Microfluidic Circuit Designs for Nanoliter-Scale Flow Control and Highly Sensitive Quantitative Bioanalysis

by

Jean Teorice Negou Negou

A dissertation submitted to the Graduate Faculty of
Auburn University
in partial fulfillment of the
requirements for the Degree of
Doctor of Philosophy

Auburn, Alabama
December 16^{th}, 2017

Keywords: Microfluidics, droplet-microfluidic, Lock-in-detection, autoregulator, Free-fatty-acid, protein quantification

Approved by

Christopher J. Easley, Chair, Knowles Associate Professor of Chemistry and Biochemistry
Curtis G. Shannon, Andrew T. Hunt Professor and Chairman of Chemistry and biochemistry
Wei Zhan, Associate Professor of Chemistry and Biochemistry
Mark L. Adams, assistant Professor of Electrical and Computer Engineering

Abstract

Within this dissertation, we have developed several new microfluidic circuit components that permit precise flow control at the nanoliter scale, and we have demonstrated their successful applications in either proof-of-concept experiments or in true bioanalytical settings.

We first introduced key concepts of microfluidics (Chapter 1), the following two chapters are focused on improvements in the microfluidic sample chopper (μChopper). Secondly, we improved upon our μChoppers performance by adding automation with on-chip pneumatic valving (Chapter 2). The device, in combination with lock-in analysis, was shown to significantly reduce 1/f noise, which is a challenging problem in small scale detection of low magnitude signals. This device allowed tightly phase-locked fluorescence detection with a bandwidth of only 0.04 Hz for droplets generated at 3.5 Hz, which resulted in a detection limit of only 12 pM fluorescein (3.1 x 10^{-19} moles) or 9.3 nM insulin (1.9 x 10^{-16} mol) using homogeneous immunoassays. The device was finally applied to the quantification of free fatty acid (FFA) uptake by 3T3-L1 adipocyte cells, and for the first time, single adipocyte FFA uptake was measured at 3.5 x 10^{-15} mol cell^{-1}. Thirdly, we expanded the applicability of this high performance detection system by designing and testing a multi-channel μChopper. The device consisted of six sample input channels and one oil input, again with automated control using seven on-chip valves. The next-generation μChopper was shown to perform various modes of analyses such as constant calibration mode, mixed mode, multiplex mode, and standard addition mode. Each mode was characterized for future application using fluorescein to mimic biological assays. We present result showing that this next-generation μChopper can not only reduce 1/f noise, but also reduce human error. Furthermore, analysis times were significantly faster since all calibrations could be completed in a single run of the device.

Fourthly, we implemented a new strategy for rapid, on-chip protein detection by combining a customized rotary mixer design with a novel, homogeneous (mix-and-read) protein assay (Chapter 3). Rapid mixing of a few nanoliters of each assay component (sample and probes) was achieved within 2.2 seconds. Aptamer or antibody-oligonucleotide based assays were used to measure protein quantities in these small-volume mixers. By combining the benefits of automated rotary mixer with homogeneous protein assays, we demonstrated that proteins could be detected at quantities as low as the attomole range.

Finally, we outlined a frequency-dependent study on passive microfluidic flow control components, namely autoregulators (Chapter 5). Using an autoregulator design developed by others, we sought to characterize the component's frequency dependence to gauge its usability in more complex microfluidic circuits. Our approach first relied on simulation of the microfluidic circuit using electrical circuit analogies. The results confirm that the autoregulators were functional as nonlinear components, permitting feedback control of the output fluidic flow rate and giving constant output flow rates at a range of input pressures. We also confirmed for the first time that these components are functional at relatively high switching frequencies-up to 16 Hz-a result that matched well with circuit simulations. Finally, we applied this knowledge to design and demonstrate a new microfluidic circuit, a flow rate mirror. Results showed that an autoregulator could control the flow rate in a parallel fluidic path, essentially independent of the downstream flow resistance. Within this work, we also demonstrated two new methods for characterizing fluidic circuit components based on real-time microscopy (fluorescence and transmission modes) to allow continuous measurements of pressures and flow rates in these devices.

Overall, we have demonstrated several new microfluidic circuit designs for nanoliter-scale flow control that allow sensitive bioanalytical measurements or provide novel flow control methodologies that should be useful for future studies in microfluidic systems.

Acknowledgments

First of all, I would like to dedicate this PhD degree to my parents. First, to my father from whom I learned to never give up no matter the odds against you, and second to my mother who succeeded in raising me and my siblings in extreme poverty conditions, some days without anything to eat, and I thank her for her unconditional love for us.

The journey to my PhD degree has been long and full of obstacles. I won't have made it without the help of a number of people. First, I would like to thank my advisor Dr. Easley for his patience, support and guidance. He is a role model for me and will always look up to him throughout my future career.

Second, I would like to formally thank my brother Oscar for whom I won't be where I am today. He financed my studies and gave me advice from the middle school to college. I really appreciate all his effort, and I wish him more success in his businesses.

Third, I would like to thank pass and present members of the Easley's group especially Dr. Xiangpeng Li with whom I collaborated in some of my projects, Dr. Joonyul Kim who gave me advice and directions when I first joined the lab, Dr. Kennon Deal who trained me for microfludics chip fabrication, Dr. Adriana Avila, Dr. Jessica Brooks, Dr. Lea Godwin, Subramaniam Somasundaram, Mark Holtan, Katarena Ford, Juan Hu, Hui Jin, and Nan Shi. I will miss you guys.

Table of Contents

Abstract ii

Acknowledgments iv

List of Figures x

List of Tables xvi

1 Introduction 1

1.1 Introduction to Microfluidic Techniques 1

1.1.1 History of Microfluidics 1

1.1.2 Microfluidic electric circuit analogue 3

1.1.3 Flow Regime in Microfluidic Systems 5

1.1.4 Droplet Microfluidics 10

1.2 Microfluidic Chip Design and Fabrication 22

1.2.1 Mask design 22

1.2.2 Photolithography 23

1.2.3 Polydimethylsiloxane (PDMS) 25

1.2.4 Plasma Oxidization 27

1.3 Flow characterization in Microfluidic Channels 28

1.4 Automated Flow Control Methods 33

1.4.1 Microfluidic Valves 33

1.4.2 Passive Components 39

1.5 Detection in microfluidic systems 40

1.5.1 Fluorescence detection 41

1.5.2 Automated lock-in detection 46

1.5.3 LabView control 47

1.5.4 Concluding remarks 48
2 An automated microfluidic droplet-based sample chopper for detection of small fluorescence differences using lock-in analysis 50
2.1 Introduction 50
2.2 Materials and Methods 52
2.2.1 Materials and Reagents 52
2.2.2 Microfluidic Device Fabrication 53
2.2.3 Flow Control 54
2.2.4 Droplet Fluorescence Measurements and Data Analysis 55
2.2.5 Adipocyte Culture, Treatment, and Lysis 56
2.2.6 Homogeneous Immunoassays 57
2.3 Control Experiment 58
2.3.1 Adipose Tissue Explant Isolation 58
2.3.2 Adipose Explant Titration with Free Fatty Acid 59
2.4 Results and Discussion 59
2.4.1 Microfluidic Device Design and Operation 59
2.5 μChopper Device Characterization 60
2.6 Real-Time Drift Correction 62
2.7 Free Fatty Acid Uptake Quantification 64
2.7.1 Homogeneous Immunoassays in Droplets 69
2.8 Concluding remarks 70
3 A Multichannels μChopper for continous calibration or multiplexed analysis . . 72
3.1 Introduction 72
3.2 Experimental Section 74
3.2.1 Materials and Methods 74
3.2.2 Microfluidic Chip Fabrication 74
3.2.3 Sample manipulation 74

3.2.4 Fluorescence measurements and data analysis 75
3.2.5 Constant calibration mode 77
3.2.6 On-chip standard addition 77
3.3 Results and Discussion 77
3.3.1 Chip design and modes of operation 77
3.3.2 Constant calibration mode 79
3.3.3 Mixed mode 81
3.3.4 Multiplex mode 84
3.3.5 Standard addition mode 84
3.4 Conclusion 85
4 Quantitative measurement of proteins at attomole levels via active microfluidic sampling and homogeneous proximity assays 88
4.1 Introduction 88
4.2 Experimental section 90
4.2.1 Reagents and materials 90
4.2.2 Microfluidic Chip Fabrication 91
4.2.3 Valve and flow control 92
4.2.4 Sample metering 94
4.2.5 Mixing time measurement 94
4.2.6 On-chip serial dilution and channels hydrophilicity treament 94
4.2.7 Thrombin quantification by pFRET assay 95
4.2.8 Insulin pFRET assay on chip 96
4.3 Result and discussion 97
4.3.1 Device design and Operation 97
4.3.2 Rotary mixer design allows rapid mixing 97
4.3.3 Nanoliter Serial Dilution 100
4.3.4 Thrombin quantification on-chip 102

4.3.5 Insulin quantification on-chip . . . 102
4.4 Conclusion . . . 105
5 Frequency Dependence Characterization in microfluidic autoregulator . . . 106
5.1 Introduction . . . 106
5.2 Experimental Section . . . 108
5.2.1 Materials, Reagents, and Methods . . . 108
5.2.2 Falstad Circuit Modeling . . . 108
5.2.3 Microfluidic Chip Fabrication . . . 109
5.2.4 Flow control and regulation . . . 111
5.2.5 Flow rate measurement . . . 111
5.2.6 Characterization of flow regulation with Frequency . . . 112
5.2.7 Current mirror experiment . . . 113
5.3 Results and Discussion . . . 114
5.3.1 Prelude experiments of autoregulator . . . 114
5.3.2 Chip designs and operation . . . 118
5.3.3 Characterization of autoregulator . . . 120
5.3.4 Frequency effects on membrane . . . 123
5.3.5 Real time flow Rate measurement . . . 124
5.3.6 Application of autoregulator in microfluidic current mirror . . . 126
5.3.7 Characterization of the microfluidic flow rate mirror . . . 127
5.4 Conclusion . . . 132
6 Chapter 6: Conclusion and Future work . . . 133
6.1 Conclusions and Achievements . . . 133
6.2 Future works . . . 135
6.2.1 Autamated μChopper . . . 135
6.2.2 Microfluidic chromatography using rotary mixer . . . 136
Bibliography . . . 138

7 Apendix A 155
7.1 LabView programs 155
8 Apendix B 173
8.1 Rights and permissions 173

List of Figures

1.1 Single molecule detection with droplet microfluidics. 4

1.2 Microfluidic electronic analogue 6

1.3 Illustration of laminar flow 7

1.4 Some applications of continuous flow microfluidic devices 9

1.5 Schematic of the droplet formation geometries 12

1.6 Surfactants role in droplet biocompatibility 14

1.7 Various methods for droplets manipulation 18

1.8 Droplets mixing mechanism 19

1.9 Soft lithography process 24

1.10 Photoresist chemical structure 26

1.11 Cross-linking reaction of PDMS 28

1.12 Plasma oxidization 29

1.13 Channel size and shapes 31

1.14 Microfluidic valves 35

1.15 Example of non-pneumatic valve 38

1.16 Quake style valves: Closing profile of multilayer soft lithography (MSL) valves . 39

1.17 The two main types of micropumps 39

1.18 Diagram of typical setup for fluorescence detection on microfluidic device 42

1.19 Illustration of molecular pincer assay 45

1.20 Block diagram of lock-in detection 47

2.1 Previous example of lock-in detection using droplet microfluidics. 52

2.2 Automated μChopper chip design 56

2.3 3T3-L1 cells free fatty acid uptake and lysis 58

2.4 Automated μChopper chip operation 61

2.5 Automated μChopper chip characterization with fluorescein 63

2.6 FFT analysis 64

2.7 Real time drift correction 65

2.8 Drift correction with PMT offset move 66

2.9 Single cell FFA uptake 67

2.10 FFA uptake by adipose tissue explants 68

2.11 Homogeneous immunoassay in droplets 70

3.1 Novel 6 channels μChopper cross-section 75

3.2 6 channels μChopper design and operation 78

3.3 Modes of operation of the 6 channels μChopper 79

3.4 Characterization of the 6 channels μChopper 82

3.5 Temporal sampling analyses 83

3.6 Standard curves of different analyses modes 86

4.1 Schematic of the pFRET assay 90

4.2 Valve controling system 93

4.3 Rotary mixer chip design 98

4.4 Rotary mixer chip operation 99

4.5 Rotary mixer characterization 100

4.6 Nanoliter volume serial dilution 101

4.7 Quantification of Thrombin protein using pFRET 103

4.8 Insulin quantification by pFRET 104

5.1 Autoregulator channel cross-sections 110

5.2 Experimental setup for flow rate measurements 112

5.3 Fluidic current mirror ROI channel cross-sections 112

5.4 Autoregulator design for simple flow rate measurements 114

5.5 Flow rate measurement preliminary results 116

5.6 Flow rate measurement by fluorescence intensity 117

5.7 Autoregulator new design 119

5.8 Autoregulator circuit simulation 121

5.9 Channels behavior 123

5.10 Evaluation of the frequency effects on regulation 125

5.11 Flow rate measurement with downstream valve pulsing at various frequencies . 126

5.12 Current mirror microfluidic design and circuit simulation 128

5.13 Flow ratio measurement 130

5.14 Flow ratio response to pressure 131

6.1 Chip design for cellular secretion dynamics study 136

6.2 Next-generation rotary mixer for chromatography 137

7.1 Automated Lock-in LabView Program front panel 155

7.2 Automated Lock-in LabView Program block diagram 156

7.3 Automated Lock-in LabView Program block diagram step 1 156

7.4 Automated Lock-in LabView Program block diagram step 2 157

7.5 Automated Lock-in LabView Program block diagram step 3 157

7.6 Automated Lock-in LabView Program block diagram step 4 158

7.7 Automated Lock-in LabView Program block diagram step 5 158

7.8 Automated Lock-in LabView Program block diagram step 6 159

7.9 Automated Lock-in LabView Program block diagram step 7 159

7.10 Automated Lock-in LabView Program block diagram step 8 160

7.11 Automated Lock-in LabView Program block diagram step 9 160

7.12 Automated Lock-in LabView Program block diagram step 10 161

7.13 Automated Lock-in LabView Program block diagram step 11 161

7.14 6 channels automated Lock-in LabView Program front panel 162

7.15 6 channels automated Lock-in LabView Program block diagram step 1 162

7.16 6 channels automated Lock-in LabView Program block diagram step 2 163

7.17 6 channels automated Lock-in LabView Program block diagram step 3 163

7.18 6 channels automated Lock-in LabView Program block diagram step 4 164

7.19 6 channels automated Lock-in LabView SubVI front panel step 5 164

7.20 6 channels automated Lock-in LabView SubVI block diagram 165

7.21 Rotary mixer LabView program front panel 165

7.22 Rotary mixer LabView program blockdiagram step 1 166

7.23 Rotary mixer LabView program blockdiagram step 2 166

7.24 Rotary mixer LabView program blockdiagram step 3 167

7.25 Rotary mixer LabView program blockdiagram step 4 167

7.26 Rotary mixer LabView program blockdiagram step 5 168

7.27 Rotary mixer LabView program blockdiagram step 6 168

7.28 Rotary mixer LabView program blockdiagram step 7 169

7.29 Autoregulators LabView program front panel 170

7.30 Autoregulators LabView program blockdiagram step 1 171

7.31 Autoregulators LabView program blockdiagram step 2 171

7.32 Autoregulators LabView program blockdiagram step 3 172

7.33 Autoregulators LabView program blockdiagram step 4 172

List of Tables

Table 1.1: Summary of some critical design rules information

List of Abbreviations

LOC Lab-on-Chip

μTAS Micrototal Analyses

SPE Single phase extraction

POC Point of care

PDMS Polydymethyl siloxane

PMMA Polymethylmethacrylate

PCR Polymerase chain reaction

CV Coefficient of variation

PFO Perfluorooctanol

PFPE Perfluoropolyether

PEG Polyethylene glycol

EWOD Electrowetting on dielectrode

FACS Fluorescence activated cell sorting

SDA Static droplet array

UV Ultraviolet

PAC Photoactive compound

DNQ Diazonaphtho-quinone

mLSI Microfluidic large scale integration

MEMS Microelectromechanical system

NC Normally closed

NO Normally opened

DMF Digital microfluidics

MSL Multilayer soft lithography

LIF Laser-induced fluorescence

MS Mass spectroscopy

ICP-AES Inductively coupled plasma-atomic emission spectroscopy

MALDI Matrix assiated laser desorption ionization

FRET Fröster energy transfer

CCD Charge coupled device

PMT Photon multiplier tube

TFA Thermofluorimetric analysis

pFRET Proximity Fröster energy transfer

ELISA Enzyme linked immunosorbent assay

ROI Region of interest

VI Virtual instrument

LOD Limit of detection

μChopper Microfluidic Chopper

FFA Free fatty acid

FBS Fetal bovine serum

FFT Fast Fourier transform

HPLC High performance liquid chromatography

BSA Bovine serum albumin

MOSFET Metal-oxide semiconductor field-effect transistor

Chapter 1

Introduction

1.1 Introduction to Microfluidic Techniques

1.1.1 History of Microfluidics

Since the 20th century, electronic technology has evolve exponentially thanks to the discovery of semiconductors and the enhancements made possible due to the development of photolithographic techniques to enable miniaturization[1, 2]. To date, electronics devices continue to be smaller and smaller. Similarly, laboratory experiment also felt a need for miniaturization especially in biological laboratories where being able to work with small volumes is important but can be not-trivial. Therefore, deriving from the same techniques used to miniaturized electronic components, a novel scientific field named microfluidics was created [3].

Microfluidics is the science that studies the behavior of fluids confined into channels of size ranging from 10 to 100 micrometers [4]. It is a technique where all laboratory equipment and glassware can theoretically be reduced into a single chip, generally about one inch square in dimensions. Therefore the platform is often referred to as Lab-on-chip (LOC) . This technology primarily focuses on the manufacture of microfluidic chips where small volume of fluids (down to femtoliter) can be controlled and manipulated. Due to its advantages such as small volume consumption, low cost, and short analyses time, this field is gaining more popularity in biology, chemistry, and engineering. Over the years, the field of microfluidics has greatly expanded with more research groups being created as well as more investment from the industries. In fact, microfluidics publication in engineering, multidisciplinary science, biology, and medicine journals sees a significant increase in the number of

publications every year, and the microfluidics market also is observing a growing number of companies[5, 6, 7]. The success of microfluidics is most probably due to the fact that it allows large flexibility in the design of the devices to include the flow regime, functionality, and application. Advantages such as low sample volume consumption, faster analyses time, and its low fabrication cost are not to be omitted.

The bioscience field presents a wide variety of tools for analyses but when miniaturization is necessary, there is an option of choosing between the microtiter plate, the microarray, and microfluidics. Although these tools can all achieve similar results, microfluidics surpasses the other techniques with better advantages. Lion et al. have compared these three devices in their review and placed microfluidics on top in terms of analytical sampling volume, and analysis time [8]. To explain the faster analysis time observed in microfluidic systems, we can consider the analogy where two molecules placed in a large volume takes more time to come to a close proximity and react than when placed in a smaller environment such as the microfluidic channels. Furthermore, microfluidics can integrate different functionality into one device to create a system known as Micrototal Analyses (μTAS). For a device to be consider a μTAS, all components and processing steps should be integrated, it should be portable, and also provide all of the possible analyses in the same device with no user interaction required except for initialization. Examples of such devices have integrated sample preparation, solid phase extraction (SPE) , dilution, electrophoresis, mixing, incubation, and detection into a single device[9, 10, 11, 12]. Another advantage of microfluidics is the low cost of material which can be less than a dollar per chip. These advantages arguably make microfluidics the best candidate for field applications and point of care detection (POC) .

The evolution of microfluidics as an analytic tool have lead to usage of a wide range of materials for fabrication. The materials mainly used are glass, paper, or polymers such as polydimethyl siloxane (PDMS). Other polymers such as polymethylmethacrylate (PMMA), photocurable perfluoropolyether, biodegradable polymers, photosensitive polymers, and polymerized hydrogels have been used to make microfluidic channels[13, 14, 15,

16, 17] Paper microfluidics is more suitable for point of care detection (POC) and can be used in developing world for diagnostic applications. On the other hand, glass, PDMS and PMMA microfluic are mostly used in research and medical laboratories as well as in the industry.

Microfluidics is a multidisciplinary technique because it finds applications in chemistry, biology, physics, and engineering. Some applications include protein crystallization[18], cell culture[19], high throughput drug screening, cell sorting, generation and manipulation of monodisperse droplets, etc. One of the biggest achievements of microfluidics system is the detection of a single DNA molecule by polymerase chain reaction (PCR). Figure 1.1 depicts single molecule encapsulation, PCR amplification and detection[20, 21]. In this method, single copies of DNA strands are encapsulated in femtoliter volume droplets and are enzymatically amplified. Positive droplets (green) can be digitally counted with high precision.

1.1.2 Microfluidic electric circuit analogue

We know that lab-on-a-chip technology is directly related to electronic circuits because materials and fabrication techniques are similar, and it has similar goal to combine components with different fonctionality in a small chip. As such every microfluidics component can be thought of as having an equivalent electronic component. Therefore a microfluidic chip can be directly compared to an electronic chip in terms of component functionality. Figure 1.2 illustrates a few microfluidic components that behave similarly to electronic components. In general, fluid pressure, fluid flow, and flow resistance can be modeled by electric voltage, current, and resistance respectively. So the Ohm's law can easily be applied to microfluidics by replacing the voltage, current, and resistor by their microfluidic analogue.

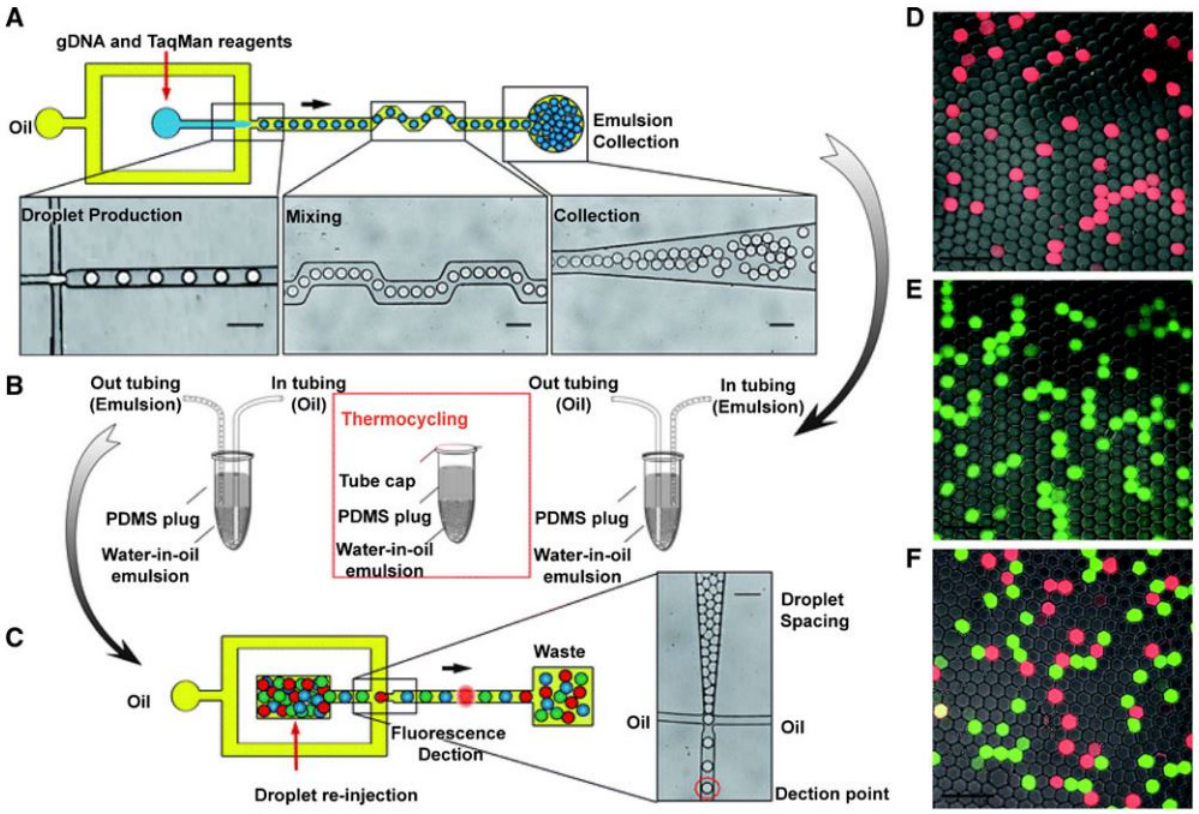

Figure 1.1: Single molecule detection with droplet microfluidics.
(A) Microfluidic design for compartmentalization and amplification of single DNA molecules. (B) Droplet emulsion collection for PCR amplification. (C) Droplet re-injection onto the microfluidic chip for fluorescence imaging. (D-F)) Fluorescence confocal microscopy analysis of thermocycled droplets showing the wild-type DNA (D), the mutated DNA (E),and both the wild type and the mutated DNA (F). This Figure was reprinted with permission from ref [21] Copyright 2011, Lab-on-Chip.

$\Delta P = \phi R_{Fluidic}$ Equation 1.1

where ΔP is the change in pressure, ϕ is the flow rate, and $R_{Fluidic}$ is the fluidic resistance.

Fluid control and manipulation can be done by using other components such as microfluidic diodes, capacitors (illustrated in Figure 1.2), and transistors (or switches) that are often fabricated by modifying the design and the functionality of microfluidic valves[22, 23, 24].

The Quake research group have pioneered microfluidic fabrication of electronic circuit analogues. They have fabricated a microfluidic multiplexer[25] and another device capable of memory storage tasks[26]. Similarly, a work showing a microfluidic shift register have been published[27]. The electronic analogies enable a deeper understanding of fluid dynamics at the microscale and for predicting reaction conditions. However, further investigation needs to be done to fully understand device function. For instance, newly described microfluidic components should be further studied for their frequency dependence and dynamic function to enable improved integration into complex devices. In fact, frequency responses of several components are shown within this dissertation.

1.1.3 Flow Regime in Microfluidic Systems

The basis of microfluidics is to be able to flow very little amount of fluids into micrometer channels and therefore perform reactions at the microscale. When fluids are allowed to flow in such small space, the forces acting on the fluid are different than those at the macroscale. Fluid behavior in microscale channels is governed by laminar flow (Figure 1.3) where plates of fluids flow side-by-side and in a uniform fashion as opposed to turbulent flow where the layers of fluids flow in a chaotic fashion and can be quickly mixed. Those plates or layers of fluids can only mix with the neighboring layers by slow diffusion. In such systems, inertial forces and gravity are negligible and the dominants forces are surface tension, van de Waals interaction, and surface roughness[28, 29]. The viscous force within the fluid is also more important than the inertial force. Another important characteristic of flow in microfluidics is the capillary forces or simply capillary number, which is the ratio between viscous forces and the surface tension. I will elaborate more on this particular characteristic in the droplet subsection bellow.

Flow can be initiated in microfluidic devices by using a pressure or vacuum source, peristaltic pump, or electro-osmosis. A simple syringe pump or pressurized syringe can be used to apply vacuum or pressure to flow reagents in the channels. Peristaltic pumps are

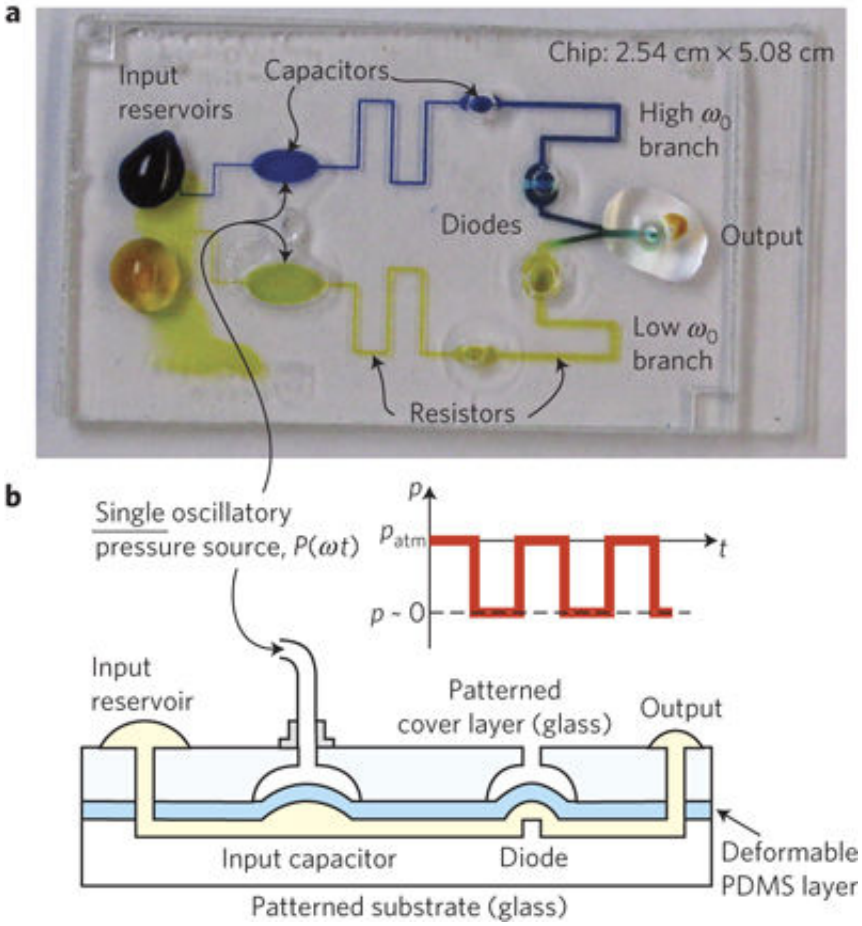

Figure 1.2: Microfluidic electronic analogue
(a) A microfluidic chip depicting fluidic components analogue to electric circuit such a fluidic resistors, capacitors and diodes. (b) A cross-section on the microfluidic chip showing the same components. This Figure was reprinted with permission from ref [24] Copyright 2009, Nature Physics.

exclusively used in automated systems where no continuous external force is needed to move or mix the fluids. Electroosmotic flow is initiated by applying a potential across the channel to move fluids; it is mostly used for microfluidic electrophoresis. This dissertation work only focuses on pressure and vacuum driven flow with or without valves in single phase and multiphase microfluidics.

Continuous Flow Microfluidics

A microfluidic device is in the continuous flow regime when the fluid is the same throughout the channel and have the same density. In general, only the aqueous phase is used in the system. In this flow regime the channel size and the hydrophilicity of channel walls

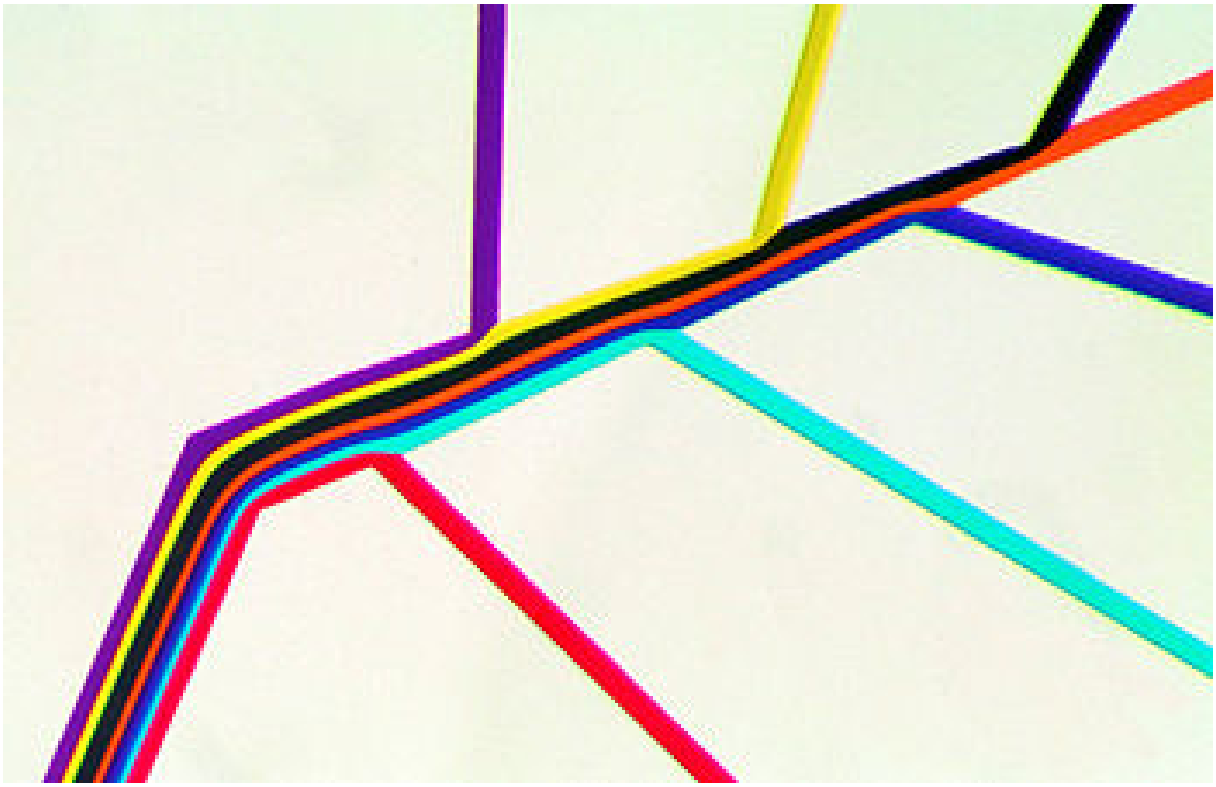

Figure 1.3: Illustration of laminar flow
An image of the laminar flow process in the microfluidic channel showing 7 layers of fluids flowing side-by-side without mixing. This Figure was reprinted with permission from ref [28] Copyright 1999, Science.

give important characteristics which is the large surface-to-volume ratio. This is the most common and the simplest flow regime, and it is present in almost all microfluidic systems.

The first microfluidic device functioned on single phase flow and was used for gas chromatography to analyze ambient air[3]. The single phase has since evolved to using aqueous reagents to perform chemical reactions on-chip. Implementation of this flow regime can be found in various microfluidics techniques going from simply using pressure or vacuum to flow liquids in channels to highly complex, automated systems such as the high-density microfluidic chip for large scale integration fabricated by the Quake group[25]. This device consisted of complex fluidic networks controlled by thousands of micromechanical valves and contained hundreds of individually addressable chambers that together function much like an electronic multiplexer. The same group presented other microfluidic devices based on continuous flow fluid manipulation, one that could flux stabilize flow and act as flip-flop memory[26], and another that was capable of segmenting precise volume of fluid for effective mixing[30]. Utilizing the continuous flow regime in microfluidics is beneficial for point of care (POC) detection (Figure 1.4, A and B)[31, 32], to mimic blood flow in the case of organ-on-chip devices (Figure 1.4C)[33], and is the only type of flow possible in some type of microfluidic devices such as the compact disk microfluidic (Figure 1.4D)[34] and paper microfluidic (Figure 1.4E) devices[35].

Microfluidics systems employing the continuous flow have found applications in fluid handling, point-of-care detection, cell separation, solid phase extraction (SPE), and on-chip assays. As mentioned in the previous paragraph, fluid control and manipulation using single phase flow are mostly applied to microfluidics electronic analogues to prove that microfludic can perform similar tasks as electronic circuits. Point of care diagnosis including paper microfluidics are simple and disposable devices that require only sample and reagent to react and be detected through color change. Cell sorting has also been done by flowing different types of cells in the same stream and using different geometries and mechanism to sort the cells[36].

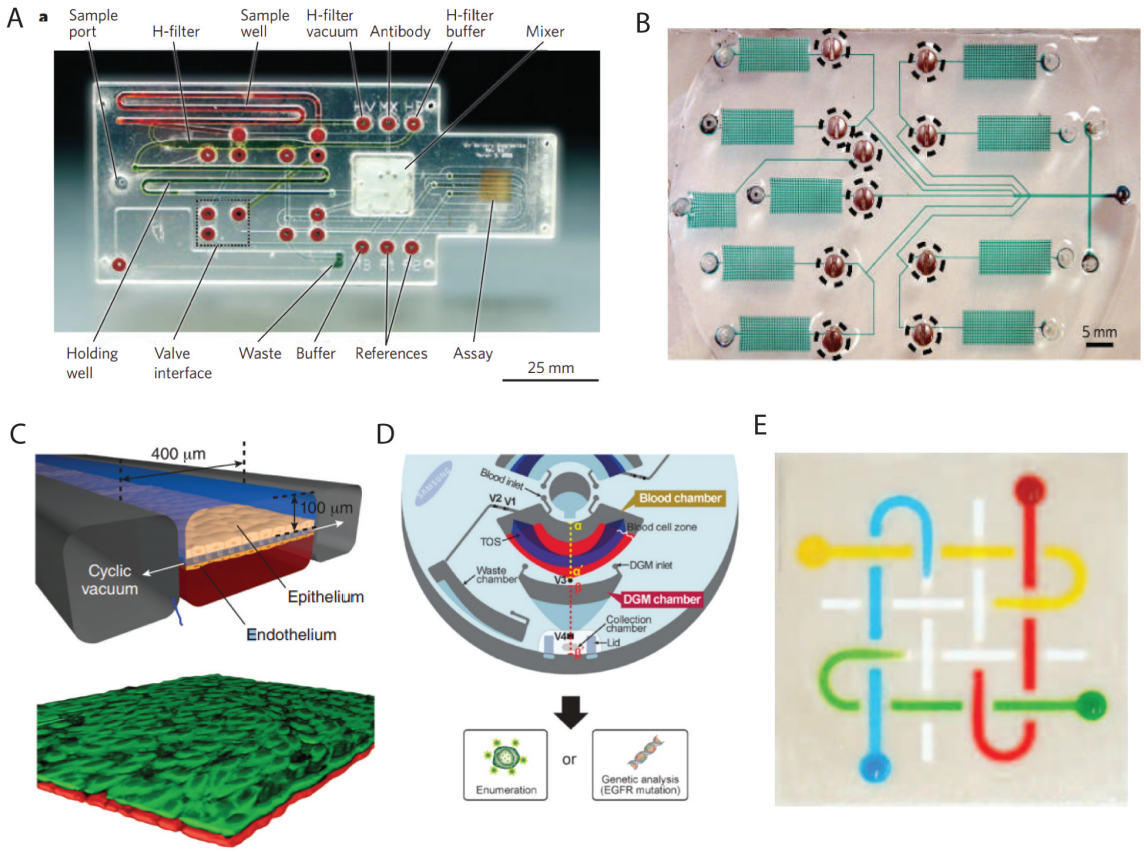

Figure 1.4: Some applications of continuous flow microfluidic devices
(A) An integrated disposable diagnostic card for analyses of filtered saliva in point of car (POC) detection. (B) A disposable microfluidic device for sandwich immunoassays used in POC detection. (C) Microfluidic organs-on-chip, an image depicting lung-on-chip. (D) A microfluidic compact disc device for isolation of rare circulating tumor cells (CTCs). (E) A 3D paper microfluidic device showing streams of fluids crossing each other. Figure A, B, C, D, and E were printed with the permission from ref [31] Copyright 2006, Nature; ref [32] Copyright 2005, Anal. Chem. ACS; ref [33] Copyright 2014, Nature Biotechnology; ref [34] Copyright 2014, Anal. Chem.; and ref [35] Copyright, 2008 PNAS.

1.1.4 Droplet Microfluidics

Droplet microfluidics is a sub-field of microfluidics where monodisperse bubbles or droplets (typically from fL to nL volume) of a dispersed gas or liquid phase in a continuous liquid stream are generated and manipulated. Since it was first introduced[37], droplet microfluidics has undergone rapid progress as it offers unique advantages and a wide range of applications, notably for single molecule analysis, digital PCR, protein crystallization, and high throughput screening. The driving force of droplet microfluidics is its ability to serve as individual, small volume compartments in which to isolate and study chemical or biochemical systems. Isolation of droplets by the immiscible fluid allows them to behave as individual test tubes or microreactors where millions of reactions or assays can be performed at the same time.

Droplet formation

Droplets are formed at the region where two immiscible fluids streams merge. The characteristics involved in droplet formation and break-out are directly related to the local geometry and surface chemistry of microchannels. Several geometries designed for passive droplet formation have been proposed and are being used by researchers, namely the cross-flow, the co-flow, and the flow focusing designs. The choice amongst these design is a matter of preference since they can all produce stable and monodisperse droplets with consistent size at a prescribed frequency[38].

Cross-Flow

When the dispersed and the continuous phase channels meet at an angle, the geometry is referred to as cross-flow (Figure 1.5A, and B)[39]. The most commonly used cross-flow geometry is the T-junction where the two phases of fluid meet at an orthogonal cross section between the channels (Figure 1.5A). It was introduced by the Quake group in 2001 when they created the first droplet microfluidic device (Figure 1.5B)[37]. The coefficient of variation

(CV), in droplet volumes using this geometry was less than 2%, thus making it the simplest method of producing monodispersed droplets and therefore the most widely used geometry. There is another T-junction design where the angle between the two phases is modified and the effect of varying the angle affects droplet breakup. The original T-junction design can also be used but with the two immiscible fluid coming in a straight channel in opposite directions and flowing together in an orthogonal channel after droplet formation. This T-junction style is called "head-on device" and form a Y-shape. If there is a need to flow two different population of droplets in the same channel, another channel can be added orthogonally to the carrier fluid channel (Figure 1.5A, bottom). The result is a production of alternating pairs of droplets where one could serve as reference droplet[40]. We have exploited this geometry for our lock-in detection discussed in section 1.5.2 and chapter 2 of this dissertation. Similar droplet pairs are produced with a Y-shape cross-flow design when using a parallel dual T-junction geometry. Other cross-flow geometries found in literature are the K-junction, and the V-junction[39].

Co-flow and flow focusing geometries

In the flow focusing droplet generation geometry, three fluidic streams converge into a main channel through a narrow pathway. In this configuration, two streams of the continuous phase surround the dispersed phase stream (Figure 1.5C, and D)[41].

The co-flow droplet generation geometry is based on injection of the dispersed phase in a central microchannel placed in the middle of another microchannel with larger dimension. The dispersed and continuous phase fluids flow in parallel streams and meet at the injection tip where droplets break-up(Figure 1.5E) . The device can be either 2D planar or 3D coaxial configuration[39].

There are few factors that characterize droplets size in co-flow systems, for example the flow rate. When the continuous phase droplet is faster, the droplets produced are smaller. Conversely, when the dispersed phase is faster, the droplets become larger. Another factor

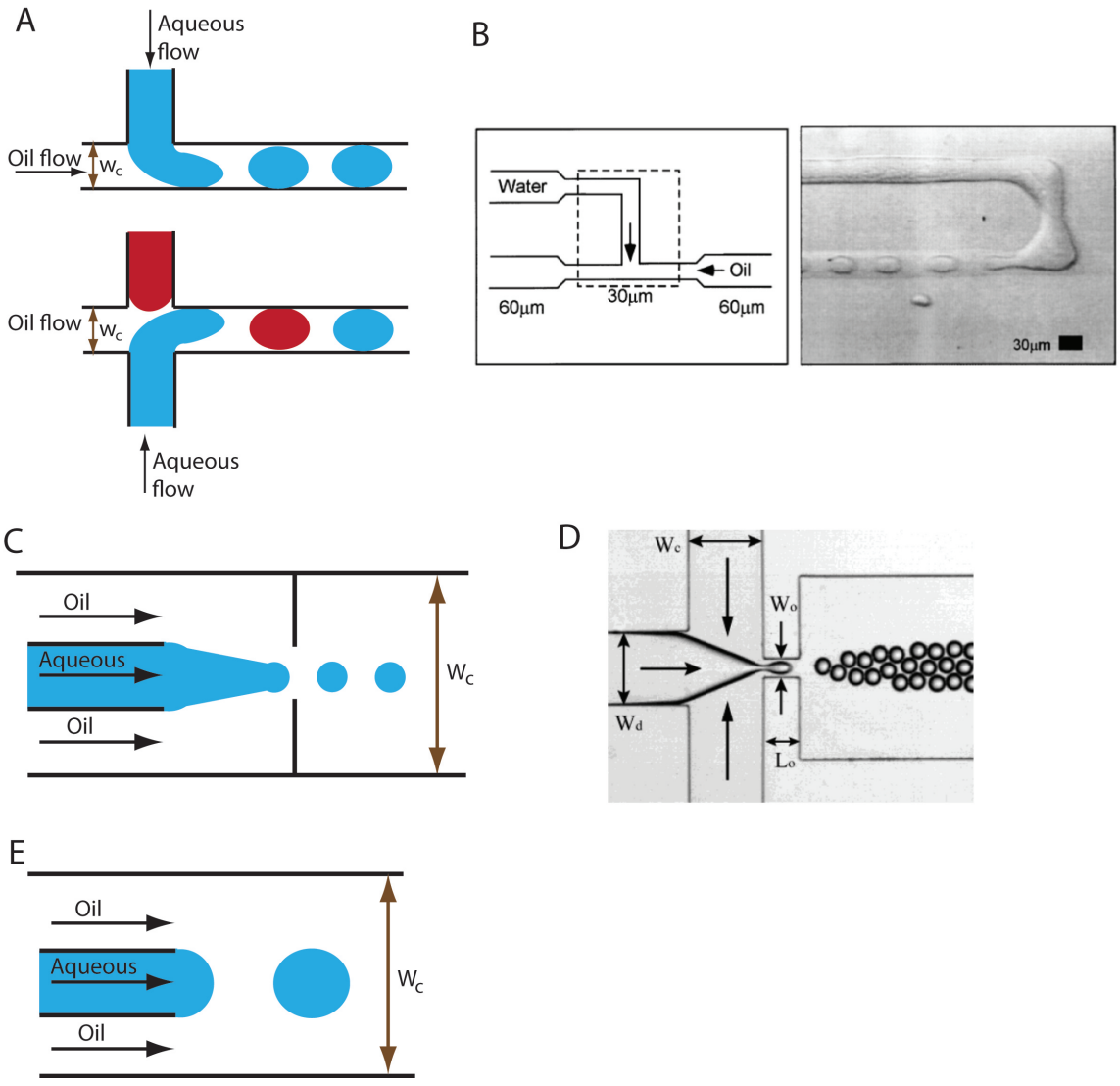

Figure 1.5: Schematic of the droplet formation geometries (A)T-junction geometries, single (top), dual T-junction (bottom); (B) Schematic and image of the first droplet formation device. (C) Planar flow focusing geometry. (D) The first flow focusing device. (E) Co-flow system. Figure B, and D were printed with permission from ref [37] copyright 2001, Physical Review Letters, form ref [41] Copyright 2011, Int. J Mol, Sci.

characterizing droplet size is the geometry of the co-flow system. The fact that the continuous flow surrounds the dispersed phase allows sub-micron droplets generation in co-flow systems[42, 43].

Droplet surface biocompatibility

One crucial element in droplet microfluidics is the use of surfactants. By definition, surfactants are amphiphilic molecules that lower the interfacial tension between two immiscible liquids. In addition, in droplet microfluidics technology they essentially form a shell that stabilize droplet interface,to make the system biocompatible, and to minimize cross-contamination between droplets(Figure 1.10A). This is a basic requirement for biochemical reactions for each droplet to become a stable individual reaction vessel without coalescing especially when conducting millions of reaction in picoliter volumes. Surfactants are part typically of the mixture of the oil carrier. Fluorinated surfactants are widely used for the stabilization of droplets. Although they have been well reported for their biocompatibility, they still present some limitations for water in oil interfaces. There have been many attempts to increase the biocompatibility of fluorinated oils by modifying the fluorocarbons. For example, perfluorooctanaol (PFO) with short fluorinated tails that is used as therapeutic agents in lung deficiency have been applied to microfluics. The limitation of the technique is the non-specific interaction of the surfactants with fibrinogen. However, changing the head groups of the PFO can lead to an increase or decrease in protein adsorption depending of which head group is used. There are few examples of a truly biocompatible surfactant. The solution is sometimes to chemically bond another organic group to the fluorosurfactants[44]. One example is the perfluoropolyethers (PFPE) with hydrophilic head group, shown in Figure 1.6B[45]. While the PFPE stabilize the droplet, the PEG prevents adsorption of biomolecules to the droplet surface. These type of biocomapatible surfactants are now commercially available. For instance Picosurf 1, commercialized by Dolomite Microfluidics, can be mixed with oil and has been proven to be very effective.

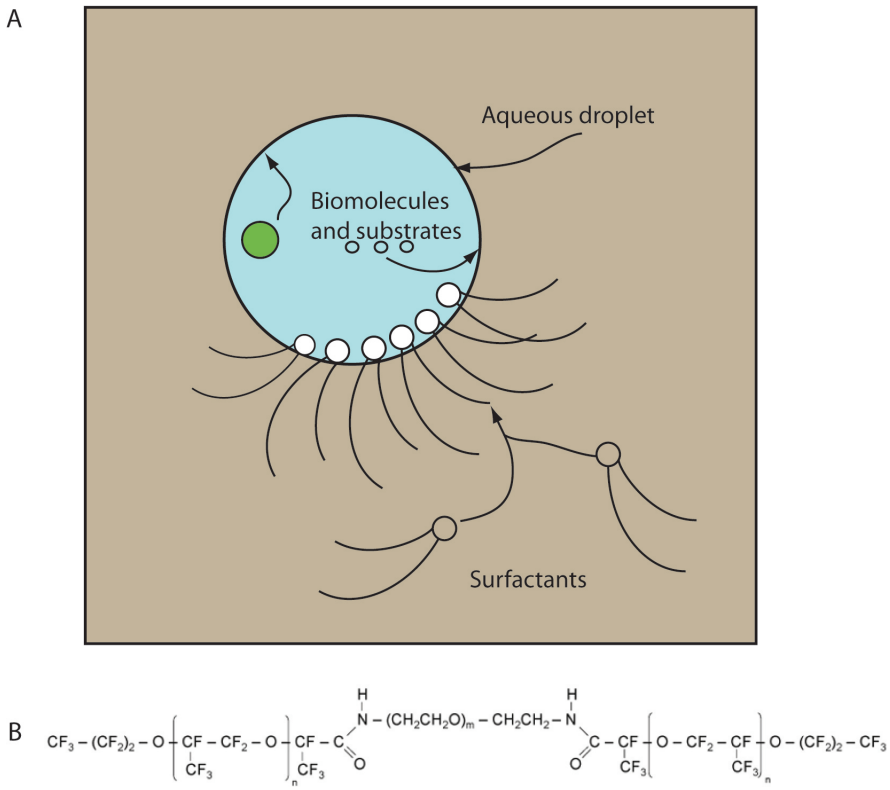

Figure 1.6: Surfactants role in droplet biocompatibility
(A) Schematis of a droplet in oil and surrounded by surfactants that prevent molecules or cells from entering or exiting the droplet. (B) An example of surfactant chemical structure. Reprinted with permission from ref [45] Copyright 2008, Lab-on-Chip.

Advantages of droplets microfluidics

Droplet trapping

After the droplets are produced, they can be directly detected or they can be manipulated to produce other benefits for biological and chemical analyses. For this purpose, discrete volume of droplets can be trapped, split (fission), merged (fusion), and sorted. Because stable droplets will make it difficult to perform these different tasks, manipulation of droplets is done often without surfactants.

Droplet trapping allows the parallel processing and monitoring of chemical and biological assays (Figure 1.7A). Drug screening, microbiology and cell biology have benefited from the use of droplet array technologies. Traditional methods such as the 96-well plate have been the only avenue for such applications in the past[46]. However, the well-plate or microtiter plate require tedious labor to dispense reagents into each well, it consumes larger amounts of expensive biological sample, and analysis time takes several hours to obtain results. In microfluidics, thousands of droplets can be produced in high frequency and trapped into microfluidic trapping channels to form droplets array. Taking advantage of the small volume of droplets (down to femtoliter), reagents can be saved. Also, microfluidics reaction times are faster (from minutes to seconds). Therefore microfluidic droplet trapping presents itself as an excellent alternative to microtiter plates. Additionally, droplet trapping is well suited for incubation, detection, and making observations. Many droplets trapping geometries involve channels with narrow regions (sometimes a membrane valve) where droplets can be trapped and a detour channel where the next droplet can bypass and be trapped in the next narrow region[46, 47, 48, 49]. A pillar array have also been used to trap and fuse droplets[50].

Droplet merging or splitting

Another purpose of droplet trapping is to fuse or merge the trapped droplet with another droplet. The main purpose of droplet merging is that it offers precise control over the reaction

mixture. Since chemical and biological reaction often involve the combination of different reagents, droplet merging provides ease of performing on-chip reagent mixture or dilution (Figure 1.7B)[48]. Droplet merging device geometries are often similar to that of trapping but require a larger chamber before the narrow region where two or more droplets can be trapped and merged. For two droplets to fuse together, they must achieve temporal and spatial synchronization. Therefore if two droplets are to be fused, the environmental conditions should only allow the two droplets to fuse at a time. One strategy has been to add surfactants in the continuous phase to make the fuse droplet more stable. However, the presence of surfactant in the solution could make the fusion difficult. The best alternative is to design geometries that would be favorable to droplet merging. One of the simplest techniques is to produce the droplet in a narrower channel and moved it into a widened channel where it can expand, be trapped, and coalesce with the next droplet[48, 51]. The efficient control of the continuous flow velocity is also a key factor.

Since the droplets can be fused to achieve some chemical and biological purposes, they can also be split as well. The importance of splitting droplet can be used to remove certain reagents in a droplet for assay operation or simply to replicate droplets. For example, Abate et al. designed a droplet spitting devices that could split larger droplets several times to form emulsion droplets in a much faster rate (Figure 1.7C top)[52]. The splitting mechanism relies on a sharp channel edge where the droplet with a large circumference can be split in two.

Droplet mixing

Mixing reagents in a droplet is a crucial aspect of droplets manipulation. Mixing establishes a homogeneous mixture of reagents inside a droplet and therefore allows faster reaction. Without faster mixing techniques in microfluidic devices, mixing would rely solely on the diffusion of molecules, which is time consuming and will compromised one of the most lauded advantages of microfluidics which is faster reaction time. Figure 1.8 shows the most

commonly used mixing mechanism involved in droplet microfluidics[53, 54]. The mixing is useful for size of droplets that are large enough to come in contact with the channels wall. The channel is designed in a serpentine fashion to allow each droplet to fold itself when passing through the sharp turn(Figure 1.8a). The folding increases the laminar plates (Figure 1.8b) while reducing their thicknesses; after each turn the droplet folds into itself and reorient for the next folding and leave an exponential number of thin laminar plates where diffusion happens at much faster rate. Figure 1.8c is another channel design for droplet mixing where the same result is obtained.

Electrowetting

So far, the droplet manipulation techniques discussed use passive flow control where droplet manipulation is constrained by the geometry the devices. Droplet digital microfluidics is a microfluidic sub-field where electrical power is used to mix, merge, and split droplets (Figure 1.7D)[55]. The technique is called electrowetting on dielectric (EWOD). In this method, and array of electrodes is used to modify the wettability and the contact angle of the surface. The drawbacks of this method is complexity of microfluidic device fabrication and the use of external electrical equipment that could interfere with biochemical reactions.

Droplet manipulation for high throughput application

Droplet microfluidics is a powerful technique because it produces micro-size droplets that act as ideal reactor chambers for different biological and chemical reactions. It also provides large flexibility in terms of droplet manipulation and application. Droplet sorting and pico-injection are the most important techniques of droplet manipulation or application because they allow high throughput and accurate analytical solution in cellular biology, biotechnology, and medicine.

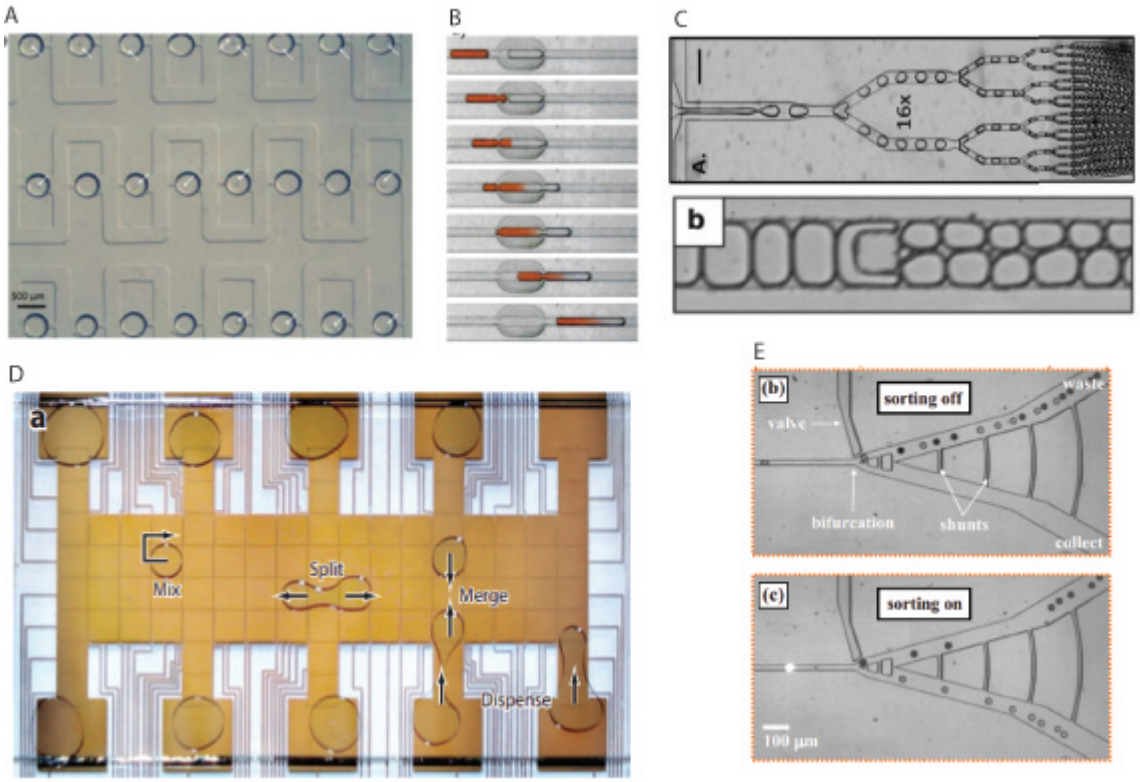

Figure 1.7: Various methods for droplets manipulation
(A) Image of droplets encapsulated with worms trapped in an array of 24. (B) Image of droplet trapping and merging. (C) Droplet splitting techniques. (D) Digital microfluidics device capable of mixing, merging, and splitting droplets. (E) Valve-based droplet sorting. Figure A, B, C, D, and E were reprinted with permission from ref [46] Copyright 2008, Lab-on-Chip, ref [48] Copyright 2013, Lab-on-Chip, ref [52] Copyright 2011, Lab-on-Chip,[55] Copyright 2015 New Biotechnology, and ref[56] Copyright 2010, Aplied Physics Letters.

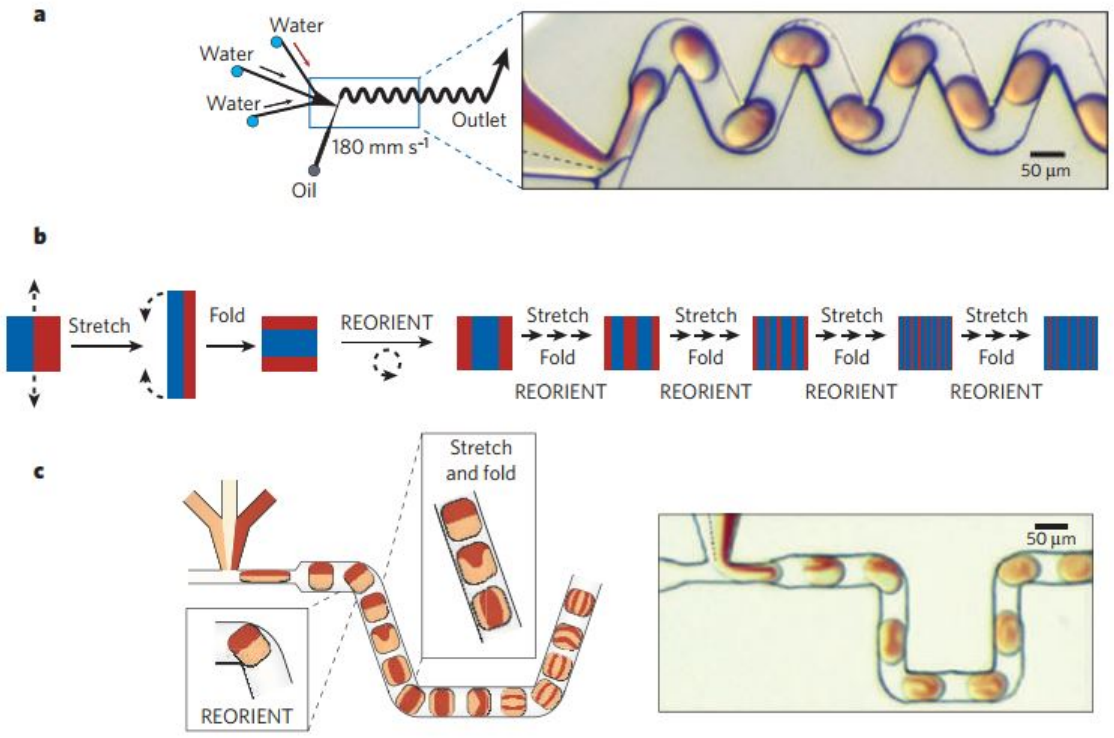

Figure 1.8: Droplets mixing mechanism
(a) Serpentine channel showing chaotic mixing in microchannel. (b) Schematic of the fluid element undergoing chaotic stretching, folding, and reorientaion steps for mixing in serpentine channels. (c) Another channel configuration for chaotic mixing. This figure was reprinted with the permission from ref [**?**] Copyright 2006, Nature.

Droplet sorting

Droplet sorting enables differentiation of droplets depending on their content for further analysis. It is used in microfluidic analyses to sort encapsulated cells or molecules from complex, heterogeneous mixtures in a sample[57]. For example, droplet technology offers the advantage of encapsulating a single cell into a droplet for analysis and facilitate diagnosis of malignant cells for early cancer detection or simply enrich or purify cell samples into well-defined populations[58, 59]. Other example include encapsulation and sorting of enzymes[60], bacteria[61], Proteins, and microbeads[62]. There are two main methods used in microfluidics to sort droplets. One is the use of pneumatic forces to divert detected droplet from the main stream. For example the system developed by Adam Abate (Figure 1.9E) where high speed fluorescent droplets sorting can be performed using a membrane valve that can be actuated to squeeze an asymmetric channel and divert fluorescent droplets. Another sorting technique is based on applying electromagnetic forces to sort droplets[56]. One most famous example is the fluorescence activated cell sorting (FACS) where cells can be sorted at very high rate (2000 droplet/s) with an error of less than 1 in 10^4 droplets[63].

Droplet pico-injection

Droplet pico-injection is a technology used to add reagent into droplets. Its importance is crucial in the case where multistep reactions which require mixing reagent at different times is needed. There are a few other methods of mixing reagents in droplet microfluidics including droplet merge mentioned above. Pico-injection offers a much simpler method of adding reagent in droplets because it does not require synchronization of droplets, and surfactants can be used. While initial technologies used metal electrodes to inject reagent in droplet[64], Abate and coworker have developed methods using a channel with dissolved electrolyte in solution[65, 66].

Static microfluidic droplet devices

Droplets can also be produced and manipulated without moving them through microchannels. Similar to the microtiter plate and the droplet trapping microfluidic device mentioned above, such systems are usually made to produce a droplet array platform for high throughput screening.

The static droplet array (SDA) device is the closest analogue of the 96-well plate. In this system an array of droplet is produced by first flowing the sample into a microchannels network with a repeated sequence of loops. Fluidic trap regions and bypass channels are the combination at every loops. First, sample is flowed to fill the channels, and plugs of the sample are trapped in the fluidic trap regions. Next, oil is flowed in the channels to remove sample in the channels and leave only the trapped sample droplets. The volume of droplets trapped varies from nanoliter (nL) to picoliter (pL) and is well suited for single DNA and cell screening. Some of these devices are capable of performing reactions with concentration gradients[67]. An automated static droplet device that is capable of generating, transport, immobilize in fusing, storing, analyzing, and retrieving droplet have been reported[68].

The SlipChip is another device where static droplets can be analyzed. This device is made of two plates in close contact to each other. In the bottom plate, there are prefabricated wells where reagents are to be loaded as well as ducts for the sample. The top plate serves as lid to the bottom plate but it also has wells where sample are to be loaded. The device contains a fluidic network where sample can be flowed to fill the sample wells and ducts. To initiate a reaction, the top plate is "slipped", or moved so that the top wells overlap with the bottom wells containing the reagents. The reaction between sample and reagent occurs by diffusion. This device can be applied for multiplexed reactions where there is a need to evaluate the reaction of one sample exposed to many reagents in small volume[69]. This technology has been commercialized to offer microfluidic platforms for quantitative measurements of nucleic acids and proteins.

1.2 Microfluidic Chip Design and Fabrication

1.2.1 Mask design

The first step into the fabrication of a microfluidic device is to make a photomask which is a predefined pattern made of opaque film with transparent areas to allow light to pass through. It is a glossy plastic used in the microelectronic industry, and in microfluidics during photolitography process. The mask can be positive or negative depending on which photoresist will be used. After deciding all features and functionalities of the device a program such as Adobe Illustrator is used to design the microfluidic channels. The predefined patterns dimensions (length and width) will be directly imprinted onto a silicon wafer after the photolithography process. To ensure that the device will operate as expected, the designing and manufacturing process must be carefully performed. Starting from the design in Adobe Illustrator, the dimensions should be carefully chosen according the flow rate, reaction time, and functionality needed. When all the design and features are done, the design files is sent to a company for photomask printing.

Other very important rules should be taken into consideration when designing a microfluidic device. For example, alignment marks should be included in all devices. This helps for alignment on the mask aligner especially when fabricating a multilayer device. Hole punch sizes, generally 3 mm for reservoirs and 1.5 mm for tygon tubings, should be predefined on the photomask. Flow channels should be designed according to acceptable aspect ratios to avoid channel collapse after fabrication, low (1:10) and high (4:1) aspect ratio limits are generally advised. Space on the photomask should be arranged to carry the maximum number of chips. Our designs usually carry no more than 6 devices at a time for $\sim 1\ in^2$ chips. The lines separating the 6 devices indicate where the chip should be diced. The device should be designed to function with a 30 μm tolerance to account for alignment and dicing errors. For multilayer microfluidics where valves are used, the cross section between control and flow channel should be designed to achieve nominal valve area; for example if

the flow channel is 35 μm, the valve area should be at least 150 μm x 150 μm and the closing pressure is at least 5 psi[70]. The PDMS membrane thickness should be less than 30 μm for the valve to properly close.

1.2.2 Photolithography

After the photmask is created, the next step is to fabricate the silicon wafer substrate. This is done by the photolithographic process where the design printed on the photomask is transfered to the surface of a silicon wafer. This process was developed for the semiconductor industry in the 1940s with the synthesis of photoresist. In fact, the process was first developed by Niepce as a photographic printing method using ink and paper[1]. In modern semiconductor fabrication, photolithography uses optical radiation to print an image of the design from the mask to a silicon wafer. The process begins with cleaning of the wafer to remove contamination, following by dehydration to remove water, and sometimes addition of an adhesion promoter. Next, a light photocurable material called photoresist is spin-coated on the surface of the wafer at a desired thickness. To remove solvent, the spin-coated wafer is baked (a process called soft bake) on a hot plate at a given temperature depending on the photoresist used. After removing the solvent the design imprinted photomask is placed on top of the wafer in a mask aligner, then aligned to make sure that all the design fit the wafer. UV exposure is done at this stage to change the solubility of the resist during the developing step. The last two steps are to bake in order to remove excess solvent (post-exposure bake) and to develop using a photoresist developer and reveal a positive relief imprinted design on the mask[71]. In microfluidics where soft polymers such as PDMS are used, photolithography is referred to as soft lithography. This process is illustrated in Figure 1.9.

As noted, the process uses an organic material called photoresist which reacts to the Ultraviolet (UV) light. There are two categories of photoresist, positive and negative photoresist. They react in an opposite manner upon exposure to UV light.

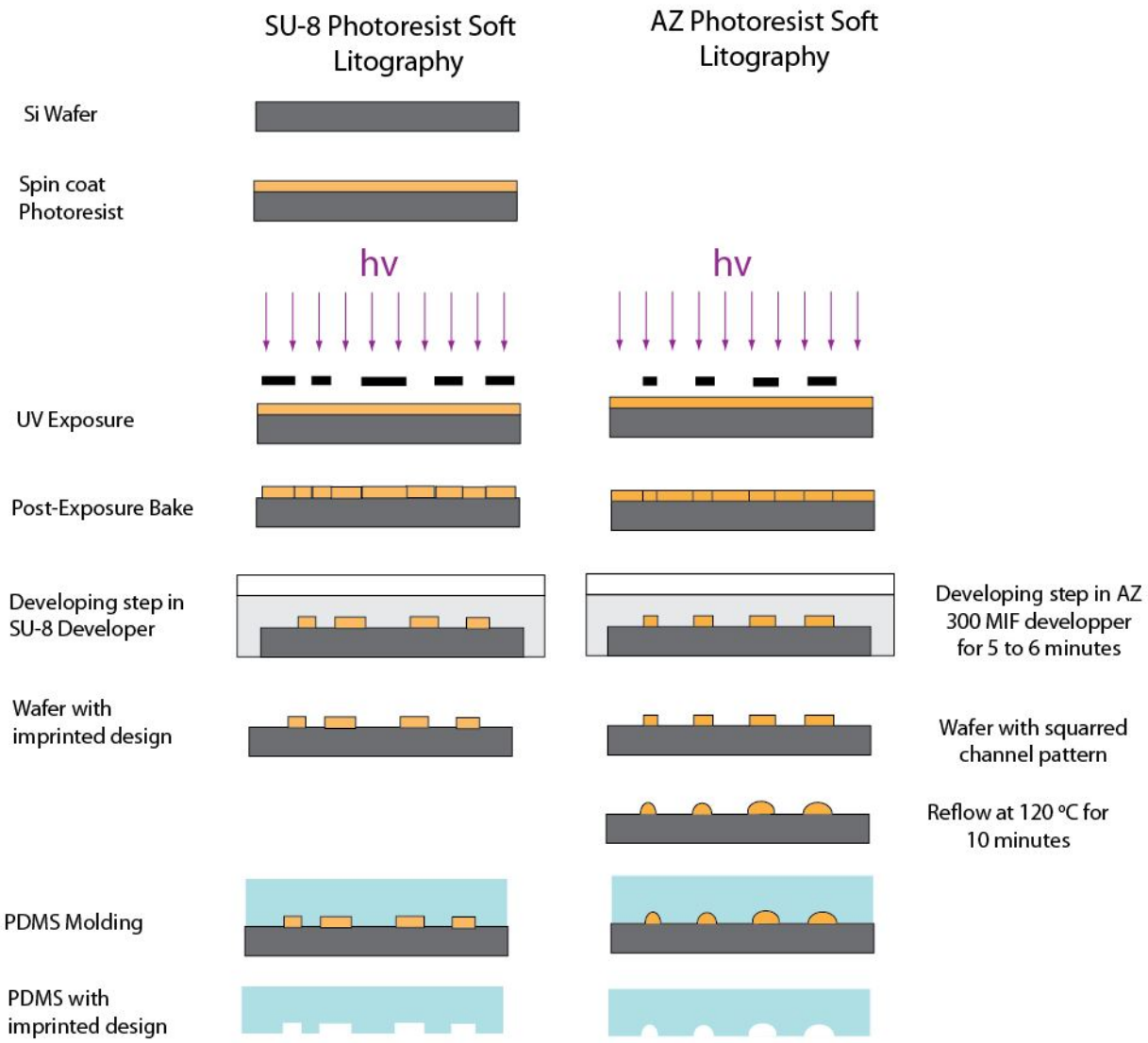

Figure 1.9: Soft lithography process
Schamatic of photolithography using negative (SU-8) photoresist (left) and positive (AZ) photoresist (right)

Positive Photoresist

Positive photoresist is a material that when exposed to UV light, the underlying material is removed. The resist is made so that the exposure to UV light changes the chemical structure to react with the developer and dissolve, leaving the unexposed underlying material. The chemical structure of an example positive photoresist is shown on Figure 1.12A. The basic compound used in this type of phoresist is a photo active compound (PAC) that belongs to the group of diazonaphtho-quinones (DNQ). UV-light triggers a reaction where nitrogen gas is released and water is absorbed. DNQ is converted to carboxylic acid, and the alkaline solubility is increased. An example of positive photoresist is the AZ 40XT used in this dissertation to make rounded channels. This photoresist allows the photoresist pattern to be directly transferred to positive-relief structures on the wafer.

Negative Photoresist

As opposed to the positive photoresist, the negative photoresist when exposed to UV-light reacts in the opposite way. One of the negative photoresists mostly used in microfluidics is the SU-8 (Figure 1.12B) to create squared channels. It is a chain of biphenol-A having 8 epoxy group at their ends. The exposure to UV-light causes the SU-8 molecules to becomes crosslinked or polymerized, and the exposed pattern remains on the wafer surface after developing. In this case, the developer is used to wash out the unexposed areas of the SU-8. The image transferred onto the wafer in this case is an inverse copy of the photomask pattern.

1.2.3 Polydimethylsiloxane (PDMS)

The development of soft lithography techniques has provided an inexpensive method for microfabrication and has played a large contribution in the advancement of microfluidics[29, 72, 73]. As I mention in the previous section, the term soft lithography is used because the basis of this fabrication technique is the soft rubbery polymer polydimethylsiloxane (PDMS).

It is an organic polymer that is purchased in liquid form and when mixed with a desired ratio of curing agent, the monomers become cross-linked and a ruber like polymer is obtained at the end[74]. The reaction (shown in Figure 1.13) is preferably carried out at 60 °C or above and the reaction time is depending on the polymer to curing agent ratio. PDMS is a widely used silicon-based polymer in the microfluidic field for the fabrication of channels because it possess mechanical and optical properties that are favorable for analytical usage and it is easy to make. The optical property of PDMS is that it is transparent from ∼3580-900 nm with a refractive index of 1.41 and therefore easy to see through with a visible light microscope. It is also inert meaning that the chance of reacting with other reagent flowing in the channels is relatively low. PDMS is a very flexible material, making it a good candidate used in mimicking organs as well as biological environment[33, 75, 76, 77]. Another advantage promoting its usage for cell and organs-on-chip application is the porosity of PDMS making it air permeable while effectively preventing water leakage and evaporation. PDMS is also non toxic and is used in the shampoos and as food additive as well as anti-foaming agent in beverage or in lubricating oil. The elastomeric feature of PDMS makes it a suitable material

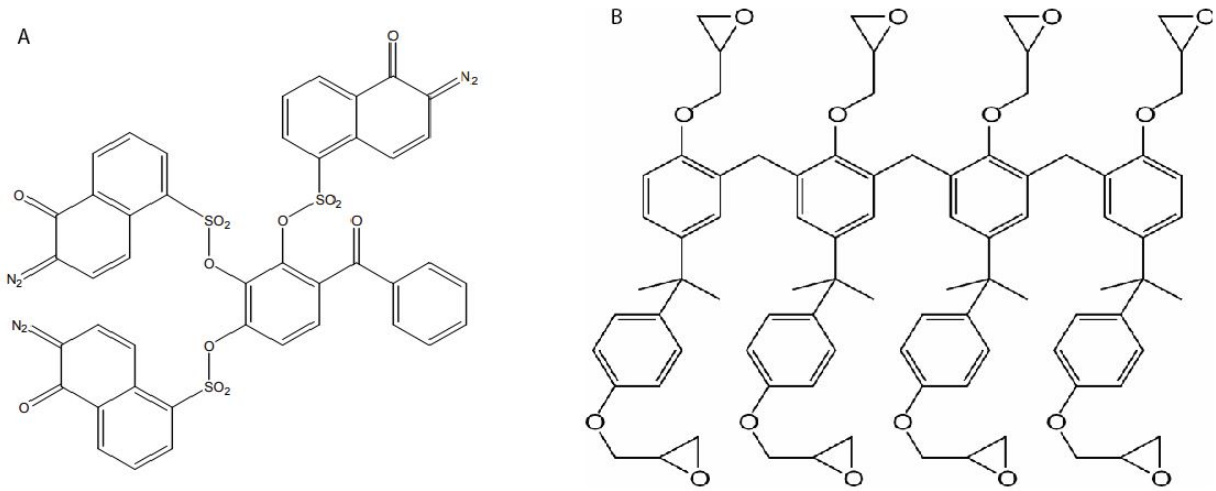

Figure 1.10: Photoresist chemical structure
(A) Positive photoresist. (B) Negative photoresist.

to mimic muscle tissues[78]. In fact, a new field referred to as "soft robotics" has been created using PDMS to fabricate small robots[79]. Depending on the application, different ratios of PDMS elastomer and curing agent can be used for the fabrication of microfluidic chips. When only one layer is used, the ratio is generally 10:1 (elastomer : curing agent). For double layer PDMS chip (used when making microfluidic valves), the thin layer, at the bottom, typically has a ratio of 20:1, and the thick layer is 5:1. The difference in ratios allows the excess curing agent in the thin layer to react with the thick layer that has less curing agent after bonding, fusing the layers together. This protocol has permitted the fabrication of intricate, multilayer devices that mimic electric circuits[25].

1.2.4 Plasma Oxidization

To complete the microchannel fabrication, the opened channels imprinted on the PDMS must be covered with a glass slide. Plasma oxidation is the process in which PDMS is covalently bonded to glass slide. It is often the final process in microfluidic chip fabrication. During this process, the surface chemistry of PDMS and glass slide are changed. The hydrocarbon groups are oxidized to silanol (SiOH) on the surface. The plasma oxidization time takes about 45 seconds in the plasma oxidizer (Figure 1.14A). Upon contact with another oxidized PDMS or glass slide, a condensation reaction occurs and creates an irreversible bonding (Si-O-Si) at the interface of the PDMS and glass cover (Figure 1.14B). Leak-free channels are created in the process. Plasma oxidization is also one of the techniques used to change surface properties of the PDMS channels and to make them hydrophilic[80]. However, the hydrophilicity in this case can only last for few hours due to the hydrophobic recovery caused by diffusion of unreacted oligomers to the surface. Vickers and coworkers have developed a method to stop the hydrophobic recovery of PDMS by first extracting the oligomers using organic solvents and secondly by plasma oxidization[81].

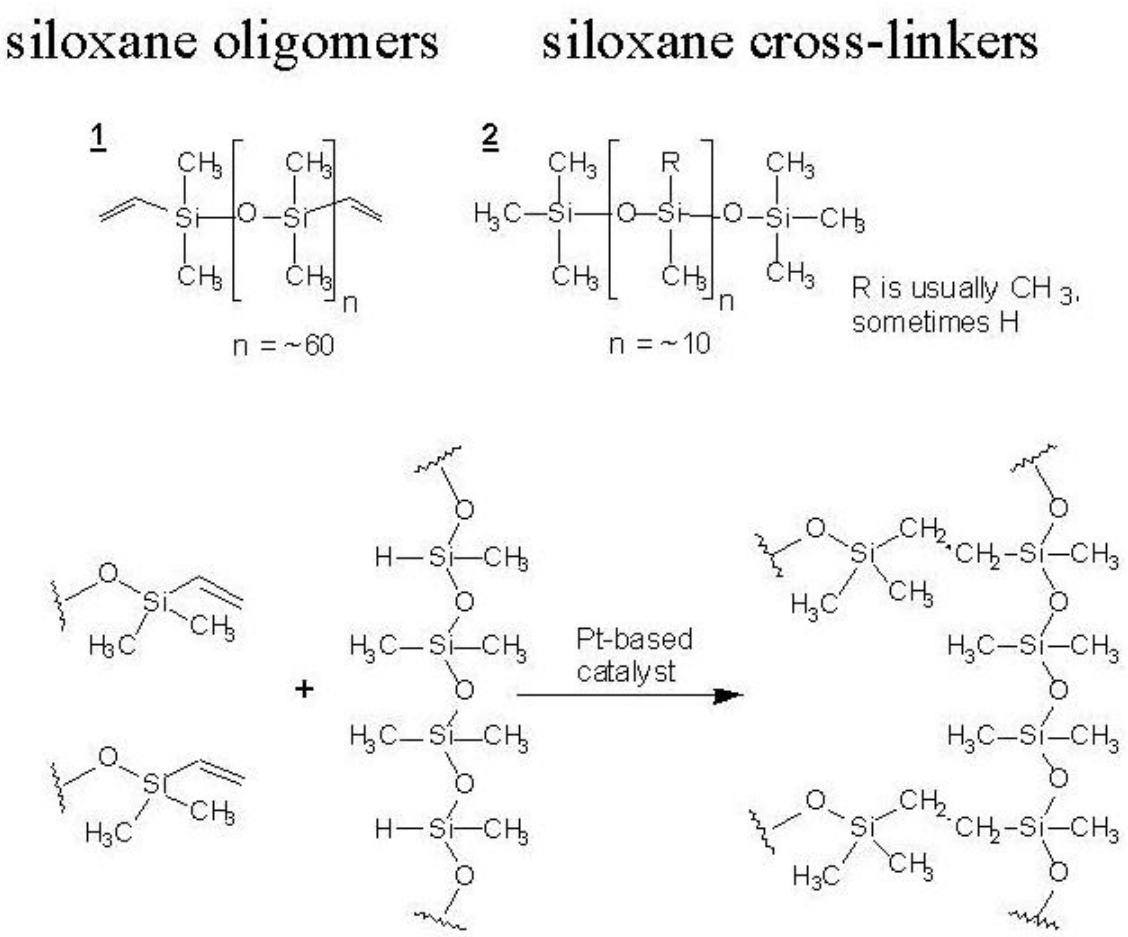

Figure 1.11: Cross-linking reaction of PDMS
(Top) The two forms of PDMS; vinyl terminated (1) and the fragmented formula (2).
(Bottom) Methylhydroxilane oligomer and cross-linker hydrosilanization reaction to produce a flexible polymer PDMS.

1.3 Flow characterization in Microfluidic Channels

Flow in microfluidic channels is characterized by few elements such as the geometry of the channels, the Reynolds number, and the Capillary number.

Channel size and shape

When including other functionality such as valves on a microfluidic chip, one very important factor is the channel's shape. Microfluidic channels are usually rectangular, or rounded

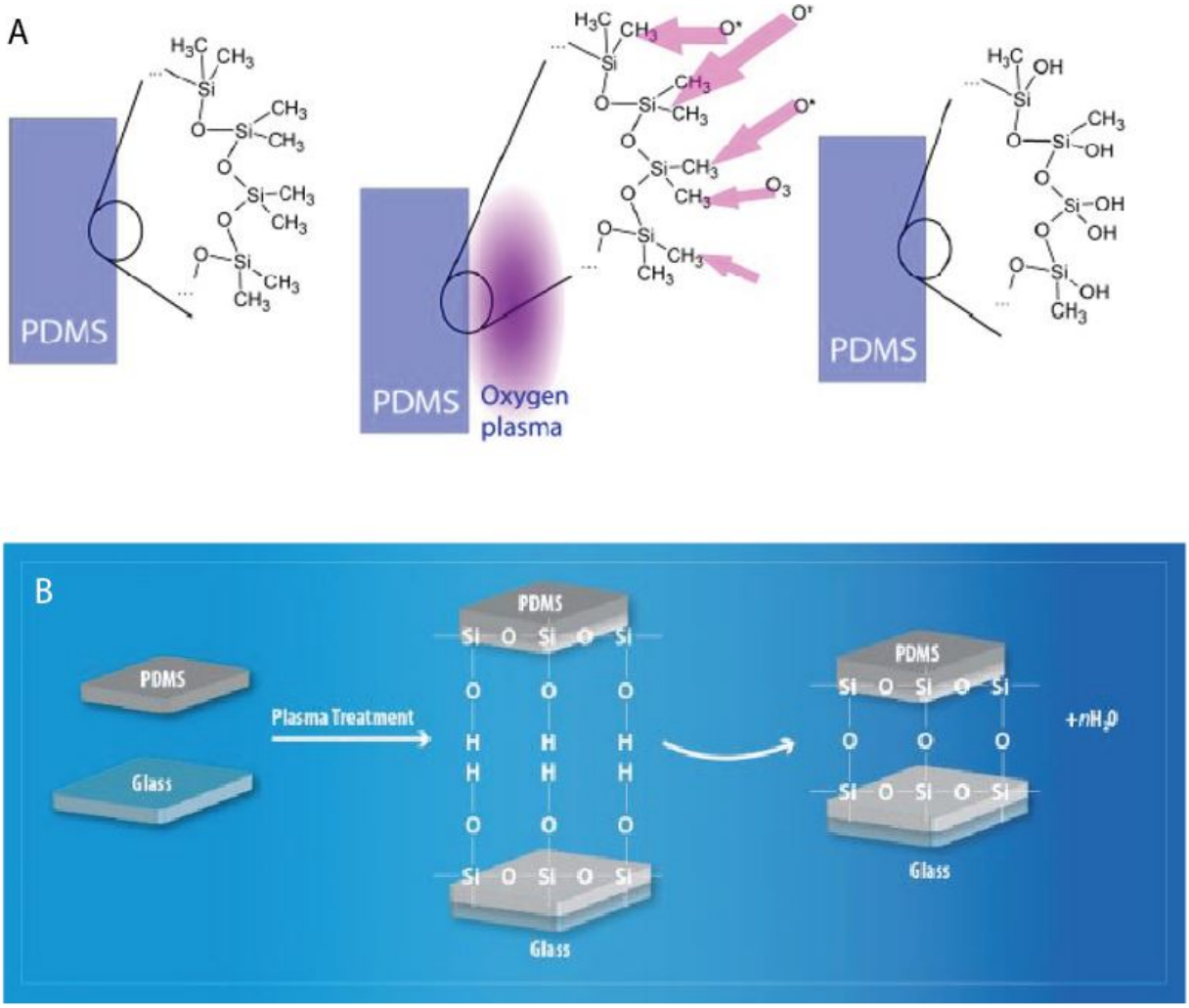

Figure 1.12: Plasma oxidization
(A) Plasma oxydation process on the glass surface. (B) PDMS-glass bonding reaction.

in shape. The most popular device fabrication method is soft lithography method that was described earlier. However, chemical (or wet) etching and deep plasma (or dry) etching can be used. Etching methods[82, 83] leaves rounded channels and to obtain squared or rectangular cross-section of the channels, another process must be added. For the PDMS, whether using the SU-8 or the AZ photoresist, the channels shape will be rectangular after phololitography and developing. However, the AZ material can be reflowed to create rounded features. Therefore, to make rectangular or squared cross-section channels, SU-8 is used and to make rounded channels, AZ is used (Figure 1.13A).

The second most important factor is the channel's size. To assure better flow control, optimum conditions for the channels must be respected for the design and fabrication of PDMS channels. For example, aspect ratio, for channels involving valves, must be lower than 1:10 (height:width) otherwise, the structure will collapse. For passive flow, the resistance and the change in pressure (ΔP) are used as the major tool to control flow rate. In addition to this, flow in automated systems is control by valves and pumps. Therefore, it is important to carefully choose the depth, width, and length of the channel. The microfluidic resistance is defined by

$$R_{Fluidic} = \frac{12\eta \mathrm{L}}{wh^3F} \quad \text{Equation 1.2}$$

where $R_{Fluidic}$ is the fluidic resistance, η is the viscosity, L is the channel length, w is the channel width, h is the channel height,and F is the geometric form factor for rectangular shape channels. This formula is based on rectangular channels, therefore channel that are not perfectly rectangular (Figure 1.13B) can cause some error in calculating fluidic resistance value with Equation 1.2[84].

Reynolds Number

A major factor that characterizes flow in microfluidics is the Reynolds number which is the ratio between viscous forces and inertial forces. It determines whether flow will be either laminar or turbulent. The laminar flow regime (Figure 1.3) often occurs at low Reynolds

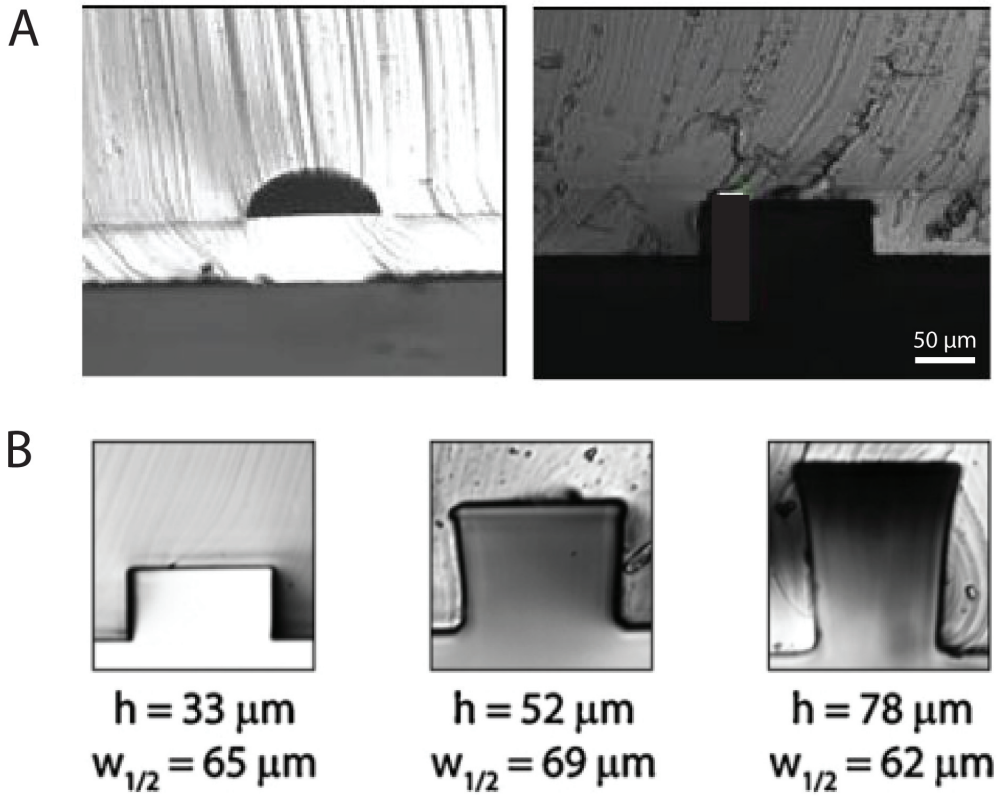

Figure 1.13: Channel size and shapes
(A) Rounded (left) and squared (right) channels feature. (B) Different shapes of squared channels. From left to right, perfect to deformed squared channels. This Figure was reprinted with the permission from ref [84] Copyright 2012, Anal Chim Act.

number (Re), in general when Re is less than 2000, and when Re is more than 4000, the flow becomes unstable, and the turbulent flow regime occurs[85]. Using aqueous solution in microchannels, the Reynolds number becomes lower and lower as the flow path and the fluid velocity gets smaller. In microfluidics, viscous forces become the dominant forces over the inertial forces allowing only laminar flow to occurs, and the Reynolds number in this case, is estimated to be less than 1. Equation 1.3 displays the equation of the Reynolds number (Re) where ρ is the density, v is the fluid velocity, L is the characteristic length of the channels, and η is the dynamic viscosity of the fluid.

$$R_e = \frac{\rho \mathrm{v} \mathrm{L}}{\eta} \qquad \text{Equation 1.3}$$

Capillary Number

While the Reynolds number characterizes flow in all microfluidic systems, in addition to this, another important factor also characterizes flow in the case of two immiscible fluids, namely the capillary number, which is the ratio of the viscous forces and the surface tension acting on the interface between liquid and gas or between two immiscible fluids. In droplet microfluidics for example, the capillary number acts on the interface between oil and liquid. Droplets are formed when the viscous force exerted by the outer liquid phase grows linearly with the droplet diameter, and break up when it exceeds the capillary force. The following equation describes the capillary number (Ca):

$$Ca = \frac{\mu \mathrm{v}}{\gamma} \quad \text{Equation 1.4}$$

where μ is the fluid viscosity, V is the flow rate of the carrier fluid, and γ is the surface tension. Ca is used to measure the ability of droplets to form. At low Capillary number, the shear stress acting on the droplet causes it to break off[86]. The capillary number in microfluidic droplet formation devices is estimated between 10^{-3} to 10^{1}[41, 87].

1.4 Automated Flow Control Methods

There are two essential components used in microfluidics to permit automated flow control: the microfluidic valves which function like electrical switches to interrupt or allow flow in the channels, and the micropumps which are series of valves on a channel. Valved microfluidics and micropumps present many advantages compared to passive flow control. In droplet microfluidics for example, introduction of a valve system provides a tunable droplet size and frequency by controlling droplet formation time and/or by controlling the oil phase only. In passive flow these parameters are dictated by the channel size and the change in pressure, which are sometimes are difficult to control and present some inconsistencies. Furthermore, automated valve systems allow the integration of multiple functions into one device, for example the microfluidic large-scale integration (mLSI) where thousands of valves and control components are integrated in a single chip, enabling hundreds of assays to be carried out in parallel. Microvalves control flow direction, timing, separation of fluids, and allow precise volume control. Micropumps, on the other hand, can provide temporal and tunable direction of flow as well as precise volumetric movement of liquid and they are also used to reduce amount external hardware. Because they tune the flow direction and move precise volume of liquid, they are used to mix reagents in microfluidic channels. There are numerous valving and micropumps techniques presented in the literature, and this dissertation relies heavily on the technology.

1.4.1 Microfluidic Valves

Valves are the basic component of fluid control in microfluidic large scale integration (mLSI). Just like transistors in electronics, microvalves are key to mLSI. They give the ability to combine different tasks and create highly complex systems for micro-total analysis. The first microvalve was created by Kovacs and coworkers using silicon microelectromechanical system (MEMS). The valve was etched into a silicon microchip and could be actuated mechanically[88]. Unfortunately, the fabrication of this valve was highly complex and could

not be adapted to large scale integration. Soon after, a number of valves technique were also developed using silicone rubber membrane on etched silicon or glass and could be actuated pneumatically. Nowadays, microvalve fabrication technology has greatly evolved with various techniques being proposed.

There are two main types of valves, a normally-open (NO) valve which closes upon actuation, and normally-closed (NC) valve for which actuation is opposite that of NO valves. Many types of valves have been developed with different actuation modes. Microfluidic valves can be actuated manually, electrochemically, and pneumatically to name a few. Figure 1.14 displays some microfluidic valves found in the literature. Some valves have latches than can be used to manually or electrically actuate the opening and closing. An example of such valve is in Figure 1.14A where an inserted screw can be turned to actuate the valve. This types of valves are more advantageous for point of care (POC) applications because they do not need external connections, and they do not require a computer a program to function[32, 89, 90, 91]. However, they lack in volume precision, and the basis of its functionality is prone to human errors.

Without any doubt, the most popular valves in the microfluidic field are pneumatic valves. Baek et al. fabricated a normally closed microvalve consisting of 3 layers of PDMS and one bias-relief plate with 3D flow path that could effectively control and regulate flow (Figure 1.14B). This type of valve is called a Plunger microvalve[92]. They are fabricated through a complex process involving multiple steps PDMS bonding. Mathies valves (Figure 1.14C) are one of the most widely used in microfluidics. They where developed by professor Richard A. Mathies from the University of California Berkeley. The valve is made of a PDMS membrane "sandwiched" between the control channel and the flow channel which are made in glass. The particularity of this valve is that the amount of off-chip controller is reduced therefore, a single vacuum source can control many valves[93, 94].

The simplest and most commonly used microfluidic valve was developed by the Quake group from Stanford University[95, 96]. It is a normally opened valve that provide precise

fluid control and timing. They are easy to fabricate by simply bonding two layers of PDMS together, a process called multilayer soft lithography (MSL). Each layer plays an essential role which is to control the flow and to flow liquids. The microvalve is formed by crossing the control channel and the flow channel perpendicular to each other, leaving a thin membrane of PDMS in between them. The control layer can be above (push-down valve) or bellow (push-up valve) the flow layer (Figure 1.16). For the valve to function properly, some design rules must be taken into consideration. First, the flow channel must have a rounded profile to allow the valve to fully close when actuated. Secondly, a nominal valve area and the PDMS memebrane thickness must be respected for a given closing pressure. For example, a valve area of 100 μm x 100 μm with flow channels of 5 to 15 μm depth and a PDMS membrane $\sim$10 μm in thickness requires a closing pressure of at least 10 psi for a push-down and 5 psi for a push-up valve. Thirdly, appropriate aspect ratios must be respected for channels not to collapse (see soft lithography section above). Last but not least, maximum and minimum channels dimension are given in the table below[97]. For the push-down valve, the maximum

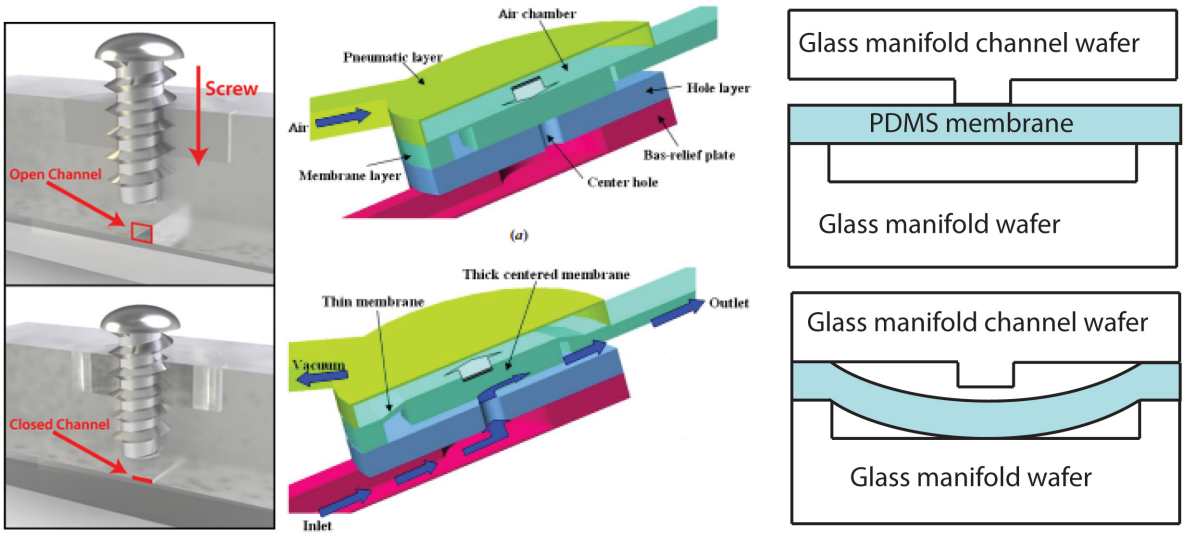

Figure 1.14: Microfluidic valves
Example of some valves used in microfluidics. A manually activated crew-valve for point of care use (left), Plunger valve with 3D flow path (middle), and the Mathies valve in close position (top right) and open position (right bottom). Figure A and B were reprinted with the permission from ref [32] Copyright 2005, Anal Chem and ref [92] Copyright 2005, J Micromech and Microeng.

flow channel height is limited to 15 μm, and it requires higher pressure to close. Conversely, the push valve can have a maximum flow channel height of 45 μm and can be closed with much smaller pressure. Investigation of closing pressures at different channels dimensions for the Quake valve was performed by Fordyce et al., who measured the dimensions and closing pressures of up to 120 different valves both before and after rounding. They found out that valves dimensions before and after rounding are proportional to aspect ratios[98].

Non-pneumatic valves are also well reported in literature and actuation mode varies depending on the application. Electrokinetic valves for example are best suited for microfluidic electrophoresis (Figure 1.15). They are used to control electoosmotic flow by changing the potential from one channel to the other. This is depicted on Figure 1.15 from b to d where the flow is switched between sample and buffer. Another valve that does not require pneumatic actuation is the check microvalve. Although the pressure is used to generate flow in the channels, valve actuation is based on the flow direction. When the sample and the reagent are flowing in the same direction, the valve opens and the two solution flow in the same stream. If the reagent flow direction is reversed, the valve closes itself[99]. The drawbacks of these valves are their cost of fabrication and the precision of control.

Table 1.1: Summary of some critical design rule information

Parameter	Value (μm)
Minimum overall chip thickness	3
Maximum overall chip thickness	7
Minimum flow channel height (push-down valve)	5
Maximum flow channel height (push-down valve)	15
Minimum flow channel height (push-up valve)	5
Maximum flow channel height (push-up valve)	45
Minimum possible feature width	15
Maximum possible feature height (rectangular profile only)	150
Nominal control channel height	10 or 25
Minimum spacing between borders of adjacent devices	2.0
inimum center-to-center spacing between punch holes (for 20 gauge)	1.5
Minimum center-to-center spacing between punch holes (for 15 gauge)	2.0

Microfluidic pumps

In addition to microvalves, microfluidic pumps or micropumps can be integrated into microfluidic chips, adding another important functionality on-chip to generate flow and reduce the number of external input such as pressure sources. When it comes to microfluidic large scale integration (mLSI), micropumps play an essential part just like valves because they can drive flow, control flow direction, and even mix liquids relatively fast despite the laminar flow[30]. Although passive micropumps have been reported[100], active micropumps are mostly used in microfluidics because of their ability to better control flow. The simplest active pump consists of series valves put one after the other along a flow channel. The pumps function by applying a sequential opening and closing of the valves across the flow channel.

Most active micropumps are actuated pneumatically by applying and external pressure to the series of valves. This pumping mechanism is refer to as a peristaltic pump. Activation

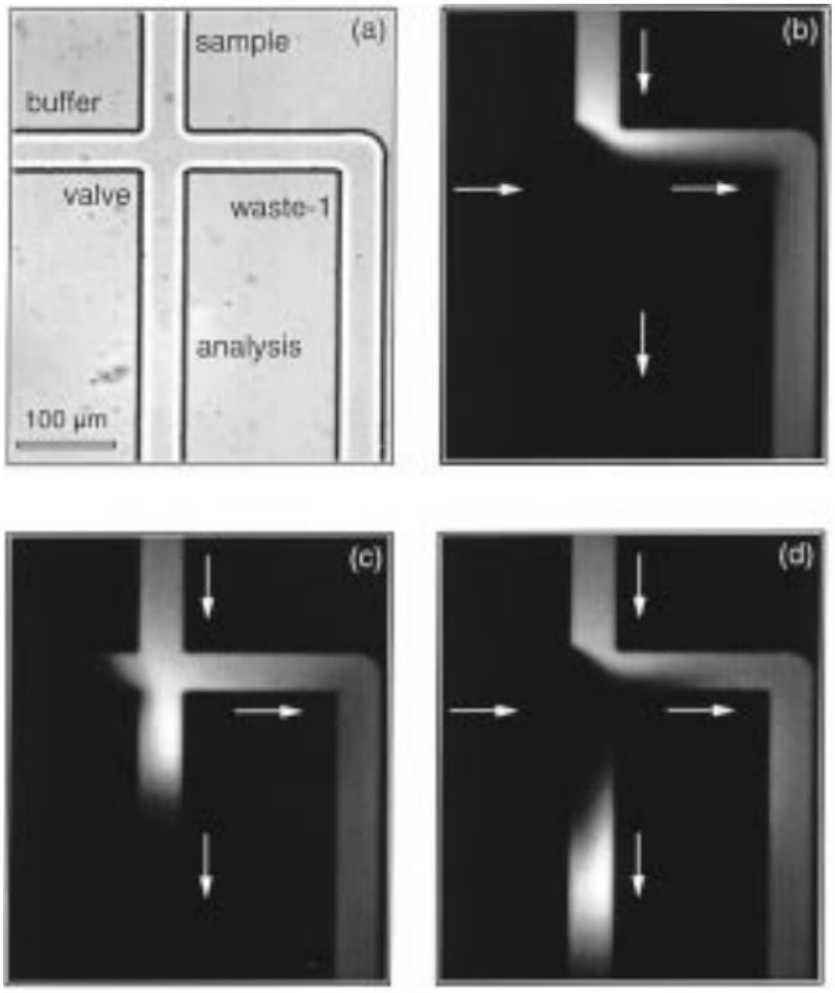

Figure 1.15: Example of non-pneumatic valve
(a) Image of an electrokinetic valve that can perform sample loading (b), dispense (c), and analysis (d). This Figure was reprinted with the permission from ref [99] Copyright 1999, Anal Chem.

of valve membranes creates a vacuum that pulls a certain volume of liquid, often set by the central valve volume. The sequential actuation of the valves moves the same volume in one direction with each pump cycle. The two most popular pneumatic pumps are made with Mathies valves[101] or Quake valves. Figure 1.17 depicts micropumps made with these two types of valves.

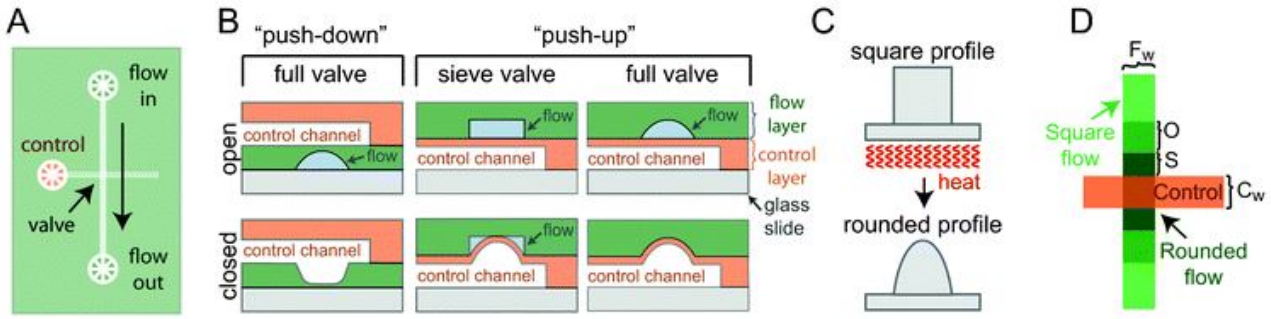

Figure 1.16: Quake style valves: Closing profile of multilayer soft lithography (MSL) valves (A) Valve formed at the intersection between flow and control channels. (B) Quake's push-down and push-up valves. (C) Squared channel reflowed to obtain rounded profile. Valve area defined by the cross-section area between the two channels (D). This figure was reprinted with permission from ref [98] Copyright 2012, Lab-on-Chip.

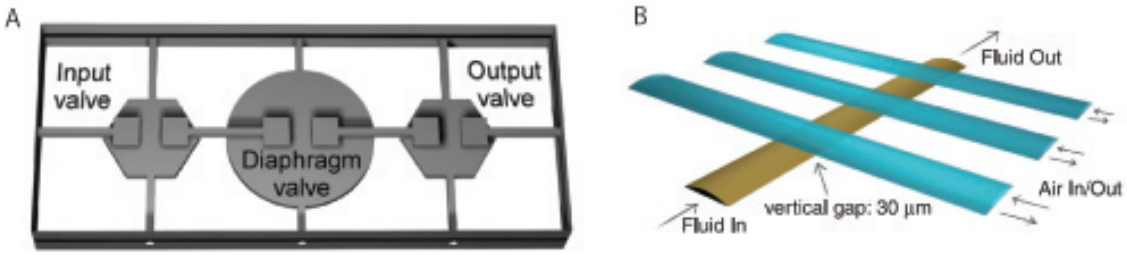

Figure 1.17: The two main types of micropumps
(A) Micropump made with Mathies style valves. (B) Peristaltic pump made with Quake valves. Figure A, and B were reprinted with permission from ref [30] Copyright 2000, Science; and ref [101] Copyright 2003, Sensors and Actuators B: Chemical.

1.4.2 Passive Components

So far we have only explored flow controlled by active components. Microfluidic flow can also be controlled with built-in components that function in response to flow conditions. Those components are directly derived from electronics and play an important role in microfluidic large scale integration systems. Each components, often made of valves, respond to flow by functioning as diodes, capacitors, or fluidic transistors acting as flow regulators[102]. The microfluidic diode for example is useful in drug delivery systems where backflow could be a major issue[103, 104, 105]. Microfluidic capacitors can be used to periodically store fluid and has been used to study oscillation[106], and dielectric permittivity of fluids[107].

As mentioned above, valves in microfluidic are analogues to the transistors and can be used passively to regulate flow in microfluidics when the valve and the fluidic channel are connected to the same pressure source[108]. Chapter 5 of this dissertation essentially covers autoregulators as a passive component.

1.5 Detection in microfluidic systems

Since the development of microfluidics, analytical chemists have implemented new methods for on-chip detection and/or adapted well established bench-top detection techniques on microfluidic chips. Although fluorescence microscopy is the most widespread detection technique, the success in the application of other methods for on-chip detection is indisputable. Amongst the detection methods reported are Raman spectroscopy[109], mass spectroscopy (MS)[110], UV-vis absorption[111], laser-induced fluorescence (LIF)[112], chemiluminescence[113], colorimetric detection[114], electrochemical detection[115], and inductively coupled plasma-atomic emission spectroscopy (ICP-AES)[116]. The choice of detection method often depends on the analyte to be studied or the type of microfluidic device used. For example, mass spectroscopy (MS) is used for proteomic, glycomic, and small molecules analyses because of microfluidic's ability to deal with such complicated sample analysis. Other abilities such as ease of automation and parallelization to meet the demands of high throughput are the driving forces of microfluidic mass spectroscopy[117]. Proteomic detection methods using mass spectrometry rely on soft ionization methods such as matrix assisted laser desorption/ionization (MALDI) and electro-spray ionization (ESI). Interfacing microfluidics with both of these techniques is a major challenge in the field. Mass spectroscopy is usually performed on glass or PDMS microfluidics with an off-chip or on-chip electro-spray emitter. Raman spectroscopy is used to detect structural properties of various analytes in one sample. It is often used as an alternative to fluorescence detection because it is a label-free technique. In this method, every analyte is recognized by the fingerprint of Raman shift,

and the amount is proportional to the peak intensity. Using Raman spectroscopy, it is possible to detect multiple analytes simultaneously and to perform high throughput detection and/or high spatial resolution. These advantages have been used in droplet microfluidics to profile the concentration of two compounds at different points along the microchannel[109]. Electrochemical detection can be used in immunoassays to detect or quantify biomolecules. It works with paper, PDMS, as well as glass microfluidics. Colorimetric detection is used in paper microfluidics for the detection of any reaction that results in color change. ICP-AES is used for the detection of trace metal. It has been successfully adapted to microfluidics for on-chip trace metal detection. UV-vis absorption has also been reported in the microfluidic field for various purposes; proving that Beer's law can also be succesfully applied on narrower pathlengths such as microfluidic channels[111, 118, 40]. Laser-induced fluorescence is just one of many fluorescence based method used in microfluidics. The next subsection explores the basics of fluorescence detection and it's use in microfluidics. Chemiluminescence is used in microfluidics and it is also used as an alternative to fluorescence because it does not require any light source or any expensive optical system. The use of microfluidics not only promotes miniaturization of the instrumental detection, but it also simplifies equipment, personnel, and laborious operations. Furthermore, microfluidics technology provides sensitive, low-cost, and rapid diagnosis that is ideal for point-of-care (POC) settings.

1.5.1 Fluorescence detection

Fluorescence is the most frequently used detection technique in the microfluidics field by chemists, biologists, and biochemists to study biomolecules. It consists of measuring the amount of light emitted when a fluorescent molecule is excited. The excitation wavelength is lower (higher energy) than the emission wavelength. Fluorescence emission occurs when molecules undergo absorption and subsequent re-radiation of light. The fluorescence process is relatively fast with absorption and emission of light being nearly simultaneous. In fact, the time between absorption of the light and the emission of the photon is in terms of

nanoseconds. During the of fluorescence process, a molecule primarily at the ground state is excited to a higher energy state and looses some energy trough relaxation process, and emits light in the process of returning to the ground state. Using fluorescence for detection provides many advantages. First, fluorescence has greater sensitivity compared to other methods such as absorption. Second it uses wells characterized fluorescent dyes to label the analytes of interest. A fluorescent label can be a small molecule, protein, or quantum dot

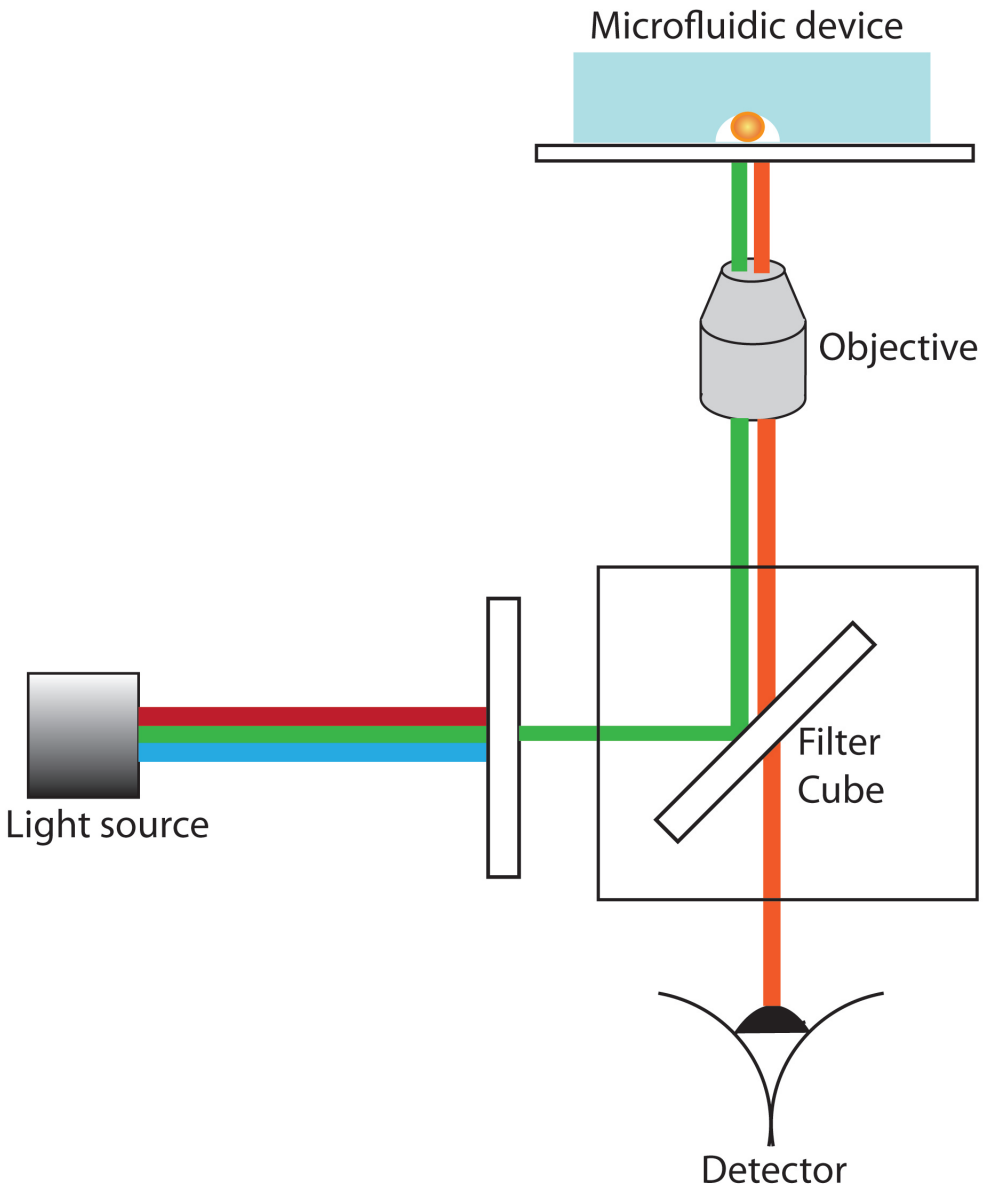

Figure 1.18: Diagram of typical setup for fluorescence detection on microfluidic device

that is used to tag a target such as a proteins, nucleic acids, or lipids. The labels chemically bond to the analyte and form a complex which is capable of providing quantitative and qualitative information[119]. Fluorescent dye molecules are used in in-vivo experiments to localize specific cells and their counterparts. There are a wide range of fluorescent reporters or dyes commercially available. They can be found in multitude of colors and the choice for fluorescent label could simply depend on the instrument used. This includes the optical filters, the detector, and the excitation source. The assay to be used is also a determining factor; one must also look for compatibility of dyes with certain samples, the pH sensitivity, and the stability to photobleaching. Finally, fluorescence gives the ability to quantitatively measure molecules in solution as well as obtaining structural information on macromolecules through high resolution Forster resonance energy transfer (FRET).

The basic setting for lab-on-chip fluorescence detection is illustrated in Figure 1.18. The instrument used is generally an upright or inverted microscope with a light source restricted to a narrow range of wavelengths, a dichromatic mirror which serves as wavelength selector or filter, an objective, and a detector. The detectors commonly used are the charge couple device (CCD) and the photonmultiplier tube (PMT). The sample holder here is a microfluidic or LOC device (Figure 1.18) where the sample to be analyze is confined in small channels.

Forster Resonance Energy Transfer (FRET)

When a an excited fluorescent molecule called a donor transfer its energy to a nearby acceptor molecule, the process is called Forster resonance energy transfer (FRET). In this process, the donor is at its excited state, and its emission energy overlaps with the absorption energy of the acceptor. It is a very sensitive fluorescence technique with the distance between the donor and acceptor typically ranging from 1 to 10 nm. Homogeneous methods of nucleic acid detection have benefited largely from this technique. They use a fluorophore as the donor and a quencher as the acceptor both attached to two different DNA probes. The

alteration of fluorescent signal when the donor and acceptor are in close proximity can help to determine the number of target strands that are present[120].

Oligonucleotide based FRET can also be used for protein detection. The most famous example is the pincer assay developed by Heyduk and coworkers (Figure 1.19). They utilize two specific antibody-oligonucleotide conjugates as sensors. These sensors were designed to perform homogeneous, antibody-based, rapid protein detection. A target protein with antibodies that specifically recognize non-overlaping epitopes of the protein, increases the stability of the complementary oligonucleotides, resulting in efficient FRET. As a result of this FRET, fluorescence signal changes can be measured to homogeneously quantify the target protein[121].

In our laboratory, we use similar homogeneous assays that exploit the FRET for protein detection. Several of these assays employ thermofluorimetric analysis (TFA) which is based on using a qPCR instrument to thermally scan the sample to distinguish between bound proteins (signal) and unbound probes (background). In one format, bivalent antibody-oligonucelotide or aptamers can be used as probes to selectively bind proteins. This technique was successfully applied to human serum, human plasma, and cell secretion[122] which are the main subjects studied in our lab. Another version of the assay uses the proximity FRET assay (pFRET). Here, two antibody-bound oligonucleotides are also used to selectively bind a protein of interest. One of the antibody-bound oligonucleotide is labeled with a fluorophore while the other is labeled with a quencher. Similar to the pincer assay (Figure 1.19), the antibody binding to the target protein results in an increase in the protein and antibody-bound oligonucleotide probe complex. A complementary oligonucleotide that serves as connector anneals with the two oligonucleotides and brings the quencher at close proximity to the fluorophore and a reduction in fluorescence signal is observed. These homogeneous assays are appealing substitutes to widely used sensitive protein detection assay like the enzyme linked immunosorbent assay (ELISA) where multiple washing steps are involved. Protein

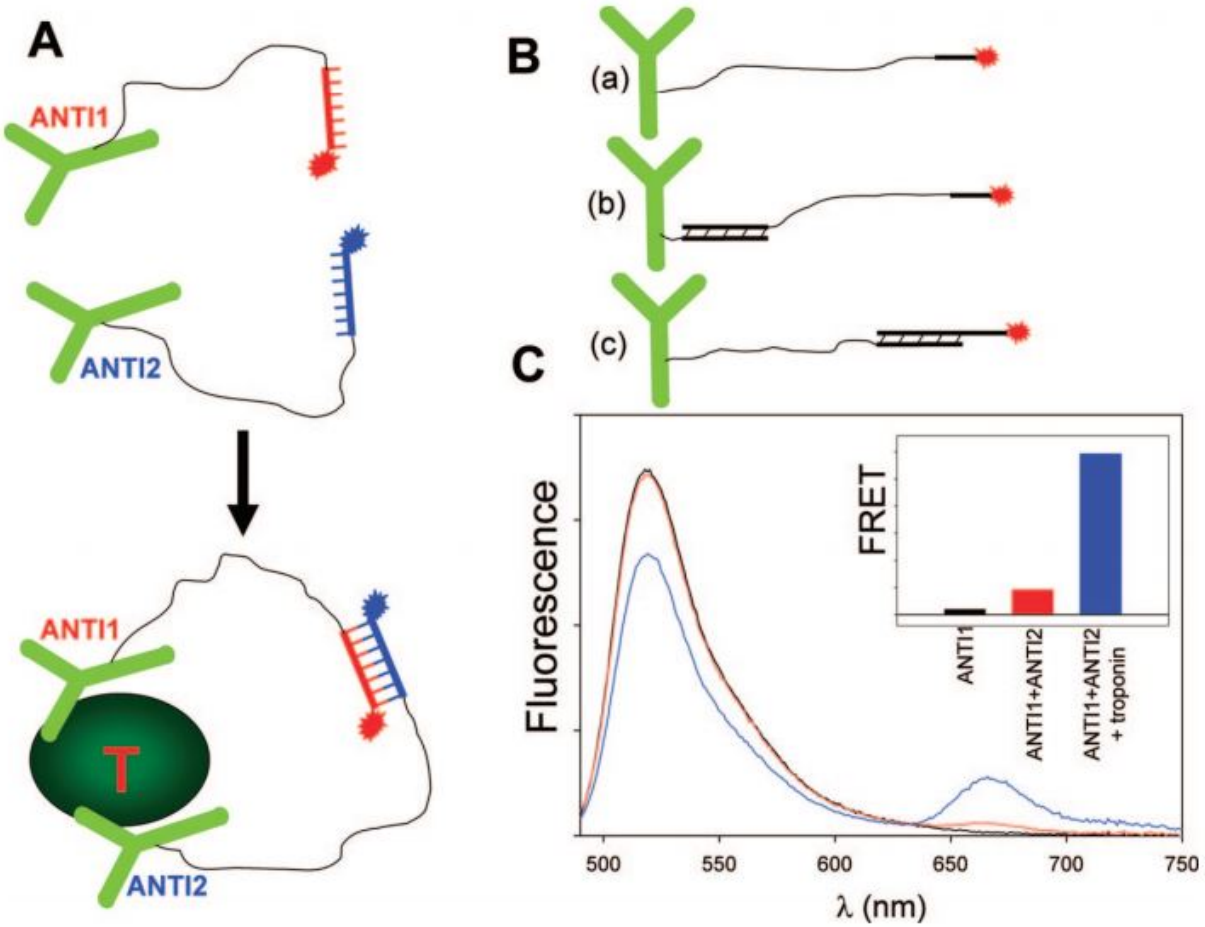

Figure 1.19: Illustration of molecular pincer assay
(A) Antibodies labeled with signaling oligonucleotides specific to the target protein T. (B) Different configurations for the labeling of antibody with signaling oligonucleotides, and illustration of signal reduction due to FRET. This figure was reprinted with permission from ref [121] Copyright 2008, Analytical Chemistry.

detection on microfluidic devices will benefit substantially from these homogeneous assay for rapid and sensitive on-Chip protein detection.

1.5.2 Automated lock-in detection

Principle of Lock-in detection

Lock-in detection is an analytical method that is mostly used by instrument developers to extract weak signals in an overwhelming noise environment. The measured amplitude of signal is modulated at the same frequency with the reference amplitude signal. This way, the frequency of the signal of interest is "locked-in" to the reference frequency signal, and all other frequencies are ignored. A small signal normally undetectable due to noise can therefore be extracted from noise[123]. The optical chopper used in labs, cameras, and industrial machines work in combination with lock-in amplifiers to reduce background noise. Lock-in detection was first applied to microfluic droplets in our lab by Deal et al[40]. As an analogue to the optical beam chopper, we used two opposing T-junction microfluidic channels where reference and sample droplet can be chopped in alternating manner. Here instead of chopping the optical beam, the sample is chopped fluidically to mimic the optical beam chopper (Figure 1.20, bottom) [124] allowing constant referencing between the sample droplets. The aqueous channels in a opposite T-junction configuration allow self modulation of the reference signal at same frequency and phase to that of the sample. This method was applied to absorbance detection of bromophenol blue where lock-in method was used to significantly reduce 1/f noise. This method greatly improved sensitivity with a limit of detection (LOD) of bromophenol blue as low as 500 nM on a pathlength of only 27 μm. The device was self regulated, and flow was initiated by just pulling a hand-held syringe to generated self alternation droplets.

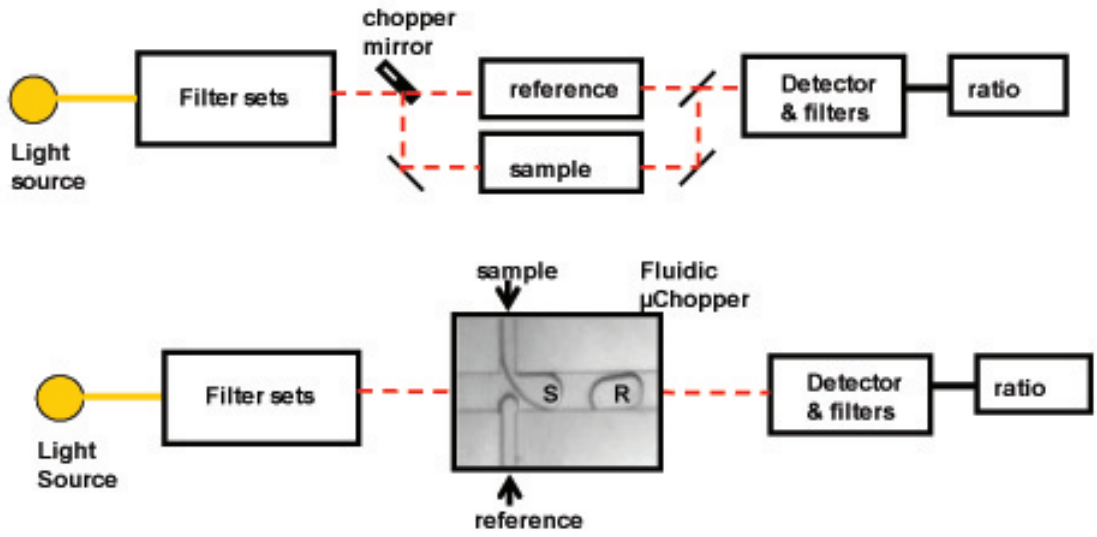

Figure 1.20: Block diagram of lock-in detection
Representation of lock-in detection system: Diagram of the optical beam chopper (top), droplets fluidic chopper (μChopper) analogue for beam chopper (bottom). This figure was reprinted from ref [124], Copyright 2013, Auburn University.

Automated Microfluidic Sample Chopper: Application in lock-in detection

The microfluidic lock-in detection concept was later improved by adding automation on the device. This was done in order to provide more control over the droplet formation and the measuring time as well as more accurate measurements. In the new device, droplet formation is controlled by pneumatic valves through a computer program to automatically control droplet formation and allow a phase-locked and precise fluorescence detection. The precision is made possible by stopping the droplets at the region of interest (ROI) and recording the signal only when the droplet is present. The lock-in analysis was also performed using a computer program. The entire chapter 2 of this dissertation provides extensive details about this new lock-in device.

1.5.3 LabView control

The automated lock-in detection is enabled by a computer program interfaced with the microfluidic device. A National Instruments program called"LabView" is best suited for

interfacing with microfluidic chip for control and data acquisition. Labview is a graphical programming software that is used in most laboratories by engineers and scientists. It uses icons instead of lines of text to create executable tasks or applications. The coding is made on a platform called Virtual Instrument or VI. Codifications or programs can be made for a wide range of applications. Some applications include testing and measurement, data acquisition and analysis, hardware control, image processing etc. For microfluidic devices, LabView is used to control the valves by actuating a solenoid system connected to the valves. LabView was used for various projects throughout this dissertation.

1.5.4 Concluding remarks

This chapter introduced the background as well as the basics of microfluidic chip fabrication. A survey of different techniques and application of microfluidics was also presented with an emphasis to the detection of small amounts or low limits of detection (LOD). Various techniques of fluid handling at the microscale and their importance in life science were also highlighted.

Microfluidics is touted for its advantages over bench-top techniques mostly for the small volume consumption and faster analysis time. Droplet microfluidics, for example where volume can be down to femtoliter level is popular for single molecule detection. However, quantitative measurements of droplets, namely direct concentration measurements inside droplets, is still rarely reported in literature. As microfluidic operate at a very small scale, detection would require a powerful technique to filter overwhelming noise in the system for accurate detection. For example, absorbance detection would be nearly impossible in microfluidic channels due to limitation of Beer's law which is pathlength dependent. At the micrometer scale, the optics cannot discern any difference between the sample and the reference. Similarly, fluorescence detection for quantification purposes is also a tedious task. Even though fluorescence have been proven to possess high sensitivity and low background noise, it is still difficult to detect small amount of analyte inside a droplet using this techniques.

Not only the optical system poses an issue for the detection in microchannels, but also some major issues are caused by the signal drift (1/f noise) and human error introduced during experimental settings. Taking all these factors into consideration, it is important to develop new detection techniques for microfluidic systems that will eliminate most of these drawbacks and allow an ease of detection at low concentration. We have attempted to address some of these limitations within this dissertation.

Moreover, it is important to study fluid behavior at the microscale in order to improve existing designs and to develop new microfluidic devices with better performance. The best method to employ would be to passively control fluidic transport in microfluidic system. By doing so, the complexity of device operation is reduced. Most of the time, fluidic control is done by connecting external devices to the microfluidic chip, which adds to the robustness of the device. However, adding external hardware to microfluidic will take away some of its advantages such as portability and the use for point-of-care detection. As such, another theme of this dissertation is simplifying flow control with passive devices such as autoregulators.

Chapter 2

An automated microfluidic droplet-based sample chopper for detection of small fluorescence differences using lock-in analysis

2.1 Introduction

To maximize sensitivity in optical measurements, noise reduction is an important issue to address. When signal levels are low, at similar magnitude to the noise floor, background drifts due to optical system fluctuations or detector noise begin to complicate signal collection. Low frequency noise (1/f noise or drift) is particularly detrimental to measurements and is often indistinguishable from signals. A fitting and well-established solution to this problem is the lock-in amplifier, which effectively modulates the signal of interest to a higher frequency, removes low frequency noise, and then demodulates the signal for recovery[125, 126, 127, 128]. Signals at levels several orders of magnitude lower than the noise can be recovered using this technique, which typically employs optical beam choppers and electronic phase-locking of photodetectors[129].

In the field of microfluidics, particularly for droplet fluidics, fluorescence is ideally suited, as optical probe volumes can be reduced to match channel and droplet dimensions[130]. However, practical limitations exist, since high numerical aperture lenses are limited to submillimeter working distances and are often unsuitable to interrogate a variety of fluidic and substrate architectures. By integrating optics onto the microdevice, the subfield of optofluidics has addressed many of these challenges. Integrated waveguides, lenses, filters, detectors, etc., in microfluidic systems, have been applied in fields ranging from cell biology to energy conservation[131, 132, 133, 134, 135]. On the other hand, typical optofluidic systems obligate fabrication complexities that can serve as barriers to widespread use. What remains

is a need for alternative, generalizable approaches to reduce noise in more standard optical detection systems used with microfluidic devices.

A common detection system used for droplet microfluidics is a standard fluorescence microscope, based on the similarity of optical probe volume and droplet volume. It is certainly possible to implement optical beam choppers and phase-locked detectors into microscope optics, yet this approach has been rare and is unlikely to gain widespread use due to its impracticality. Recently, our group and others have shown that constant droplet referencing can be used in lieu of optical choppers, allowing lock-in detection to be applied to both absorbance[136] and Raman spectroscopy[137] with relatively simple optical systems (Figure 2.1). In our passively controlled microfluidic device (μChopper), alternation of sample and reference droplets at $\sim$10 Hz each permitted the use of phase sensitive detection, i.e., lock-in detection, and 1/f noise was greatly reduced. This μChopper device promoted quantitative absorbance measurements at nanomolar concentrations through a path length of only 27 μm[136]. Oil phase referencing was also proven useful by our group using fluorescence[138] and by Marz et al. using Raman spectroscopy[137]. However, such passively controlled systems[139, 140] are inherently limited by the frequency-domain bandwidth of droplet formation. The main sensitivity limitation then shifts to the precision of droplet generation frequency, for which passively operated devices are prone to frequency-domain drifts.

In this work, we extend our μChopper concept to fluorescence detection with standard wide-field microscope optics. Notably, these devices show greatly improved droplet formation precision after integrating pneumatic valving,[95] and we show herein that this enhanced precision leads to concomitant improvements in drift correction and limit of detection. Finally, we present biological validation of the methodology by quantifying free fatty acid uptake in single adipocytes and by homogeneous protein detection at the attomole level. Thus, a significant performance enhancement can be achieved by combining droplet fluidics with actively controlled valves that are phase-locked with the detection system, resulting in a novel

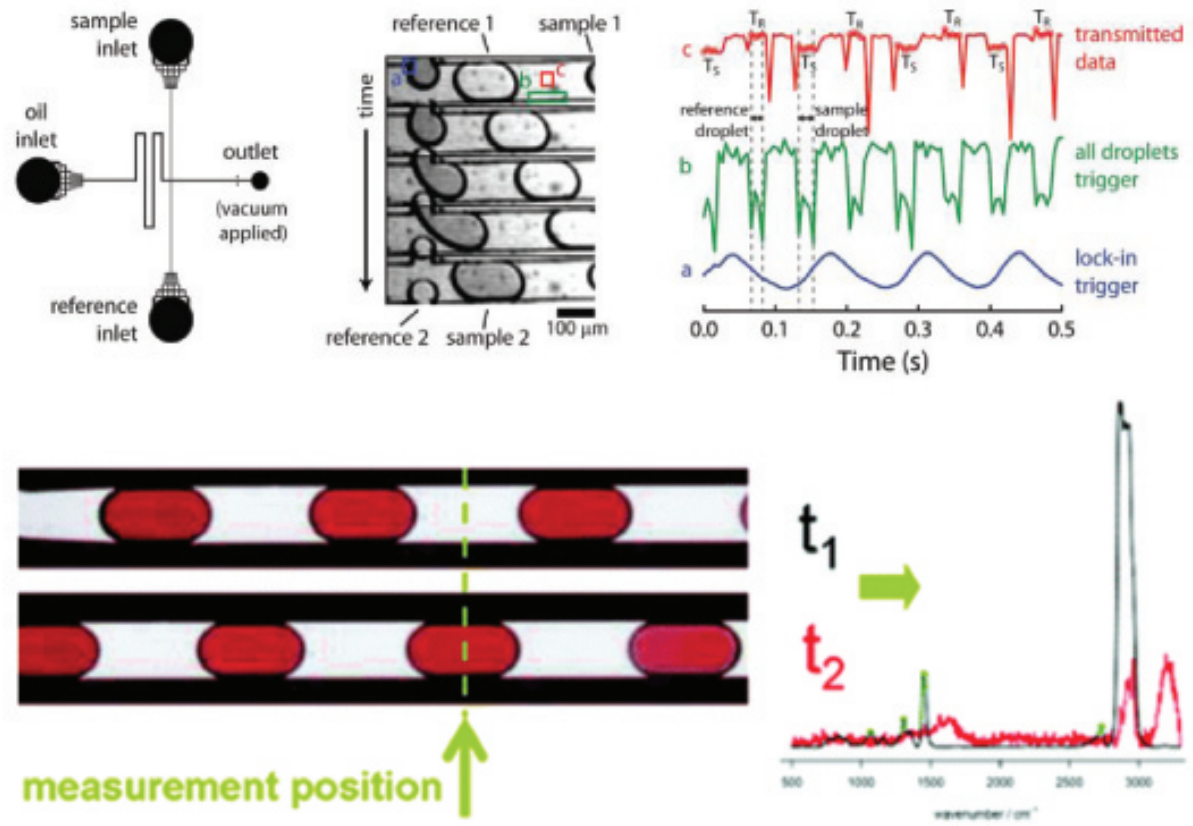

Figure 2.1: Previous example of lock-in detection using droplet microfluidics. Passively operated μChopper device achieved the absorbance detection of low concentration of bromophenol blue on pathlength of only 27 μm (top). Baseline correction of Raman spectrum using constant referencing between oil and droplets (bottom). Reprinted with the permission from reference [40]; copyright 2012 ACS and reference [137]; copyright 2011 ACS.

microfluidic platform that should be well-suited to a variety of single-cell or small-volume analyses.

2.2 Materials and Methods

2.2.1 Materials and Reagents

Polydimethylsiloxane (PDMS) precursors, Sylgard 184 elastomer base, and curing agent were purchased from Dow Corning (Midland, Maryland, USA). Silicon wafers were acquired from Polishing Corporation of America (Santa Clara, CA, USA). AZ-40-XT photoresist, AZ

300 MIF developer, and SU-8 photoresist and developer were purchased from Microchem (Westborough, MA, USA). Tubing (TGY-020-5C; 0.02 in. ID, 0.06 in. OD, 0.02 in. wall) and blunt needles (NE-223PL-C 22G) to interface syringes and devices were obtained from Small Parts (Logansport, IN, USA). Fluorescein was obtained from Alfa Aesar (Ward Hill, MA, USA). Fetal bovine serum (FBS) was purchased from VWR (West Chester, Pennsylvania, USA) and Aquapel from Pittsburgh Glass Works (Pennsylvania, USA). KH_2PO_4, NaH_2PO_4, 42-hydroxyethyl-1-piperazineethanesulfonic acid (HEPES), phosphate buffered-saline solution (PBS), insulin, penicillin/streptomycin, 3-isobutyl-1-methylxanthine (IBMX), dexamethasone, and D-glucose were obtained from SigmaAldrich (St. Louis, Missouri, USA). BODIPY FL C_{16} (termed as FFA*) and Dulbeccos Modified Eagle Medium (DMEM) were obtained from Invitrogen (Thermo Fisher Scientific). Surfactant solutions were made by dissolving Pico Surf 2 (Dolomite Microfluidics, Royston, UK) surfactant in HFE-7500 oil (3M, St. Paul, MN, USA) to make 1.0% w/w solution. This not only helps to minimize exchange of compounds between aqueous and oil phases but also prevents adsorption to the PDMS.

2.2.2 Microfluidic Device Fabrication

Microfluidic devices were made of two layers of patterned PDMS following standard soft lithography guidelines[96]. While standard methods employ photolithography using a mask aligner and UV light source, we employed an in-house built UV lithography source[141] based on 365 nm LEDs, after a few modifications to the recent design detailed by Groisman and co-workers[142]. Two master wafers for fluidic and pneumatic channels were fabricated. All channel layouts were designed in Adobe Illustrator, and photolithographic masks were printed at 50 800 dpi resolution by Fineline Imaging (Colorado Spring, CO). For the pneumatic control channels (thin lower layer), 30 μm thick negative photoresist (SU-8 2050) was spin-coated onto a silicon wafer. The wafers were then baked on a hot plate at 95 °C for 5 min. UV exposure was carried out through the mask at $\sim$330 mJ/cm^2 on the in-house built UV LED exposure unit. The wafer was hard baked for 5 min at 105 °C and then developed

for 5 min in the SU-8 developer. For the fluidic channel layer, 45 μm thick positive photoresist (AZ-40-XT) was spin-coated onto another silicon wafer. The wafer was then baked at 105 °C for 5 min followed by UV exposure at ∼330 mJ/cm^2 . After another baking step at 105 °C for 5 min, followed by wafer development in AZ developer for about 5 min, the master wafer was baked at 115 °C for 6 min to anneal the AZ photoresist and create a more rounded cross-section of the fluidic channel template. All silicon wafers were exposed to trimethylsilyl chloride vaper for 30 min before use to enhance PDMS removal. Channels were later characterized by slicing an assembled PDMS device with a razor and imaging the channel cross section. To fabricate the lower, pneumatic layer, a thin PDMS valving membrane (∼15 μm membrane above control channels) was made by spin-coating a 20:1 ratio mixture of PDMS precursors and curing agent, respectively, onto the SU-8 defined control wafer. The upper, fluidic layer was made by pouring a 5:1 ratio mixture of PDMS precursors and curing agent to form a thick (∼0.6 cm) substrate over the rounded, AZ-defined fluidic channels. Both layers were cured at 65 °C in an oven for ∼35 min. Thereafter, the thick fluidic layer was quickly peeled from the silicon wafer, cleaned with methanol, air-dried, and then aligned and bonded to the thin pneumatic layer. The assembled layers were again cured at 65 °C in an oven for ∼35 min to facilitate interlayer bonding. Following this process, the resultant microfluidic devices were peeled from the wafer, cleaned with methanol, air-dried with a stream of N^2, plasma oxidized, and bonded to a glass slide. The flow channels were treated with Aquapel then rinsed with methanol to repel aqueous solution, facilitating aqueous-in-oil droplet formation.

2.2.3 Flow Control

Microfluidic flow control was enabled by active pneumatic push-up valves, initially developed by the Quake group[95], which are formed at the intersections between the control and the flow channels. An in-house written application in LabVIEW (National Instruments) was interfaced to a control system of solenoid valves (Lee Co.; LHDA0533115H) to permit

on-demand droplet formation. Valve actuation was powered by a regulated pressure source of ∼20 psi, and flow was promoted by vacuum applied to the outlet channel via a hand-held 100 mL glass syringe (SGE Analytical Science).

2.2.4 Droplet Fluorescence Measurements and Data Analysis

Fluorescence calibration standards and stocks were initially evaluated using a Nanodrop 1000 spectrophotometer or Nanodrop 3300 fluorospectrometer (Thermo Scientific, Grand Island, NY USA). These calibration standards were diluted in 20 nM HEPES buffer solution (pH = 7.5) and analyzed in triplicate. Wide-field or fluorescence imaging and measurements in the μChopper device were performed with either a cooled CCD camera (CoolSnap HQ2; Photometrics Scientific) or more typically using a PMT (Hamamatsu). These detectors were interfaced to a Nikon Ti-E inverted fluorescence microscope via a green fluorescence filter cube (excitation: 470 ± 20 nm; emission: 525 ± 25 nm). The PMT was set to 10^{-3} A V^{-1} sensitivity with a 0.5 ms time constant and a one-time, manually adjusted amplifier offset at the onset of measurements.

The device (μChopper) included a reference inlet (either buffer or high fluorescence), a sample inlet, and an oil channel inlet (Figure 2.2). Using pneumatic microvalves and the LabVIEW application, droplets were generated in an alternating fashion[40]; each droplet was moved to the region of interest (ROI) and stopped, and the fluorescence emission was collected with the PMT. This customized software allowed instantaneous separation of the sample and reference signals into two different data arrays, greatly simplifying data analysis compared to previous device iterations[40]. Droplets could be reliably formed at 3.50 Hz each (0.04 Hz bandwidth) while maintaining software-based phase-locking to the detector. Reference droplet signals were subtracted from sample droplet signals over time to correct for drift, and this analysis was carried out for up to 100 droplets for each sample. Alternatively, fast Fourier transform (FFT) analysis was carried out in Matlab, where sample and droplet

data arrays were recombined in time, and the primary frequency-domain peak intensity at 3.50 Hz was used as the processed signal.

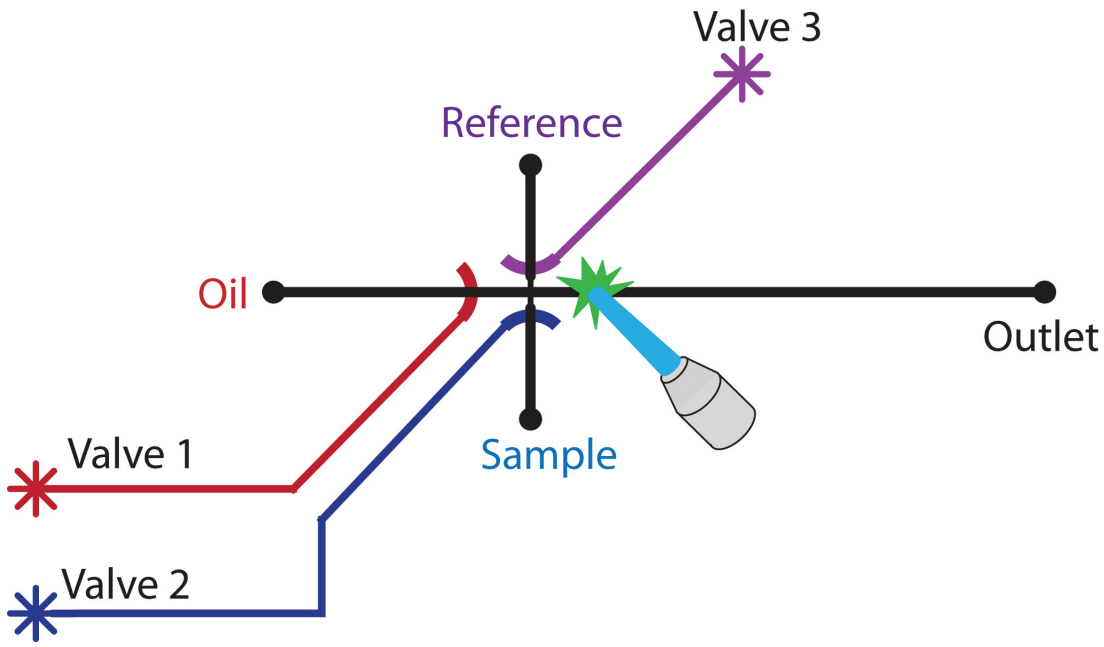

Figure 2.2: Automated μChopper chip design
Channel layout depicts flow channels (black), control channels (blue, red, and purple), and the fluorescence detection region of interest (ROI). This figure was reprinted with permission from Negou et al. Copyright 2017, ACS.

2.2.5 Adipocyte Culture, Treatment, and Lysis

Murine preadipocytes (3T3-L1; ATCC) were seeded on 35 mm culture dishes and kept in DMEM supplemented with 10% FBS and penicillin/streptomycin (5%) at 37 °C in an atmosphere of 5% CO_2. After confluency was reached, differentiation was induced by adding DMEM supplemented with 0.5 mM IBMX, 250 nM dexamethasone, 1.0 μM insulin, and 10% FBS. Three days later, DMEM supplemented with 1.0 μM insulin was added, and the cells were maintained for an additional 3 days in this media. Thereafter, cells were set in DMEM supplemented with 10% FBS before use, usually between 5 and 8 days. Differentiated adipocytes were subjected to starvation for 1.0 h in DMEM without phenol red and FBS, supplemented with 3.0 mM glucose and 50 pM insulin at 37 °C in an atmosphere of

5% CO_2. Subsequently, this starvation media was replaced with DMEM without phenol red and FBS, containing 19.0 mM glucose, 2.0 nM insulin, and 1.0 M BODIPY FL C_{16} (FFA*). The cells were maintained for 1 h under the same conditions previously mentioned for starvation. Next, the differentiated cells were washed four times with 2.0 mL of phosphate buffered-saline solution (PBS). Carefully, ∼100 adipocytes were detached with a 10 μL pipet tip and transferred into 200 μL of PBS. The solution was gently mixed with the pipet to disaggregate the cells. Using a tissue culture microscope and a 10 μL micropipette, 10, 3, 1, or 0 adipocytes were transferred into 30 μL of RIPA Lysis and Extraction Buffer (Thermo Fisher Scientific). Each solution was mixed and kept in ice during the lysis process. Samples were then immediately centrifuged at 12 000 rpm for 10 min, and the supernatant was analyzed in our Chopper device. For adipocyte imaging, differentiated 3T3-L1 cells were fixed and stained with lipid-staining LipidTOX and nucleus-staining DAPI. LipidTOX emission was collected at 525 ± 25 nm after excitation at 470 ± 20 nm, and DAPI emission was collected at 460 ± 25 nm after excitation at 350 ± 25 nm. Differential interference contrast (DIC) images were also collected. Images were overlaid using ImageJ software[143], and false coloring was applied for visualization (green for LipidTOX, blue for DAPI, gray for DIC).

2.2.6 Homogeneous Immunoassays

Insulin was quantified in droplets using a homogeneous fluorescence assay (Human Insulin FRET-PINCER Assay Kit; Mediomics, St. Louis, MO), where higher insulin levels caused decreases in fluorescence due to target-specific probe quenching. Various concentrations of insulin (0, 11, 22, 44, 88, and 176 nM) were premixed with both antibodyoligonucleotide probes (16-fold larger than recommended in kit; ∼160 nM each) and incubated for 30 min; then, fluorescence emission was measured using the Nikon Ti-E inverted fluorescence microscope via a green fluorescence filter cube (excitation: 470 ± 20 nm; emission: 525 ± 25 nm) interfaced to a CCD camera (Coolsnap HQ2; Photometrics). To provide a constant,

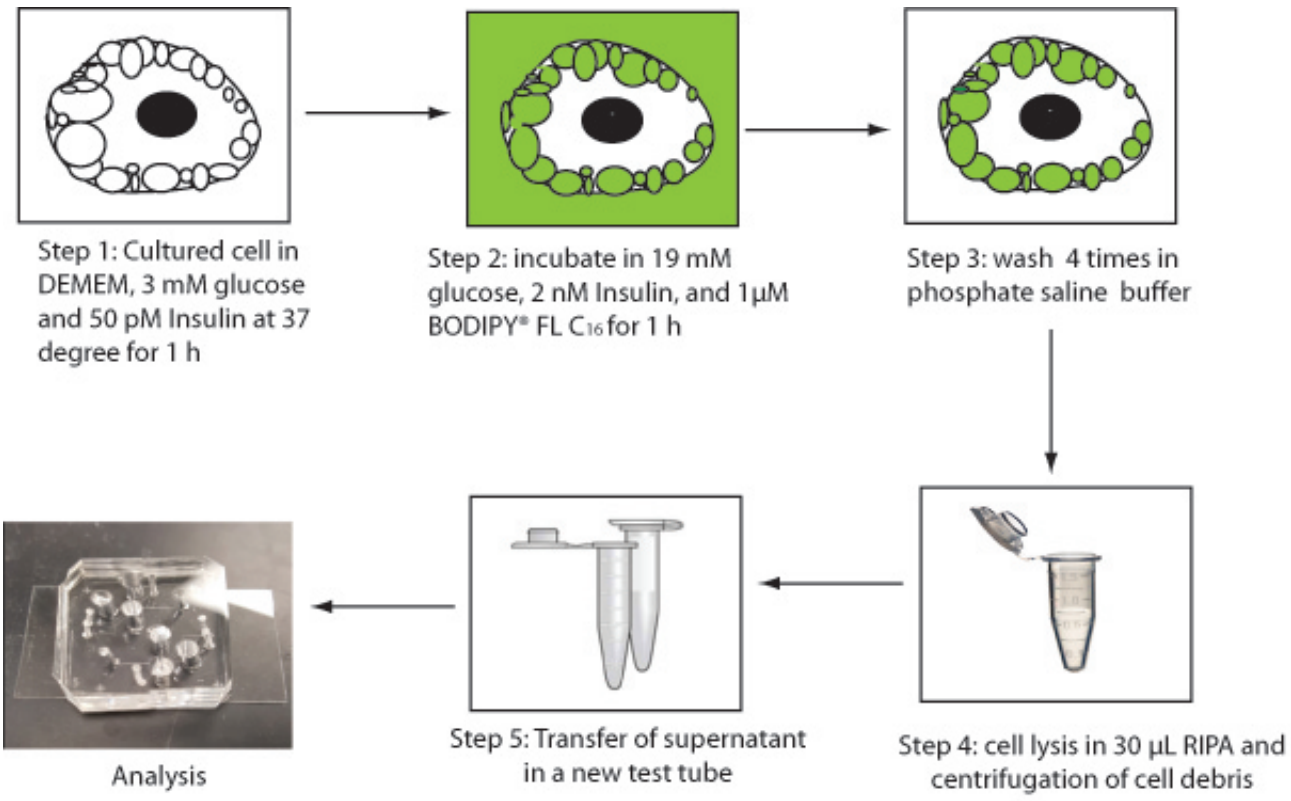

Figure 2.3: 3T3-L1 cells free fatty acid uptake and lysis
Step-by-step Adipocyte cells preparation for on-chip single cell free fatty acid (FFA) uptake.

unquenched emission, reference droplets consisted of ∼80 nM of only the fluorophore-labeled probe. Unless otherwise noted, 30 droplet pairs (sample and reference) were analyzed for each concentration.

2.3 Control Experiment

2.3.1 Adipose Tissue Explant Isolation

Epididymal fat pads were isolated from C57BL/6 male mice as described previously[144, 145, 141, 146]. Following isolation, fat pads were transferred to a 60 mm petri dish containing a few mL of fresh phosphate-HEPES buffer. Excess vasculature and other non-adipose tissue was excised using micro surgical scissors. A 3-mm diameter sterile biopsy punch was used to form aliquots of the fat tissue. As explants were punched, they were transferred

with surgical tweezers into a glass tube with 3-4 mL of phosphate-HEPES buffer. Explants were centrifuged at 1000 rpm for 3 min. Infranatant was removed with an 18-gauge, 1.5-inch needle. 3-4 mL of phosphateHEPES buffer was added back to the tube. Cells were centrifuged and washed in this fashion one additional time with phosphateHEPES buffer and 2 additional times with fat serum media. After the final rinse, explants were transferred to individual microcentrifuge tubes as described below.

2.3.2 Adipose Explant Titration with Free Fatty Acid

Six 3-mm diameter explants were incubated with 100 μL DMEM in micro-centrifuge tubes separately. Each explant was treated with 100 μL of either high insulin/glucose (10 nM/20 mM) or low insulin glucose (50 pM/5.5 mM) solution in DMEM buffer. Next, 20 μL of 3 μM FFA* was added and mixed by pipetting to a final concentration of 0.5 M. After 10 min, 20 L from each explant tube was transferred to a microplate well that had been preloaded with 60 μL of DMEM. In this titration experiment, every 10 min we added 20 μL of 3 μM FFA*, and after mixing by pipetting, 20 μL of the solution was transferred to the microplate for readout (zero net change in volume). We used buffer solution with no explants as our control.

2.4 Results and Discussion

2.4.1 Microfluidic Device Design and Operation

We previously reported a droplet-based μChopper for microfluidic absorbance detection consisting of three inputs (sample, reference, oil) and a single output. The device was passively self-regulated, alternating sample and reference droplets simply based on the opposing droplet T-junction geometries with manually applied vacuum at the outlet. Constant alternation of sample and reference droplets is a key feature of the lock-in analysis, because noise at frequencies and phases different from that of the droplets are largely rejected. This allowed nanomolar analyte detection limits (femtomole amounts) with absorbance[40], even

in short path-length microchannels. However, this passive approach lends itself to drifts in droplet frequency over time that must be tracked in data analysis. For this reason, we hypothesized that a more precisely controlled droplet formation system would permit further improvements in detection sensitivity and would simplify data analysis. Following this logic, here, we have applied the μChopper device concept to fluorescence detection while also adding active control using pneumatic valving. Droplet formation was automated by software, and phase-locked detection was applied in real time. The device design is depicted in Figure 2.2. The automated device is made of two layers of PDMS with fluidic channels (black) and the control channels (red, blue, and purple). With automated droplet formation and real-time, phase-locked fluorescence detection, a considerable reduction in data analysis was permitted compared to our prior work[40, 138]. Since the software was in control of the type of droplet being placed into the focal region, the fluorescence emission measurements by the PMT (green trace in Figure 2.4B) could be instantly stored into separate data arrays for sample and reference droplets, rather than relying on complex image analysis methods. Downstream data analysis required mere subtraction of reference traces from sample traces (or vice versa), which is easily built into the LabVIEW application.

2.5 μChopper Device Characterization

Since droplet formation was now intimately phase-locked with detection using microvalves, we expected that the μChopper would permit quantitative measurements of small differences between the fluorescence emission from sample and reference droplets, even at levels far below the magnitude of the drift or 1/f noise at the detector. This concept could be implemented for a low concentration fluorescence measurement using buffer as the reference ("signal on" assay), or the reference solution could be defined as having a constant fluorescence emission "signal of" assay), for example, with a quenching based assay. Our device was characterized in both situations. First, we characterized the system with buffer (no fluorescence) as the reference and fluorescein as the sample (Figure 2.5A). Following

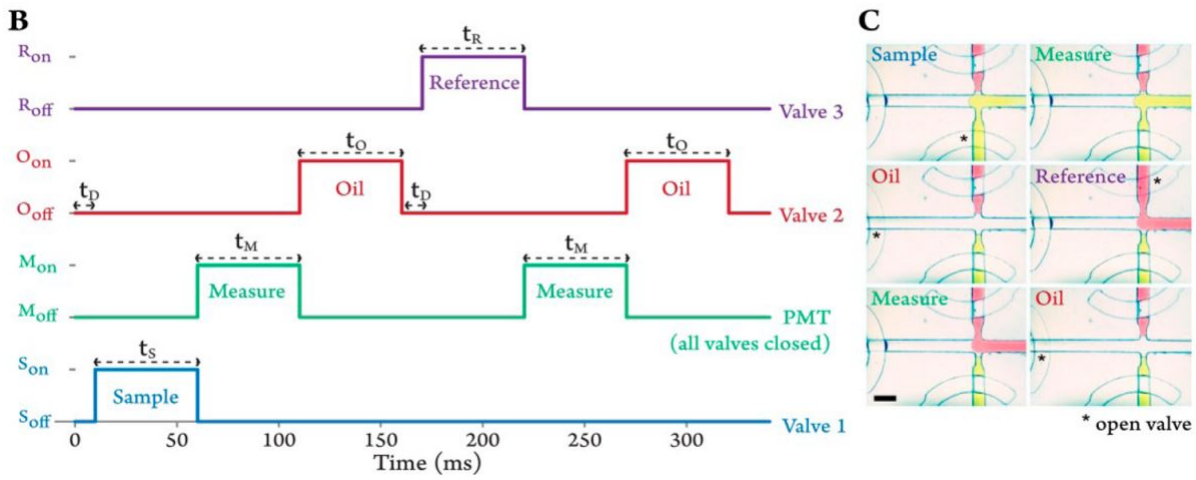

Figure 2.4: Automated μChopper chip operation
(B) Schematic of valve-automated chip operation cycle: t_D is the delay time, t_S is the sample flow time, t_M is the measuring time, t_O is the oil flow time, and t_R is the reference flow time. Droplet position was phase-locked with the detector collection cycle. (C) An image montage showing segments of a video collected during automated droplet formation on the μChopper. Open valves are marked with asterisks. Scale bar represents 200 μm. This figure was reprinted with permission from Negou et al. Copyright 2017, ACS.

lock-in analysis, we observed a highly linear response ($R^2 = 0.9997$) in the picomolar range. Using buffer as the reference, the PMT could be tuned to maximize sensitivity, at 9.65 V nM^{-1} . The LOD was determined to be 12 pM when sampling 2070 droplets (180620 nL). When only a single droplet was analyzed, the concentration LOD was higher at 35 pM, but this represents an amount of only 310 zeptomoles (3.1 x 10^{19} mol) of fluorescein detected. Notably, when the same data was analyzed without the lock-in approach, the noise magnitude (and thus the LOD) was 54-fold higher, validating the use of the μChopper system for noise reduction (3σ magnitudes marked with horizontal dotted lines). Interestingly, the inset graph in Figure 2.5A shows that, as the number of analyzed droplets was increased from 1 to 20, noise was reduced significantly, yet when analyzing >70 droplets, noise began to increase slightly. This trend was also observed in our prior work[40] and is likely due to buildup of the nonzero noise (white and 1/f) in the narrow band at 3.5 $\pm$ 0.04 Hz with increasing signal collection time. The noise increase in this study is more attenuated compared to prior work, which is reasonable considering the much narrower bandwidth. Nonetheless,

it is important to note the observation of an optimal, lower noise range of droplet number. Next, we characterized the μChopper with a fixed fluorescence signal as the reference, which would be useful for quenching based, indirect assays. As shown in Figure 2.5B, this placed a limit on the PMT sensitivity settings; with higher reference concentrations, lower sensitivities must be used. Again, highly linear responses were observed ($R^2 > 0.99$). In these analyses, the independent variable was defined as a detectable change in fluorescein concentration (Δ- [fluorescein]). With a reference of 50 nM, the μChopper could resolve as low as a 0.39 nM change in fluorescein; i.e., the system could discriminate 49.61 nM from 50 nM. With a reference of 10 nM, a 0.16 nM change was resolvable. The frequency response of the system was also characterized, as shown in Figure 2.6. FFT analysis was performed on the data from Figure 2.5A after recombining the sample and reference traces in the time domain, creating approximate square wave signals. The frequency domain in Figure 2.6 exhibited the standard square wave spectrum, with a fundamental peak at 3.50 Hz along with the odd harmonics at higher frequencies (10.5 and 17.5 Hz, etc.). The intensities of these peaks were clearly dependent upon the difference between the sample and reference concentrations. The inset log-scale spectra show a clear peak at 3.50 Hz, even at the lowest tested concentration of 39 pM. Here, the bandwidth was calculated as 0.042 Hz, which confirms the exquisite control that was provided by automated droplet formation using on-chip valves. Using postprocessing via FFT, the LOD of the system for fluorescein detection was further improved to 5.4 pM (data from all 100 droplets analyzed), although the real-time processing described above is much more practical.

2.6 Real-Time Drift Correction

To fully appreciate the noise and drift correction achievable with the μChopper, it is instructive to view the time domain data, as shown in Figure 2.7. Using standard microscope optics, the μChopper device allowed real-time drift correction by constantly referencing signal from the sample droplets (red trace) to that of the reference droplets (blue trace) at 3.5 Hz,

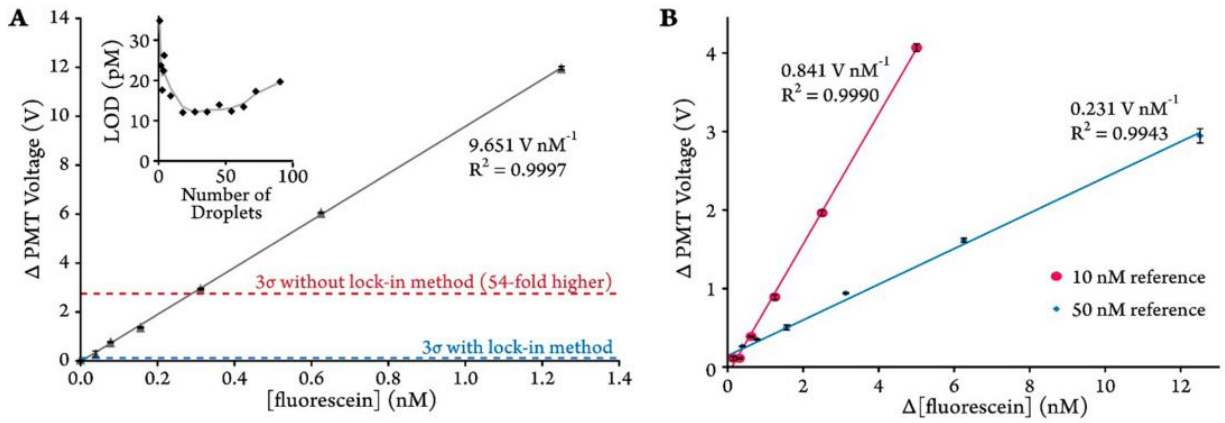

Figure 2.5: Automated μChopper chip characterization with fluorescein
(A) With a buffer reference, high sensitivity and an LOD of 12 pM were possible. Inset graph shows dependence of LOD on droplet number (moving average shown as a guide). (B) With fluorescent reference droplets, lower PMT sensitivities were required, but the system was highly linear, resolving small signal differences (0.39 and 0.16 nM). This figure was reprinted with permission from Negou et al. Copyright 2017, ACS.

in a phase-locked manner. It is clear from the difference signal (green trace) that larger system drifts (e.g., at the ∼10 or ∼70 s time range) were corrected using this approach. The difference signal trace was shown to be directly proportional to the sampled fluorescein concentrations. Further evidence of this drift correction is shown in Figure 2.8, where the PMT offset was intentionally varied as proof-of-concept. High measurement precision was also achieved with the μChopper. Responses recorded in Figure 2.5A,B were highly linear (R^2 = 0.9997, 0.9990, and 0.9943) with minimal measurement error at each concentration. Interestingly, this high precision exposed what appears to be slight human errors in sample preparation in one of the samples from Figure 2.5B (3.125 nM data point with 50 nM reference). Considering the other data sets in Figure 2.5 match the linear models very well, this deviation is most likely human error related and not a result of a poor regression model. Moreover, it is to be expected that fluorescence emission intensity will be linear versus concentration, since consistent optical settings were applied.

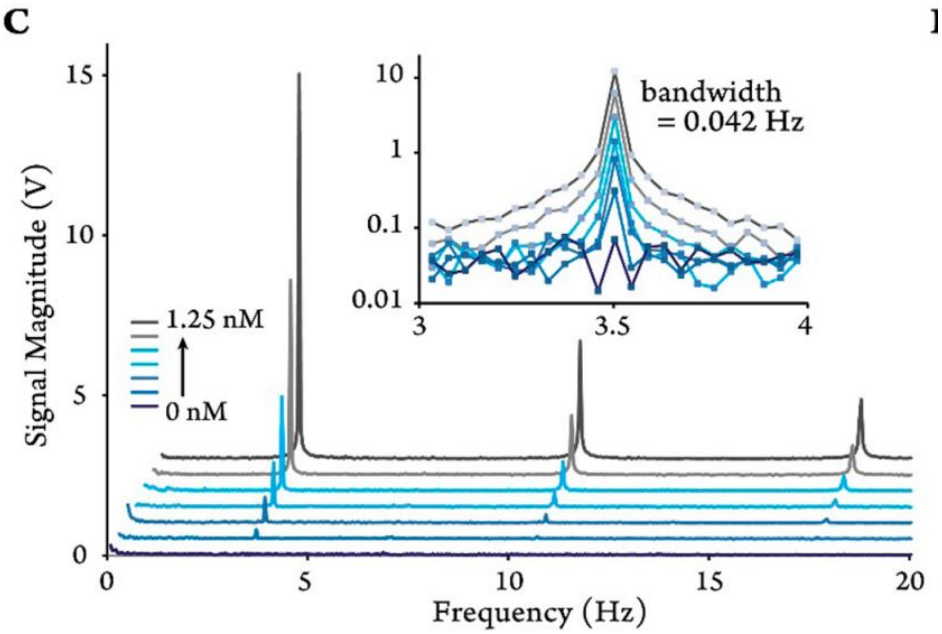

Figure 2.6: FFT analysis
Fourier analysis showed the expected square wave spectrum, with the fundamental peak at 3.50 Hz showing linear concentration dependence. Inset plot shows log-scale intensities and the highly regulated bandwidth of 0.042 Hz. This figure was reprinted with permission from Negou et al. Copyright 2017, ACS.

2.7 Free Fatty Acid Uptake Quantification

Methodology for single-cell analysis is critical in studying the variability in cell populations[147], preventing inaccuracies in taking averages of entire cell populations. However, single cell studies are often limited by the difficulties associated with analyzing small amounts of starting material. Microfluidic approaches are ideal in handling small volumes, allowing manipulation of small numbers of cells and minimizing sample dilution, for instance, after cell lysis[148]. Single-cell analyses using droplet microfluidics have been previously reported[149, 150, 151]. However, these studies were focused mainly on cell screening or gene expression analysis. Studies including breakdown, absorption, and uptake of metabolites are scarce and mostly not quantitative. It has been reported that fatty acid accumulation is cell-to-cell heterogeneous[152]; therefore, it is critical to quantify the amount of uptake from single cells rather than averaging uptake of larger groups of cells in bulk conditions.

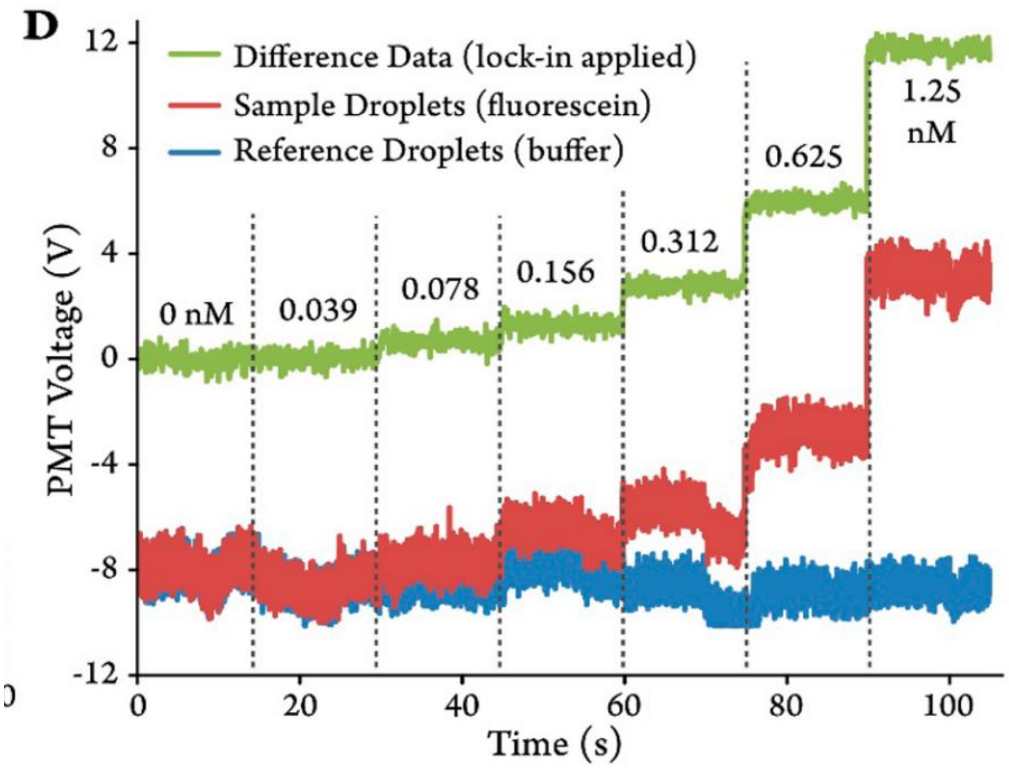

Figure 2.7: Real time drift correction
Time domain data illustrates the benefits of real-time drift correction using the μChopper. This figure was reprinted with permission from Negou et al. Copyright 2017, ACS.

Such information should contribute to gaining a better understanding of factors that lead to obesity[153, 154, 155, 156] and type 2 diabetes[157, 158]. Although our prior studies of adipose tissue on microdevices were quantitative in nature[141, 146, 144] single cell resolution was not achieved. With all of this in mind, we validated the μChopper system by applying it to quantify the amount of labeled free fatty acid (FFA*) that was taken up by small numbers of 3T3-L1 adipocytes. As shown herein, due to its extraordinary noise reduction and ability to discriminate very small fluorescence differences, our μChopper system could successfully quantify FFA* uptake by even a single 3T3-L1 adipocyte by simply lysing the cell in bulk solution. Fully differentiated adipocytes were incubated with a fluorescently labeled fatty acid solution (BODIPY FL C_{16}, or FFA*). Small numbers of adipocytes (0, 1, 3, or 10) were washed and then lysed in 30 μL aliquots of lysis buffer. Following centrifugation, the supernatant was analyzed directly with our μChopper device and lock-in analysis method.

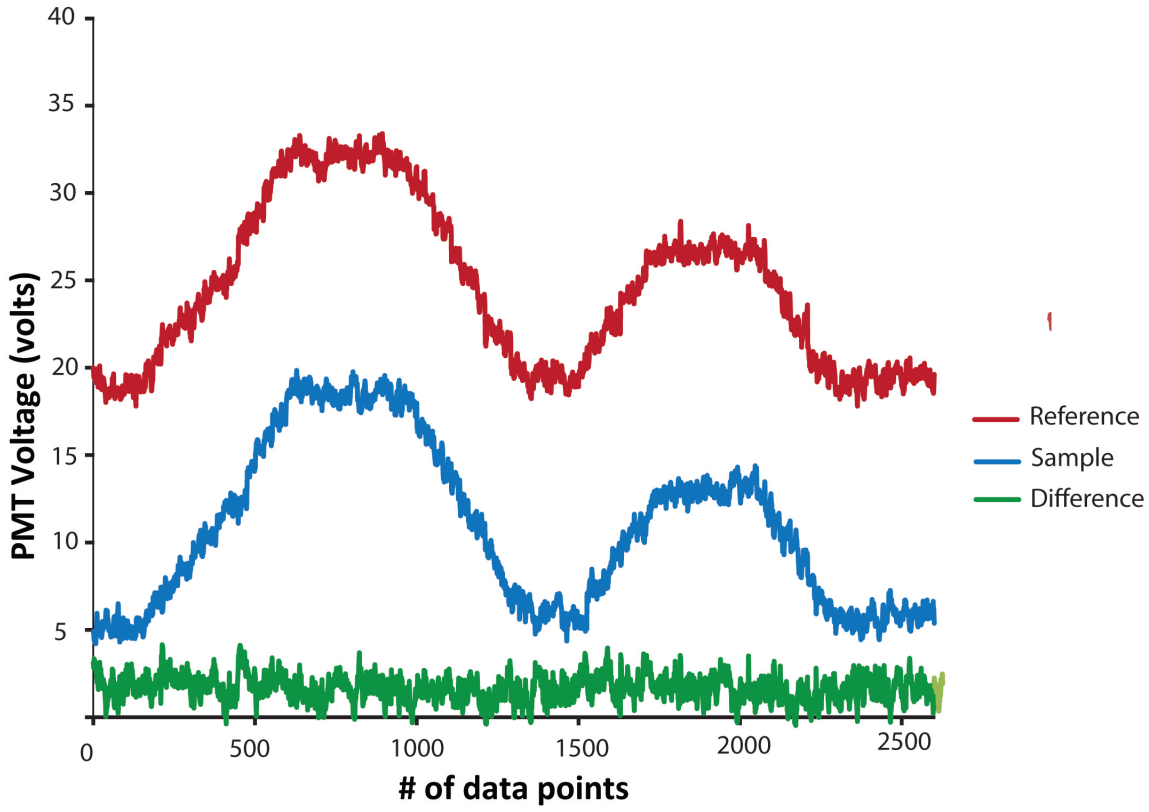

Figure 2.8: Drift correction with PMT offset move
The offset of the photomultiplier tube (PMT) amplifier was manually adjusted as a proof-of-concept of the drift correcting capabilities of the μChopper device. Sample droplets contained fluorescein (red trace), and reference droplets contained buffer (blue trace), but these data traces were artificially positioned in the y-axis for purposes of clarity in the chart above. The difference trace (green) shows the true voltage determined by the μChopper system; the constant voltage reading in this trace shows that the manually introduced amplifier offsets were nicely corrected by the lock-in analysis. This figure was reprinted with permission from Negou et al. Copyright 2017, ACS.

As shown in Figure 2.9, our system permitted single-cell FFA uptake rates to be quantified at 3.5 ± 0.2 10^{-15} mol cell^{-1}. To our knowledge, this is the first report of single cell uptake rates, and the value correlates well with confirmatory experiments using primary adipose explants (Figure 2.10). Our approach was more sensitive compared to the most recently reported methods[159, 160] since we were able to quantitatively measure FFA* uptake by a single cell. Slight deviations from the linear regression model at low cell number are likely due to human error related to the multistep cell isolation and preparation, as discussed above.

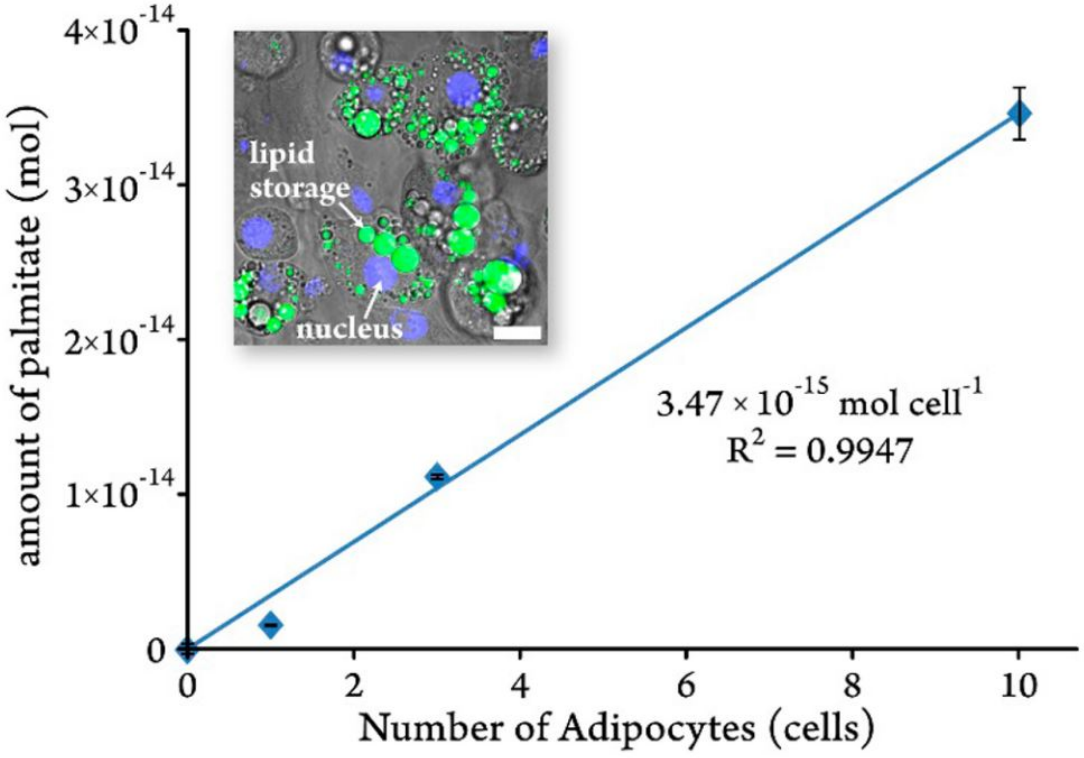

Figure 2.9: Single cell FFA uptake
Labeled free fatty acid (FFA*) uptake by 3T3-L1 adipocyte cells was quantifiable down to the single cell level using the Chopper system with lock-in analysis. Single cell FFA* uptake was quantified at 3.5 ± 0.2 x 10^{15} mol cell1 for the first time. The inset image shows a confocal fluorescence scan of fixed and stained adipocytes, where lipid storage is stained in green and nuclei are stained in blue. Scale bar represents 20 μm. This figure was reprinted with permission from Negou et al. Copyright 2017, ACS.

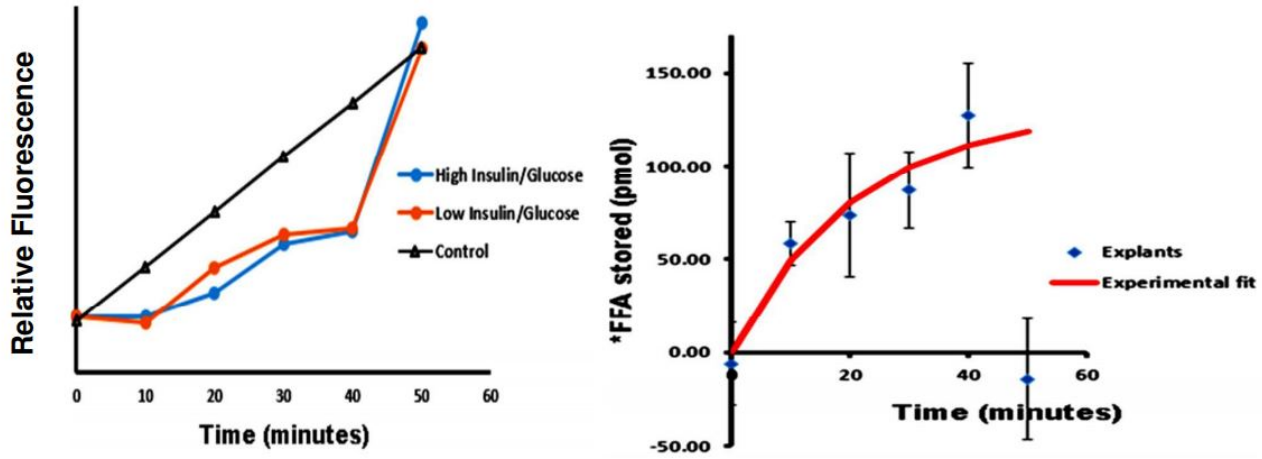

Figure 2.10: FFA uptake by adipose tissue explants
Six adipose tissue explants were titrated with FFA* as described above, under varying insulin and glucose levels. (Left) When compared to the control titration into buffer (black trace, triangles), it is clear that all explants absorbed FFA* during the experiment until the 50 min time point, where all six explants reached saturation and could no longer absorb FFA*. (Right) These data could be converted to the amount of FFA* stored per explant (in pmol), and the single exponential fit (red curve) gave a saturation point of 1.30 x 10^{-10} mol explant^{-1}. Considering that the average 3-mm diameter explant (∼0.3 mm height) contains approximately 32 400 spherical adipocytes of 50 m diameter, this uptake saturation rate equates to about 4.0 x 10^{-15} mol cell^{-1}, a value in good agreement with the Chopper determined value of 3.5 ± 0.2 x 10 $^{-15}$ mol cell^{-1} discussed in the main text. his figure was reprinted with permission from Negou et al. Copyright 2017, ACS.

2.7.1 Homogeneous Immunoassays in Droplets

Since the device was also shown to be useful with a fixed fluorescence signal as the reference (see Figure 2.5B), here, we show proof-of concept that a fluorescence quenching based, homogeneous immunoassay can be used to quantify small amounts of proteins in droplets using the μChopper. The device allowed homogeneous quantification of insulin in droplets with a concentration LOD of 9.3 nM using 30 droplet pairs and a mass LOD of 1.9 x 10^{-16} mol (190 amol) using 2 droplet pairs (Figure 2.11). A four-parameter sigmoidal fitting method was used for the insulin calibration curve shown in Figure 2.11 of the main text. This type of fitting is typically used for immunoassays such as sandwich enzyme-linked immunosorbent assays (ELISAs) and is appropriate for the sandwich type format of the homogeneous Pincer assay. The equation for the fitting is included below as Equation 2.1. The best-fit to the data in Figure 2.11 gave parameter values as follows: (A, B, C, D,) = (0.1201, 1.2323, 98.042, 0.5596).

$$y = D - \frac{(A - D)}{1 + (\frac{x}{c})^B} \quad \text{Equation 2.1}$$

This fitting method was applied to the sandwich type assay; observed deviations from this model are likely a result of a human induced bias in sample preparation rather than device error. As shown in the inset plot, reference droplets (red trace) contained a constant fluorescence reference (unquenched antibodyoligonucleotide probes), while sample droplets contained continuously varying insulin concentrations mixed with both homogeneous immunoassay probes. Again, the reference trace (red) can be used to validate the usage of the μChopper device, since time-dependent optical system drift is readily observed at magnitudes that would be detrimental to the assay without correction. The lock-in detection approach used here allows for much of that drift to be corrected. Such a system would be ideal to apply to real-time cell secretion quantification for any protein with an available homogeneous

immunoassay, and droplet sampling provides the potential for significant improvements in temporal resolution[138].

2.8 Concluding remarks

We have now shown that our droplet phase-locking approach with microfluidics (μChopper) is applicable to both absorbance[136] and fluorescence detection systems, and others have recently used a similar strategy with Raman spectroscopy in droplets[138]. Phase-locking with droplets can be done passively, but in our application to fluorescence herein, we demonstrated that significant bandwidth reduction was possible using on-chip pneumatic valving. Considering these results together, it should be relatively straightforward to apply the technique

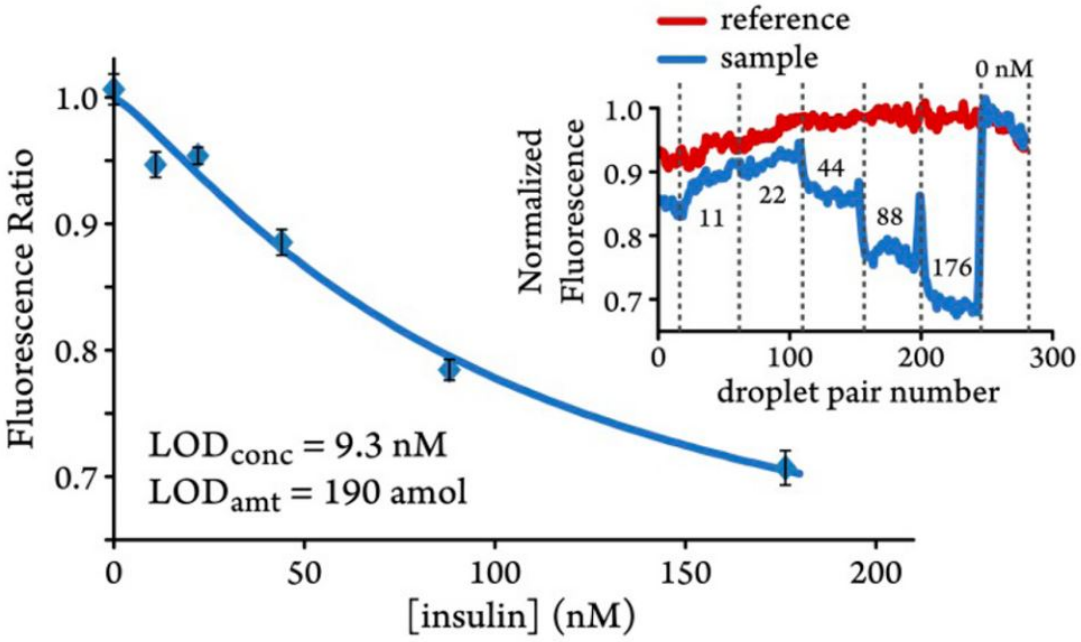

Figure 2.11: Homogeneous immunoassay in droplets
Homogeneous quantification of insulin in droplets was possible at levels as low as 9.3 nM (30 droplet pairs) or 190 amol (2 droplet pairs) using the μChopper system. Reference droplets contained unquenched antibodyoligonucleotide probes. Calibration plot includes a 4-parameter sigmoidal fit curve obtained by nonlinear least-squares fitting. Inset graph shows a typical real-time data collection as insulin standards are sequentially added to the sample droplet reservoir. his figure was reprinted with permission from Negou et al. Copyright 2017, ACS.

to improve any optical readout method without modifying the optical assembly, particularly for groups already employing droplet microfluidics. Furthermore, it is theoretically possible to apply this droplet phase-locking technique to any droplet-integrated detection method to eliminate signal drifts. For example, ion collection in droplet-interfaced mass spectrometry[161, 162] could be phase-locked with droplet formation to help recover signal from low abundance analytes. Alternatively, electrochemical detection in droplets[163] could be phase-locked with droplet formation to recover lower analyte currents. Although a >50-fold reduction in noise was exhibited here, in theory, this system could be further improved by phase-locking to higher frequency droplet formation. Droplets are now routinely generated at kHz frequencies[164], a sampling range that is known as a quiet region of the noise spectrum[129]. If kHz range pneumatic valve actuation frequencies could be achieved, this ultimate low-noise sampling bandwidth should be attainable. Overall, using the improved μChopper device presented here, we have further demonstrated the compatibility of droplet fluidics with phase-sensitive (lock-in) detection. In many existing droplet microfluidics systems, this approach should provide significant noise reduction with relatively few design modifications. Such microsystems are ideal for analyzing precious specimens such as cells or biological reagents and for quantifying samples of limited volume.

Chapter 3

A Multichannels μChopper for continous calibration or multiplexed analysis

3.1 Introduction

Droplet-based microfluidics has enabled breakthrough experiments on many chemical and biological processes and provided a resourceful platform of analyses to be performed in a given experiment[165, 166, 167]. However, many microfluidic devices in the literature are designed for a specific analysis and require manual change of solutions during experiment, which is time consuming, labor demanding, and can introduce human errors during the process. A switchable microfluidic device that can perform various analytical modes would greatly reduce analysis time and facilitate experimental procedures. Automation in microfluidics allows rapid and sensitive chemical analyses[168, 145]. The ease of formation and manipulation of monodispersed droplets where different reactants can be comparmentalized into small volumes ranging from femtoliter to nanoliter through a computer program has many advantages. For example, a single microfluidic chip can be programmed to perform a variety of analyses without redesigning and using the same optical detection method. Moreover, there is a possibility of performing high throughput assays at high temporal resolution.

Recently, we have designed an automated droplet microfluidic device (μChopper) for fluorescence detection that could perform highly precise (strictly phase locked at 0.04 Hz bandwidth) and sensitive measurements[169]. This device was designed as analogue to optical beam chopper where picoliter of sample and reference droplets form alternately. This constant referencing technique have been proven to be a powerful tool for noise reduction[40, 137]. Coupled with the lock-in detection method, the key application of this device was to greatly reduce signal drift (1/f noise) without the need of complex optical readout and to detect small difference between two samples. However, to change solutions on these devices

required manual user pipetting steps that were tedious and could cause inadvertent optical misalignment.

Herein, we present a novel generation of μChopper with 6 input channels and one input oil that can not only achieve the performances of the previous device but also perform many experiments in a single process without the need to manually change samples. Because this device can accomodate up to six solutions, several analytical modes can be operated. First, the novel μChopper can perform the same constant referencing technique as before to reduce 1/f noise for the detection of low concentrated sample in a single run for up to 5 samples (multiplex mode). Second, this new devices can be used for continuous calibration mode with one unknown sample and five calibration solutions which can be used to monitor the dynamics of a continuously changing sample as compared to 5 fixed calibration solutions (constant calibration mode). Another posibility is to analyze several unknown samples and several calibration solutions (mixed mode). A fourth mode of operation is to employ the standard addition in complex matrices, where the sample is spiked with increasing concentrations of standard (in all 6 wells) to correct for interferences within the sample matrix (standard addition). Finally, these analysis modes should normally be applied to high throughput analyses since the device is automated. For example, in future work we could validate the pincer assay in human serum using the standard addition method with the multiplex mode. Later, we will also attempt to monitor temporal changes in glycerol secretion using an enzyme assay with constant calibration mode. This device could be applied to many other biological assays to analyze precious samples since it can measure small differences in signal, while achieving low limits of detection and good temporal resolution. Practically, the upper limit on the number of sample wells is limited only by the value control system.

3.2 Experimental Section

3.2.1 Materials and Methods

Polydimethylsiloxane (PDMS) precursors, Sylgard 184 elastomer base, and curing agent were purchased from Dow Corning (Midland, Maryland, USA). Silicon wafers were acquired from Polishing Corporation of America (Santa Clara, CA, USA). AZ-40-XT photoresist, AZ 300 MIF developer, and SU-8 photoresist and developer were purchased from Microchem (Westborough, MA, USA). Tubing (TGY-020-5C; 0.02 in. ID, 0.06 in. OD, 0.02 in. wall) and blunt needles (NE-223PL-C 22G) to interface syringes and devices were obtained from Small Parts (Logansport, IN, USA). Fluorescein was obtained from Alfa Aesar (Ward Hill, MA, USA). Human serum (FBS) was purchased from Bioreclamation IVT (Charleston, Maryland, USA) and Aquapel from Pittsburgh Glass Works (Pennsylvania, USA).Surfactant solutions were made by dissolving Pico Surf 2 (Dolomite Microfluidics, Royston, UK) surfactant in HFE-7500 oil (3M, St. Paul, MN, USA) to make 1.0% w/w solution. This not only helps to minimize exchange of compounds between aqueous and oil phases but also prevents adsorption to the PDMS.

3.2.2 Microfluidic Chip Fabrication

The microfluidic device was fabricated as previously described. Briefly, the chip is made of two layers of pattern PDMS following standard soft lithography guidelines, the top being the fluidic (thick PDMS) layer with rounded features and the bottom being the control (thin PDMS) layer with squared features. Figure 3.1 shows a cross-section of the channels and the dimensions.

3.2.3 Sample manipulation

Sample droplet formation and manipulation are controlled by an in-house-written LabVIEW application (National Instruments, Austin, TX). This program is interfaced with the

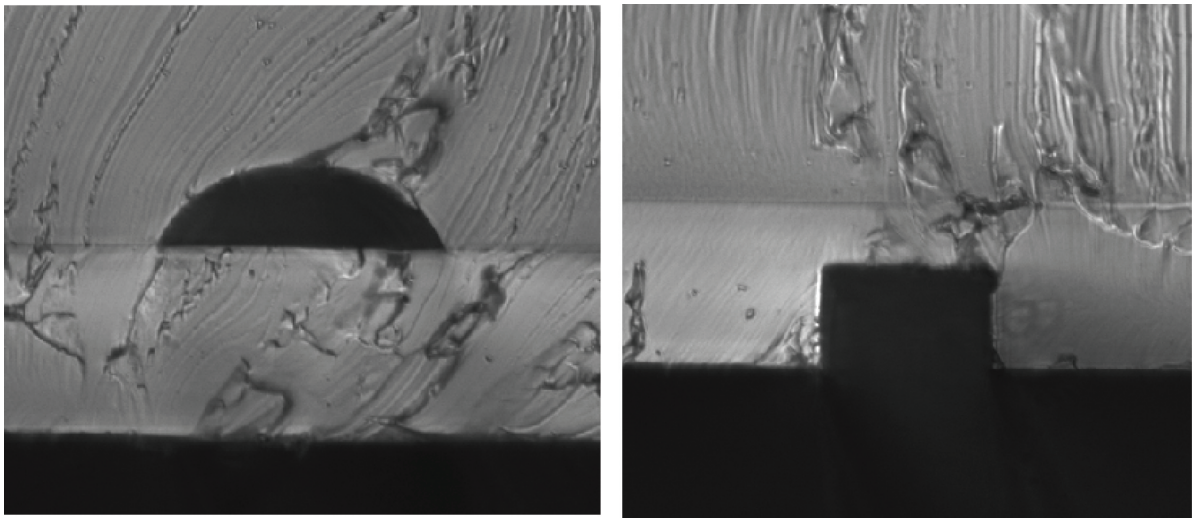

Figure 3.1: Novel 6 channels μChopper cross-section
A cross-section of the two bonded PDMS layer of the 6 channel μChopper. (Left) thick PDMS layer showing the cross-section of the rounded channel; Channel dimension width = 134 μm, depth = 39 μm. (Right) thin PDMS layer with the squared control channel cross-section; Channel height = 52 μm, width = 92 μm (control channel), valve membrane thickness = 32 μm.

microfluidic chip through a solenoid valves system (Lee Co.; LDHDA0533115H) which are controlled by an Arduino program. These solenoids are used to control fluidic movements in the microfluidic channels by pneumatically actuating microvalves. The valves are formed at the intersection of the control and the flow channels where the pneumatic action induces a push-up of a PDMS membrane to close the fluidic channel[95]. The valves actuation is powered by a regulated pressure source set at ∼20 psi. To initiate flow, a hand-held 100 mL glass syringe (SGE Analytical Science) was used.

3.2.4 Fluorescence measurements and data analysis

For device characterization, fluorescein solutions were diluted in 20 mM HEPES buffer solution (pH = 7.5) according to each mode of operation. The stock solution was diluted and the concentration was evaluated by measuring its absorbance at 490 nm wavelength on a Nanodrop 1000 spectrophotometer (Thermo Scientific) with 1 mm optical pathlength. Six samples are to be loaded on the device at the same time, therefore six solutions were made

for each analytical mode. Fluorescence measurements and fluorescence imaging in the 6 channels μChopper device was realized with a PMT (Hamamatsu, Japan) or a cooled CCD Camera respectively. Both detectors were interfaced with a Nikon Ti-E inverted microscope equipped with a green filter cube maintaining the same settings as previously described.

On-demand droplet formation was performed using pneumatic valves. The six reservoir inlets were filled with solutions, either one unknown and 5 standards, or 3 unknown and 3 standards. The unknown could be a fixed concentration solution or a solution that changes concentration over the course of the experiment. The LabVIEW program generates droplets in a given order. In one cycle time, the program can either generate droplets starting from the unknown sample and going to standard 1 through 5 or it can operate by alternating five standards with one reference or unknown. Similar to our previous work[169], droplets are moved to the region of interest (ROI) and stopped for measurement. Each step is assigned a code in the LabVIEW program to facilitate downstream analysis. Specifically, the first inlet of the channel, which is mostly used for unknown, is assigned a code of 0 (zero) and the next sample (standard 1) is assigned a code of 1 and so on to make codes numbered 0 through 5 for the 6 channels. The oil was assigned a code of 0 or 1 indicating whether it is off or on, respectively. The measurement is also assigned a code of 0 or 1 for inactive or active states. After making all the measurements, the data are sorted in an Excel worksheet using their assigned codes and analyzed. The LabView application was programmed to assign equal timing for the droplet formation, measurement, and oil flow. For example, droplets can be formed, measured, and moved away for 100 ms each steps. The total timing in this case would be 1.8 seconds for a complete cycle (to analyze all 6 droplets) plus an additional 10 ms wait time. The number of cycles depends on the number of droplets to be sampled or the analysis mode.

3.2.5 Constant calibration mode

The constant calibration solutions were made by dilution six standards with HEPES buffer. The first standard was 5 nM and the other were ranging from 10 to 165 nM. 10 μL of the first standard was loaded in reservoir 1 and 35 μL each of the other standards were loaded in reservoir 2 through 5. The experiment was carried out for 5 minutes and then 10 μL of high concentration fluorescein (82.5 nM) was added. To make sure that the solution diffuse faster in the channels to the droplet formation region, the solution was added to bottom of the reservoir and closer to the channels inlets. At 10 seconds time point, another 10 μL of 82.5 nM of fluorescein was added to the same reservoir following the same procedures.

3.2.6 On-chip standard addition

Standard addition method was characterized on our new μChopper by pipetting 10μL of the unknown fluorescein solution into 6 micro-centrifuge test tubes. In the first test tube, 30 μL of HEPES buffer was added. Next, 10 μL of 10.3, 20.6, 41.2, 42.5,and 165 nM of fluorescein solutions were pipetted in test tubes numberd from 2 to 6. Finally, buffer solutions were pipetted into each of the test tubes to make a total volume of 30 μL. The solutions were transferred into the 6 reservoirs of the μChopper in an increasing concentration order.

3.3 Results and Discussion

3.3.1 Chip design and modes of operation

This next-generation μChopper contains 6 aqueous input channels, and one oil input and a single output. The six channels each form a T-junction geometry with the oil channel. The aqueous channels are narrowed at the intersection between aqueous and oil channels to facilitate droplet formation. Figure 3.2 shows the design and operation of the 6 channel μChopper. Similar to previous design, the 6 channel device (Figure 3.2A) consists of a control layer (red) and a flow layer (black). Flow is initiated by applying vacuum to the

outlet of the device. Droplet generation is enabled with a LabView application; the 7 control valves can automatically form droplets in a predefined sequence, for example from valve 1 to 6 (Figure 3.2C) or in an alternating fashion (not shown). After each droplet is formed, the droplet is placed in the region of interest (ROI) for measurements then moved away by flowing oil. A video montage of droplet formation (made of diluted food coloring) in the 6 channels is shown on Figure 3.2B.

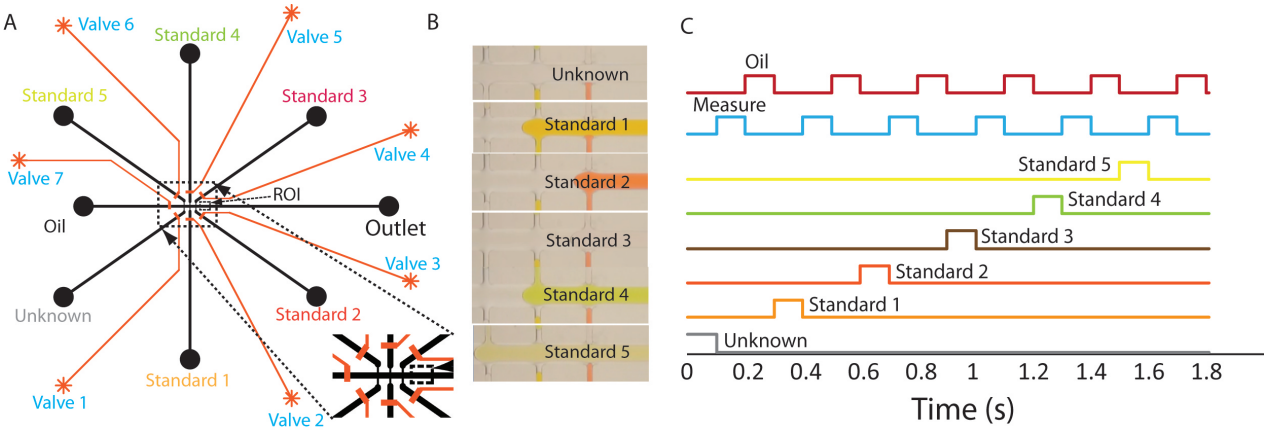

Figure 3.2: 6 channels μChopper design and operation
(A) Channels design depicting flow channels (black), control channels (orange), and detection point (squared dots). (B) Image montage showing droplets formation. This are segments of a video collected during automated droplet formation on the 6 channels μChopper. (C) Schematic of the valve-automated chip operation cycle, on-demand sample separated by measurement and oil flow is indicated over time

While the previous design focused only on reducing 1/f noise for a better limit of detection in absorbance[40] or fluorescence[169] measurements, this device offers the possibility not only to reduce 1/f noise but also to remove human error introduced when manually changing solutions between experiments. Since up to 6 solution can be handled at a time, this device also offers a wide range of possible analyses including dynamic changes in solutions. For example, dynamic changes or kinetics of the pincer assay can be studied in this chip, or cell secretion assays could be employed. Figure 3.3 displays four modes of operation that is applied to this device. It also displays sample loading order for the four modes (order can be interchanged). The reservoir are numbered with the valve number code therefore

valve 1 through 6 is actuated to form a droplet from the unknown to standard 5 (counter clockwise on the pictures) for the continuous calibration mode. The same order is made for the other modes except the multiplex mode where a reference droplet can sometimes be formed after each sample droplet (not shown).

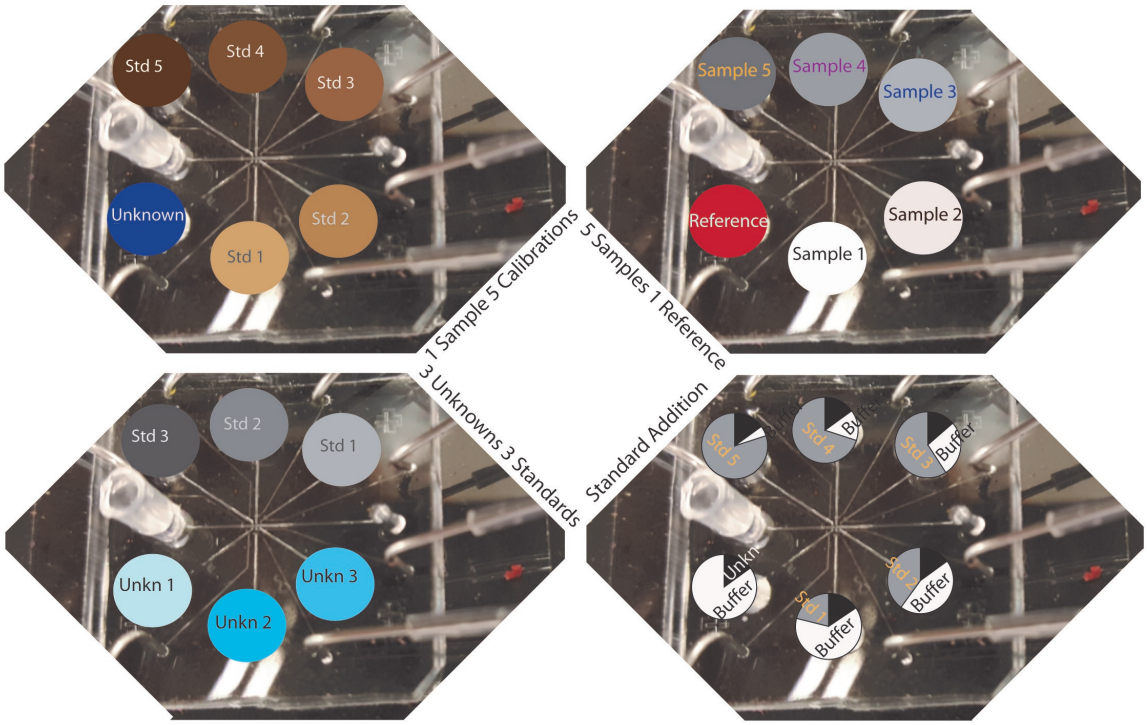

Figure 3.3: Modes of operation of the 6 channels μChopper
Images of an actual 6 channels μChopper showing sample loading for four different modes of analyses. In a duty cycle, a single droplet is formed for every sample in a counter clockwise manner for every mode of analysis. (Top left) The continuous calibration mode. (Top right) Multiplex mode with constant referencing. (Bottom) Mixed mode(left) and continuous calibration with an application in standard addition (right).

3.3.2 Constant calibration mode

As a proof of concept, we first characterized our novel μChopper for four modes of analyses using fluorescein solutions. For characterization purposes, the PMT settings were changed depending on the samples concentrations used and the sensitivity was maximized above 9 V nM^{-1}. The voltage and the offset were adjusted according to analysis mode to fit

a 20 volts window. Since up to six samples can be measured in only one run, we have the possibility to study the temporal response of the samples and to confirm the calibrations by observing the slope, the y-intercept, and the R^2 over time.

The constant calibration mode was performed by loading 6 calibration standards made of fluorescein into the reservoirs. During the first 10 seconds of the experiment, a high concentration is spiked in the first reservoir twice to create a changing concentration of unknown leaving 5 constant calibration standards (See Figure 3.2A). This will help to obtain dynamic information for some assays as well as the kinetics, for instance the kinetics of the pincer assays in human serum. We have mimic these type of assay with fluorescein solution in four modes of operation as explained above and we present the temporal response in this section. Figure 3.4 displays the raw data with intensity profile for every droplets for 30 seconds measurement time on the left and one duty cycle on the right. Experiment for this mode lasted nearly 20 minutes sampling more than 3.5k droplets in total (616 cycles). The full range data shows an increasing unknowns peak during the period of the experiment ($\sim$ 20 minutes) while the standard peaks remain constant. The real time fluorescence trace analysis (Figure 3.5A) also shows the same result. More interestingly, the standard and sample trace can be seen over time with the unknown trace (blue) increasing over time. The PMT offset and the voltage were intentionally adjusted during the experiment (after 12 minutes time point) to fit the 20 volts window and to confirm the stability of our system. After the modification of the system's setting the unknown trace continued its increase following the same path. The linear response of the system is also shown on Figure 3.6 A with two curves representing the data before and after modification of the system's settings. The slope, y-intercept, and R^2 are also constant over time even after the offset and voltage change confirming accurate 1/f noise removal. To confirm the accuracy of the measurement, the unknown concentration was calculated using the data at the end of the experiment and the value was found to match the known value which is the same as standard 4.

The peak intensities shown in Figure 3.4 all displayed the expected trend meaning that our method could distinguish between samples concentrations, even the lower concentration for some cases. As for the constant calibration, once the standard solution were loaded, the unknown reservoir previously filled with 5 nM of fluorescein is spiked with a high concentration fluorescein that diffuses over time. The corresponded peak intensities (Figure 3.4A) for this mode clearly shows a difference between droplets concentrations and an increasing unknown peak for the full length of the data (∼20 minutes).

3.3.3 Mixed mode

For the mixed mode, various concentrations of unknown and calibration standard can be used. In the present study, 3 unknowns and 3 standards were used. Expected peak intensities were also observed (Figure 3.4B) for the three calibration solutions as well as the three unknown samples. A real time trace of the 3 unknowns as well as the 3 standard droplets signal is shown on Figure 3.5B. The traces show variation of the signal throughout the experiment with a significant decrease happening to all the signals at the beginning. This variation is probably due to channel clogging or certainly an accidental movement of the chip out of the ROI. The second possibility is more probable because the peak signal (Figure 3.4B, right) seem to be recording the droplet edge since the peak intensity is partially recorded in the data. These abnormally can be seen in other plots such as the slope, the y-intercept, and the R^2. However, even with the variations we were able to obtain distinct signals between all samples and the linear response (Figure 3.6B) was acceptable. We were also able to calculate the values of the unknowns which were close enough to the true values nearly 83% for unknown 1, 86% for unknown 2, and 72% for unknown 3.

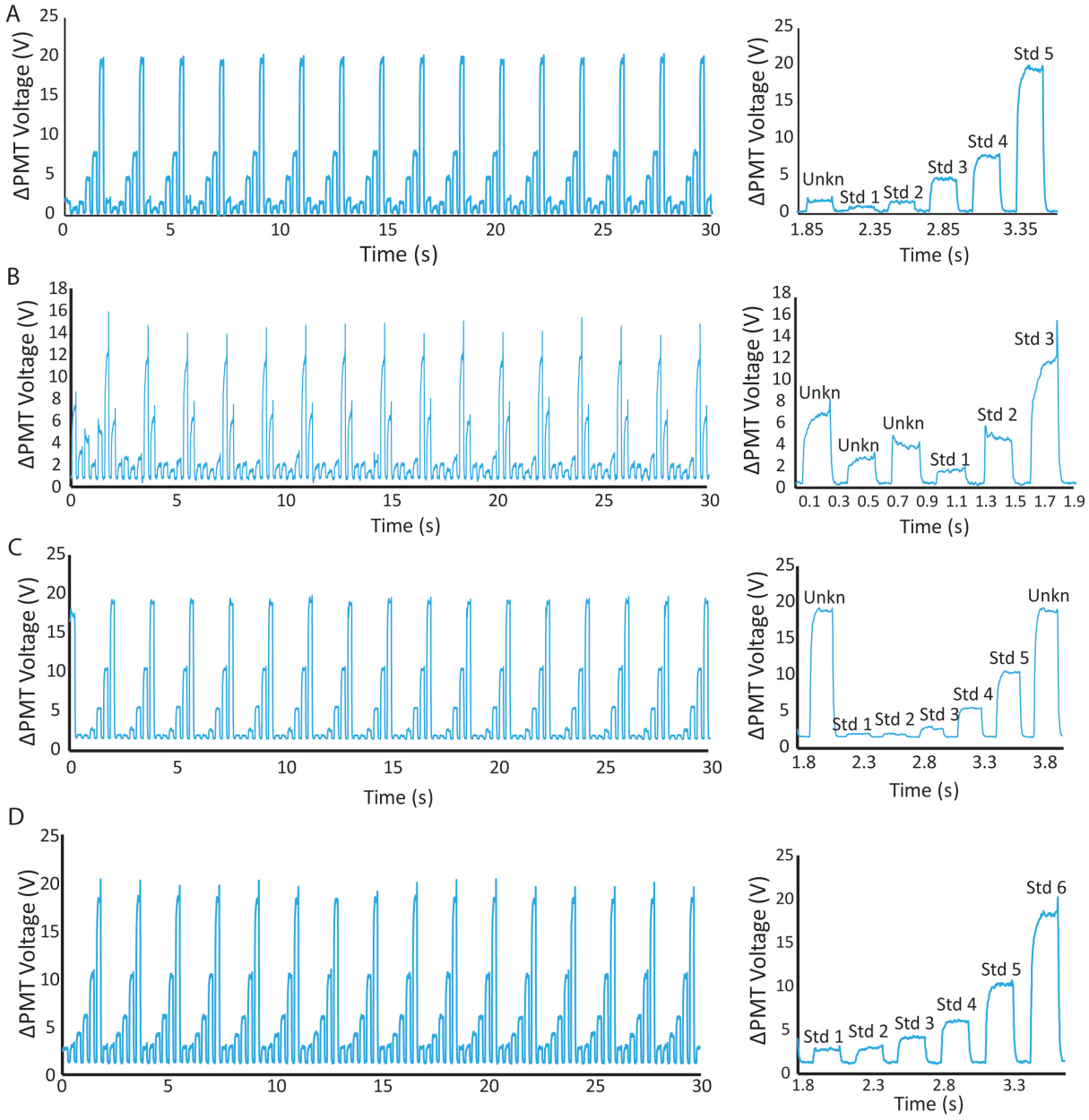

Figure 3.4: Characterization of the 6 channels μChopper
Droplets peak intensities for 30 seconds data (left) and a zoom in representing on duty cycle for each mode (right). (A) Temporal sampling in the constant calibration mode; (B) 3 samples 3 calibration in the mixed mode; (C) 5 point calibration with one unknown in one run; (D) on-chip standard addition method in continuous calibration mode

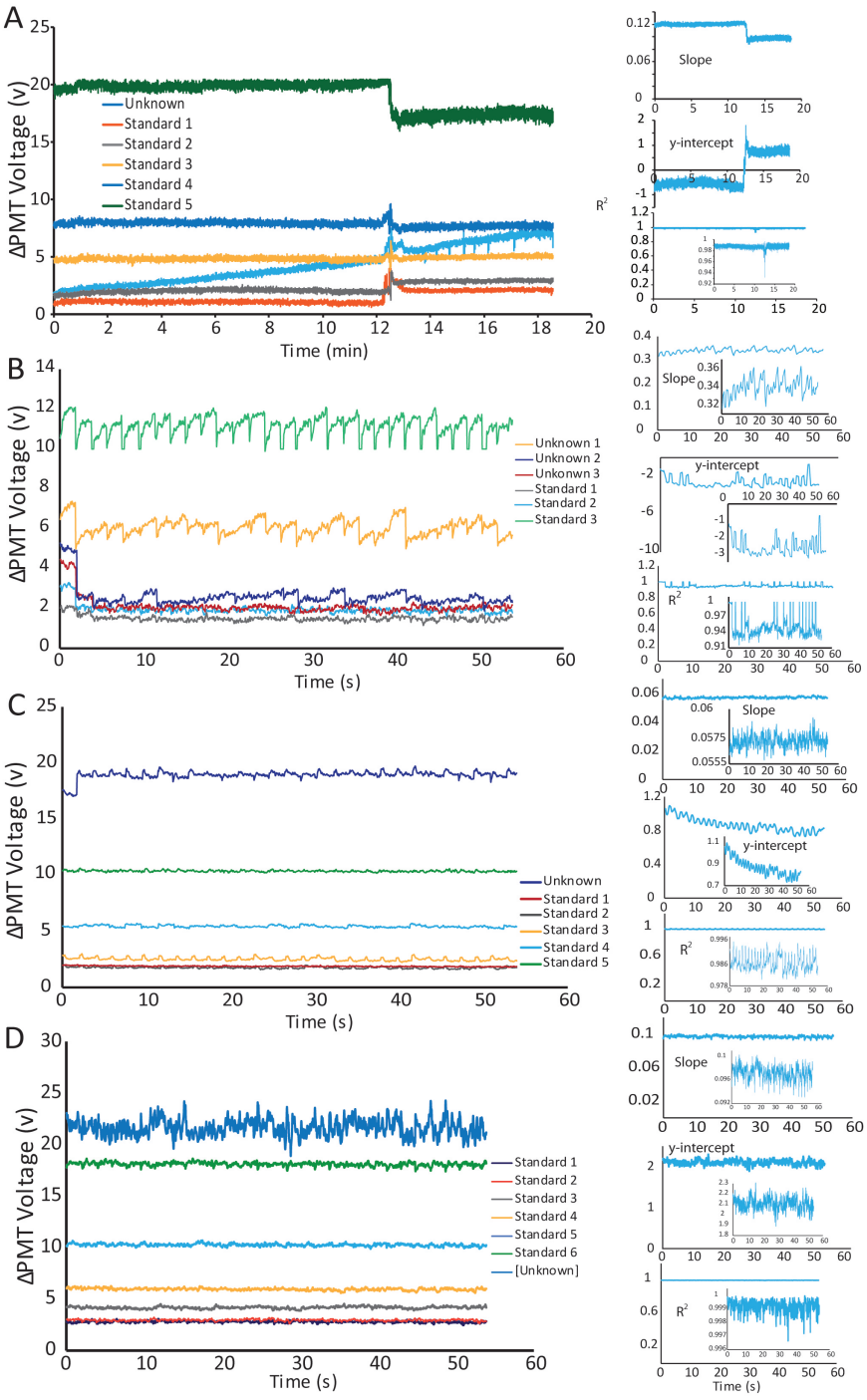

Figure 3.5: Temporal sampling analyses

Temporal response of all modes (left) with their slope, y-intercept, and R^2 (right from top to bottom). (A) Temporal sampling experiment showing the unknown signal increasing over time while the standard remain constant; PMT offset intentionally moved after 12 minute time point.(B) Mixed mode with 3 unknown samples and 3 calibrations; signal is constant for all samples. (C) Continuous calibration mode with one unknown and 5 calibrations. (D) Standard addition method showing all six standard and the unknown concentration to be constant throughout the experiment

3.3.4 Multiplex mode

Since previous device could only perform one sample and one reference at a time, we evaluate the multiplex capability of our device by using 1 reference and 5 calibration samples. This can be done by constant referencing each sample droplet with the reference or referencing after the 5 sample droplets. To characterize this mode, very high concentration of reference was used, and PMT was calibrated according to its signal. This was to mimic assays where the signal is reduced during the course of the reaction such as the pincer assay. A buffer can also be used as reference. The voltage was turned down to fit the reference signal in the window for recording. We present partial peak data (the first 30 seconds) on Figure 3.4C where the droplet peak intensities of the 5 samples (standards) and the unknown can be seen. Since the sensitivity was turned down, the first two droplets are not distinguishable from each other. However, the 3 other standards are distinguishable and can be used for calibration which is another advantage of this device. The real time observation of the droplets show constant signal for all sample concentrations as well as the reference (Figure 3.5C). While the R^2 and the slope seem to remain constant for the duration of the experiment with values around 0.986 and 0.0565 respectively, the y-intercept shows a slight decrease. This is decrease is probably resulting from the weak signals from the lower concentrations standards. Despite this minor issue, the linear response of this mode (Figure 3.6C) was acceptable.

3.3.5 Standard addition mode

For the standard addition method, since six standards each containing the same volume of unknown at different ratios with the buffer was prepared(Figure 3.3), the PMT was set according the the highest concentration standard. This was done to mimic a complex matrix of sample containing the same unknown such as the human serum. We intent to measure the human albumin inside a complex human serum matrix. We analyzed the unknown sample contain in our six standards. The fluorescence droplets intensity can be seen on Figure

3.4D with the six standards peaks different from each other. We also present the temporal sampling analysis (Figure 3.5D) showing constant droplet traces for all the standards as well as constant slope, R^2, and y-intercept. The concentration trace of the unknown (dark blue) is also shown in this figure and seems to be noisier than the standard. The noise is also present in the slope, R^2, and y-intercept trace (see inset in Figure 3.5D). We suspect that this noise is generated in the calculation from the lowest concentration standards that have similar signal. We obtained a very linear response from the system (Figure 3.6D) with and R^2 of 0.9995 from the system proving that our system is best suited for analyses of complex matrix. The unknown concentration not only matches the known concentration but also matches the results obtained from the mixed mode since unknown 1 from that experiment was used.

3.4 Conclusion

This work took the automated microfluidic sample chopper μChopper one step further by increasing the number of samples to be analyzed in a single run. The next generation μChopper included six sampling channels and was capable of performing various analytical modes. We have successfully investigated the constant calibration mode, the mixed mode, the multiplex mode, and the standard addition mode and we have shown real time signal measurement with temporal characteristics such as the slope, the y-intercept, and the R^2. A continuously changing sample with constant standard was characterized with fluorescein and our device successfully measured the changing concentration even when the settings were intentionally changed proving 1/f noise reduction in the system. For the case where there is multiple unknowns to be analyzed, we have set up a mixed mode with 3 unknowns and 3 calibration standards, and successfully determined the concentration of the unknowns even with abnormality occurring at the droplet formation regions. We also investigated the multiplex mode where a single reference was used to measure 5 different sample in a single run. With this mode up to 3 reference can be used to measure 3 different sample

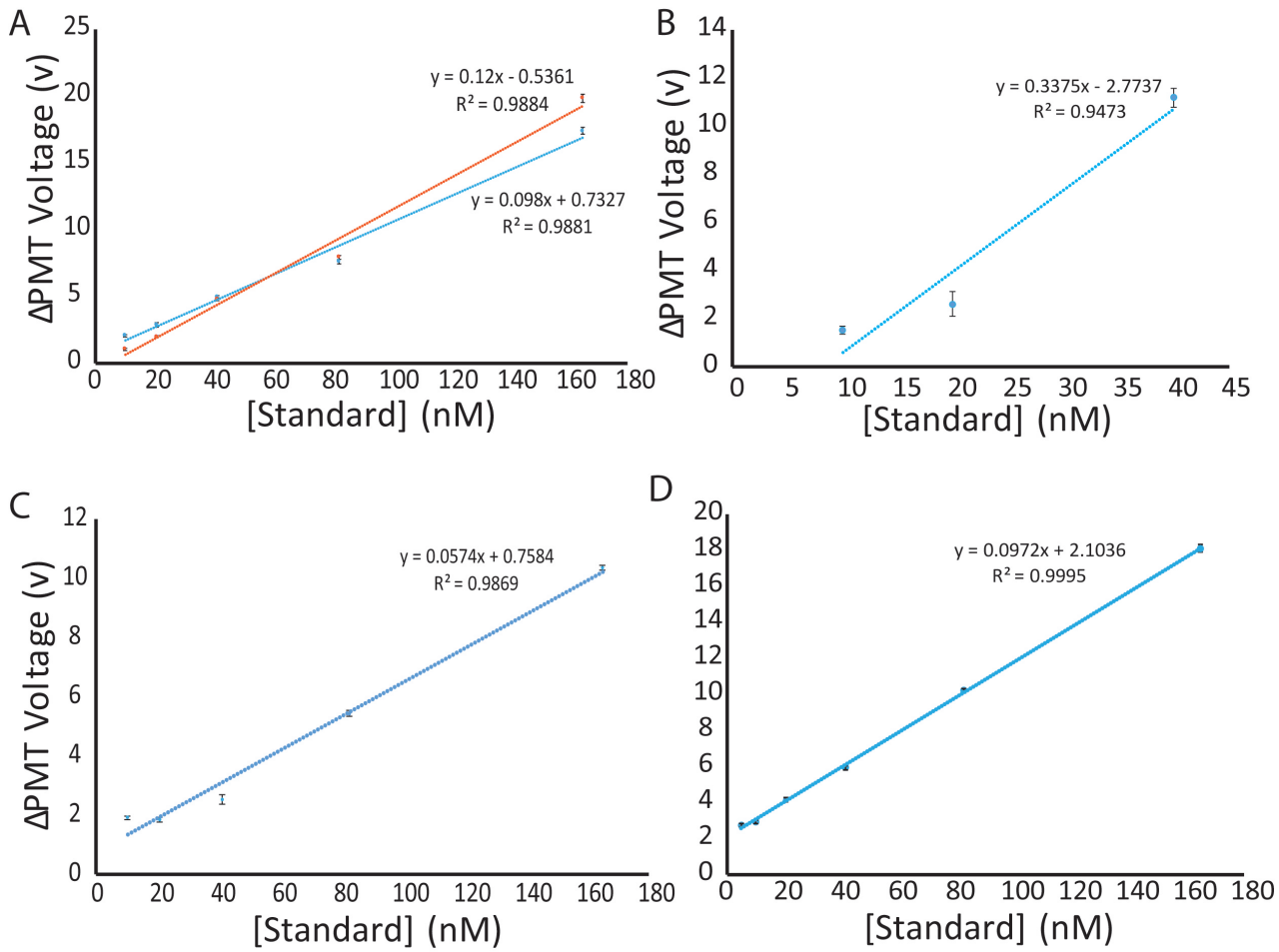

Figure 3.6: Standard curves of different analyses modes
(A) Standard curve of the temporal sampling with constant calibration showing the standard curves of data before PMT offset move (red) and after PMT offset move (blue). (B) Mixed mode (3 unknown samples and 3 calibration points). (C) 5 points calibration in continuous calibration mode. (D) on-chip standard addition method in continuous calibration mode.

thus increasing the multiplexity. Last but not least, we have successfully perform on-chip standard addition method which is useful for complex matrix samples, and we accurately determined the unknown concentration in the matrix. According to these results, we can now measure a continuously changing sample namely, the gylcerol enzyme assay, various unknown at the same time, lock-in detection with constant referencing of samples, and human albumin contained in complex matrix such the human serum. Our next-generation μChopper is the ideal tool to perform rapid measurements and to greatly reduce 1/f noise and human error.

Chapter 4

Quantitative measurement of proteins at attomole levels via active microfluidic sampling and homogeneous proximity assays

4.1 Introduction

Rapid and sensitive proteins quantification methods are fundamental requirements for advances in medicinal diagnostics. Especially for metabolic diseases where early detection can be vital for a patient. An example of such disease is the diabetes melitus where the body's ability to produce or respond to the hormone insulin is impaired. The survival of a patient suffering from this disease is uniquely based on regulating the amount of insulin produced by the body. To do so, it is necessary to measure the amount of insulin in the blood[170, 140, 145, 146]. Immunoassays are well equipped for protein detection in miniaturirized devices. However, these assays involve tedious chemical processes that require complex device engineering. The enzyme linked immunosorbent assay (ELISA) is the traditional and most widely known protein detection method used in microfluidics[171, 172, 173] because of it high specificity and dynamic range. This assay uses a captured antibody attached to the surface of a microplate well to specifically bind a target protein. However, ELISA is a tedious and expensive assay because of large volume sample and reagent consumption an require washing steps. There remain a need for method permitting rapid insulin quantification with simple mix-and read workflow. In the microfluidics field the current focus is being on adapting tedious assays such as polymerase chain reaction (PCR)[174], the recombinase polymerase amplification (RPA)[175, 176], bead-based assays using antibodies or aptamers[177, 178, 179], and quantum dots (QD)[180] to microfluidic platforms. A homogeneous assay that require only one step mix-and-read process is ideal for protein detection[121]. We have previously present a homogenous assay where temperature could be used to discriminate between bound

and unbound complexes[181]. Here we present a novel homogeneous mix-and read assay which uses aptamers or antibodies, and is based on the proximity of a fluorophore and a quencher when the the antibody/aptamer binds to the target protein.

Microfluidics is well known for its low volume sample consumption and has been successfully applied to protein detection[182, 183]. However, the fluids in such system possess laminar flow behavior and require relatively long time to diffuse and then produce chemical reaction. The difficulty of mixing in continuous flow microfluidics has prone some device engineering to overcome the laminar flow[184]. However, these mixing technique have low efficiency and require complex fabrication processes. The Quake group had invented a device where a peristaltic pump can be applied to a ring to perform rapid mixing. This method proved very efficient and its implementation into various application is poorly exploited.

In this work, we combine a custumized nanoliter rotary mixer[30] with our newly developed proximity assay, which permit selective, direct-readout fluorescence quantification of proteins in picoliter-to-nanoliter volumes. The assay is a homogeneous "mix-and-read" assay[185, 121], where immoblization of antibodies and washing steps are not required. It based on Förster resonance energy transfer principle (FRET) with a pair of highly specific DNA oligo-conjugate antibodies or aptamers, where one is labeled with a fluorophore and the other is labeled with a quencher, and a connector. The connector is a complementary short DNA strand that anneals with the 5' of one DNA oligo-conjugate and the 3' of the other and brings the fluorophore and the quencher at close proximity (Figure 4.1). As a result, the fluorescence signal is reduced. Thus, the assay is refered to as proximity FRET assay (pFRET). The rotary mixer microfluidic device has been proven to achieve rapid effective mixing compared to other mixing techniques in continuous flow systems[186, 187, 188, 189]. We have modified the rotary mixer to minimize dead volume, increase pump volume, sample metering, and loading. Our modified rotary mixer is capable of performing fast mixing in only 2.2 seconds and we also demonstrated protein detection and quantification using thrombin and insulin.

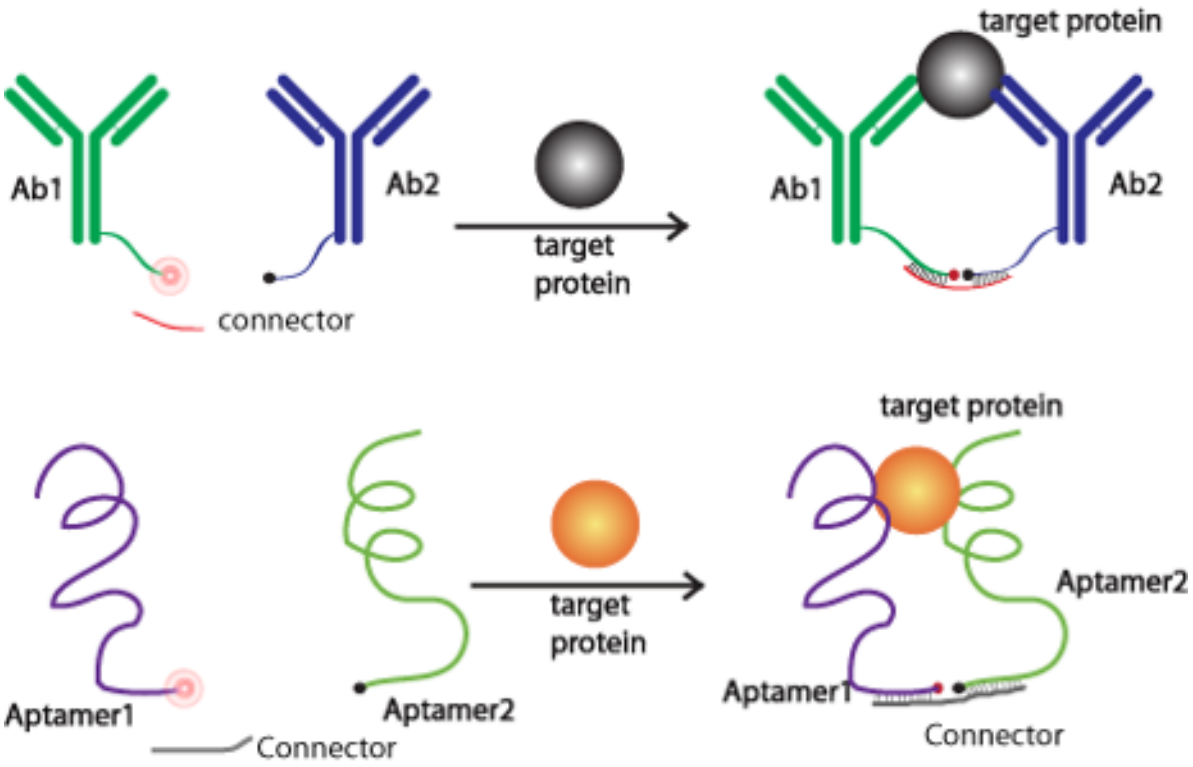

Figure 4.1: Schematic of the pFRET assay
The pFRET assay uses a pair of antibodies or aptamers and a connector. Ab1 or aptamer1 is labeled with a fluorophore and Ab2 or aptamer2 is labeled with a quencher. At the presence of a target (grey or orange) protein, a complex is formed bringing the fluorofore and the quencher at close proximity.

4.2 Experimental section

4.2.1 Reagents and materials

Polydimethylsiloxane (PDMS) precursors, Sylgard 184 elastomer base and its curing agent were purchase from Dow Corning (Midland, MI). AZ 40XT-11D positive photoresist and AZ 300 MIF developer was from AZ Electronic Materials USA (Somerville, NJ). The negative photoresist, SU-8 2050 was obtained from Michrochem (Westborough, MA). Silicon wafers for PDMS molding was acquired from Polishing Corporation of America (Santa Clara, CA). Tubing (TGY-020-5C; 0.02 in. ID, 0.06 in. OD, 0.02 in. wall) and blunt needles (NE-223PL-C 22G) to interface syringes and devices were obtained from Small Parts (Logansport, IN, USA). All solutions were prepared with deionized, ultrafiltered water (Fisher

Scientific). Bovine serum albumin (BSA, 98%) were from EMD Millipore (Darmstadt, Germany). Insulin antibodies (clones 3A6 and 8E2) were from Fitzgerald Industries (Acton, MA). The following reagents were from Sigma-Aldrich (St. Louis, MO) and used as received: Human thrombin, Sodium chloride (NaCl), Tris(hydroxymethyl)aminomethane hydrochloride (tris-HCl), Magnesium chloride ($MgCl_2$), agarose (low gelling temperature, A9414-5G). Fluorescein was obtained from Alfa Aesar (Ward Hill, MA, USA). Oligonucleotides were obtained from Integrated DNA Technologies (IDT; coralville, Iowa), with purity and yield confirmed by mass spectrometry and HPLC, respectively. Sequences for aptamer based pFRET and antibody based pFRET were as follows. Thrombin aptamer A (Thr1_BHQ1): CAG TCC GTG GTA GGG CAG GTT GGG GTG ACT TTT ACT TTC TGC ACG ACA CTT TGG AAC AGC /3IABkFQ/; Thrombin aptamer B (Thr2_TAMRA): /55-TAMK/ AAT AAC GTC AGA ATC GTA CTC GGG TGT GAC TAC TGG TTG GTG AGG TTG GGT AGT CAC AAA; connector (Thr-C20): TGA CGT TAT TGC TGT TCC AA; Insulin antibody arm A (AbA_BFQ): /5AmMC6//iSp18/ TCG TGG AAC TAT CTA GCG GTG TAC GTG AGT GGG CAT GTA GCA AGA GG/3IABkFQ/; Insulin antibody arm B (AbB_TAMRA): /55-TAMK/ GTC ATC ATT CGA ATC GTA CTG CAA TCG GGT ATT AGG CTA /iSp18//3AmMC6T/; insulin pFRET connector(C'10-10): GAA TGA TGA CCC TCT TGC TA.

4.2.2 Microfluidic Chip Fabrication

The microchip device was fabricated using standard multilayer soft lithography[95, 190, 191]. The microfluidic channel layout photomask was designed in Adobe Illustrator software, and printed by Fineline Imaging (Colorado Spring, CO) at 65024 DPI resolution. Photolitography processes were carried out in the clean room facility of the Alabama Microelectronics Science and Technology Center. The SU-8/silicon master was fabricated using standard negative photolithography (see Figure 1.11) with channels in length (need to measure the cross section) and served as the pneumatic control channels (thin PDMS layer) mold. Briefly, 32

μm thick negative photoresist (SU-8 2050) was spin-coated onto a silicon wafer and baked for 5 minutes on a hot plate at 95 °C followed by UV exposure using a Karl Suss MA6 mask aligner. The last steps are the post exposure baking of the wafer at 95 °C for 5 minutes and development in SU-8 developer. The AZ-40XT/silicon master was made with positive photolithography (see Figure 1.11) following similar procedure as described for the SU-8 and channel was rounded by reflowing at 120 °C for 7 min.

The device comprises two layers of PDMS. The control layer was obtained by spin coating a mixture of 20:1 ratio of PDMS elastomer and curing agent mixture on the SU-8/silicon master. The fluid layer ($\sim$5 mm thick) was made by a mixture of 5:1 ratio PDMS pouring on the AZ-40XT/silicon wafer master. Both layers are partially cured in the oven for 35 minutes, then the thick layer was peeled off from master, cut, and holes punched (3.5 mm inner diameter for input reservoir, 1.5 mm inner diameter for outlet interfacing with tubing). The PDMS stamps were carefully aligned on the top of the control layer and permanently bonded together by placing in the oven at 65 °C for at least three hours. PDMS replicas were then peeled off form the AZ-40XT/silicon wafer, hole punched (1.5 mm diameter for pneumatic valves control), plasma oxidized,and bonded on a glass substrate. Before loading samples, microfluidics flow channels were treated with Chitosan and O-[(N-succinimdyl)succiny]-o-methyl-poly(ethylene glycol) (mPEG) to make the surface hydrophilic and biocompatibile[192].

4.2.3 Valve and flow control

The pneumatic valves controlling system is shown in Figure 4.2 and comprises a pressure source connected to a pressure regulator, a selenoid system with tubing interfacing with the microfluidic chip, a data acquisition system, and an in-house build valve controller. The valves are actuated automatically with solenoid switchers (LHDA0531415H, The Lee Co., Westbrook, CT) controlled by a multifunction data acquisition system (USB-6002, National Instruments co., Austin, TX). The house nitrogen source provides a pressure source with

a pressure regulator adjusted to 20 psi. Since the PDMS is air permeable, the dead ended control channels were filled with yellow food dyes to prevent air infiltration through PDMS membrane. Valve actuation is regulated through an in-house written LabView application. The LabVIEW program mainly include a case structure within a while loop. The LabView program function in a four steps process, sample loading, mixing, incubation, and washing. Each steps is coded by a seven digit of the binary code associated with the 7 control channels. The samples were loaded into the reservoirs with micropipette and vacuum were applied by pulling the syringes connected to the channel for driving the solution flow through the two channel outlets when valves open.

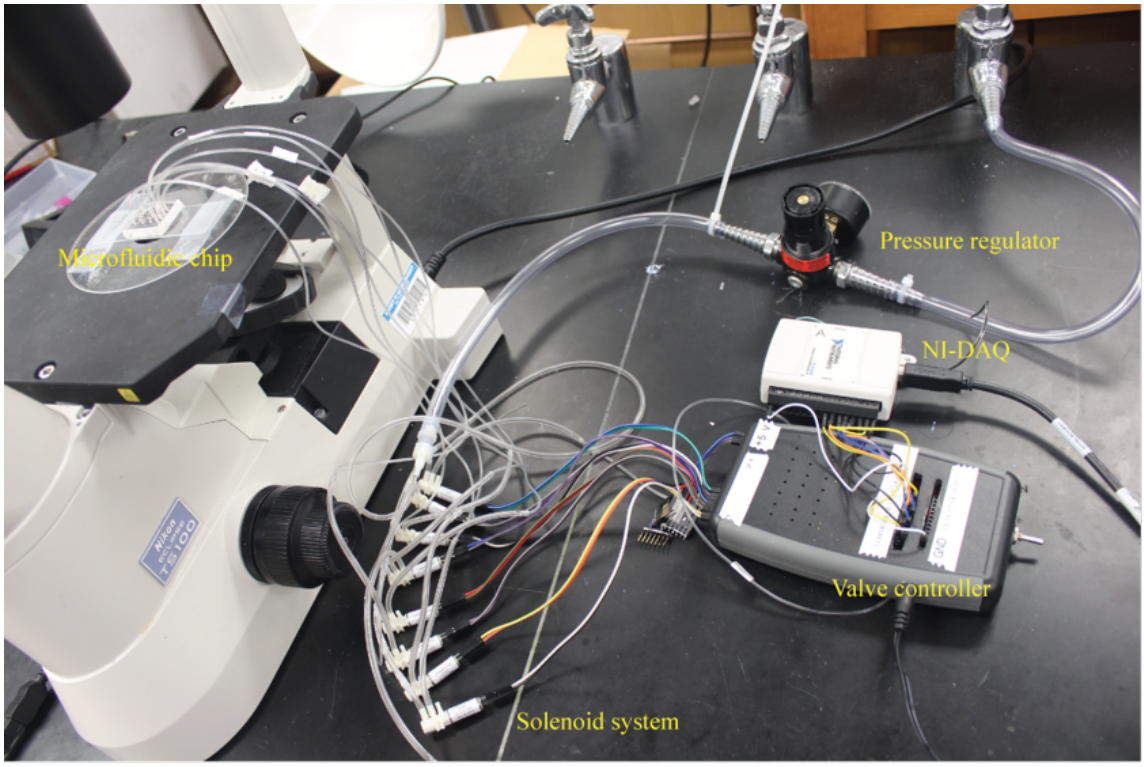

Figure 4.2: Valve controling system
Image of the valve controlling system. Pneumatic valves were connected to a solenoid-switched pressure source (compressed N_2 gas), which was interfaced with a Labview NI-DAQ system. Wide-field and fluorescence measurement was performed directly with a Nikon Ti-E inverted fluorescence microscope.

4.2.4 Sample metering

The assay used in this work requires an equal volume mixture of the antibody oligo-conjugates/aptamers and the target protein to function properly. Therefore, our microfluidic rotary mixer was designed for this purpose(see Figure 4.3). The rotary mixer ring is delimited with microvalves to accurately meter a precise volume of sample on both sides of the ring before mixing. More specifically, there are a total of seven valves on our microfluidic rotary mixer chip where four serve for sample metering. The central valve separates the ring in two parts, one part for sample A and the other for sample B for example. At each side of the ring, there is one valve at the inlet and another at the outlet of the ring to precisely meter 9 nL volume of sample.

4.2.5 Mixing time measurement

Microchip characterization was made by recording videos of the mixing of red and green food dye (Kroger) with a Nikon 1 camera attached to a Nikon Eclipse TS 100 microscope. Green dye was loaded in reference reservoir as well as in sample reservoir A. Red dye was loaded in sample reservoir B. Then vacuum applied to the outlets to fill the channels. Green and red dye were mixed by the 5-step peristaltic pumping with step time at 1 ms, 2 ms, 5 ms, 10 ms, 15 ms, 25 ms, 50 ms, 100 ms, 150 ms, and 200 ms. Viscosity effect was investigated by repeating the experiment with red and green food dye in 0.5% agarose solution. Data analysis was performed using ImageJ and mixing was considered complete when the percent red in the RGB image of the solution was stabilized to <2% deviation.

4.2.6 On-chip serial dilution and channels hydrophilicity treament

Fluorescein was dissolved into Tris-HCl (2.5 mM tris-HCl buffer, pH 8.0) to make 36.5 mM of stock. Next, 200 nM fluorescein was made from the stock(200 nM in 2.5 mM tris-HCl buffer, pH 8.0). This solution was then used as starting concentration for our on-chip serial dilution experiment. The two samples were mixed and the fluorescence pictures of

fluorescein in the channel were recorded by the camera attached to the microscope with 20X lens. Images were obtained with a fluorescence microscope (Nikon Eclipse Ti) and analyzed with imageJ. The mixing and measurement were repeated. This process was repeated 8 times. The fluorescent intensity was normalized by the reference fluorescein (200 nM in 2.5 mM tris-HCl buffer, pH 8.0) in the reference channel.

Channels modification was made following the protocol described in reference [192]. In short, the process started by pumping the Chit solution (pH=6.00, 0.01%, w/v) through the PDMS microfluidic channels with a vacuum pump. This followed by incubation for 5 minutes to allow the Chit to be adsorbed by the PDMS. After PDMS adsorption, the channels are flushed with distilled water for 10 minutes then the channels are filled with NSS-mPEG solution and kept at room temperature for 4 h. The final step in the process was to flush the channels with BGE for 10 minutes. Lastly, to protect the channels from hydrophobic recovery, the microfluidic chips are wrapped in plastics and stored at 4 °C. The hydrophlicity was tested by performing serial dilution of fluorescein in the channels.

4.2.7 Thrombin quantification by pFRET assay

All pFRET assays were performed in Tris binding buffer: (50 mM Tris (pH7.5), 100 mM NaCl, and 1 mM $MgCl_2$, with or without 1% BSA). Fluorescence images were recorded on a Nikon Ti microscope with a filter set for TAMRA. Thrombin aptamers (1 M) were dissolved in binding buffer, heated at 94 °C for 7 min, and then quickly cooled in iced water. After these treatments, each aptamer would form its specific secondary structure. Then the probe mix was made by diluting two aptamers (Thr1_BHQ1, Thr2_TAMRA) to 300 nm in binding buffer (1% BSA), and mixing with the connector (Thr-C20, 1% BSA binding buffer) at a 1 : 1: 1 ratio. Various concentrations of thrombin were diluted in binding buffer (1% BSA) as the samples. The probe mix (10 μL) and sample (10 μL) were added into sample reservoir and the probes reservoir, respectively, and then mixed by the 5-step peristaltic pumping with step time at 10 ms for 90 s. The LabView program was made to automatically switch

between sample loading, mixing, incubation, and wash steps. Therefore, right after mixing, the mixture was incubated at room temperature in channel, and the fluorescent images were taken in a selected squared area including both the reference channel and sample channel every 3 min for 30 min. To reduce photo-bleaching effects, the light source was only turned on right before measurement and turned off after. When all the measurement of one sample finished, the microchannel was washed as flollows: the solution in the reservoirs were taken out with pipette, washed with binding buffer (1% BSA, 20 μL) twice, and loaded with binding buffer (1% BSA). After loading the buffer, a vacuum was applied to both of the channel outlets for 30 s to fill the channels. Then the fresh buffer was driven circulated in the channel automatically for 90 s to remove any residues from the previous solution. The rinsing and circulation steps were repeated one more time before the loading the next sample. Data analysis was performed using ImageJ and the photo-bleaching effect was corrected by the reference probe mix in the reference channel.

4.2.8 Insulin pFRET assay on chip

The insulin pFRET probes were made as previously described[193, 122] by covalent attachment of AbA_BFQ to insulin antibody 3A6 (probe: 3A6_BFQ) and AbB_TAMRA to insulin antibody 8E2 (probe: 8E2_TAMRA), respectively. Conjugation and purification were accomplished using the Antibody-Oligon-conjugate All-In-One Conjugation Kit (Solulink), according to the manufacturers instructions. The final conjugate concentrations were determined via the BCA protein assay. For insulin pFRET, the probe concentration were as follows: 50 nM each of the pair of insulin antibody-oligonucleotide conjugates and 70 nM of DNA connector. The rotary mixer chip was placed in the 37 °C incubator on the microscope stage. The measurement were similar as the thrombin pFRET: Various concentrations of insulin were diluted in binding buffer (1% BSA) as the samples. After the probe mix (10 μL) and insulin sample (10μL) were loaded and mixed, the fluorescent images were taken in the square area including both the reference channel and mixer every 15 s for 15 minutes. The

reservoir and the channels were rinsed twice with the next sample before each measurement. Data analysis was performed using ImageJ.

4.3 Result and discussion

4.3.1 Device design and Operation

The rotary mixer chip design consist two layers of PDMS (Figure 4.3). The pneumaic control layer is made of a thin PDMS (40 μm) and contain 7 channels (black). The fluidic layer is made of a thick PDMS (5.5 mm) and contains the rotary mixer ring of diameter 1.72 mm with two input and two output channels, and a reference channel. The total volume of the rotary mixer is 18 nL, with about 9 nL on each side. The ring of the rotary mixer has been twisted toward the center, in order to reduce the dead volume to nearly zero. To increase the mixing efficiency the pump volume was increased by enlarging one portion of the ring at the cross section with the central valve of the peristaltic pump. Automatic control of the rotary mixer was enabled with a LabView program. The chip operation and the valve actuation scheme are presented on Figure 4.4. The two side of the ring was divided by the control valve 2, and samples and reagents were loaded into the half of the ring separately so there is no risk of diffusion between reagents before mixing. Furthermore, accurate volume metering and sample manipulation are achieved with this method. First, sample A (e.g. pFRET antibody probes) and sample B (Protein target) are loaded respectively by opening valve 1 and 3 and applying vacuum at the outlets. Second, The solutions in the ring were confined by closing the valve 1, 3, and 7, and mixed by opening valve 2 and applying peristaltic pump using valve 4, 5, and 6. Last, after the mixing step, the homogeneous mixture is incubated, measured and washed to prevent contamination of the next sample.

4.3.2 Rotary mixer design allows rapid mixing

We have designed a microfluidic rotary mixer for fast mixing of reagents. The mixing is performed by peristaltic pump[95]. Since the pump volume is determined by the central

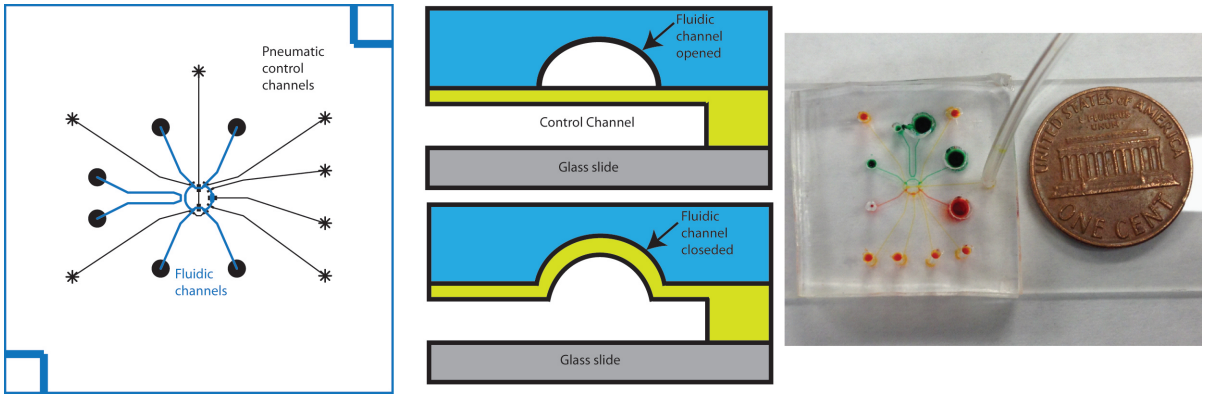

Figure 4.3: Rotary mixer chip design
Microfluidic rotary mixer device layout (left) with fluid channels in blue and pneumatic control channels in black. The diameter of the rotary mixer ring is 1.7 mm, with sampling volumes of 9 nL and a total volume of 18 nL. Chip fabrication was accomplished by multilayer soft lithography (middle). Flow channels were molded into polydimethylsiloxane (PDMS) using patterned AZ 40XT positive photoresist, rounded by thermal reflow; squared control channels were molded into PDMS using patterned SU-8 negative photoresist. Rounded flowing channel ensures complete closure of fluidic channels by valves. Image of rotary mixer chip (right).

valve of the peristaltic pump, the key to achieve fast mixing was the enlargement of the central valve area. The rotary mixer fluidic channels were filled with red and green food dye on both sides respectively and the control channels were filled with yellow food dye (Figure 4.3 right). Rapid mixing of the food dyes was recorded with a Nikon 1 camera and analysed with imageJ. The mixing is done by opening valve 2 separating both fluids in the ring and pumping the fluids around the ring for a defined period of time while maintaining valve 1, 3, and 7 closed. The mixing occurs due to the parabolic profile of the Poiseulle flow in microfluidic channels. As two fluids rotating in the rotary mixer, the center of each fluid flows faster than the edges. Therefore, the interface between the two fluids keep stretching and wrapping around each other, thus forms a long and thin stream, which allows the diffusion to occur quickly across the interface and results in fast mixing. So the mixing efficiency of the rotary mixer is determined by the pumping frequency and the volume pumps in each cycle. The volume of sample injected by the peristaltic pump in each pump cycle equals to the dead volume under the middle valve of the peristaltic pump[194]. We investigated the

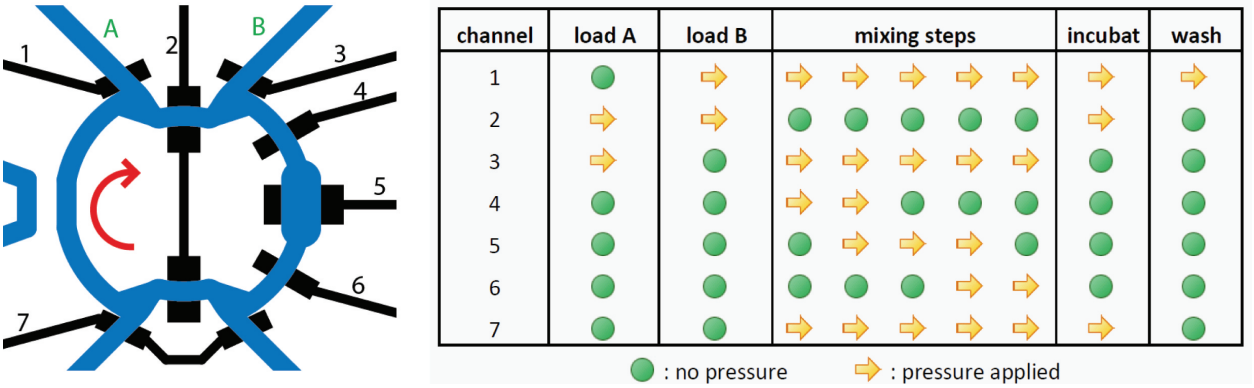

Figure 4.4: Rotary mixer chip operation
The rotary mixer is automatically controlled by applying pressure to the 7 pneumatic valves (left) with the tabulated program (right).

pumping efficiency of our rotary mixer and the result is shown in figure 4.5. The channel of the rotary ring is 137 μm wide, and the width of enlarged valve is 270 μm. The channels area is of a half ellipse with a height of 28 μm. With these parameters we obtained a maximum pumping volume per cycle of 356μL/s and maximum pump frequency of 200 Hz. These values are by far higher than other rotary mixers found in literature[194, 195].

The mixing time was extensively investigated with red and green food dye in the rotary mixer (Figure 4.5). As shown in Figure 4.5A, rapid mixing was achieved, as fast as 2.2 s. We also investigated the viscosity effect by diluting red and green food dyes in a solution containing 0.5% agarose , the fastest mixing time of 2.44 s at cycling time of 25 ms, which suggest our device is suitable for the fast mixing of viscose fluids. The Reciprocal of mixing time showed a linear response with cycle frequency between 1 Hz to 20 Hz (Figure 4.5B). The mixing time at higher frequency diverged from the linear line due to the responding time requirement of the solenoid system or the valve membranes, which suggest the optimal mixing frequency is around 20 Hz (50 ms cycling time). Figure 4.5C shows snapshots video of the mixing where the red and green food dyes can be seen in the rotary mixer before, during, and after mixing.

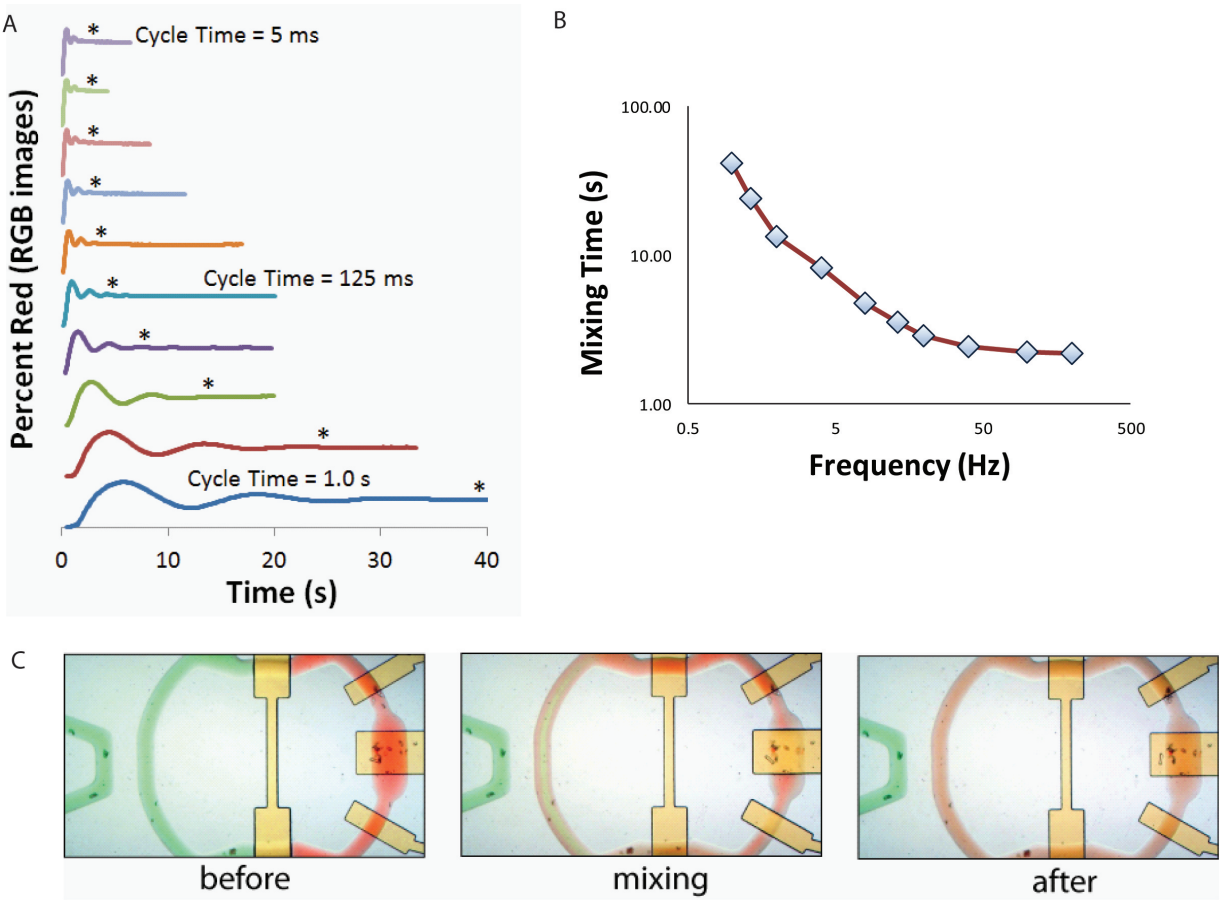

Figure 4.5: Rotary mixer characterization
(A)The extent of mixing over time was studied as a function of pumping cycle time. Mixing was considered complete when the percent red in the RGB image of the solution was stabilized to <2% deviation. Rapid mixing was achieved, as fast as 2.2 s, a significant advantage for secretion sampling purposes. (B) The plot of mixing time with cycle frequency shows that mixing is optimal at a cycle frequency of around 20 Hz. (C) Characterization of the device was accomplished initially with food dyes. the rotary mixer ring was filled with 9 nL each of red sample and green probes (left), which were then mixed by peristaltic pumping around the ring.

4.3.3 Nanoliter Serial Dilution

Accuracy of the mixing volume between the two sides of the ring channel is studied by serial dilution of fluorescein into Tris buffer. Theoretically, the standard dilution curve follows the equation $C_n = a^n C_0$, with **a** as the dilution factor, C_n as the diluted concentration, C_0 as the initial concentration, and **n** as the dilution number. The relative fluorescence ratio between fluorescein and the buffer solution was measured. Images was recorded with a

CCD camera on an inverted fluorescence microscope. As shown in Figure 4.6 (left), the experimental standard dilution curve lies perfectly on the theoretical curve with dilution factor of 0.456. Although the experimental dilution factor is different from that of the theoretical dilution factor (0.5), this would not affect the efficiency of our assay since the difference in volume is only about 9%. The difference in the dilution factor is due to the enlarged volume of the central valve of the peristaltic pump, and the difference between the volumes of two sides of the ring, the device still ensure the accuracy in sample preparation and metering samples for biological assays. The result also proved the surface treatment prevented the non-specific binding of fluorescein to the PDMS surface. Since no fluorescence adsorption by the PDMS channels is observed in Figure 4.6 (right), we can conclude that our channels wall were biologically compatible.

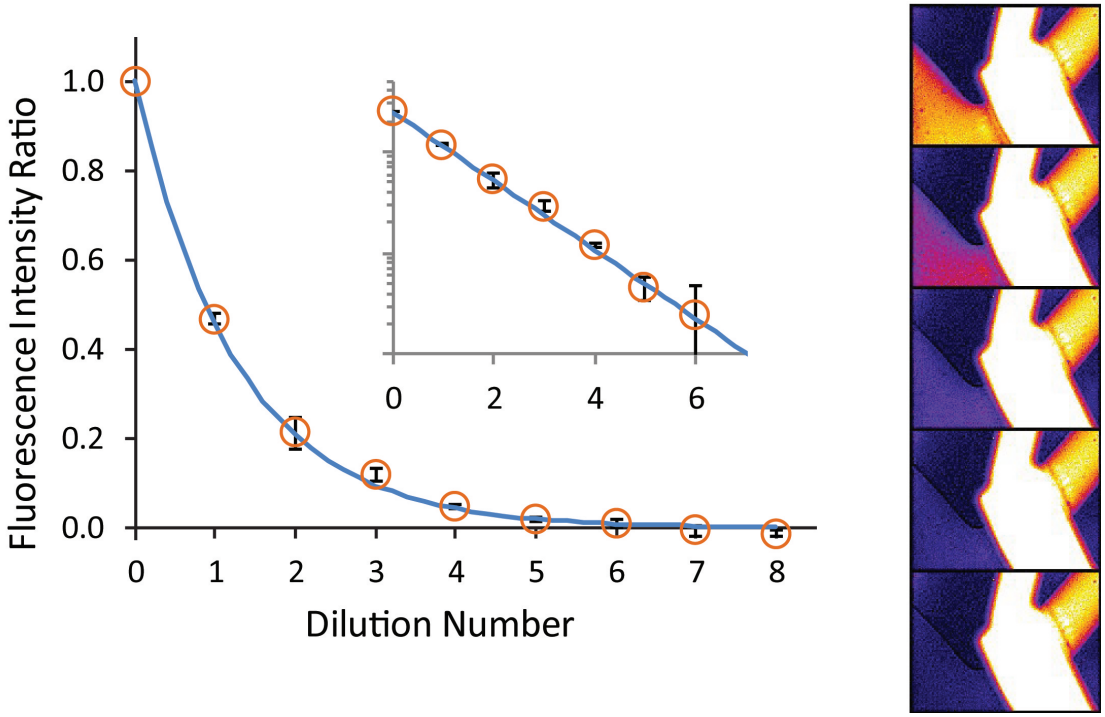

Figure 4.6: Nanoliter volume serial dilution
The experimental serial dilution curve with a 0.455 perfectly fitted the theoretical serial dilution curve. The inset curve is the logscale of the serial dilution curve showing the linearity of the method (left). Fluorescence images of the serial dilution showing a gradual decrease in fluorescence intensity (lower left corners). These images also account for the surface treatment done with the Chit-mPEG to render the channels surface hydrophilic.

4.3.4 Thrombin quantification on-chip

To demonstrate the potential utility of the device for direct optical protein quantification, thrombin concentration was measured with pFRET assay. For this experiment highly specific Thrombin binding aptamer was used. The aptamers were purified using HPLC and GC. Two atptamers (Thr1_BHQ1, Thr2_TAMRA) that bind to different sites on thrombin molecule were used as affinity probes, and a 20-base connector was used to bring the FRET pair (Tamra and Black Quencher) labeled aptamer tails together to ensure a high and consistent FRET efficiency. Varying concentrations of thrombin and fixed concentration probes were loaded and mixed in the device. During the incubation, the relative fluorescence of the sample decreased as a first order reaction kinetics (Figure 4.7). The least square fitting of the data into the first order reaction exponential decay $K = A*e^{(-\lambda t)}+B$. The extent of fluorescence quenching (pre-exponential factor of fit curves, A) was directly proportional to the concentration of the thrombin (Figure 4.7 left). The limit of detection was 180 attomoles. Note that our input sample volume is only around 9 nL. So without extensive optimization, we have detected thrombin at about 180 attomole level. The fluorescence starts to level off after 20 min, but the fluorescence different between samples could be distinguished even at 3 min, which suggest that accurate measurement can be achieved in less time. To minimize the cross contamination between different runs, two-step washing was done, and the assay was did in the order from 0 nM, 100 nM, 20 nM, 150 nM, to 40 nM. The linear response between preexpontential factor and thrombin concentration suggests a sufficient washing, not cross-contamination, and a biocompatable PDMS surface.

4.3.5 Insulin quantification on-chip

We have successfully showed that direct quantification of human thrombin was possible on our device. Here we would like showcase further application to prove that our rotary mixer could be used for sampling and quantification of hormone secretion, which is useful for the detection of early diabetes. With this in mind, we have applied our device to insulin

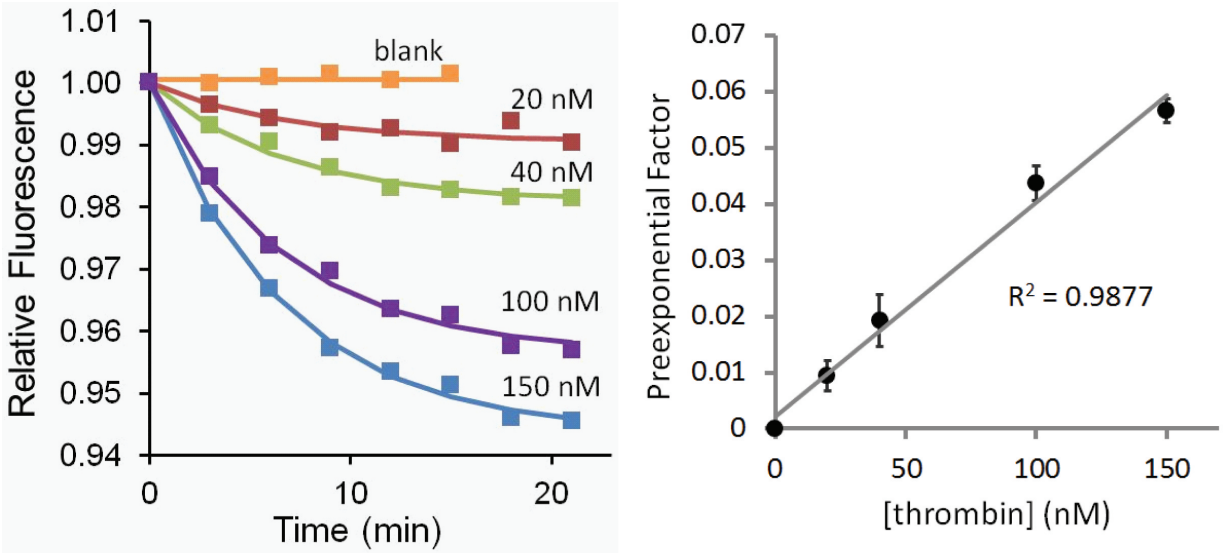

Figure 4.7: Quantification of Thrombin protein using pFRET
Direct optical quantitation of human thrombin using pFRET was achieved by continuous sampling and segmentation of varying concentrations of sample and fixed probe concentration. During incubation, the relative fluorescence of the sample decreased (left). The rates of fluorescence quenching (preexponential factor of fit curves) were directly proportional to the concentration of thrombin (right). Without extensive optimization, we have detected thrombin at the 180 attomole level.

detection since its amount is directly proportional to diabetes mellitus. Since our pFRET assay is perfect for direct readout of small concentration of protein, we diluted 6 concentration of insulin going from 0 to 100 nM. Using these concentrations and a fixed concentration of antibody oligo-conjugate probes at 1:1 ratio mixture and as reference, we loaded reservoir A and reservoir B with sample and probes respectively. The data were recorded after every 0.5 minute using a standard fluorescence microscope equipped with a CCD camera and analysed using imageJ and Excel. Because the on-chip islets culture need to be at 37 °C, we performed the insulin pFRET assay in the rotary mixer at 37 °C with insulin antibody-oligonucleotides conjugates pFRET probes and 10-10 connector which is optimized for 37 °C[122]. The binding of the two antibodies to one insulin molecule bring the FRET pair (TAMRA and BHQ) labeled oligonucleotide tails together to ensure a high and consistent FRET efficiency. With the 10-10 connector, the target-independent DNA annealing, which cause the background signal, was not favored at 37°C. However, the protein-dependent proximity effect largely

increase the complex stability, which result a protein-dependent fluorescent quenching. The insulin quantification pFRET data is shown in Figure 4.8. Similar to the thrombin experiment above, the fluorescent quenching follows first order reaction kinetics and the extent of fluorescence quenching (pre-exponential factor) was directly proportional to the concentration (Figure 4.8 left). The standard curve (Figure 4.8 right) was also obtained using the pre-exponential factor A from the Figure 4.8 left versus the concentrations of the insulin. Overall, we was able to observe the fluorescence decay from 6.25 nM insulin concentration in only 1.5 minutes. Thus, we were able to quantify insulin as low as 128 attomoles proving that with our microfluidic rotary mixer is useful for rapid quantification of proteins. Therefore, can be used for detection of metabolic diseases at their early stage.

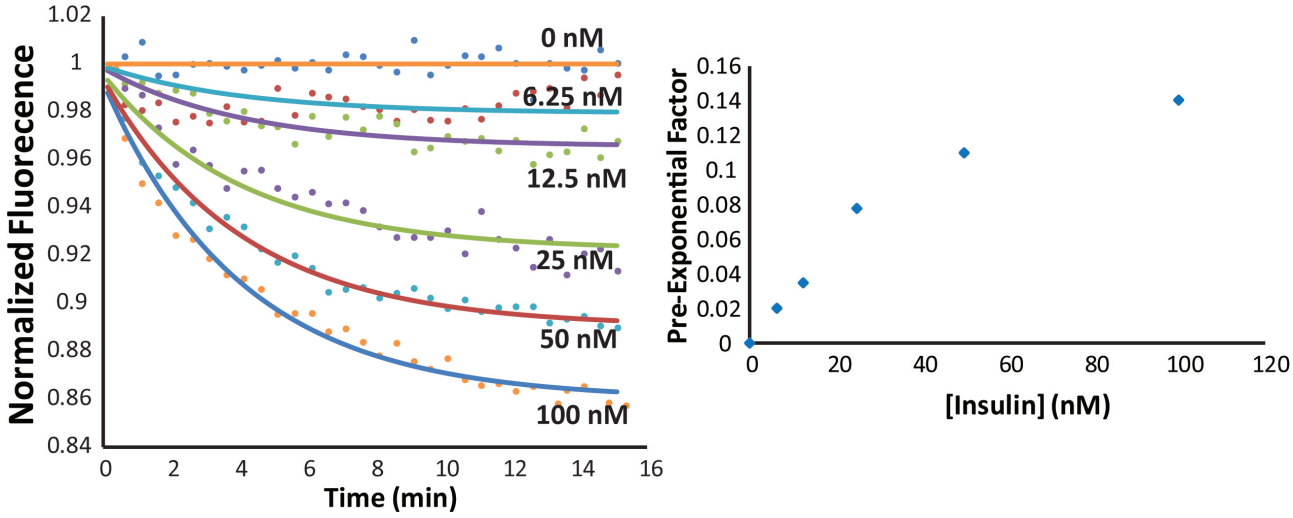

Figure 4.8: Insulin quantification by pFRET
The microfluidic rotary mixer was used for the quantitation of small amount of insulin using pFRET assay in a simple optical system. The relative fluorescence intensity decreases when the target insulin molecule is present in the solution; the raw data are shown as doted lines and the exponential fit curve as solid lines (left). Standard curve of insulin pFRET experiement (right).

4.4 Conclusion

We designed a microfluidic rotary mixer that we successfully applied for rapid protein quantification using proximity assay. In this study, we showed proof-of-concept of rapid, sensitive, and selective protein quantitation in a nanoliter continuous flow system using a simple optical readout. Due to automation enabled by a valve system, we obtained a mixing time of only 2.2 s. Protein quantification was performed using homogenous pFRET assay with thrombin and insulin as the target proteins. The amount of protein detected was as low as 180 attomoles for thrombin and 128 attomoles for insulin. Therefore we believe that by combining our homogenous pFRET assays with valved microfluidic systems, it should be possible to capitalize on the true potential of these systems for sampling and quantifying hormone secretion. Since pFRET utilizes a dual probe format[193], we should be able to quantify minute quantities of any protein with two antibodies using this system. In particular, our functional insulin pFRET assays should be ideally suited for secretion quantitation from pancreatic islets.

Chapter 5

Frequency Dependence Characterization in microfluidic autoregulator

5.1 Introduction

Microfluidic self-regulators are the impending solution to greatly reduce the necessity of expensive and complex external flow controllers (i.e. syringe pumps)[196, 197, 198, 199]. Maintaining a constant flow rate (Q) over a wide range of pressure (ΔP) could provide time reslolved information when studying cell secretion or organs on chip[138, 200, 201]. Therefore, controlling flow rate can be imperative especially where there is a need to mimic dynamic environment. Microfluidic self-regulators not only increase the integration and miniaturization capability of the device but also they are useful where flow control is a contributing factor to the task in hand[202, 203, 204, 205]. The microfluidic autoregulator design involves a straight fluidic channel with a detour forming a Quake valve (normally open valve, NO)[196, 108]. This device has been demonstrated to effectively maintain a non-linear relationship between the flow rate (Q) and the change in pressure (ΔP). However, the frequency response of the PDMS membrane forming the regulator valve has not yet been studied. This is a very important factor to consider when integrating the autoregulator function in conjunction with other function in an integrated system.

In microfluidics, an integrated system combines multiple functionalities into a single microfluidic chip to achieve one common goal. Just like an electronic circuit, a microfluidic device posseses analogue components that are used to perform similar tasks. For example, the flow rate in microfluidics is an analogue to the electric current, the pressure to the voltage, the fluidic channel to the electric resistor, the membrane deflection to the capacitors, and the valve to the transistors[24]. Therefore, electronic circuit have been used to design microfluidic analogue devices. Some prominent example include the works where microfluidic devices

have been designed to function as digital logic circuits[94, 206, 207] band-pass filters[24], and oscillators[105, 208]. These electric circuit models accurately predicted the microfluidic analogue behavior and confirmed the close proximity between electronic and microfluidic components.

Similarly, an electronic model of a circuit with a current flow that is independent to the voltage could help us to understand the behavior of microfluidic self-regulators, especially the dynamic response of a normally open (NO) valve during regulation. A step-wise approach is necessary for this study which we initiate in this chapter. First, the electronic circuit is designed to simulate response to current and voltage. Second, these responses are used to predict the response of the microfluidic analogue. Finally, a microfluidic analogue of the circuit is fabricated to closely match the characteristics of the electronic circuit, and the fluidic circuit is tested for its similarities and differences. These steps help in the design and to better study microfluidic components in a more complex system.

In the present study, we report a microfluidic self-regulator (i.e. autoregulator) with a downstream valve placed after the regulator valve to enable frequency studies. The valve can be pulsed at different frequencies to observe the dynamic response of the regulator's membrane valve. To do so, we first simulated the autoregulation of the device with a computer program to predict the membrane behavior. Since microfluidic devices behave like electric circuits, the goal was to match the operation of our electronic simulation to our microfluidic autoregualtor and obtain useful information about the regulation membrane's behavior. Real time measurement of the flow rate at various frequencies is also reported using a fluorescence microscopy technique. Finally, we introduced a current mirror fluidic circuit exploiting an autoregulator that controls the flow rate within its circuit as well as a parallel circuit. This fluidic flow mirror is also characterized at varying frequencies.

5.2 Experimental Section

5.2.1 Materials, Reagents, and Methods

Materials for the microfluidic chip fabrication were obtained as follows: Silicon wafers from Polishing Corporation of America (Santa Clara, CA, USA), AZ-40-XT photoresist and AZ 300 MIF developper from AZ Electronic Materials (Branchburg, NJ, USA), polydimethylsiloxane (PDMS) procursors, Sylgard 184 elastomer base and curing agent from Dow Corning (Midland, Maryland, USA), SU-8 phoresist and SU-8 developper from Microchem (Westborough, MA, USA), and Tygon tubing (TGY-020-5C; 0.02 in. ID, 0.06 in. OD, 0.02 in. wall) and blunt needles from Small Parts (Logansport, IN, USA). The reagents used in this work were obtained as follows: 4-2-hydroxyethyl-1-piperazineethanesulfonic acid (HEPES) buffer from Sigma-Aldrich (St. Louis, Missouri, USA),Tris(hydroxymethyl)aminomethane hydrochloride (tris-HCl)and fluorescein were from Alfa Aesar (Ward Hill, MA). USA).

5.2.2 Falstad Circuit Modeling

A free electronic circuit simulation software (http://www.falstad.com/circuit/) was used to build a prototype circuit with a constant current flow at various potentials. The basis of self-regulation relies on a p-channel MOSFET where the source and the gate are connected to the similar voltage source. The voltage source used is variable and produces real time current flow. The resistance of the circuit is represented by a 140 Ω and 25 Ω placed before the source and after the drain respectively. The circuit is then connected to the ground to allow the current flow. When the voltage is varied to a certain threshold (25 volts), the current flow tends to becomes constant. Similarly, another circuit is build to simulate current mirror[209, 210] with a 30 Hz variable voltage source and keeping the resistors at the same values. Next, a microfluidic analogue of the electronic circuit was designed and fabricated matching the analogous values of the electric circuit components. Time units (s) were held consistent, while units of fluidic resistance (kPa.s.mm^{-3}), pressure (kPa), and flow rate (mm^3

s^{-3}) were assumed to be equivalent to their electrical counterparts of resistance (Ω), voltage (V), and current (A), respectively by adjusting the values of a microfluidic system.

5.2.3 Microfluidic Chip Fabrication

The microfluidic device fabrication begins with the design of the channels layout using Adobe Illustrator software. After that, the design is sent to Fineline Imaging (Colorado Springs, CO) for photomask printing at 50 800 dpi resolution (positive and negative images respectively). The positive and negative photomask are used to fabricate two master wafers where one is used for the pneumatic control layer and the other for the fluidic layer. The photolithography for master fabrication is perform with an in-house built UV light source based on 365 nm LED array after a few modification of the recent design detailed by Groisman et al.[142]. The last step in the fabrication is to make a two layers of patterned PDMS microfluidic chip following standard soft lithography guidelines[96]. The total thickness of the PDMS microfluidic chip is 5 mm including the pneumatic control layer (thin lower layer) making 70 μm thick. The channels high is defined by spin coating the SU-8 2050 (negative photoresist) and AZ-40XT (positive photoresist) onto a silicon wafer. Both wafers are used for the pneumatic channels and the fluidic channels respectively. For the pneumatic control layer, the wafers are baked on a hot plate at 95 °C for approximately 5 minutes before the exposure to the 330 $\sim$mJ/cm^2 UV LED source. To obtain the SU-8 patterned master, the wafer is hard baked for 5 min at 95 °C and then developed for 5 min in the SU-8 developer to reveal the pattern. The fluidic channel is made by spin-coating 40 μm AZ-40XT positive photoresist onto another wafer and soft bake at 126 °C for 5 minutes, followed by wafer development in AZ 300 MIF developer to obtain squared feature channels. The rounded cross-section channels are made by heating the wafer at 120 °C for 7 minutes in a process called "reflow".

After photolithograpy procedures, the two layers PDMS microfluidic device can now be molded. Firstly, the bottom (control) layer is made by spin-coating 20:1 ratio mixture of

PDMS precursor and curing agent respectively onto the SU-8 patterned wafer to make a thin PDMS layer, 20 μm membrane above the channels. Secondly, the upper layer (thick fluidic layer) is made by pouring 5 mm of 5:1 PDMS ratio mixture of PDMS precursor and curing agent onto the AZ patterned wafer with rounded features. Both PDMS layers are partially cured at 65 °C for ∼35 minutes. Thereafter, the thick fluidic layer is quickly peeled off, hole punched for the fluidic inlets and outlets, cleaned with methanol, air dried and then aligned to the thin control layer using a top view microscope. Thirdly, the assembled layers are cured at 65 °C in an oven for 3 hours to allow the two layers to permanently bond. Fourthly, the bonded layers are peeled off the wafer and hole punched for the pneumatic control inlets. To connect the control and the fluidic layer, a via is punched using an in-house buil CO_2 laser tube with focusing optics purchased from Cole Technology C. LTD (Hefei, Anhui, China). This via allows the fluid to flow from the fluidic channels to the detour channel which is a key part of the self-regulation. Afterwards these PDMS layers are again cleaned with methanol, air dried, plasma oxidized, and bonded to a glass slide.

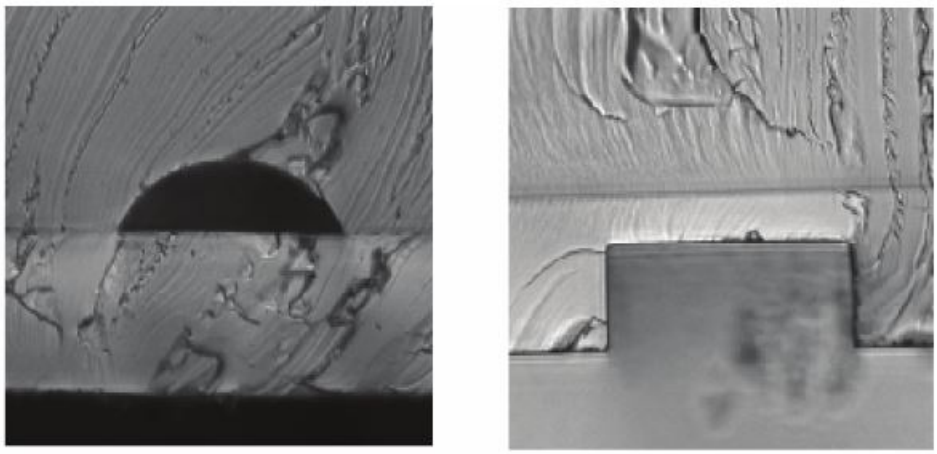

Figure 5.1: Autoregulator channel cross-sections
Az-master made rounded channels of 53 μm height and 112 μm width (left) which were used as the main fluidic channels. Squared channel made with SU-8 master with 143 μm width and 42 μm height (right) which was used as the self-regulated channel that operates a push-up membrane into the rounded fluidic channel. ROI region cross-section for the autoregulator current mirror (38 μm high and 477 μm wide).

5.2.4 Flow control and regulation

The microfluidic devices reported in this chapter control and automatically regulates flow. All devices consist of a regulator valve with upstream feedback to the flow channel by a via connection. This regular valve is 400 x 200 μm. For devices with active flow control at a range of frequencies (1 - 32 Hz) we use a pneumatic push up valve ($\sim$200 x 200 μm), which is a normally open (NO) valve formed by intersecting a seoarate control channel with the and fluidic channel[95]. Periodic valve actuation is enabled by an in-house build electronic box coupled to a solenoid system (Lee Co.; LDHA0533115H) and interfaced with an in-house written Labview program (National Instruments). Valve actuation was powered by a regulated pressure source at $\sim$20 psi, and flow was promoted by a manually pressurized 100 mL glass syringe (SGE, Analytical Science). The flow was pulsed periodically by opening and closing the control valve to initiate the regulating membrane response.

5.2.5 Flow rate measurement

In simple devices without active vakves, flow rate was quantified by measuring the displacement of fluid inside a piece of tubing over time. Figure 5.2 shows the experimental setup with a microfluidic chip, a syringe, a 30 cm ruler, a timer, and a stereo microscope. Approximately 80 cm tubing connects the inlet of the microfluidic chip to the syringe and the outlet tubing taped on the ruler. Green or red food dye (Kroger) is filled on the inlet tubing and pressurized through the chip. The flow rate is measured at different pressures ranging from 4 to 70 kPa. The fluid displacement is observed through the microscope by recording the time and and the position of the meniscus at every pressure in triplicate.

For real-time flow rate measurements in later iterations, an imaging method was developed. This method is based on measuring the flow ratio at a ROI and estimating the flow rate with the channel dimension over time. Since the the two fluids meets at the ROI and flow in laminar fashion, the estimated flow rate of both solutions can be calculated using the ROI dimension (Figure 5.2) over time. For example, when the ratio is one-to-one, the flow

rates of both fluids are equal and when the ratio is different, the flow rate is obtained by the percentage of each fluids given by the ratio.

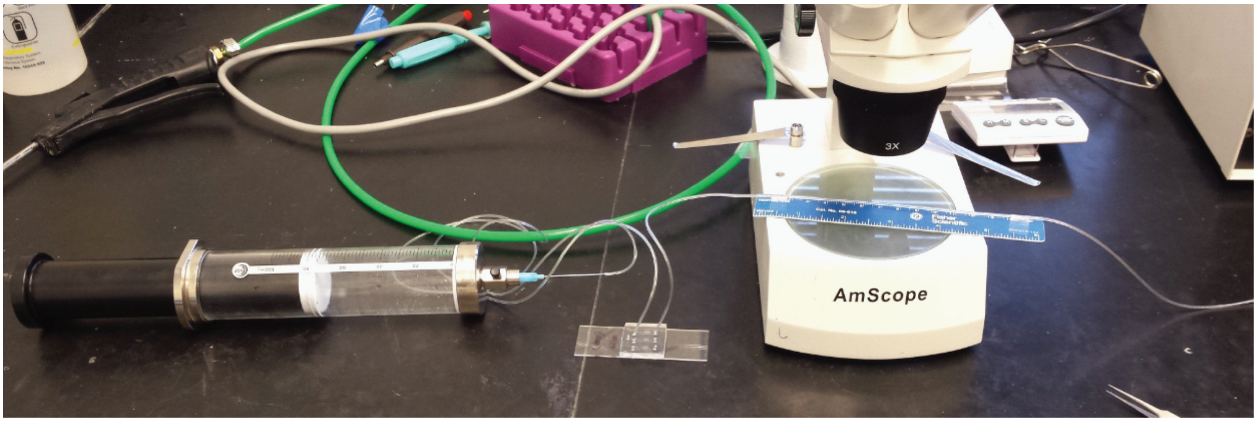

Figure 5.2: Experimental setup for flow rate measurements
Flow rate measurements by fluid displacement in tygon tubings.

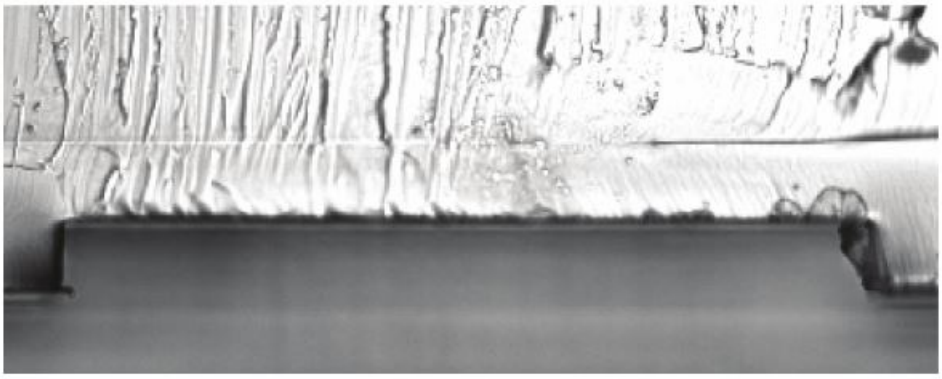

Figure 5.3: Fluidic current mirror ROI channel cross-sections
ROI region cross-section for the autoregulator current mirror (38 μm high and 477 μm wide).

5.2.6 Characterization of flow regulation with Frequency

Measurement of the regulator valve membrane deflection was performed at different frequencies ranging from 1 to 32 Hz by measuring the fluorescence intensity of fluorescein with an inverted fluorescence microscope (Nikon Ti-E). For this measurement, a high concentration (500 μM) of fluorescein was used to permit short exposure times. The fluorescence intensity was recorded with a PMT detector (Hamamatsu) with green fluorescence filter cube

(excitation: 490 ±2 nm; emission 525 ±2 nm. The PMT was set to 10^{-3} μA V^{-1} sensitivity with 0.5 ms time constant and one-time, manually adjusted amplifier offset at the beginning of measurements with voltage range from -10 to 10 volts. Images of the membrane deflection were also recorded using a cooled CCD camera (CoolSnap HQ2; Photometric Scientific). As noted earlier, an in-house built Labview program was connected to one downstream valve placed after the the regulation valve so that the valve actuation could have a direct effect on the the regulator membrane.

Autoregulator devices with active flow control included one inlet and one outlet. Before the experiment, the control channels are filled with water by pressurizing the water into the dead end channels. Since the detour channel is connected to the fluidic channel, the water is pressurized at the inlet through the via keeping the downstream valve closed. This way, the regulator valve is filled with water to avoid air bubbles from leaking into the fluidic channels. For the higher frequency membrane response measurements, the PMT window was focused on a region of interest (ROI) located at the center of the regulation valve. PMT data analysis was analyzed using Excel and the fast Fourier transform (FFT) was carried out using Matlab to obtain membrane displacement magnitude at each frequency.

5.2.7 Current mirror experiment

Fluidic current mirror circuit simulations were performed using the Falstad software. The microfluidic chip fabrication was the same as above. A red color food dye and DI water were used as solution and comprise two mirrored channels and inlets and one outlet. Two 50 mL BD Luer Lock graduated syringes were used to provide equal pressures to the two inlets. To make sure that the syringes will apply the same pressures at the same time, a syringe pump was used to move the syringes at the desired locations and then stopped for measurement(no pumping). The flow rate ratio was observed varying the pressure from 25 to 102 kPa. Video images of the flow rate ratios was obtained with a CCD camera (CoolSnap) and analyzed with NIS Elements software (Nikon) and ImageJ as described in section 5.2.5.

5.3 Results and Discussion

5.3.1 Prelude experiments of autoregulator

As a proof of concept, we first tested the flow rate autoregulation by designing a microfluidic chip similar to that of Kartalov and coworkers [196]. Two chips were designed, one with larger resistor (Chip A) and the other with smaller resistor(Chip B). The chip consisted of one inlet reservoir and one outlet. The device had two patterned PDMS layers where the bottom layer included the detour/regulation channel, and the fluidic channels at the top layer (Figure 5.4). To maximize the space usage on the chip, we included 3 designs on a single 25 mm x 25 mm device. Initially, vias were manually punched using a needle and a tweezer to remove the debris. The two chip design with different resistance values were fabricated by spin coating PDMS at 4 different thicknesses namely, 24, 26, 34, and 36 μm.

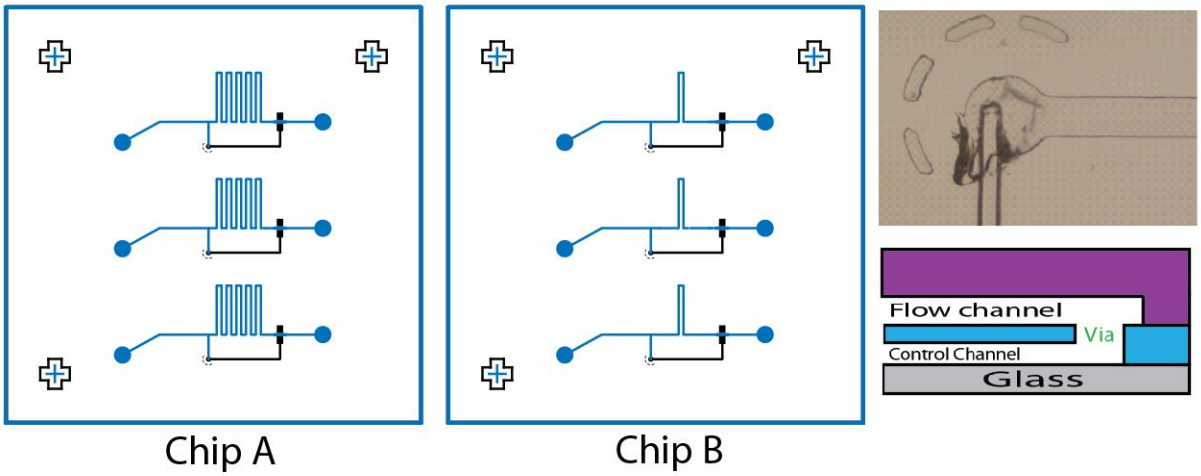

Figure 5.4: Autoregulator design for simple flow rate measurements
Chip A High resistor (left); Chip B low resistor (middle), fluidic channel (blue) and detour channel (black); manually punched via and its schematic(right)

The first attempt in flow rate measurements was done by using vacuum with a syringe connected at the outlet where vacuum was manually applied. The goal was reproduce Kartalov's results where pressure was used to produce a constant flow rate after a threshold pressure. One reason for attempting to use vacuum instead of pressure is because in our

lab, the vacuum system is better suited for many of our applications in cell secretion measurement. Since pressure and shear stress can affect the structure and function or even be harmful to the cells[211], if we intend to apply the autoregulators to study cell secretion, it is advisable to use vacuum at an outlet channel and keep cells in an inlet reservoir. However, we performed flow rate measurements multiple times and where unable not only to produce similar results as with pressure, but also our results varied widely from chip to chip (Figure 5.5). Therefore, it was difficult for us to confirm the feasibility of the autoregulator using vacuum. At the time, we believed that the inconsistency was caused by the difficulty to measure flow rate by fluid displacement in the tubing. In the microfluidic field, traditional gravimetric methods and interface tracking methods are mostly used. Unfortunately, evaporation of fluid is a major issue due to the fact that we are dealing with very small volumes. Therefore, other more elaborate methods are advised, for example flow rate was measured using multiplexed fluidic resistance (MFR) where the flow rate was obtained by measuring the mass of food dyes in an outlet[102]. This technique requires a relatively tedious process using absorbance detection and concentration after flow to back-calculate the flow rate of the food dyes, and it is not possible to achieve dynamic flow rate measurements.

Our second attempt was to measure flow rate by fluorescence. Using the same design, we sought to measure flow rate by recording the fluorescence intensity at the regulation valve. Knowing that when the valve is at its resting position, the flow rate encounters no resistance due to valve deflection. Therefore the fluorescence intensity should reflect the membrane position, be proportional pressure, and remain steady at constant flow rate. When the valve is at the regulation mode, the fluorescence intensity should be proportional to the valve position, with the lowest intensity meaning that the valve is almost closed. Ideally, the flow rate can be calculated using the valve dimensions and the time although several asumptions must be made. Therefore, we performed flow rate measurement by fluorescence using vacuum. Interestingly, we were able to measure pressure differences and estimate flow rate using this technique. We used Chip A and Chip B with the PDMS valve membrane

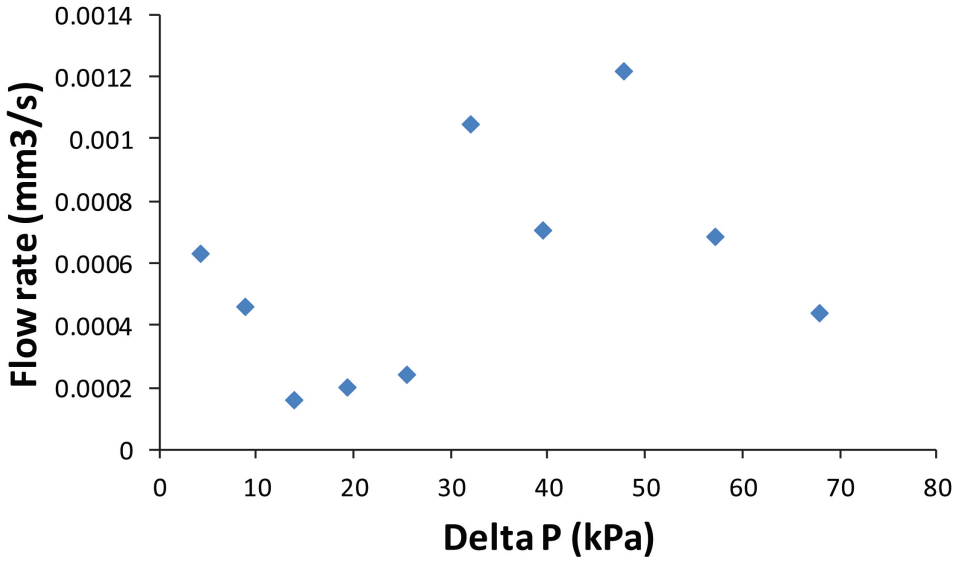

Figure 5.5: Flow rate measurement preliminary results
A plot of flow rate (Q) vs change in pressure (ΔP) showing inconsistency in the flow measurement.

thicknesses described above. We present the data on Figure 5.4. ImageJ was used to analyze videos from the experiment. Unfortunately, after several attempt we rand into the same inconsistency as above. The flow rate seems to be very low in most cases suggesting that the membrane distance does not truly reflect the flow rate. The second hypothesis is that, since the vacuum is applied on the lower resistance side of the chip and closer to the regulation valve, the effect is different than when applying pressure. For example we observed that the membrane was deflecting more towards the downstream channel rather than the center of the valve. Furthermore, we believe that the forward and reverse bias described by Kartalov and coworkers[196] may not function the same way with the vacuum. They described two biases. The forward bias when positive pressure is applied to the channels, and a reverse bias when a resistance is created at the valve area due to membrane deflection. They stipulated that when pressure is applied, the first current in the detour channel saturates (forward bias) and behaves linearly in the Reverse bias[196, 108]. The repeating process of Forward and Reverse bias maintains a constant flow rate as the Reverse bias cancels the flow created

by the Forward bias as the pressure increases. We believe that these effects are not being observed with our system using vacuum (negative pressure) since it is the pressure applied at the inlet that creates saturation in the forward bias.

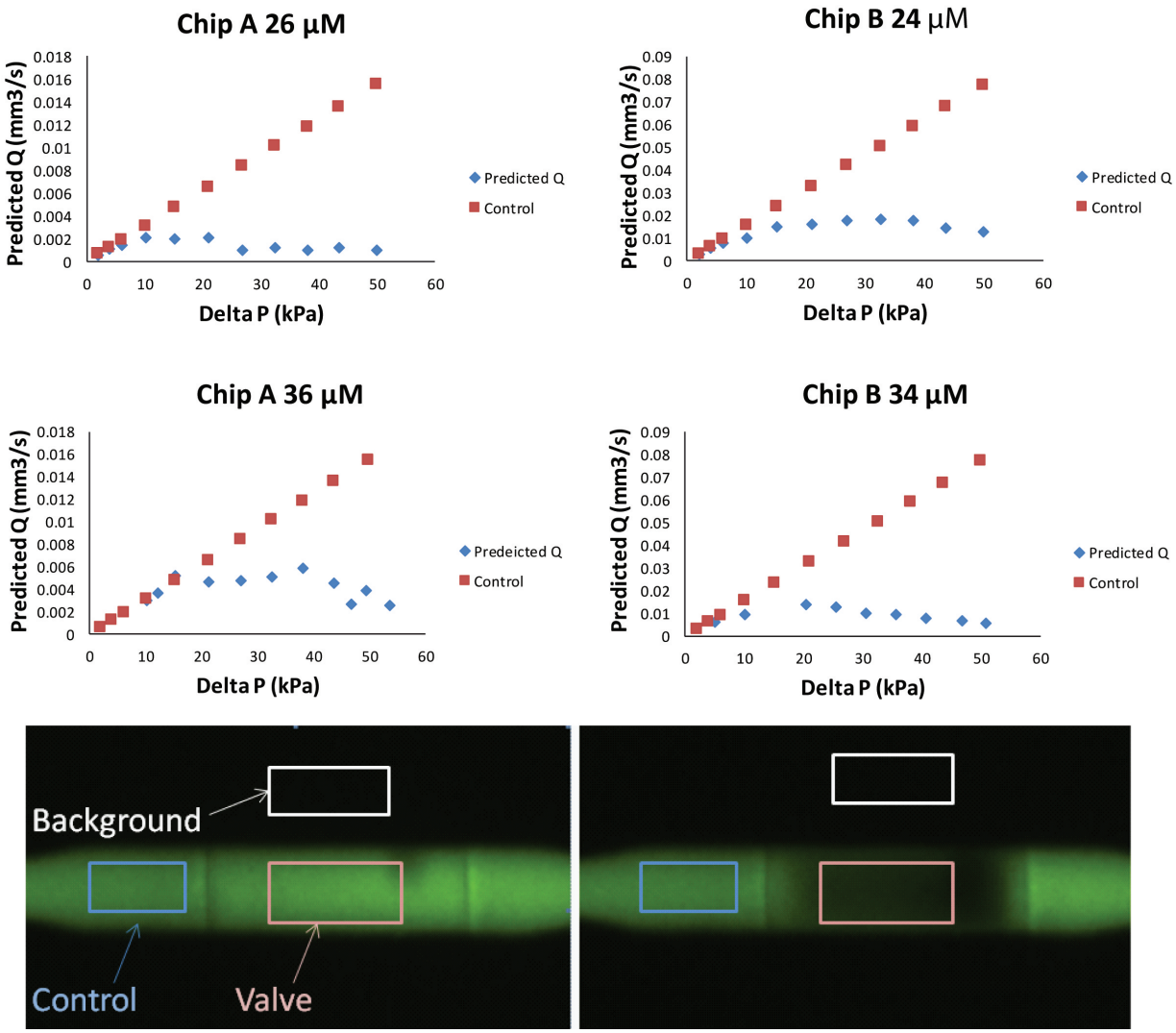

Figure 5.6: Flow rate measurement by fluorescence intensity
(Top) Flow rate measurement using fluorescence intensity and channels dimensions. Plots of flow rate (Q) vs change in pressure (ΔP) for both Chip A and Chip B with thin membarnes (24 and 26 μm) and thicker membrane (35 and 36 μm) showing inconsistency in the flow measurement. (Bottom) Snapshot of the video showing channel willed with fluorescein solution and showing the region of interest where the measurements were taken.

Since the original plan was to show that microfluidic self-regulators that have already been developed could be integrated into a microfluidic large scale integration system (MSL)

with other valves, we decided on another approach using pressurized input instead of vacuum. This attempt was successful, and we obtained a similar result to that of Kartalov et al. The flow rate increased linearly and started to level off from 25 kPa pressure for Chip A. We only attempted Chip A because the fluidic resistance placed between the regulator valve and the detour channel plays a major role in flow regulation and higher resistor value regulates more effectively. Therefore, we use the higher resistor value from this point on.

We have characterized this chip and found out that with a membrane thickness about 25 μm produced desirable results. We also studied smaller membranes (down to 6 μm) and obtained regulation at a lower pressure range. Any membrane above 30 μm would produce inconsistent results, since thicker membranes require higher pressure to deflect. The forward and reverse bias described in Kartalov's work used a 5 μm membrane thickness. Therefore, we have demonstrated the possibility to use thicker membranes which allow regulation at lower pressure. Our chip starts regulating around 20 kPa and continues to regulate at more than 70 kPa.

5.3.2 Chip designs and operation

To account for microfluidic large scale integration system (mLSI), we redesign our autoregulator by adding one valve downstream from the regulation valve. This periodically activated valve provokes a direct response of the regulation valve since it is placed at close proximity and the fluidic resistance between them is negligible. The new design is presented in Figure 5.6. The fluidic channels (black) have one inlet and one outlet where a 1.5 mm hole is punched to insert tubing. The detour channel (green) is connected to the fluidic channel through a 255 μm diameter via that punched using a 40 Watt CO_2 laser tube (80 cm). The laser system was cooled with water and the laser beam was guided by 90 degree turning mirrors /38 mm focal length ZnSe lens. The laser system is controlled by a custom built Arduino Nano controller, for duration and intensity control. For this particular experiment, the laser was set at 20% power at 6 ms. The laser ablates the PDMS at these power setting

without burning. After ablation, a conical shape is formed in the PDMS with the largest diameter being 255 μm. The detour channel forms a Quake valve with the fluidic channel and charges like a capacitor under pressure. The control channel (red) is used to control flow by pulsing pressure at various frequencies. The proximity of this valve to the regulation valve would have a direct effect on the regulation valve since it regulates only when ΔP across the valve is positive. Closing the downstream valve causes the regulation valve to fully open and the opposite causes the valve to be at its regulation mode. The valve is actuated at frequencies going from 1 to 32.05 Hz. The effect of these frequencies is described in the next sections.

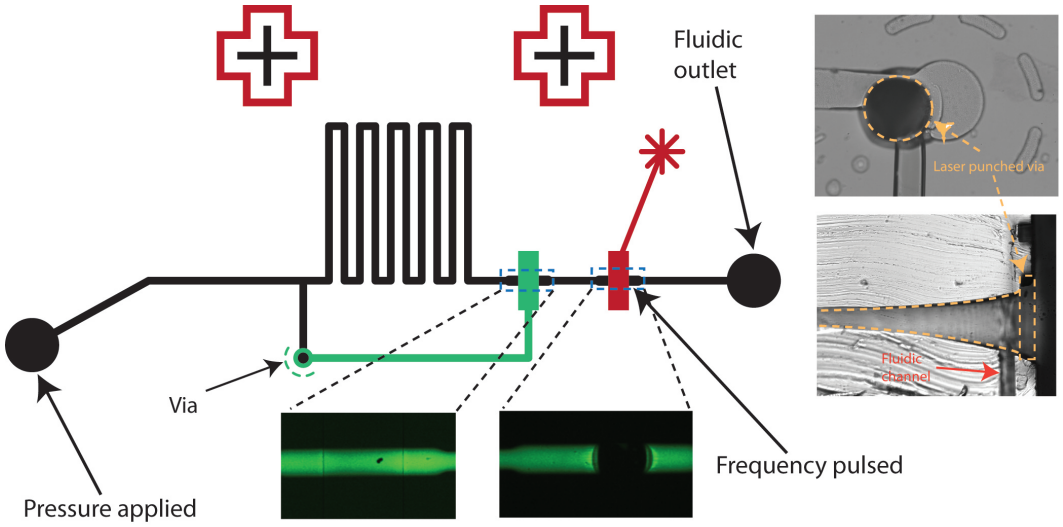

Figure 5.7: Autoregulator new design
Autoregulator with a downstream frequency valve. Fluidic channel (black), detour channel controlling the regulator valve(green), and frequency control channel (red). (Right) Image of the laser punched via, top view (top) and cross section (bottom). The highlighted areas show the regulation valve and the frequency control valve both taken in real time during measurement and showing the fluorescein solution in the channels.

5.3.3 Characterization of autoregulator

Electric circuit simulation

Although the microfluidic self-regulator functionality has been well reported, we hypothesize that adding a downstream valve to the self-regulation valve would not only mimic the presence of other microfluidic functionality in an integrated system but also help us to understand the regulator's behavior in such a system. Knowing that the concept of electrical circuit can be a useful model to predict fluidic behavior in microfluidics, we borrowed this concept for our investigation. Therefore, we first characterized our autoregualtor by simulation using the Falstad software (Figure 5.7). We build a regulator circuit using pMOSFET transistors as valves in addition to resistors and capacitors. PDMS is a soft material, and the channel wall deflection serves as a capacitor analogy in the microfluidic. Two capacitors are used in the circuit and the values are set at 30 μF and 20 μF and placed before the pulse transistor (valve) and before the regulation transistor respectively. Both transistors have a breakthrough (threshold) voltage set at a positive value rather than negative to account for the normally open architecture (35 volts). We also put resistors in the circuit with values to match the fluidic resistors. The pressure is simulated by a continuous voltage source where the input maximum voltage can be varied from 25 volts to 70 volts (for the purpose of this experiment only) simulating change in pressure (ΔP, kPa). We also used a square wave generator voltage source connected the gate of a downstream pMOSFET to simulate the downstream valve frequency actuation (pulse valve).

The self regulation was validated by varying the voltage from 5 to 70 volt at 1 Hz pulse frequency. Once we established a regulated pressure range, we then varied the pulse frequency from 1 to 32 Hz. We observed the behavior by measuring the current and the voltage at different point in the circuit. We found out that by placing a scope probe between the gate and the drain of the pMOSFET, we can capture the pressure change between them which would reflect membrane behavior in a microfluidic model. Another observation is that,

due to the presence of capacitors in the circuit and the on-and-off flow control, the capacitor charges and discharge in the circuit creating a periodic flow on the current. The maximum values of this periodic flow of the current remains constant starting from 30 volts (see graph in Figure 5.8).

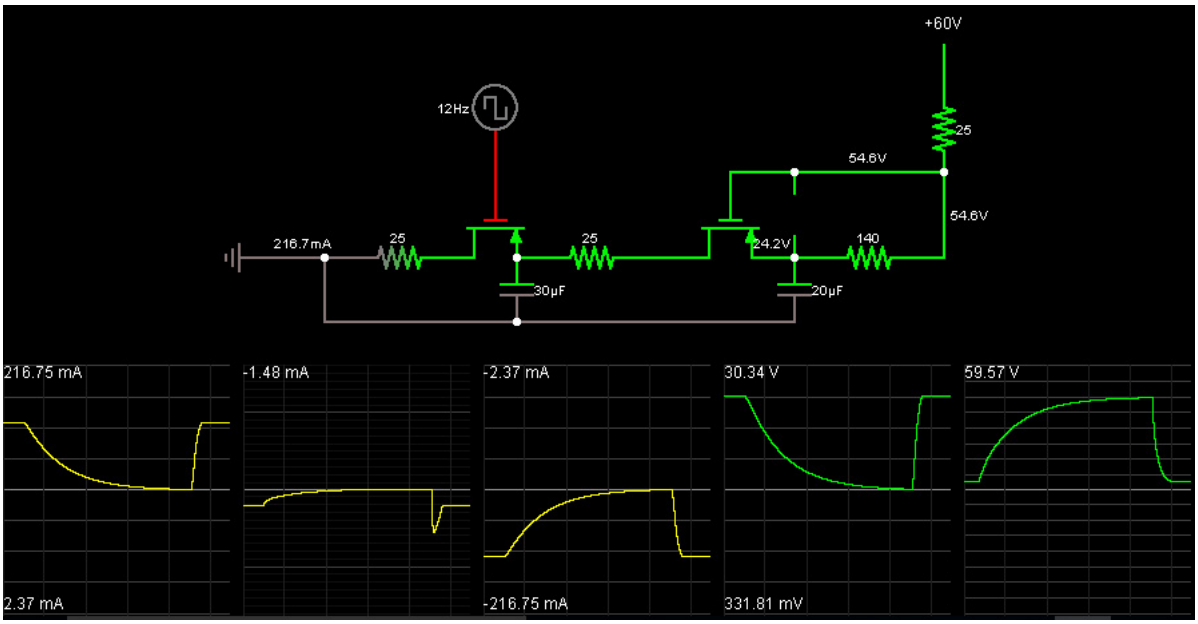

Figure 5.8: Autoregulator circuit simulation
Falstad simulation of the autoregulator. Electric circuit model of autoregulator with component values to match with the microfluidic analogue, current flows from right to left (top). Graph of current and voltages at 12 Hz pulse; from left to right 140 Ω resistor, wire between drain and the capacitor, wire at outlet of the circuit, scope probe voltage, 30 μF capacitor.

Characterization with microfluidic chip

We validated the observation from the self-regulated current electric circuit simulation on its microfluidic equivalent. The microfluidic autoregulator was characterized using highly concentrated fluorescein solution. The solution was loaded into about 80 cm tubing and pressurized into the microfluidic chip. Fluorescence intensity was recorded on 3 regions of interest (ROI) located on, before, and after the the regulation valve. Data from the ROIs was recorded for 35 seconds using a photomultiplier tube (PMT) or a CCD camera. The recording started with no pressure applied (resting state) for 5 seconds, then the downstream

valve was closed for another 5 seconds before pressure was applied to the system (Figure 5.9A). When pressure was applied, the regulator's membrane deflected quickly and returned to its resting position, causing the spike observed on the graph (10 s time point). The signal increase was due to the inflation of the valve caused by the abrupt pressure change. At the 15 second time point, the downstream valve start pulsing, the membrane deflects to its regulating position. Figure 5.9A (from 15 to 35 seconds) depicts this results for the valve pulsed at 1 Hz. At this frequency, the membrane stays at the regulation position for half the time but takes relatively longer time to come back to its resting (valve fully open) position during the rest of the cycle time. This observation is due to the capacitance behavior of the membrane.

The same effects were observed in the circuit simulation as the capacitors charged slowly and quickly discharged the current in the system. Figure 5.8B is an illustration of the microfluidic channel and membrane during the experiment. As we saw with the fluorescence signal in Figure 5.9A, during the first 10 seconds, the channels remained still even when the downstream valve is closed. When pressure was applied, the channels inflated like a balloon when air is pumped into it. From 15 to 35 second time, the membrane position fluctuates between resting and the regulating position. Note that the valve was halfway closed when the device was regulating, maintaining the balance between the forward and reverse bias. The channels region before and after the regulation valve were also investigated. We observed similar behavior as on the regulator valve with the normalized fluorescence intensity suddenly increasing when pressure is applied as well as the capacitance behavior. One important observation is the fluorescence intensity magnitude that is larger for the ROI after the regulation valve than that of before. This signals that the capacitance values is larger for the channel portion closer to the pulse valve. We made the same observation during simulation by moving the capacitor at different positions and they produced better response when placed just before each transistor.

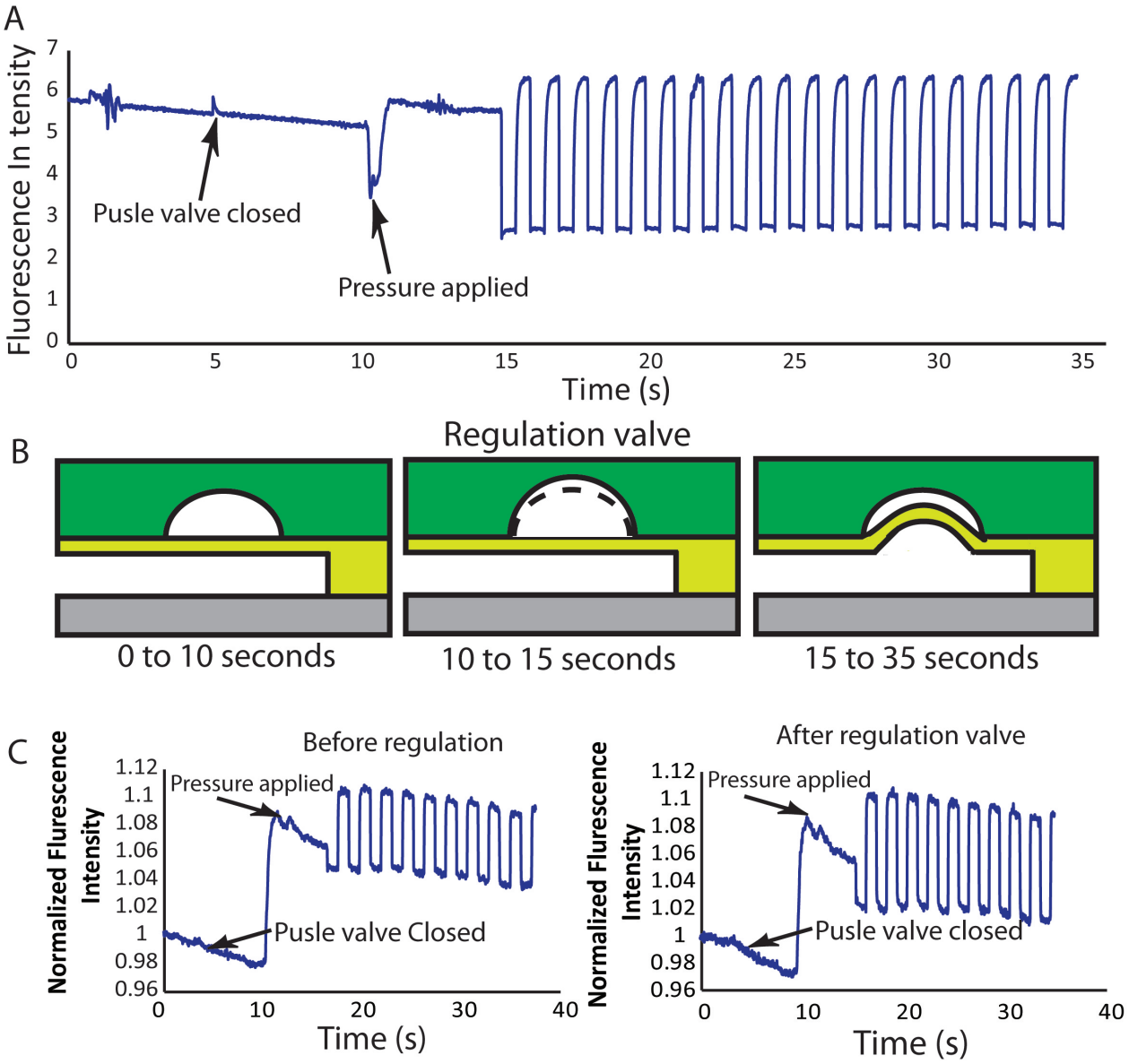

Figure 5.9: Channels behavior
(A) Time dependent response of the autoregulator fluidic channels. (B) Illustarion of the channels behavior during the experiement . (C) Time dependent response before (left) and after right) the regulation valve.

5.3.4 Frequency effects on membrane

To fully understand understand the PDMS membrane behavior in a faster paced microfluidic environment, we examined the membrane under various frequencies. As observed in the electric circuit simulation, we expect the device to regulate even at higher frequencies.

We also expect the membrane position to vary with the frequency. Therefore, we selected frequencies from 1 to 60 Hz, and we measured the membrane response. We found that after 25 Hz, the membrane response does not follow a particular cycle anymore since no clear frequency is observed in the results. This was found despite the fact that the simulation predicted a periodic response. For this reason, we only report results with frequencies as follows: 1, 1.43, 3.03, 4, 6.02, 8, 12.05, 16.06, and 25 HZ. Figure 5.10A shows the frequency response for 1, 6.02 and 25 Hz. It also depict a general trend on how the membrane behaved during regulation. The membrane goes to its regulating position as soon as the downstream valve starts pulsing (see full length of 1 Hz data above) and slowly moved back to its resting position (capacitor charging mode). As the frequency increased, the membrane tended to stay closer to its regulating position and never returned to its resting position. Interestingly, after performing the experiment we plotted the difference in peak height values versus the frequencies and the results nicely fit that obtained from the simulation (Figure 5.8B). In order to account for the membrane displacement at every frequency, we performed fast Fourier transform (FFT) analysis. We clearly see that the membrane is at different equilibrium position at every frequency. The position decrease exponentially from the resting position observed with 1 Hz frequency (Figure 5.10C).

5.3.5 Real time flow Rate measurement

We further characterized our autoregulator by measuring the average flow rate at various frequencies. To do so, we loaded food coloring in a 80 cm tygon tubing and we applied pressure with a glass syringe. Flow rate was measured under different pressure of 5.35, 11.30, 17.95,25.43, 33.91, 43.60, 54.78, and 67.82 kPa. These pressures were first characterizes in the preliminary experiment without the frequency valve. The displacement of the fluid was measured and recorded for 5 minutes for lower pressures and 3 minutes for higher pressures. The flow rates at each pressure was determined and is presented in Figure 5.11. The control experiment (blue dots) was measured using an autoregulator chip with no via punched to

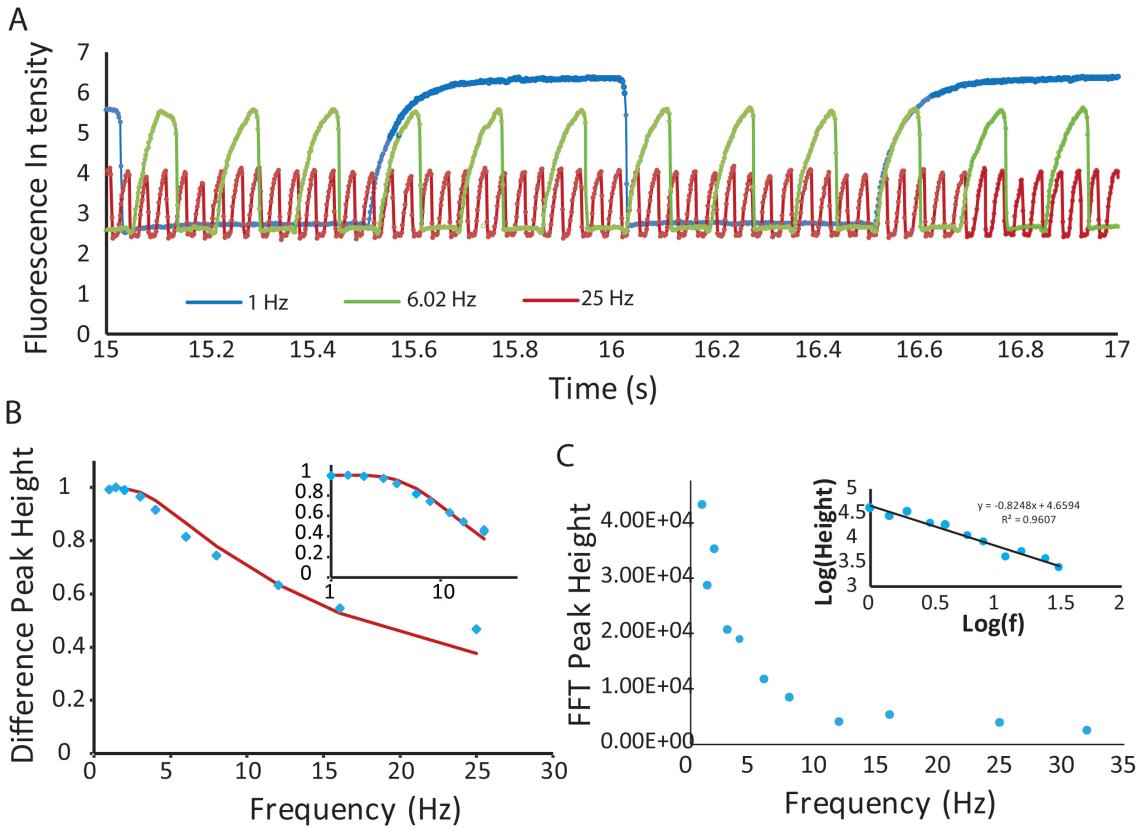

Figure 5.10: Evaluation of the frequency effects on regulation
(A) Membrane behavior in relation to frequency showing measurement at 1, 6.06, and 25 Hz. (B) Comparison of experimental membrane displacement (blue dots) at all frequencies (from 1 to 25 Hz) with the simulated displacement (red trace); the logarithmic plot is showed in the inset. (C) Fast Fourier transform analysis showing exponential decrease of the FFT peak height and the frequency, the inset figure represent the logscale of the same data.

make sure that there is no flow regulation in the chip. This experiment was performed at zero frequency (DC flow) using the same batch of chips that will be used to measure flow regulation. Subsequently, the flow rate was measured at 1, 2, 3, 4, 8, and 16 Hz. Our observation was that the frequency of the downstream valve in this range does not influence flow regulation negatively. The flow rate here follow the same trend with and without downstream valve frequency pulse. Evaporation of the fluid was no issues in these experiments because throughout the duration of the experiment, the fluid was kept inside the tubing and the microfluidic chip, and not exposed to ambient air. This result bodes well for using autoregulators of this type in more complex, rapidly switchable microfluidics.

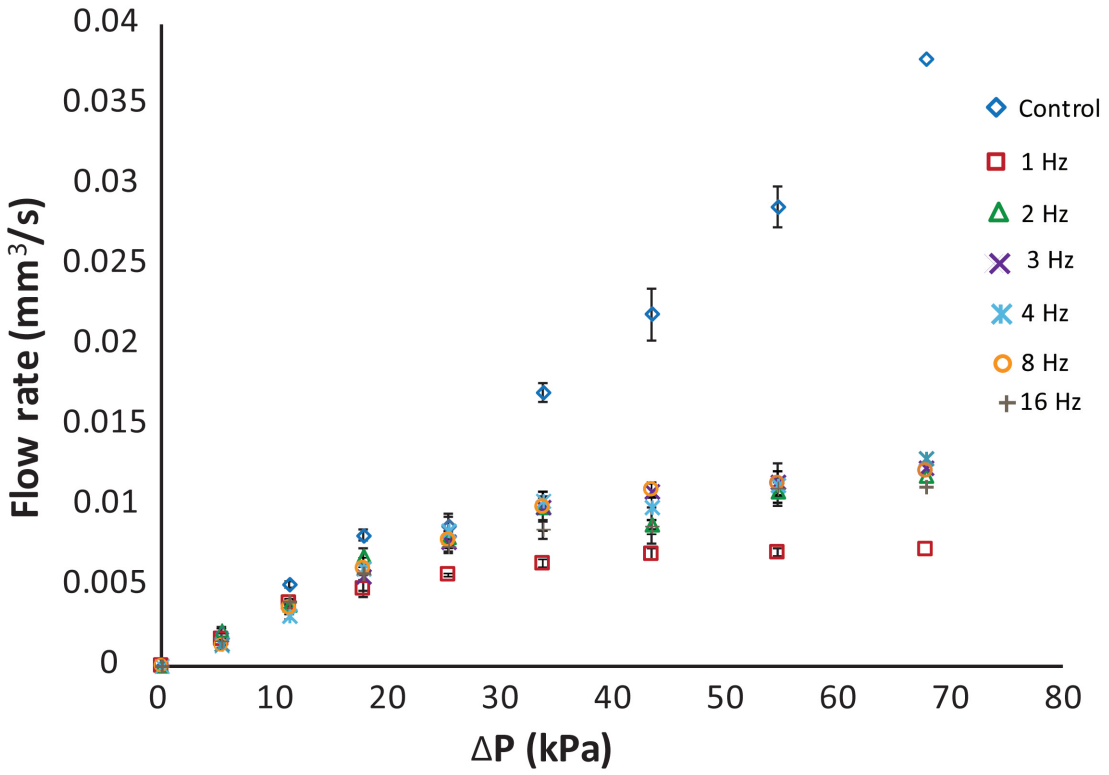

Figure 5.11: Flow rate measurement with downstream valve pulsing at various frequencies

5.3.6 Application of autoregulator in microfluidic current mirror

Another well known electrical circuit which serves as current regulator is the the current mirror. In the electric circuit, the current mirror is used to supply nearly constant current to the circuit over a wide range of resistances since the flow rate is largely controlled by a parallel circuit. It can be used for many applications including integrated circuit technology to mirror the current of one device in another. Similarly, the current mirror can be applied to microfluidics especially in microfluidic large scale integration (mLSI) to mirror the flow rate of one microfuidic channel in another. Figure 5.12 (bottom image) shows the Falstad simulation of our flow rate mirror circuit. The current flows from left to right. The top circuit mirrors the current of the bottom circuit circuit even when the resistor is changed from 200 Ω to 6Ω. This phenomenon happened only when the voltage reached the regulation threshold.

The simulation was run at only 1 Hz because the goal here is to observe the current ratio when the resistor varies from high to low on one side of the circuit.

The microfluidic analogue of the current mirror chip was designed to maintain a constant flow when the resistor of one branch of the circuit is varied from low to high (Figure 5.12 top). We thus termed this design as a "flow rate mirror". The device comprised two inlets where equal pressure was applied and one outlet where the two branches of the circuit met and flowed together in laminar flow fashion. The device is made of two layers of PDMS as described above. The ROI region is made from SU-8 photoresist and has squared channel for better estimation of the flow ratio volume. The regulation valve channels were connected by only one input via. Two other vias were punched using the laser to connect the top rounded channels to the bottom (squared) channels of the outlet. The chip functioned by applying equal pressure to the inlets. When the pressure reached the threshold, the top branch regulated the flow in the system and the constant flow is mirrored to the bottom branch even when the resistor of the branch is changed using the resistor switch valve. When this valve was actuated, the fluid had no choice but to take the longer (higher value resistor) path and when it is off, the fluid chooses the shorter path (lower value resistor).

5.3.7 Characterization of the microfluidic flow rate mirror

The microfluidic current mirror analogy was carried out by using a red color food dyes in the variable resistor branch and DI water in the other branch of the device. The two fluids flow next to each other parallel when pressurized and the flow ratio can be measured typically at a designated ROI near the outlet (Figure 5.12, top). Both branches having the same total resistance values, we expect the fluid to flow in 1:1 ratio at the ROI region when the same pressure is applied to the inlets. When the resistance of one branch is different, the flow ratio should readjust accordingly. First the experiment was performed using a microfluidic chip that has a via connecting the regulation channels to the flow channel to make sure that regulation happens. Then, we performed the control experiment with a chip

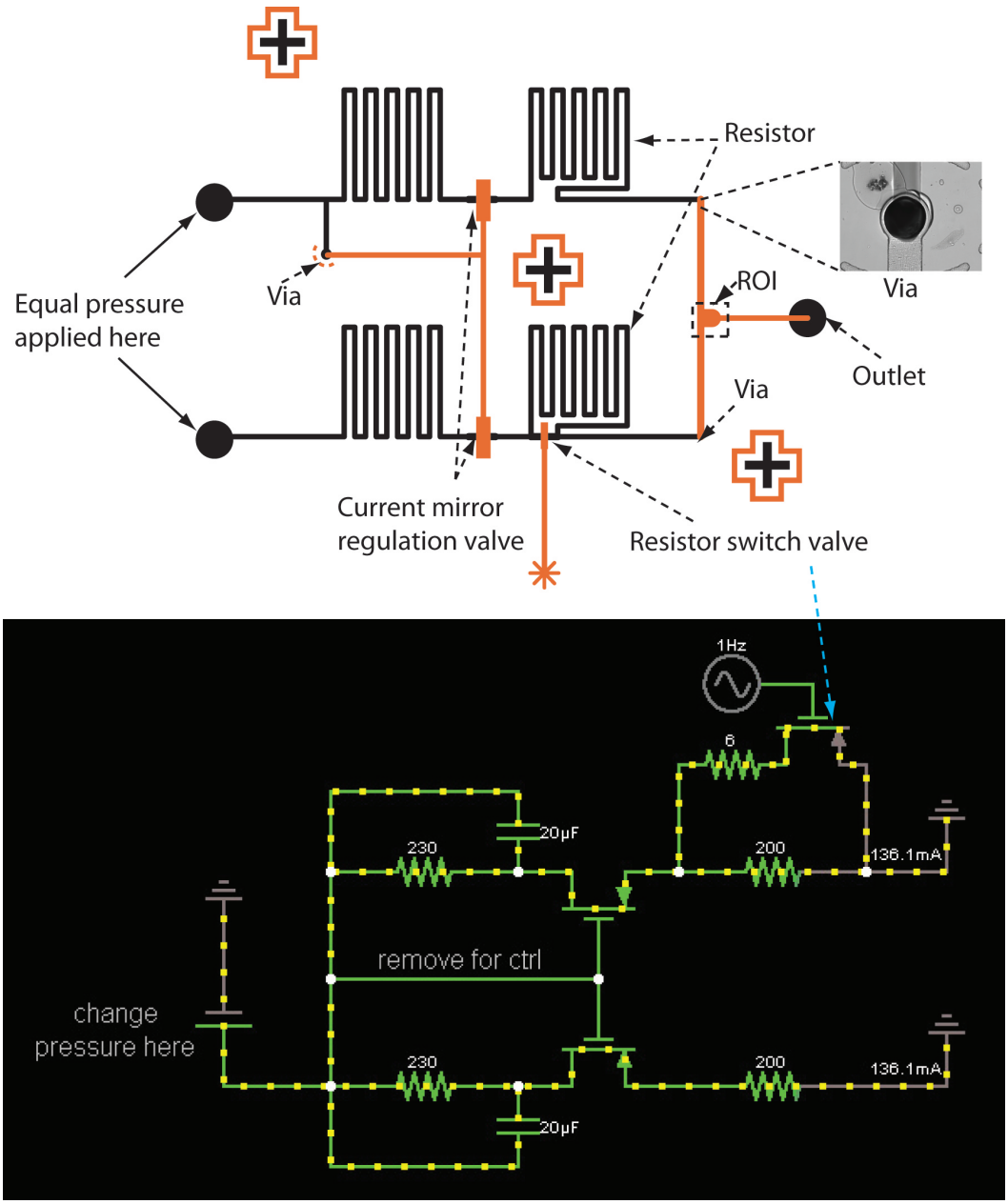

Figure 5.12: Current mirror microfluidic design and circuit simulation
(Top) Microfluidic current mirror, AZ-fabricated Fluidic layer (black), SU-8 layer(orange) serving for the control of the valves, and the ROI optical reading. (Bottom) Screenshot image of the electric circuit simulation.

that has no via punched, therefore no flow regulation should occur. Four different pressure were investigated in this experiment namely, we used 25.43, 43.6, 67.82, and 101.73 kPa. We started the experiment with the resistor valve opened (lower resistance), and we applied pressure. The syringes were elevated to the same height has the microfluidic chip to avoid

errors caused by gravitational pressure. When the flow was observed to be nearly 1:1 ratio, the resistor valve was pulsed at 0.5 Hz, and the videos of the ROI was recorded for 40 seconds.

After recording the videos, the analysis was done using ImageJ. Briefly, an 8 bit image ROI of 100 pixels x 384 pixels was selected on all videos, and binary distribution of the image was used to calculate the flow ratio between both fluids. Since the red food dye is darker and the water is clearer under black and white image, the binary analysis was performed making the red food dye to appear as black and the clear region to appear as white. Analysis of these images is shown on Figure 5.13. The top graph was obtained using the flow regulated chip. The higher the pressure, the less the flow is changed by switching the "load" resistor in the lower fluidic path. Flow rate difference occurred more at lower pressures. This is due to the fact that at lower pressure, the device is just nearing the regulation pressure threshold and only fully regulates at higher pressures. The simulation showed no change in the ratio when the system was fully regulating. However, our result showed near ideal flow rate mirror because we found only 6 % difference in flow ratio with the higher pressure. These results also show a drift (blue trace) in the flow ratio. This was probably due to artifacts in the binary data analysis. Interestingly, the flow ratio remain the same throughout the drift. For the control experiment (bottom graph), we also observed similar trend in the flow ratio from the lowest to the highest pressure. Yet, the flow ratio changes were more significant that the regulated chip. In fact, the different in flow ratio was between 50% and 40% for all pressures. This is a clear proof that there was no flow regulation and that the flow rate mirror phenomenon was not occurring as in the experiment done with the regulated current mirror chip. We have therefore introduced a novel fluidic circuit design, the flow rate mirror.

Flow ratio response to pressure

Due to the above observations, we suspected that the pressure was having an important effect on the flow ratios. At lower pressures, our microfluidic flow rate mirror system would

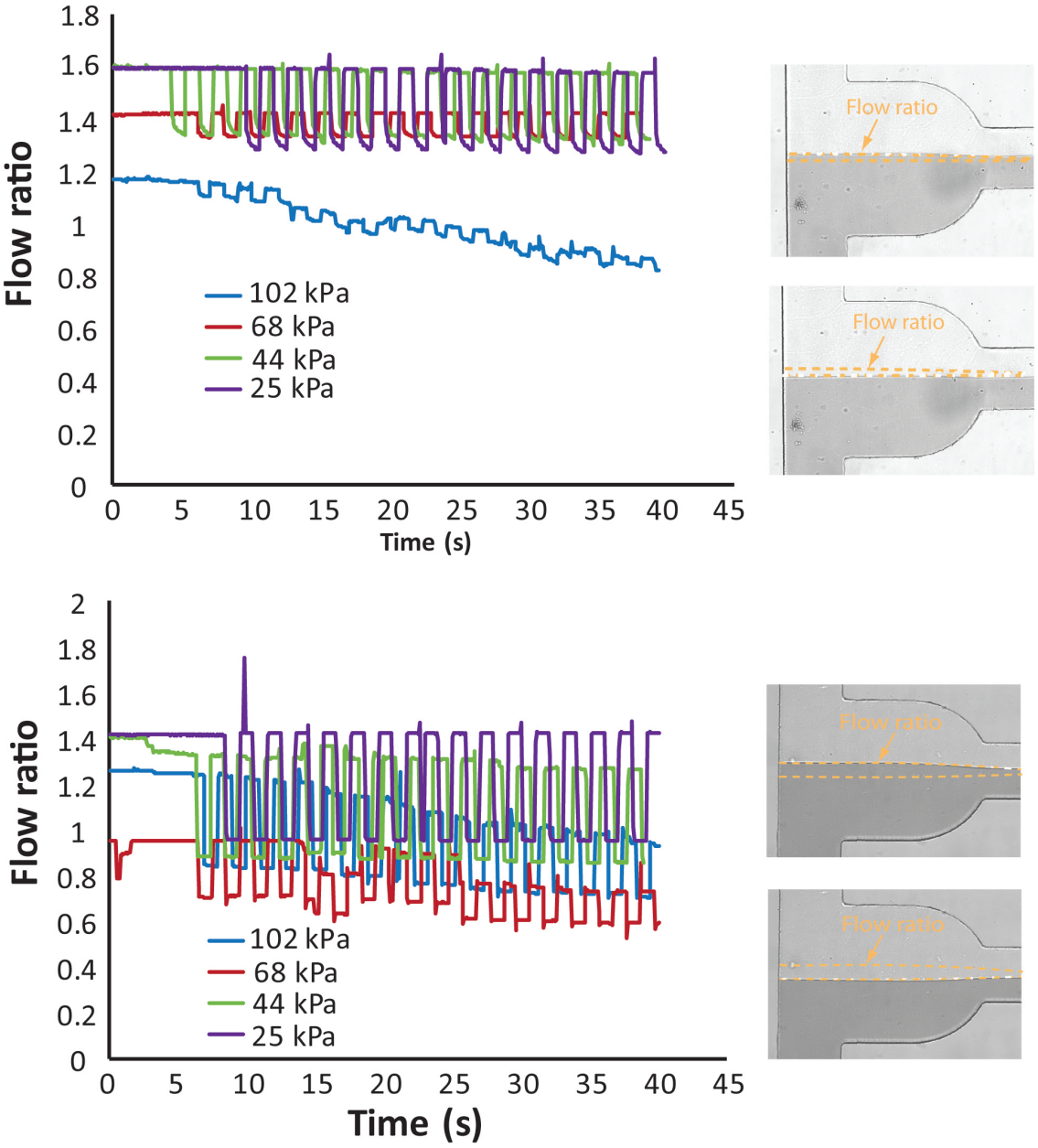

Figure 5.13: Flow ratio measurement
Graph of the flow ratio over time. (Top) Regulated flow current mirror experiment showing the flow rate beeing mirrored from one microfluidic channel branch to another with small flow ratios (left). Images of the ROI showing a real time difference in the flow ratios (right). (Bottom) Control experiement showing higher flow ratio and no current mirrored (left). Images of the ROI showing larger flow ratios in real time.

not be having a stable flow rate meaning that the system is not regulating. To clarify this assumption, we plotted the difference in flow ratios versus the pressures and they both show

a linear decrease (Figure 5.14). This plot accounts for the flow regulation. As the line approaches y=0, the more the flow is being regulated. Keeping this in mind, we note that the control experiment (red) slope is decreasing much more slowly compared to the flow rate mirror experiment (Blue). Even though both curves seem to be decreasing with increasing pressure, the flow rate mirror result decreases faster and the line approached zero. Hence, we can further confirm that our microfluidic flow rate mirror is regulating on both branches when the pressure is sufficient for operation.

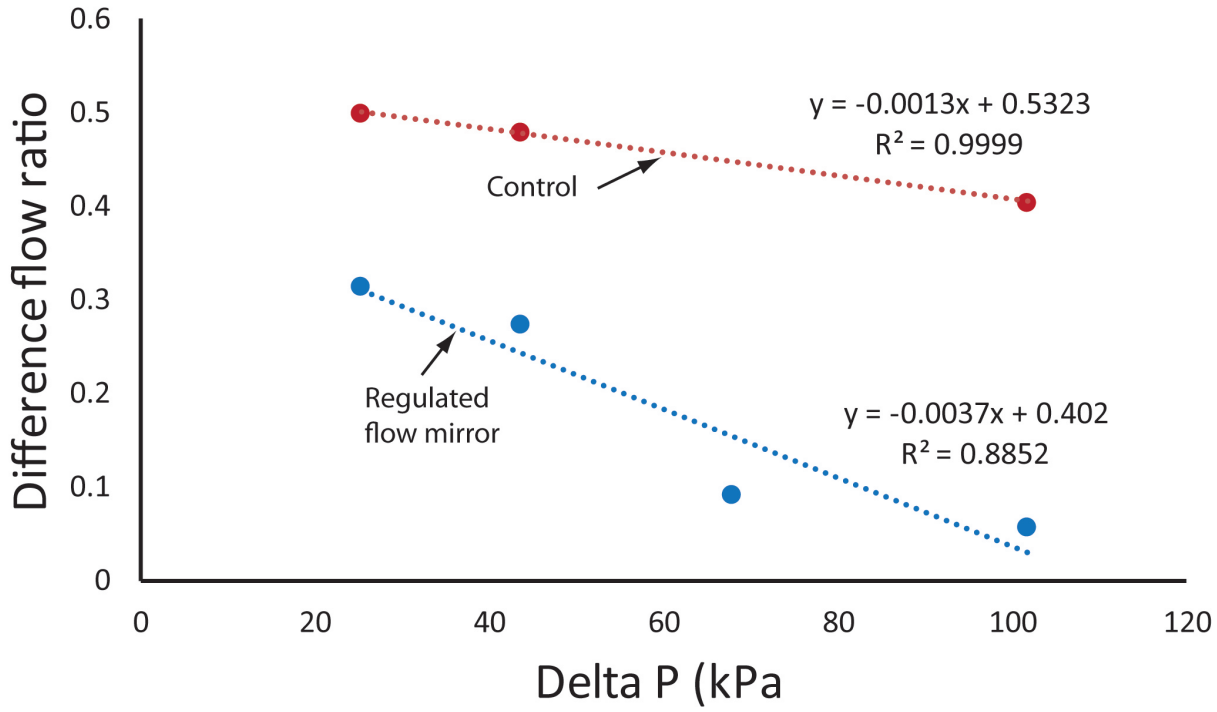

Figure 5.14: Flow ratio response to pressure
Microfluidic crrent mirror (blue), and the control experiment (red).

5.4 Conclusion

Once again, microfluidic analogy to electric circuit have been demonstrated. We have shown that electric circuit model can be used to nicely mimic microfluidic behavior. We have designed a microfluidic autoregulator with a downstream valve to study the membrane response and thus the regulation conditions. With a fixed resistor defining the regulation threshold, we studied microfluidic self regulation under various frequencies. Although several groups have proposed different design of microfluidic autoregulators, a study to demonstrate its applicability to rapidly switched circuits was still lacking in the literature up to now. Our design and study paves the way towards the application of microfluidic autoregulators. We have carefully develop our theory through simulation and we move to the experimental study to confirm our simulation results. Theoretical simulation as experimental results showed that microfluidic autoregulator can directly be applicable in microfluidic large scale integration devices.

For the first time, a microfluidic current mirror analogue was designed and implemented. From the simulation, we defined the characteristics of all the components involved, and we designed our microfuidic flow rate mirror accordingly. The current mirror principle relying on the flow regulation, our design used the regulation of one microfluidic channel to regulate another. The experimental results was very closed to that of the simulation. With this we observed only 6% difference on the flow ratio between both channels and we proved that the device is regulating more at higher pressures. An interesting possibility would be to use a single pressure source to control flow rates in any parallel fluidic circuits.

Chapter 6

Chapter 6: Conclusion and Future work

6.1 Conclusions and Achievements

In this dissertation, we have demonstrated microfluidics techniques for highly sensitive quantitative bioanalyses. We started by reviewing microfluidic techniques and their impact in science and technology. Finally, we present our little contribution in the microfluidics application for detection of biomolecules. In this chapter, we will summarized the major accomplishments of this dissertation and give future directions for possible improvements or real life application.

A droplet microfluidic (μChopper) with valves system capable of significantly improving the limit of detection (LOD) of biomolecules was developed. Deriving from previous device that was passively operated and used for absorbance detection with only 27 μm pathlength, we have shown that active control of droplets formation in addition to lock-in detection method could greatly reduce bandwidth frequency and allow highly sensitive bioanalyses. As a result, the limit of detection detection of any biomelecule can be greatly improved. We have applied this technique for the detection of free fatty acids (FFA) uptake in a single adypocite cell. This was the first time that quantitative instead of qualitative analyses of FFA was performed in science. This device is also very useful for precious samples and small volume situations and when very low limit of detection is a crucial requirement. We believe that analyses of cells with high temporal resolution, which is our goal in Easley Lab, can easily be achieved with this device.

We further developed this device to include multiple μChoppers into a single device. Our goal was to allow multiplexed experiment by avoiding sample loading steps during experiments and therefore create a robust system where where multiple samples can be

chopped into droplets and in combination with lock-in detection, human errors as well as 1/f noise can be eliminated. We have presented a proof of concept of this novel μChopper and demonstrated its ability to perform various modes of analyses and to remove 1/f noise. For example, we have shown that our device could study the temporal response of biological assays by mimic such assay with fluorescein. With this experiment, we found that 1/f noise was greatly eliminated during the experiment by showing a constant slope, y-intercept, and R^2. The unknown concentration was accurately determined at the end of the temporal study. We found similar results for other four modes of analyses. We believe that this device can perform a variety of analyses especially that it could provide accurate insight information on cells secretion with high temporal resolution.

The laminar flow presents a real challenge in microfluidics as it considerably slows the reacting process in microlfuidic channels. There was a need for a technique where reactions could be performed faster since reaction time is one of the major advantages of microfluidics. Therefore, we have built up from a previously developed rotary mixer to accelerate reactions in such systems. We have improved this device by enlarging the center valve of the peristaltic pump in order to increase pump volume. We also developed an accurate sample metering system in our device and confirmed the accuracy with serial dilution. Our system could perform mixed as fast as 2.2 seconds and was applied for protein detection. With this system, highly sensitive and selective protein quantification can be performed and it can be applied to insulin sampling secretion.

We also applied new analytical tools to study passive fluidic control circuits such as autoregulators. The electric circuit simulation of the autoregulator was built and shown to accurately predict the experimental results simply by matching the electric components values to the microfluidic analogue. The frequency dependence of the autoregulator was accurately predicted by electric circuit simulation and was shown to be a negligible factor to the regulation. We have shown that fluorescence imaging can be used similarly to a voltage reader to give ΔP vs time curve. For the first time, a microfluidic current mirror

was developed. Taking advantage of the flow regulation in one channel, the flow regulation was mirrored in a parallel channel. We showed that the laminar flow at the outlet can used as current meter and we measured the dynamic current with fluidic ratio vs pressure. These analyses allowed us to create a new device from a microfluidic autoregulator to fluidic current mirror.

6.2 Future works

6.2.1 Autamated μChopper

The Easley Lab goal has already been developing systems to analyze islets secretion. As part of a contribution in fulfilling this goal, we have successfully developed a microfluidic sample chopper (μChopper) with active valve control and proved that it could greatly reduce bandwidth frequency, and applied this device for the free fatty acid uptake by a single adiopcyte cell. We also presented a new version of this device with multichannels for performing multiplex assays with an advantage of measuring up to six concentrations in only one run. We have already proven this system in absorbance detection and fluorescence detection. We intend to directly apply this device to measure human albumin contained in human serum. Since this device can accurately measure samples in changing systems, It can also be applied to measure free fatty acid uptake from explants, the kinetics of any homogeneous assay (for example the pincer assay), and glycerol enzyme assay. This new device can be useful in many applications including absorbance as well as other optical systems such as Raman spectroscopy, mass spectroscopy, and non optical systems such as electrocemistry. Figure 6.1 shows a fully automated microfluidic chip for cellular secretion dynamics study. Utilizing the μChopper method, this device has already been tested for it application in coupled enzyme assays such as glycerol, glucose, etc... as well as homogeneous protein assays such as insulin and asprocin.

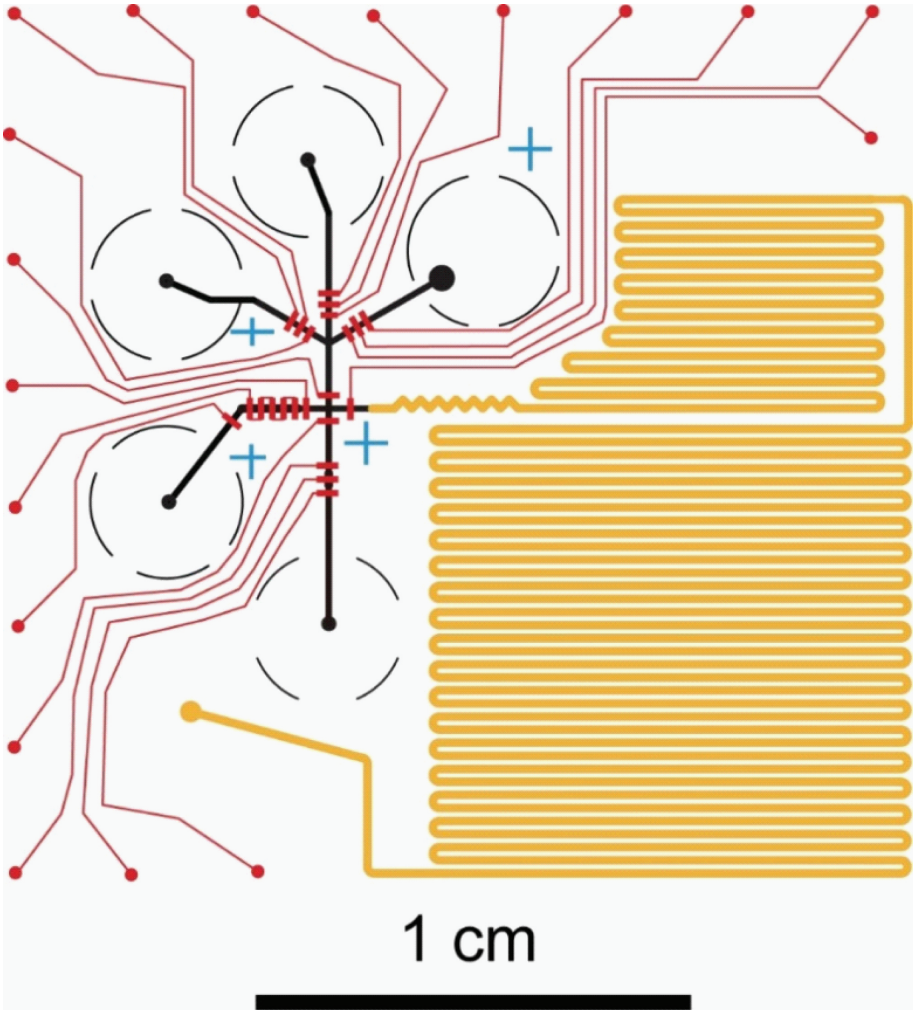

Figure 6.1: Chip design for cellular secretion dynamics study
Design of a fully-automated droplet chip for the analyses of cellular secretion dynamics. Fluidic channels (black) with 4 aqueous inlets and one oil inlet. Droplet are automatically formed with peristaltic pumping having equal mixture of reagents and incubated in the incubation channels (yellow).

6.2.2 Microfluidic chromatography using rotary mixer

Since the rotary mixer could accurately meter sample and perform sensitive and selective protein detection, we want to take it one step further by performing protein separation and detection on-chip. We have already designed a new microfluidic rotary mixer for this purpose (Figure 6.2). This device contains a microcolumn where microbeads can be packed for protein separation purposes. The separation is made possible by using protein specific antibody attached to the surface of the microbeads.

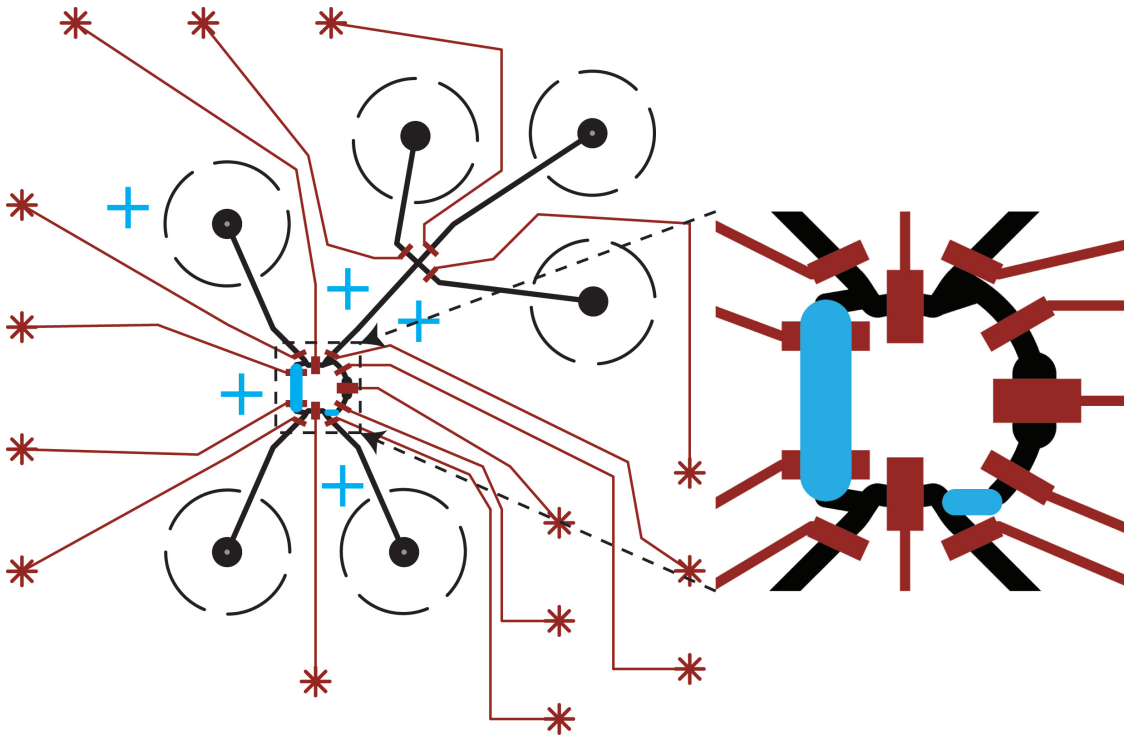

Figure 6.2: Next-generation rotary mixer for chromatography
Design of the next-generation rotary mixer. Fluidic rounded channels (black) with microbeads loading region (blue) in squared SU-8 features, and control channels (red)with 14 control valves.

Bibliography

[1] C. G. Willson, R. R. Dammel, and A. Reiser, "Photoresist materials: a historical perspective," 1997.

[2] *Fundamentals and Aplications of Microfluidics*. Artech House, 2002.

[3] S. C. Terry, J. H. Jerman, and J. B. Angell, "A gas chromatographic air analyzer fabricated on a silicon wafer," *IEEE Transactions on Electron Devices*, vol. 26, pp. 1880–1886, Dec 1979.

[4] G. M. Whitesides, "The origins and the future of microfluidics," *Nature*, vol. 442, no. 7101, pp. 368–373, 2006.

[5] R. Zengerle and J. Ducrée, "Microfluidics roadmap: The trend to use low-cost technologies and microfluidic platforms," in *Proceedings of the 9th International Conference on New Actuators (Actuator'04), Bremen, Germany*, pp. 194–199, 2004.

[6] E. K. Sackmann, A. L. Fulton, and D. J. Beebe, "The present and future role of microfluidics in biomedical research," *Nature*, vol. 507, no. 7491, pp. 181–189, 2014.

[7] I. Ahmed, H. M. Iqbal, and Z. Akram, "Microfluidics engineering: Recent trends, valorization, and applications," *Arabian Journal for Science and Engineering*, pp. 1–10, 2017.

[8] N. Lion, F. Reymond, H. H. Girault, and J. S. Rossier, "Why the move to microfluidics for protein analysis?," *Current opinion in biotechnology*, vol. 15, no. 1, pp. 31–37, 2004.

[9] C. J. Easley, J. M. Karlinsey, J. M. Bienvenue, L. A. Legendre, M. G. Roper, S. H. Feldman, M. A. Hughes, E. L. Hewlett, T. J. Merkel, J. P. Ferrance, *et al.*, "A fully integrated microfluidic genetic analysis system with sample-in–answer-out capability," *Proceedings of the National Academy of Sciences*, vol. 103, no. 51, pp. 19272–19277, 2006.

[10] S. Kumar, V. Sahore, C. I. Rogers, and A. T. Woolley, "Development of an integrated microfluidic solid-phase extraction and electrophoresis device," *Analyst*, vol. 141, pp. 1660–1668, 2016.

[11] B. C. Strachan, H. S. Sloane, E. Houpt, J. C. Lee, D. C. Miranian, J. Li, D. A. Nelson, and J. P. Landers, "A simple integrated microfluidic device for the multiplexed fluorescence-free detection of salmonella enterica," *Analyst*, vol. 141, pp. 947–955, 2016.

[12] J. S. Mellors, K. Jorabchi, L. M. Smith, and J. M. Ramsey, "Integrated microfluidic device for automated single cell analysis using electrophoretic separation and electrospray ionization mass spectrometry," *Analytical Chemistry*, vol. 82, no. 3, pp. 967–973, 2010. PMID: 20058879.

[13] G. S. Fiorini and D. T. Chiu, "Disposable microfluidic devices: fabrication, function, and application," *BioTechniques*, vol. 38, no. 3, pp. 429–450, 2005.

[14] A. Paguirigan and D. Beebe, "Gelatin based microfluidic devices for cell culture," *Lab on a Chip*, vol. 6, no. 3, pp. 407–413, 2006.

[15] J. P. Rolland, R. M. Van Dam, D. A. Schorzman, S. R. Quake, and J. M. DeSimone, "Solvent-resistant photocurable liquid teflon for microfluidic device fabrication," *Journal of the american chemical society*, vol. 126, no. 8, pp. 2322–2323, 2004.

[16] K. T. Haraldsson, J. B. Hutchison, R. P. Sebra, B. T. Good, K. S. Anseth, and C. N. Bowman, "3d polymeric microfluidic device fabrication via contact liquid photolithographic polymerization (clipp)," *Sensors and Actuators B: Chemical*, vol. 113, no. 1, pp. 454 – 460, 2006.

[17] J. Kobayashi, M. Yamato, K. Itoga, A. Kikuchi, and T. Okano, "Preparation of microfluidic devices using micropatterning of a photosensitive material by a maskless, liquid-crystal-display projection method," *Advanced Materials*, vol. 16, no. 22, pp. 1997–2001, 2004.

[18] L. Li and R. F. Ismagilov, "Protein crystallization using microfluidic technologies based on valves, droplets, and slipchip," *Annual Review of Biophysics*, vol. 39, no. 1, pp. 139–158, 2010. PMID: 20192773.

[19] I. Meyvantsson and D. J. Beebe, "Cell culture models in microfluidic systems," *Annu. Rev. Anal. Chem.*, vol. 1, pp. 423–449, 2008.

[20] Z. Zhu, G. Jenkins, W. Zhang, M. Zhang, Z. Guan, and C. J. Yang, "Single-molecule emulsion pcr in microfluidic droplets," *Analytical and Bioanalytical Chemistry*, vol. 403, pp. 2127–2143, Jun 2012.

[21] D. Pekin, Y. Skhiri, J.-C. Baret, D. Le Corre, L. Mazutis, C. B. Salem, F. Millot, A. El Harrak, J. B. Hutchison, J. W. Larson, *et al.*, "Quantitative and sensitive detection of rare mutations using droplet-based microfluidics," *Lab on a chip*, vol. 11, no. 13, pp. 2156–2166, 2011.

[22] P. Frank, J. Schreiter, S. Haefner, G. Paschew, A. Voigt, and A. Richter, "Integrated microfluidic membrane transistor utilizing chemical information for on-chip flow control," *PloS one*, vol. 11, no. 8, p. e0161024, 2016.

[23] M. Cheikh and I. Lakkis, "Microfluidic transistors for analog microflows amplification and control," *Microfluidics and Nanofluidics*, vol. 20, p. 91, Jun 2016.

[24] D. C. Leslie, C. J. Easley, E. Seker, J. M. Karlinsey, M. Utz, M. R. Begley, and J. P. Landers, "Frequency-specific flow control in microfluidic circuits with passive elastomeric features," *Nature Physics*, vol. 5, no. 3, p. 231, 2009.

[25] T. Thorsen, S. J. Maerkl, and S. R. Quake, "Microfluidic large-scale integration," *Science*, vol. 298, no. 5593, pp. 580–584, 2002.

[26] A. Groisman, M. Enzelberger, and S. R. Quake, "Microfluidic memory and control devices," *Science*, vol. 300, no. 5621, pp. 955–958, 2003.

[27] M. Zagnoni and J. M. Cooper, "A microdroplet-based shift register," *Lab on a chip*, vol. 10, no. 22, pp. 3069–3073, 2010.

[28] P. J. A. Kenis, R. F. Ismagilov, and G. M. Whitesides, "Microfabrication inside capillaries using multiphase laminar flow patterning," *Science*, pp. 83–85, 1999.

[29] S. K. Tang and G. M. Whitesides, "Basic microfluidic and soft lithographic techniques," 2009.

[30] H.-P. Chou, M. A. Unger, and S. R. Quake, "A microfabricated rotary pump," *Biomedical Microdevices*, vol. 3, no. 4, pp. 323–330, 2001.

[31] P. Yager, T. Edwards, E. Fu, K. Helton, K. Nelson, M. Tam, and B. Weigl, "Microfluidic diagnostic technologies for global public health," *Nature*, vol. 442, pp. 412–418, 7 2006.

[32] D. B. Weibel, M. Kruithof, S. Potenta, S. K. Sia, A. Lee, and G. M. Whitesides, "Torque-actuated valves for microfluidics," *Analytical Chemistry*, vol. 77, no. 15, pp. 4726–4733, 2005. PMID: 16053282.

[33] S. N. Bhatia and D. E. Ingber, "Microfluidic organs-on-chips," *Nature biotechnology*, vol. 32, no. 8, pp. 760–772, 2014.

[34] J.-M. Park, M. S. Kim, H.-S. Moon, C. E. Yoo, D. Park, Y. J. Kim, K.-Y. Han, J.-Y. Lee, J. H. Oh, S. S. Kim, W.-Y. Park, W.-Y. Lee, and N. Huh, "Fully automated circulating tumor cell isolation platform with large-volume capacity based on lab-on-a-disc," *Analytical Chemistry*, vol. 86, no. 8, pp. 3735–3742, 2014. PMID: 24641782.

[35] A. W. Martinez, S. T. Phillips, and G. M. Whitesides, "Three-dimensional microfluidic devices fabricated in layered paper and tape," *Proceedings of the National Academy of Sciences*, vol. 105, no. 50, pp. 19606–19611, 2008.

[36] C. W. Shields IV, C. D. Reyes, and G. P. López, "Microfluidic cell sorting: a review of the advances in the separation of cells from debulking to rare cell isolation," *Lab on a Chip*, vol. 15, no. 5, pp. 1230–1249, 2015.

[37] T. Thorsen, R. W. Roberts, F. H. Arnold, and S. R. Quake, "Dynamic pattern formation in a vesicle-generating microfluidic device," *Phys. Rev. Lett.*, vol. 86, pp. 4163–4166, Apr 2001.

[38] C. N. Baroud, F. Gallaire, and R. Dangla, "Dynamics of microfluidic droplets," *Lab on a Chip*, vol. 10, no. 16, pp. 2032–2045, 2010.

[39] P. Zhu and L. Wang, "Passive and active droplet generation with microfluidics: a review," *Lab on a Chip*, vol. 17, no. 1, pp. 34–75, 2017.

[40] K. S. Deal and C. J. Easley, "Self-regulated, droplet-based sample chopper for microfluidic absorbance detection," *Analytical chemistry*, vol. 84, no. 3, pp. 1510–1516, 2012.

[41] H. Gu, M. H. Duits, and F. Mugele, "Droplets formation and merging in two-phase flow microfluidics," *International journal of molecular sciences*, vol. 12, no. 4, pp. 2572–2597, 2011.

[42] A. S. Utada, A. Fernandez-Nieves, H. A. Stone, and D. A. Weitz, "Dripping to jetting transitions in coflowing liquid streams," *Phys. Rev. Lett.*, vol. 99, p. 094502, Aug 2007.

[43] R. Suryo and O. A. Basaran, "Dripping of a liquid from a tube in the absence of gravity," *Phys. Rev. Lett.*, vol. 96, p. 034504, Jan 2006.

[44] J.-C. Baret, "Surfactants in droplet-based microfluidics," *Lab Chip*, vol. 12, pp. 422–433, 2012.

[45] C. Holtze, A. Rowat, J. Agresti, J. Hutchison, F. Angile, C. Schmitz, S. Köster, H. Duan, K. Humphry, R. Scanga, *et al.*, "Biocompatible surfactants for water-in-fluorocarbon emulsions," *Lab on a Chip*, vol. 8, no. 10, pp. 1632–1639, 2008.

[46] M. Courtney, X. Chen, S. Chan, T. Mohamed, P. P. Rao, and C. L. Ren, "Droplet microfluidic system with on-demand trapping and releasing of droplet for drug screening applications," *Analytical chemistry*, vol. 89, no. 1, pp. 910–915, 2016.

[47] W. Shi, J. Qin, N. Ye, and B. Lin, "Droplet-based microfluidic system for individual caenorhabditis elegans assay," *Lab on a Chip*, vol. 8, no. 9, pp. 1432–1435, 2008.

[48] P. M. Korczyk, L. Derzsi, S. Jakieła, and P. Garstecki, "Microfluidic traps for hard-wired operations on droplets," *Lab on a Chip*, vol. 13, no. 20, pp. 4096–4102, 2013.

[49] A. Huebner, D. Bratton, G. Whyte, M. Yang, A. J. deMello, C. Abell, and F. Hollfelder, "Static microdroplet arrays: a microfluidic device for droplet trapping, incubation and release for enzymatic and cell-based assays," *Lab Chip*, vol. 9, pp. 692–698, 2009.

[50] J. Seo, S.-K. Lee, J. Lee, J. S. Lee, H. Kwon, S.-W. Cho, J.-H. Ahn, and T. Lee, "Path-programmable water droplet manipulations on an adhesion controlled superhydrophobic surface," *Scientific reports*, vol. 5, 2015.

[51] Y.-C. Tan, J. S. Fisher, A. I. Lee, V. Cristini, and A. P. Lee, "Design of microfluidic channel geometries for the control of droplet volume, chemical concentration, and sorting," *Lab on a Chip*, vol. 4, no. 4, pp. 292–298, 2004.

[52] A. R. Abate and D. A. Weitz, "Faster multiple emulsification with drop splitting," *Lab on a Chip*, vol. 11, no. 11, pp. 1911–1915, 2011.

[53] M. R. Bringer, C. J. Gerdts, H. Song, J. D. Tice, and R. F. Ismagilov, "Microfluidic systems for chemical kinetics that rely on chaotic mixing in droplets," *Philosophical Transactions of the Royal Society of London A: Mathematical, Physical and Engineering Sciences*, vol. 362, no. 1818, pp. 1087–1104, 2004.

[54] A. J. Demello, "Control and detection of chemical reactions in microfluidic systems.," *Nature*, vol. 442, no. 7101, pp. 394–402, 2006.

[55] T. Kokalj, E. Prez-Ruiz, and J. Lammertyn, "Building bio-assays with magnetic particles on a digital microfluidic platform," *New Biotechnology*, vol. 32, no. 5, pp. 485 – 503, 2015. Particle based biosensors.

[56] A. R. Abate, J. J. Agresti, and D. A. Weitz, "Microfluidic sorting with high-speed single-layer membrane valves," *Applied Physics Letters*, vol. 96, no. 20, p. 203509, 2010.

[57] H.-D. Xi, H. Zheng, W. Guo, A. M. Ganan-Calvo, Y. Ai, C.-W. Tsao, J. Zhou, W. Li, Y. Huang, N.-T. Nguyen, and S. H. Tan, "Active droplet sorting in microfluidics: a review," *Lab Chip*, vol. 17, pp. 751–771, 2017.

[58] L. Mazutis, J. Gilbert, W. L. Ung, D. A. Weitz, A. D. Griffiths, and J. A. Heyman, "Single-cell analysis and sorting using droplet-based microfluidics," *Nature protocols*, vol. 8, no. 5, p. 870, 2013.

[59] M. Girault, H. Kim, H. Arakawa, K. Matsuura, M. Odaka, A. Hattori, H. Terazono, and K. Yasuda, "An on-chip imaging droplet-sorting system: a real-time shape recognition method to screen target cells in droplets with single cell resolution," *Scientific reports*, vol. 7, p. 40072, 2017.

[60] L. Granieri, J.-C. Baret, A. D. Griffiths, and C. A. Merten, "High-throughput screening of enzymes by retroviral display using droplet-based microfluidics," *Chemistry Biology*, vol. 17, no. 3, pp. 229 – 235, 2010.

[61] Y.-J. Eun, A. S. Utada, M. F. Copeland, S. Takeuchi, and D. B. Weibel, "Encapsulating bacteria in agarose microparticles using microfluidics for high-throughput cell analysis and isolation," *ACS Chemical Biology*, vol. 6, no. 3, pp. 260–266, 2011. PMID: 21142208.

[62] Y.-C. Tan, K. Hettiarachchi, M. Siu, Y.-R. Pan, and A. P. Lee, "Controlled microfluidic encapsulation of cells, proteins, and microbeads in lipid vesicles," *Journal of the American Chemical Society*, vol. 128, no. 17, pp. 5656–5658, 2006. PMID: 16637631.

[63] J.-C. Baret, O. J. Miller, V. Taly, M. Ryckelynck, A. El-Harrak, L. Frenz, C. Rick, M. L. Samuels, J. B. Hutchison, J. J. Agresti, *et al.*, "Fluorescence-activated droplet sorting (fads): efficient microfluidic cell sorting based on enzymatic activity," *Lab on a Chip*, vol. 9, no. 13, pp. 1850–1858, 2009.

[64] A. C. Siegel, D. A. Bruzewicz, D. B. Weibel, and G. M. Whitesides, "Microsolidics: fabrication of three-dimensional metallic microstructures in poly (dimethylsiloxane)," *Advanced Materials*, vol. 19, no. 5, pp. 727–733, 2007.

[65] B. O'Donovan, D. J. Eastburn, and A. R. Abate, "Electrode-free picoinjection of microfluidic drops," *Lab on a Chip*, vol. 12, no. 20, pp. 4029–4032, 2012.

[66] A. R. Abate, T. Hung, P. Mary, J. J. Agresti, and D. A. Weitz, "High-throughput injection with microfluidics using picoinjectors," *Proceedings of the National Academy of Sciences*, vol. 107, no. 45, pp. 19163–19166, 2010.

[67] M. Sun, S. S. Bithi, and S. A. Vanapalli, "Microfluidic static droplet arrays with tuneable gradients in material composition," *Lab Chip*, vol. 11, pp. 3949–3952, 2011.

[68] S. H. Jin, H.-H. Jeong, B. Lee, S. S. Lee, and C.-S. Lee, "A programmable microfluidic static droplet array for droplet generation, transportation, fusion, storage, and retrieval," *Lab Chip*, vol. 15, pp. 3677–3686, 2015.

[69] W. Du, L. Li, K. P. Nichols, and R. F. Ismagilov, "Slipchip," *Lab Chip*, vol. 9, pp. 2286–2292, 2009.

[70] M. Lake, C. Narciso, K. Cowdrick, T. Storey, S. Zhang, J. Zartman, and D. Hoelzle, "Microfluidic device design, fabrication, and testing protocols," *Protoc. Exch*, vol. 10, 2015.

[71] A. K.-K. Wong, *Resolution enhancement techniques in optical lithography*, vol. 47. SPIE press, 2001.

[72] P. Kim, K. W. Kwon, M. C. Park, S. H. Lee, S. M. Kim, and K. Y. Suh, "Soft lithography for microfluidics: a review," 2008.

[73] D. Qin, Y. Xia, and G. M. Whitesides, "Soft lithography for micro-and nanoscale patterning," *Nature protocols*, vol. 5, no. 3, p. 491, 2010.

[74] G. C. Lisensky, D. J. Campbell, K. J. Beckman, C. E. Calderon, P. W. Doolan, R. M. Ottosen, and A. B. Ellis, "Replication and compression of surface structures with polydimethylsiloxane elastomer," *Journal of Chemical Education*, vol. 76, no. 4, p. 537, 1999.

[75] D. Huh, H. J. Kim, J. P. Fraser, D. E. Shea, M. Khan, A. Bahinski, G. A. Hamilton, and D. E. Ingber, "Microfabrication of human organs-on-chips," *Nature protocols*, vol. 8, no. 11, p. 2135, 2013.

[76] D. Huh, G. A. Hamilton, and D. E. Ingber, "From 3d cell culture to organs-on-chips," *Trends in cell biology*, vol. 21, no. 12, pp. 745–754, 2011.

[77] D. Huh, Y.-s. Torisawa, G. A. Hamilton, H. J. Kim, and D. E. Ingber, "Microengineered physiological biomimicry: organs-on-chips," *Lab on a Chip*, vol. 12, no. 12, pp. 2156–2164, 2012.

[78] N. F. Huang, R. J. Lee, and S. Li, "Engineering of aligned skeletal muscle by micropatterning," *American journal of translational research*, vol. 2, no. 1, p. 43, 2010.

[79] G. R. Gossweiler, C. L. Brown, G. B. Hewage, E. Sapiro-Gheiler, W. J. Trautman, G. W. Welshofer, and S. L. Craig, "Mechanochemically active soft robots," *ACS applied materials & interfaces*, vol. 7, no. 40, pp. 22431–22435, 2015.

[80] S. H. Tan, N.-T. Nguyen, Y. C. Chua, and T. G. Kang, "Oxygen plasma treatment for reducing hydrophobicity of a sealed polydimethylsiloxane microchannel," *Biomicrofluidics*, vol. 4, no. 3, p. 032204, 2010.

[81] J. A. Vickers, M. M. Caulum, and C. S. Henry, "Generation of hydrophilic poly (dimethylsiloxane) for high-performance microchip electrophoresis," *Analytical Chemistry*, vol. 78, no. 21, pp. 7446–7452, 2006.

[82] N. Pekas, Q. Zhang, M. Nannini, and D. Juncker, "Wet-etching of structures with straight facets and adjustable taper into glass substrates," *Lab on a Chip*, vol. 10, no. 4, pp. 494–498, 2010.

[83] C. Iliescu, H. Taylor, M. Avram, J. Miao, and S. Franssila, "A practical guide for the fabrication of microfluidic devices using glass and silicon," *Biomicrofluidics*, vol. 6, no. 1, p. 016505, 2012.

[84] L. A. Godwin, K. S. Deal, L. D. Hoepfner, L. A. Jackson, and C. J. Easley, "Measurement of microchannel fluidic resistance with a standard voltage meter," *Analytica Chimica Acta*, vol. 758, pp. 101 – 107, 2013.

[85] K. Avila, D. Moxey, A. de Lozar, M. Avila, D. Barkley, and B. Hof, "The onset of turbulence in pipe flow," *Science*, vol. 333, no. 6039, pp. 192–196, 2011.

[86] P. Garstecki, M. J. Fuerstman, H. A. Stone, and G. M. Whitesides, "Formation of droplets and bubbles in a microfluidic t-junctionscaling and mechanism of break-up," *Lab on a Chip*, vol. 6, no. 3, pp. 437–446, 2006.

[87] C. N. Baroud, F. Gallaire, and R. Dangla, "Dynamics of microfluidic droplets," *Lab Chip*, vol. 10, pp. 2032–2045, 2010.

[88] *Micromachined transducers sourcebook*, ch. . McGraw-Hill, 1998.

[89] M. M. Gong, B. D. MacDonald, T. Vu Nguyen, and D. Sinton, "Hand-powered microfluidics: A membrane pump with a patient-to-chip syringe interface," *Biomicrofluidics*, vol. 6, no. 4, p. 044102, 2012.

[90] S. E. Hulme, S. S. Shevkoplyas, and G. M. Whitesides, "Incorporation of prefabricated screw, pneumatic, and solenoid valves into microfluidic devices," *Lab on a Chip*, vol. 9, no. 1, pp. 79–86, 2009.

[91] D. B. Weibel, A. C. Siegel, A. Lee, A. H. George, and G. M. Whitesides, "Pumping fluids in microfluidic systems using the elastic deformation of poly (dimethylsiloxane)," *Lab on a Chip*, vol. 7, no. 12, pp. 1832–1836, 2007.

[92] J. Y. Baek, J. Y. Park, J. I. Ju, T. S. Lee, and S. H. Lee, "A pneumatically controllable flexible and polymeric microfluidic valve fabricated via in situ development," *Journal of micromechanics and microengineering*, vol. 15, no. 5, p. 1015, 2005.

[93] W. H. Grover, A. M. Skelley, C. N. Liu, E. T. Lagally, and R. A. Mathies, "Monolithic membrane valves and diaphragm pumps for practical large-scale integration into glass microfluidic devices," *Sensors and Actuators B: Chemical*, vol. 89, no. 3, pp. 315–323, 2003.

[94] W. H. Grover, R. H. Ivester, E. C. Jensen, and R. A. Mathies, "Development and multiplexed control of latching pneumatic valves using microfluidic logical structures," *Lab on a Chip*, vol. 6, no. 5, pp. 623–631, 2006.

[95] M. A. Unger, H.-P. Chou, T. Thorsen, A. Scherer, and S. R. Quake, "Monolithic microfabricated valves and pumps by multilayer soft lithography," *Science*, vol. 288, no. 5463, pp. 113–116, 2000.

[96] D. C. Duffy, J. C. McDonald, O. J. Schueller, and G. M. Whitesides, "Rapid prototyping of microfluidic systems in poly (dimethylsiloxane)," *Analytical chemistry*, vol. 70, no. 23, pp. 4974–4984, 1998.

[97] J. Melin and S. R. Quake, "Microfluidic large-scale integration: the evolution of design rules for biological automation," *Annu. Rev. Biophys. Biomol. Struct.*, vol. 36, pp. 213–231, 2007.

[98] P. Fordyce, C. Diaz-Botia, J. DeRisi, and R. Gomez-Sjoberg, "Systematic characterization of feature dimensions and closing pressures for microfluidic valves produced via photoresist reflow," *Lab on a Chip*, vol. 12, no. 21, pp. 4287–4295, 2012.

[99] S. C. Jacobson, S. V. Ermakov, and J. M. Ramsey, "Minimizing the number of voltage sources and fluid reservoirs for electrokinetic valving in microfluidic devices," *Analytical Chemistry*, vol. 71, no. 15, pp. 3273–3276, 1999.

[100] D. Juncker, H. Schmid, U. Drechsler, H. Wolf, M. Wolf, B. Michel, N. de Rooij, and E. Delamarche, "Autonomous microfluidic capillary system," *Analytical chemistry*, vol. 74, no. 24, pp. 6139–6144, 2002.

[101] W. H. Grover, A. M. Skelley, C. N. Liu, E. T. Lagally, and R. A. Mathies, "Monolithic membrane valves and diaphragm pumps for practical large-scale integration into glass microfluidic devices," *Sensors and Actuators B: Chemical*, vol. 89, no. 3, pp. 315 – 323, 2003.

[102] D. C. Leslie, B. A. Melnikoff, D. J. Marchiarullo, D. R. Cash, J. P. Ferrance, and J. P. Landers, "A simple method for the evaluation of microfluidic architecture using flow quantitation via a multiplexed fluidic resistance measurement," *Lab Chip*, vol. 10, pp. 1960–1966, 2010.

[103] M. L. Adams, M. L. Johnston, A. Scherer, and S. R. Quake, "Polydimethylsiloxane based microfluidic diode," *Journal of Micromechanics and Microengineering*, vol. 15, no. 8, p. 1517, 2005.

[104] R. D. Sochol, A. Lu, J. Lei, K. Iwai, L. P. Lee, and L. Lin, "Microfluidic bead-based diodes with targeted circular microchannels for low reynolds number applications," *Lab Chip*, vol. 14, pp. 1585–1594, 2014.

[105] B. Mosadegh, C.-H. Kuo, Y.-C. Tung, Y.-s. Torisawa, T. Bersano-Begey, H. Tavana, and S. Takayama, "Integrated elastomeric components for autonomous regulation of sequential and oscillatory flow switching in microfluidic devices," *Nature physics*, vol. 6, no. 6, pp. 433–437, 2010.

[106] S.-J. Kim, R. Yokokawa, and S. Takayama, "Microfluidic oscillators with widely tunable periods," *Lab Chip*, vol. 13, pp. 1644–1648, 2013.

[107] M. Demori, V. Ferrari, and P. Poesio, "A microfluidic capacitance sensor for fluid discrimination and characterization," *Procedia Engineering*, vol. 5, no. Supplement C, pp. 408 – 411, 2010. Eurosensor XXIV Conference.

[108] H.-J. Chang, W. Ye, and E. P. Kartalov, "Quantitative modeling of the behaviour of microfluidic autoregulatory devices," *Lab on a Chip*, vol. 12, no. 10, pp. 1890–1896, 2012.

[109] G. Cristobal, L. Arbouet, F. Sarrazin, D. Talaga, J.-L. Bruneel, M. Joanicot, and L. Servant, "On-line laser raman spectroscopic probing of droplets engineered in microfluidic devices," *Lab Chip*, vol. 6, pp. 1140–1146, 2006.

[110] D. Gao, H. Liu, Y. Jiang, and J.-M. Lin, "Recent advances in microfluidics combined with mass spectrometry: technologies and applications," *Lab on a Chip*, vol. 13, no. 17, pp. 3309–3322, 2013.

[111] N. J. Petersen, K. B. Mogensen, and J. P. Kutter, "Performance of an in-plane detection cell with integrated waveguides for uv/vis absorbance measurements on microfluidic separation devices," *Electrophoresis*, vol. 23, no. 20, pp. 3528–3536, 2002.

[112] X. Liu, X. Liu, A. Liang, Z. Shen, Y. Zhang, Z. Dai, B. Xiong, and B. Lin, "Studying protein-drug interaction by microfluidic chip affinity capillary electrophoresis with indirect laser-induced fluorescence detection," *Electrophoresis*, vol. 27, no. 15, pp. 3125–3128, 2006.

[113] A. M. Gracioso Martins, N. R. Glass, S. Harrison, A. R. Rezk, N. A. Porter, P. D. Carpenter, J. Du Plessis, J. R. Friend, and L. Y. Yeo, "Toward complete miniaturisation of flow injection analysis systems: Microfluidic enhancement of chemiluminescent detection," *Analytical Chemistry*, vol. 86, no. 21, pp. 10812–10819, 2014. PMID: 25275830.

[114] K. L. Peters, I. Corbin, L. M. Kaufman, K. Zreibe, L. Blanes, and B. R. McCord, "Simultaneous colorimetric detection of improvised explosive compounds using microfluidic paper-based analytical devices (μpads)," *Analytical Methods*, vol. 7, no. 1, pp. 63–70, 2015.

[115] B. J. Sanghavi, J. A. Moore, J. L. Chvez, J. A. Hagen, N. Kelley-Loughnane, C.-F. Chou, and N. S. Swami, "Aptamer-functionalized nanoparticles for surface immobilization-free electrochemical detection of cortisol in a microfluidic device," *Biosensors and Bioelectronics*, vol. 78, pp. 244 – 252, 2016.

[116] Y. Lin, D. Gritsenko, S. Feng, Y. C. Teh, X. Lu, and J. Xu, "Detection of heavy metal by paper-based microfluidics," *Biosensors and Bioelectronics*, vol. 83, pp. 256 – 266, 2016.

[117] D. Gao, H. Liu, Y. Jiang, and J.-M. Lin, "Recent advances in microfluidics combined with mass spectrometry: technologies and applications," *Lab Chip*, vol. 13, pp. 3309–3322, 2013.

[118] F. Pena-Pereira, I. Costas-Mora, V. Romero, I. Lavilla, and C. Bendicho, "Advances in miniaturized uv-vis spectrometric systems," *TrAC Trends in Analytical Chemistry*, vol. 30, no. 10, pp. 1637 – 1648, 2011. In-Vivo and On-Site Analysis II.

[119] A. Author, "Improving fluorescence detection in lab on chip devices," *Lab on a Chip*, vol. 8, no. 5, pp. 649–652, 2008.

[120] S. A. Marras, F. R. Kramer, and S. Tyagi, "Efficiencies of fluorescence resonance energy transfer and contact-mediated quenching in oligonucleotide probes," *Nucleic acids research*, vol. 30, no. 21, pp. e122–e122, 2002.

[121] E. Heyduk, B. Dummit, Y.-H. Chang, and T. Heyduk, "Molecular pincers: Antibody-based homogeneous protein sensors," *Analytical Chemistry*, vol. 80, no. 13, pp. 5152–5159, 2008. PMID: 18491925.

[122] J. Kim, J. Hu, A. B. Bezerra, M. D. Holtan, J. C. , and C. J. Easley, "Protein quantification using controlled dna melting transitions in bivalent probe assemblies," *Analytical Chemistry*, vol. 87, no. 19, pp. 9576–9579, 2015. PMID: 26372070.

[123] J. M. Masciotti, J. M. Lasker, and A. H. Hielscher, "Digital lock-in detection for discriminating multiple modulation frequencies with high accuracy and computational efficiency," *IEEE Transactions on Instrumentation and Measurement*, vol. 57, pp. 182–189, Jan 2008.

[124] PhD thesis.

[125] J. Goree, "Double lockin detection for recovering weak coherent radio frequency signals," *Review of Scientific Instruments*, vol. 56, no. 8, pp. 1662–1664, 1985.

[126] P. Horowitz and W. Hill, *The art of electronics*. Cambridge Univ. Press, 1989.

[127] A. Mandelis, "Signaltonoise ratio in lockin amplifier synchronous detection: A generalized communications systems approach with applications to frequency, time, and hybrid (rate window) photothermal measurements," *Review of Scientific Instruments*, vol. 65, no. 11, pp. 3309–3323, 1994.

[128] T. H. Wilmshurst, *Signal recovery from noise in electronic instrumentation*. CRC Press, 1990.

[129] D. A. Skoog, F. J. Holler, and S. R. Crouch, *Principles of instrumental analysis*. Cengage learning, 2017.

[130] M. E. Johnson and J. P. Landers, "Fundamentals and practice for ultrasensitive laser-induced fluorescence detection in microanalytical systems," *Electrophoresis*, vol. 25, no. 21-22, pp. 3513–3527, 2004.

[131] K.-H. Han, R. D. McConnell, C. J. Easley, J. M. Bienvenue, J. P. Ferrance, J. P. Landers, and A. B. Frazier, "An active microfluidic system packaging technology," *Sensors and Actuators B: Chemical*, vol. 122, no. 1, pp. 337 – 346, 2007.

[132] X. Fan and I. M. White, "Optofluidic microsystems for chemical and biological analysis," *Nature photonics*, vol. 5, no. 10, pp. 591–597, 2011.

[133] S. S. Guduru, F. Scotognella, A. Chiasera, V. Sreeramulu, L. Criante, K. C. Vishnubhatla, M. Ferrari, R. Ramponi, G. Lanzani, and R. M. Vázquez, "Highly integrated lab-on-a-chip for fluorescence detection," *Optical Engineering*, vol. 55, no. 9, pp. 097102–097102, 2016.

[134] L. Pang, H. M. Chen, L. M. Freeman, and Y. Fainman, "Optofluidic devices and applications in photonics, sensing and imaging," *Lab Chip*, vol. 12, pp. 3543–3551, 2012.

[135] Y. Zhang, B. R. Watts, T. Guo, Z. Zhang, C. Xu, and Q. Fang, "Optofluidic device based microflow cytometers for particle/cell detection: A review," *Micromachines*, vol. 7, no. 4, p. 70, 2016.

[136] K. S. Deal and C. J. Easley, "Self-regulated, droplet-based sample chopper for microfluidic absorbance detection," *Analytical Chemistry*, vol. 84, no. 3, pp. 1510–1516, 2012. PMID: 22191400.

[137] A. Mrz, T. Bocklitz, and J. Popp, "Online-calibration for reliable and robust lab-on-a-chip surface enhanced raman spectroscopy measurement in a liquid/liquid segmented flow," *Analytical Chemistry*, vol. 83, no. 21, pp. 8337–8340, 2011. PMID: 21916424.

[138] C. J. Easley, J. V. Rocheleau, W. S. Head, and D. W. Piston, "Quantitative measurement of zinc secretion from pancreatic islets with high temporal resolution using droplet-based microfluidics," *Analytical Chemistry*, vol. 81, no. 21, pp. 9086–9095, 2009. PMID: 19874061.

[139] C. J. Easley, R. K. P. Benninger, J. H. Shaver, W. Steven Head, and D. W. Piston, "Rapid and inexpensive fabrication of polymeric microfluidic devices via toner transfer masking," *Lab Chip*, vol. 9, pp. 1119–1127, 2009.

[140] L. A. Godwin, M. E. Pilkerton, K. S. Deal, D. Wanders, R. L. Judd, and C. J. Easley, "Passively operated microfluidic device for stimulation and secretion sampling of single pancreatic islets," *Analytical Chemistry*, vol. 83, no. 18, pp. 7166–7172, 2011. PMID: 21806019.

[141] J. C. Brooks, R. L. Judd, and C. J. Easley, *Culture and Sampling of Primary Adipose Tissue in Practical Microfluidic Systems*, pp. 185–201. New York, NY: Springer New York, 2017.

[142] M. Erickstad, E. Gutierrez, and A. Groisman, "A low-cost low-maintenance ultraviolet lithography light source based on light-emitting diodes," *Lab Chip*, vol. 15, pp. 57–61, 2015.

[143] C. A. Schneider, W. S. Rasband, and K. W. Eliceiri, "Nih image to imagej: 25 years of image analysis," *Nature methods*, vol. 9, no. 7, pp. 671–675, 2012.

[144] L. A. Godwin, J. C. Brooks, L. D. Hoepfner, D. Wanders, R. L. Judd, and C. J. Easley, "A microfluidic interface for the culture and sampling of adiponectin from primary adipocytes," *Analyst*, vol. 140, pp. 1019–1025, 2015.

[145] X. Li, J. C. Brooks, J. Hu, K. I. Ford, and C. J. Easley, "3d-templated, fully automated microfluidic input/output multiplexer for endocrine tissue culture and secretion sampling," *Lab Chip*, vol. 17, pp. 341–349, 2017.

[146] J. C. Brooks, K. I. Ford, D. H. Holder, M. D. Holtan, and C. J. Easley, "Macro-to-micro interfacing to microfluidic channels using 3d-printed templates: application to time-resolved secretion sampling of endocrine tissue," *Analyst*, vol. 141, pp. 5714–5721, 2016.

[147] V. Lecault, A. K. White, A. Singhal, and C. L. Hansen, "Microfluidic single cell analysis: from promise to practice," *Current Opinion in Chemical Biology*, vol. 16, no. 3, pp. 381 – 390, 2012. Synthetic biology / Analytical techniques.

[148] R. N. Zare and S. Kim, "Microfluidic platforms for single-cell analysis," *Annual Review of Biomedical Engineering*, vol. 12, no. 1, pp. 187–201, 2010. PMID: 20433347.

[149] E. Brouzes, M. Medkova, N. Savenelli, D. Marran, M. Twardowski, J. B. Hutchison, J. M. Rothberg, D. R. Link, N. Perrimon, and M. L. Samuels, "Droplet microfluidic technology for single-cell high-throughput screening," *Proceedings of the National Academy of Sciences*, vol. 106, no. 34, pp. 14195–14200, 2009.

[150] F. Chen, L. Lin, J. Zhang, Z. He, K. Uchiyama, and J.-M. Lin, "Single-cell analysis using drop-on-demand inkjet printing and probe electrospray ionization mass spectrometry," *Analytical Chemistry*, vol. 88, no. 8, pp. 4354–4360, 2016. PMID: 27015013.

[151] Q. Li, P. Chen, Y. Fan, X. Wang, K. Xu, L. Li, and B. Tang, "Multicolor fluorescence detection-based microfluidic device for single-cell metabolomics: Simultaneous quantitation of multiple small molecules in primary liver cells," *Analytical Chemistry*, vol. 88, no. 17, pp. 8610–8616, 2016. PMID: 27503398.

[152] A. Herms, M. Bosch, N. Ariotti, B. J. Reddy, A. Fajardo, A. Fernndez-Vidal, A. Alvarez-Guaita, M. A. Fernndez-Rojo, C. Rentero, F. Tebar, C. Enrich, M.-I. Geli, R. G. Parton, S. P. Gross, and A. Pol, "Cell-to-cell heterogeneity in lipid droplets suggests a mechanism to reduce lipotoxicity," *Current Biology*, vol. 23, no. 15, pp. 1489 – 1496, 2013.

[153] P. J. Campbell, M. G. Carlson, and N. Nurjhan, "Fat metabolism in human obesity," *American Journal of Physiology-Endocrinology And Metabolism*, vol. 266, no. 4, pp. E600–E605, 1994.

[154] M. D. Jensen, M. W. Haymond, R. A. Rizza, P. E. Cryer, and J. M. Miles, "Influence of body fat distribution on free fatty acid metabolism in obesity.," *The Journal of Clinical Investigation*, vol. 83, pp. 1168–1173, 4 1989.

[155] B. B. Kahn and J. S. Flier, "Obesity and insulin resistance," *The Journal of Clinical Investigation*, vol. 106, pp. 473–481, 8 2000.

[156] L. R. Roust and M. D. Jensen, "Postprandial free fatty acid kinetics are abnormal in upper body obesity," *Diabetes*, vol. 42, no. 11, pp. 1567–1573, 1993.

[157] R. N. Bergman and M. Ader, "Free fatty acids and pathogenesis of type 2 diabetes mellitus," *Trends in Endocrinology Metabolism*, vol. 11, no. 9, pp. 351 – 356, 2000.

[158] R. H. Unger, "Lipotoxicity in the pathogenesis of obesity-dependent niddm: Genetic and clinical implications," *Diabetes*, vol. 44, no. 8, pp. 863–870, 1995.

[159] E. Dubikovskaya, R. Chudnovskiy, G. Karateev, H. M. Park, and A. Stahl, "Measurement of long-chain fatty acid uptake into adipocytes," *Methods in Enzymology*, vol. 538, pp. 107 – 134, 2014. Methods of Adipose Tissue Biology, Part B.

[160] O. Varlamov, R. Somwar, A. Cornea, P. Kievit, K. L. Grove, and C. T. Roberts, "Single-cell analysis of insulin-regulated fatty acid uptake in adipocytes," *American Journal of Physiology - Endocrinology and Metabolism*, vol. 299, no. 3, pp. E486–E496, 2010.

[161] S. Sun, B. C. Buer, E. N. G. Marsh, and R. T. Kennedy, "A label-free sirtuin 1 assay based on droplet-electrospray ionization mass spectrometry," *Anal. Methods*, vol. 8, pp. 3458–3465, 2016.

[162] S. Sun and R. T. Kennedy, "Droplet electrospray ionization mass spectrometry for high throughput screening for enzyme inhibitors," *Analytical Chemistry*, vol. 86, no. 18, pp. 9309–9314, 2014. PMID: 25137241.

[163] X. Lin, X. Hu, Z. Bai, Q. He, H. Chen, Y. Yan, and Z. Ding, "A microfluidic chip capable of switching w/o droplets to vertical laminar flow for electrochemical detection of droplet contents," *Analytica Chimica Acta*, vol. 828, pp. 70 – 79, 2014.

[164] A. Sciambi and A. R. Abate, "Accurate microfluidic sorting of droplets at 30 khz," *Lab Chip*, vol. 15, pp. 47–51, 2015.

[165] S.-Y. Teh, R. Lin, L.-H. Hung, and A. P. Lee, "Droplet microfluidics," *Lab Chip*, vol. 8, pp. 198–220, 2008.

[166] T. Schneider, J. Kreutz, and D. T. Chiu, "The potential impact of droplet microfluidics in biology," *Analytical Chemistry*, vol. 85, no. 7, pp. 3476–3482, 2013. PMID: 23495853.

[167] M. T. Guo, A. Rotem, J. A. Heyman, and D. A. Weitz, "Droplet microfluidics for high-throughput biological assays," *Lab on a Chip*, vol. 12, no. 12, pp. 2146–2155, 2012.

[168] S. S. Aimovi, M. A. Ortega, V. Sanz, J. Berthelot, J. L. Garcia-Cordero, J. Renger, S. J. Maerkl, M. P. Kreuzer, and R. Quidant, "Lspr chip for parallel, rapid, and sensitive detection of cancer markers in serum," *Nano Letters*, vol. 14, no. 5, pp. 2636–2641, 2014. PMID: 24730454.

[169] J. T. Negou, L. A. Avila, X. Li, T. M. Hagos, and C. J. Easley, "An automated microfluidic droplet-based sample chopper for detection of small fluorescence differences using lock-in analysis," *Analytical Chemistry*, 2017.

[170] J. F. Dishinger, K. R. Reid, and R. T. Kennedy, "Quantitative monitoring of insulin secretion from single islets of langerhans in parallel on a microfluidic chip," *Analytical chemistry*, vol. 81, no. 8, pp. 3119–3127, 2009.

[171] S.-M. Han, J.-H. Cho, I.-H. Cho, E.-H. Paek, H.-B. Oh, B.-S. Kim, C. Ryu, K. Lee, Y.-K. Kim, and S.-H. Paek, "Plastic enzyme-linked immunosorbent assays (elisa)-on-a-chip biosensor for botulinum neurotoxin a," *Analytica Chimica Acta*, vol. 587, no. 1, pp. 1 – 8, 2007.

[172] M. Ihara, A. Yoshikawa, Y. Wu, H. Takahashi, K. Mawatari, K. Shimura, K. Sato, T. Kitamori, and H. Ueda, "Micro os-elisa: Rapid noncompetitive detection of a small biomarker peptide by open-sandwich enzyme-linked immunosorbent assay (os-elisa) integrated into microfluidic device," *Lab Chip*, vol. 10, pp. 92–100, 2010.

[173] N. Yanagisawa, J. O. Mecham, R. C. Corcoran, and D. Dutta, "Multiplex elisa in a single microfluidic channel," *Analytical and Bioanalytical Chemistry*, vol. 401, p. 1173, Jul 2011.

[174] S. Ishii, T. Segawa, and S. Okabe, "Simultaneous quantification of multiple food and waterborne pathogens by use of microfluidic quantitative pcr," *Applied and environmental microbiology*, pp. AEM–00205, 2013.

[175] S. Lutz, P. Weber, M. Focke, B. Faltin, J. Hoffmann, C. Muller, D. Mark, G. Roth, P. Munday, N. Armes, O. Piepenburg, R. Zengerle, and F. von Stetten, "Microfluidic lab-on-a-foil for nucleic acid analysis based on isothermal recombinase polymerase amplification (rpa)," *Lab Chip*, vol. 10, pp. 887–893, 2010.

[176] J. Y. Kim and J.-L. Lee, "Development of a multiplex real-time recombinase polymerase amplification (rpa) assay for rapid quantitative detection of campylobacter coli and jejuni from eggs and chicken products," *Food Control*, vol. 73, Part B, pp. 1247 – 1255, 2017.

[177] H. C. Tekin and M. A. M. Gijs, "Ultrasensitive protein detection: a case for microfluidic magnetic bead-based assays," *Lab Chip*, vol. 13, pp. 4711–4739, 2013.

[178] G. Shao, D. Lu, Z. Fu, D. Du, R. M. Ozanich, W. Wang, and Y. Lin, "Design, fabrication and test of a pneumatically controlled, renewable, microfluidic bead trapping device for sequential injection analysis applications," *Analyst*, vol. 141, pp. 206–215, 2016.

[179] J. A. Thompson and H. H. Bau, "Microfluidic, bead-based assay: Theory and experiments," *Journal of Chromatography B*, vol. 878, no. 2, pp. 228 – 236, 2010. IMMUNOAFFINITY TECHNIQUES IN ANALYSIS.

[180] H. Zhang, Y. Liu, X. Fu, L. Yuan, and Z. Zhu, "Microfluidic bead-based assay for micrornas using quantum dots as labels and enzymatic amplification," *Microchimica Acta*, vol. 182, pp. 661–669, Feb 2015.

[181] J. Hu, J. Kim, and C. J. Easley, "Quantifying aptamer-protein binding via thermofluorimetric analysis," *Anal. Methods*, vol. 7, pp. 7358–7362, 2015.

[182] F. Volpetti, J. Garcia-Cordero, and S. J. Maerkl, "A microfluidic platform for high-throughput multiplexed protein quantitation," *PloS one*, vol. 10, no. 2, p. e0117744, 2015.

[183] A. H. Diercks, A. Ozinsky, C. L. Hansen, J. M. Spotts, D. J. Rodriguez, and A. Aderem, "A microfluidic device for multiplexed protein detection in nano-liter volumes," *Analytical Biochemistry*, vol. 386, no. 1, pp. 30 – 35, 2009.

[184] K. Ward and Z. H. Fan, "Mixing in microfluidic devices and enhancement methods," *Journal of Micromechanics and Microengineering*, vol. 25, no. 9, p. 094001, 2015.

[185] S. Tyagi and F. R. Kramer, "Molecular beacons: probes that fluoresce upon hybridization," *Nature biotechnology*, vol. 14, no. 3, pp. 303–308, 1996.

[186] B. He, B. J. Burke, X. Zhang, R. Zhang, and F. E. Regnier, "A picoliter-volume mixer for microfluidic analytical systems," *Analytical Chemistry*, vol. 73, no. 9, pp. 1942–1947, 2001.

[187] J. Melin, G. Giménez, N. Roxhed, W. van der Wijngaart, and G. Stemme, "A fast passive and planar liquid sample micromixer," *Lab on a Chip*, vol. 4, no. 3, pp. 214–219, 2004.

[188] A. D. Stroock, S. K. Dertinger, A. Ajdari, I. Mezić, H. A. Stone, and G. M. Whitesides, "Chaotic mixer for microchannels," *Science*, vol. 295, no. 5555, pp. 647–651, 2002.

[189] Y. Z. Liu, B. J. Kim, and H. J. Sung, "Two-fluid mixing in a microchannel," *International journal of heat and fluid flow*, vol. 25, no. 6, pp. 986–995, 2004.

[190] S. R. Quake and A. Scherer, "From micro- to nanofabrication with soft materials," *Science*, vol. 290, no. 5496, pp. 1536–1540, 2000.

[191] J. W. Hong, V. Studer, G. Hang, W. F. Anderson, and S. R. Quake, "A nanoliter-scale nucleic acid processor with parallel architecture," *Nature biotechnology*, vol. 22, no. 4, pp. 435–439, 2004.

[192] A.-J. Wang, J.-J. Xu, and H.-Y. Chen, "In-situ grafting hydrophilic polymer on chitosan modified poly(dimethylsiloxane) microchip for separation of biomolecules," *Journal of Chromatography A*, vol. 1147, no. 1, pp. 120 – 126, 2007.

[193] C. J. DeJournette, J. Kim, H. Medlen, X. Li, L. J. Vincent, and C. J. Easley, "Creating biocompatible oilwater interfaces without synthesis: Direct interactions between primary amines and carboxylated perfluorocarbon surfactants," *Analytical Chemistry*, vol. 85, no. 21, pp. 10556–10564, 2013. PMID: 24070333.

[194] C. L. Hansen, M. O. A. Sommer, and S. R. Quake, "Systematic investigation of protein phase behavior with a microfluidic formulator," *Proceedings of the National Academy of Sciences of the United States of America*, vol. 101, no. 40, pp. 14431–14436, 2004.

[195] H.-Y. Tseng, C.-H. Wang, W.-Y. Lin, and G.-B. Lee, "Membrane-activated microfluidic rotary devices for pumping and mixing," *Biomedical Microdevices*, vol. 9, pp. 545–554, Aug 2007.

[196] J. Liu, Y. Chen, C. R. Taylor, A. Scherer, and E. P. Kartalov, "Elastomeric microfluidic diode and rectifier work with newtonian fluids," *Journal of Applied Physics*, vol. 106, no. 11, p. 114311, 2009.

[197] S.-J. Kim, R. Yokokawa, and S. Takayama, "Analyzing threshold pressure limitations in microfluidic transistors for self-regulated microfluidic circuits," *Applied Physics Letters*, vol. 101, no. 23, p. 234107, 2012.

[198] X. Zhang, Z. Zhu, Z. Ni, N. Xiang, and H. Yi, "Inexpensive, rapid fabrication of polymer-film microfluidic autoregulatory valve for disposable microfluidics," *Biomedical Microdevices*, vol. 19, p. 21, Apr 2017.

[199] X. Zhang, N. Xiang, W. Tang, D. Huang, X. Wang, H. Yi, and Z. Ni, "A passive flow regulator with low threshold pressure for high-throughput inertial isolation of microbeads," *Lab Chip*, vol. 15, pp. 3473–3480, 2015.

[200] S. Köster, F. E. Angile, H. Duan, J. J. Agresti, A. Wintner, C. Schmitz, A. C. Rowat, C. A. Merten, D. Pisignano, A. D. Griffiths, *et al.*, "Drop-based microfluidic devices for encapsulation of single cells," *Lab on a Chip*, vol. 8, no. 7, pp. 1110–1115, 2008.

[201] D. Chen, W. Du, Y. Liu, W. Liu, A. Kuznetsov, F. E. Mendez, L. H. Philipson, and R. F. Ismagilov, "The chemistrode: A droplet-based microfluidic device for stimulation and recording with high temporal, spatial, and chemical resolution," *Proceedings of the National Academy of Sciences*, vol. 105, no. 44, pp. 16843–16848, 2008.

[202] J. E. Purvis and G. Lahav, "Decoding the insulin signal," *Molecular cell*, vol. 46, p. 715716, June 2012.

[203] A. Capurro, F. Baroni, L. S. Kuebler, Z. Krpti, T. Dekker, H. Lei, B. S. Hansson, T. C. Pearce, and S. B. Olsson, "Temporal features of spike trains in the moth antennal lobe revealed by a comparative time-frequency analysis," *PLOS ONE*, vol. 9, pp. 1–10, 01 2014.

[204] J.-J. Chiu and S. Chien, "Effects of disturbed flow on vascular endothelium: Pathophysiological basis and clinical perspectives," *Physiological Reviews*, vol. 91, no. 1, pp. 327–387, 2011.

[205] Y. J. Heo, J. Kang, M. J. Kim, and W. K. Chung, "Tuning-free controller to accurately regulate flow rates in a microfluidic network," *Scientific reports*, vol. 6, p. 23273, 2016.

[206] E. C. Jensen, W. H. Grover, and R. A. Mathies, "Micropneumatic digital logic structures for integrated microdevice computation and control," *Journal of Microelectromechanical Systems*, vol. 16, pp. 1378–1385, Dec 2007.

[207] M. M. Hamedi, A. Ainla, F. Güder, D. C. Christodouleas, M. T. Fernández-Abedul, and G. M. Whitesides, "Integrating electronics and microfluidics on paper," *Advanced Materials*, vol. 28, no. 25, pp. 5054–5063, 2016.

[208] S.-J. Kim, R. Yokokawa, and S. Takayama, "Analyzing threshold pressure limitations in microfluidic transistors for self-regulated microfluidic circuits," *Applied physics letters*, vol. 101, no. 23, p. 234107, 2012.

[209] M.-H. Cheng and Z.-W. Wu, "Low-power low-voltage reference using peaking current mirror circuit," *Electronics Letters*, vol. 41, no. 10, pp. 572–573, 2005.

[210] P. Crawley and G. Roberts, "High-swing mos current mirror with arbitrarily high output resistance," *Electronics Letters*, vol. 28, no. 4, pp. 361–363, 1992.

[211] L. Li, Y. Yang, X. Shi, H. Wu, H. Chen, and J. Liu, "A microfluidic system for the study of the response of endothelial cells under pressure," *Microfluidics and Nanofluidics*, vol. 16, pp. 1089–1096, Jun 2014.

Chapter 7

Apendix A

7.1 LabView programs

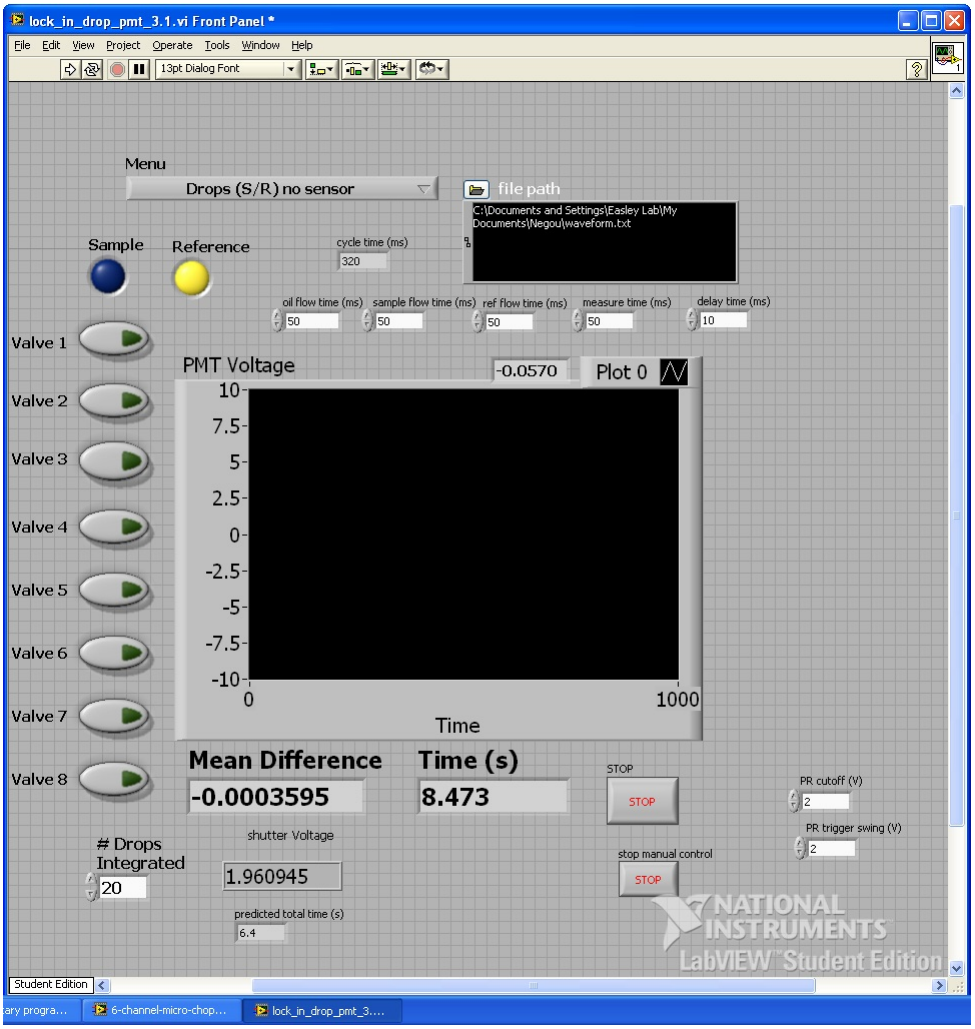

Figure 7.1: Automated Lock-in LabView Program front panel

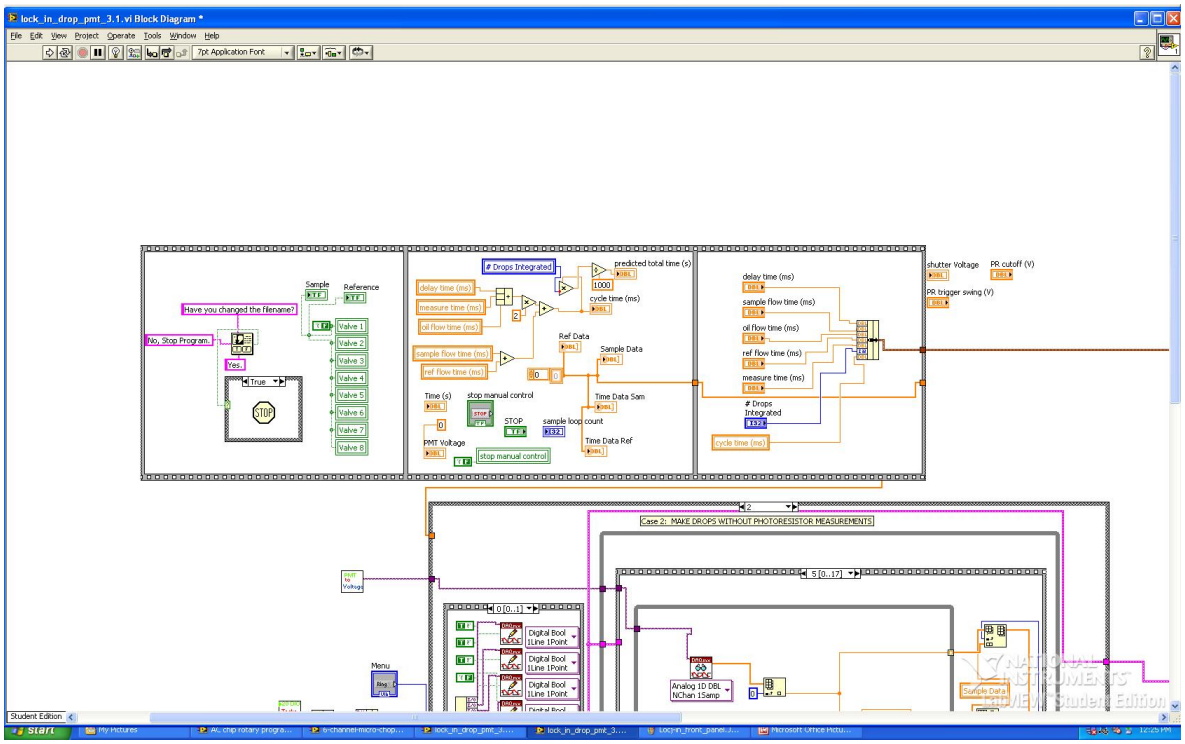

Figure 7.2: Automated Lock-in LabView Program block diagram
Lock-in data initialization

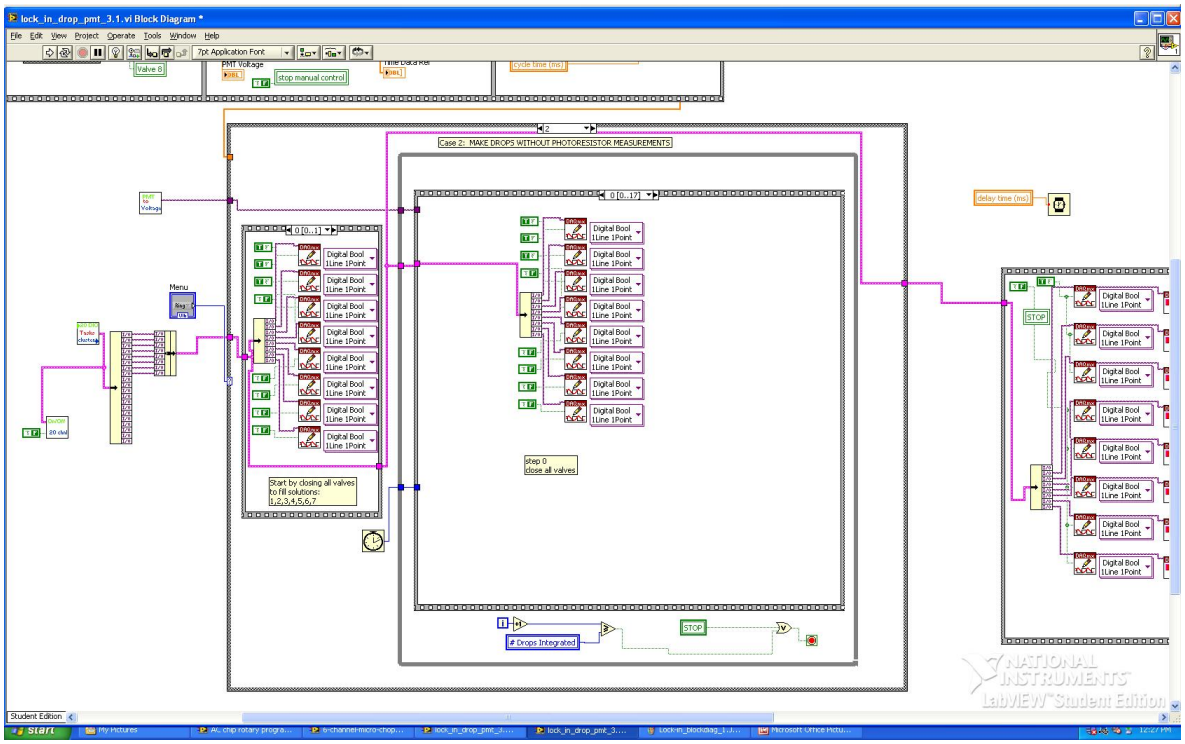

Figure 7.3: Automated Lock-in LabView Program block diagram step 1

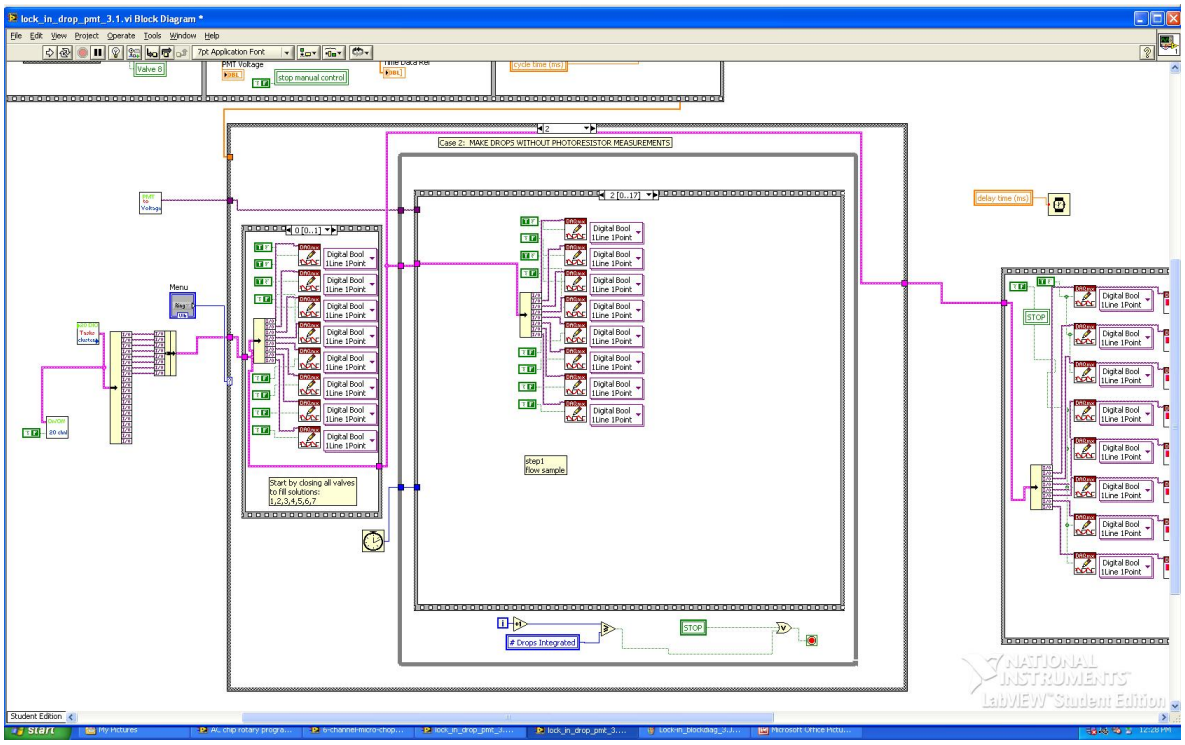

Figure 7.4: Automated Lock-in LabView Program block diagram step 2

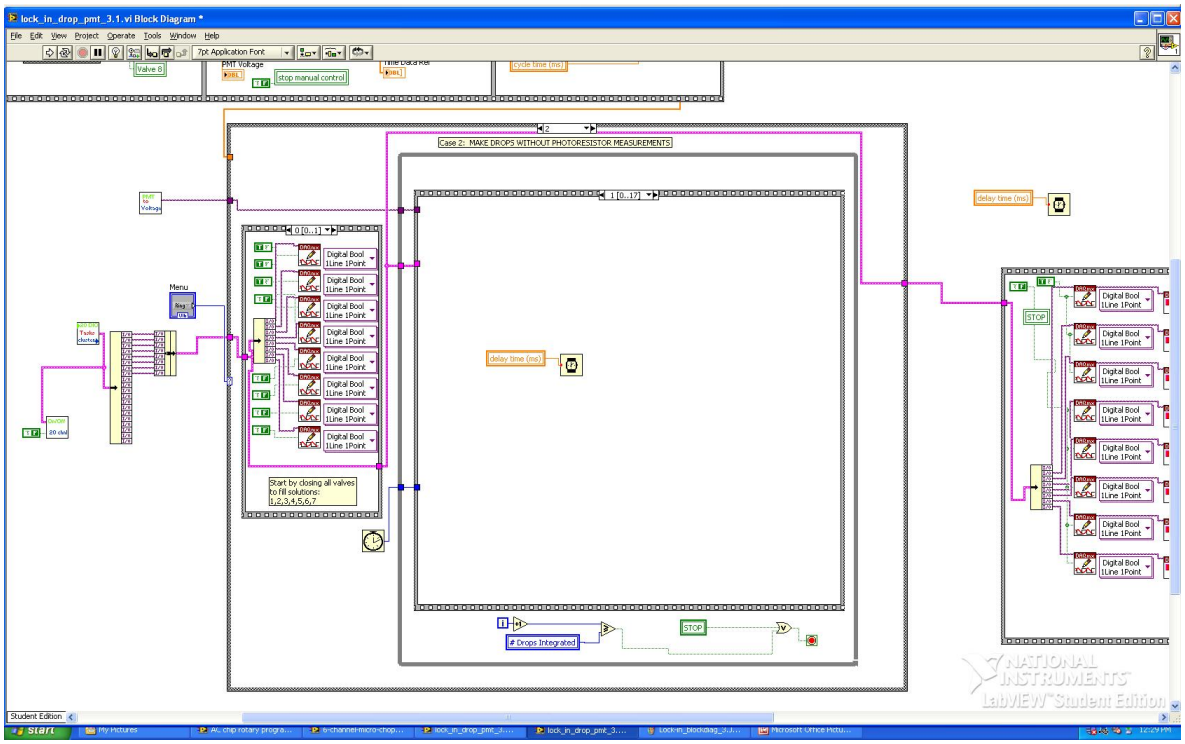

Figure 7.5: Automated Lock-in LabView Program block diagram step 3

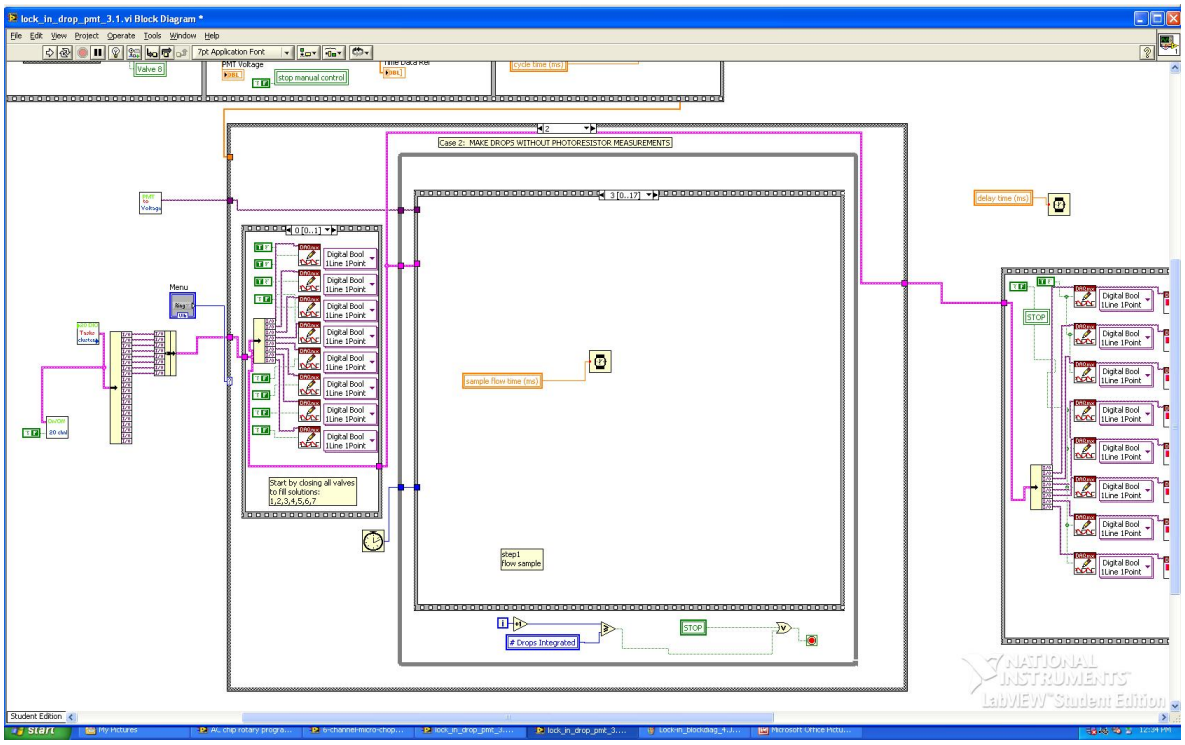

Figure 7.6: Automated Lock-in LabView Program block diagram step 4

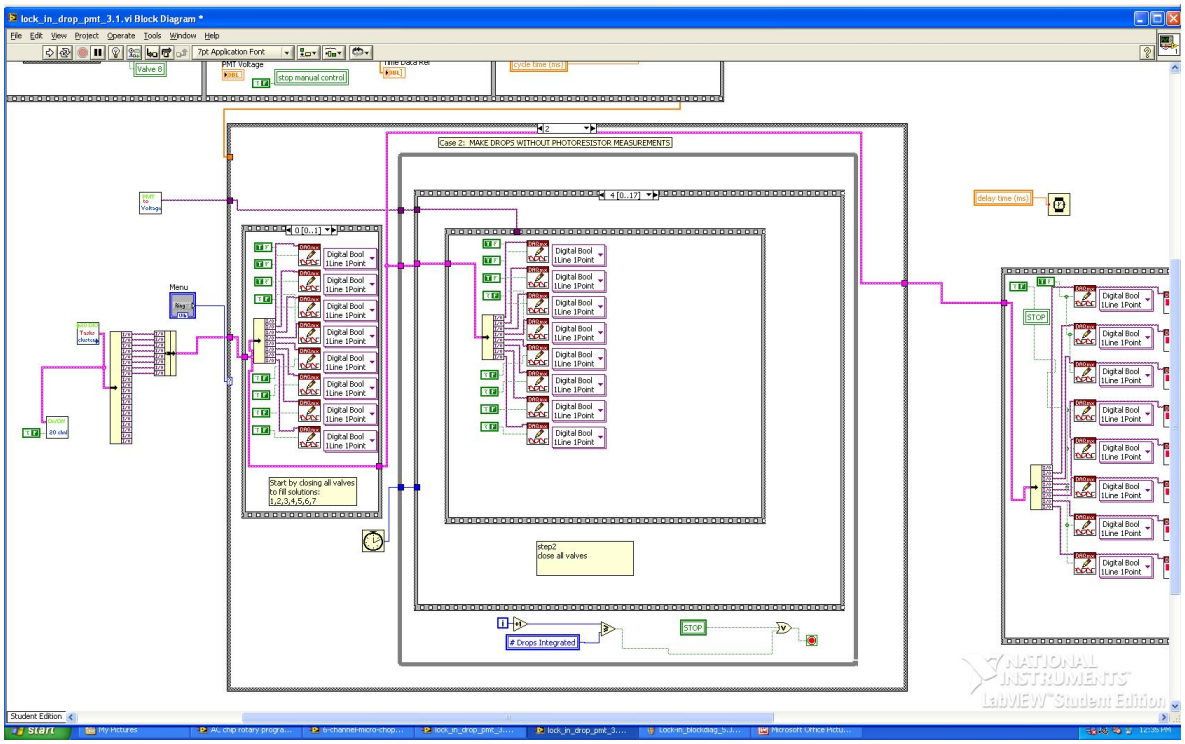

Figure 7.7: Automated Lock-in LabView Program block diagram step 5

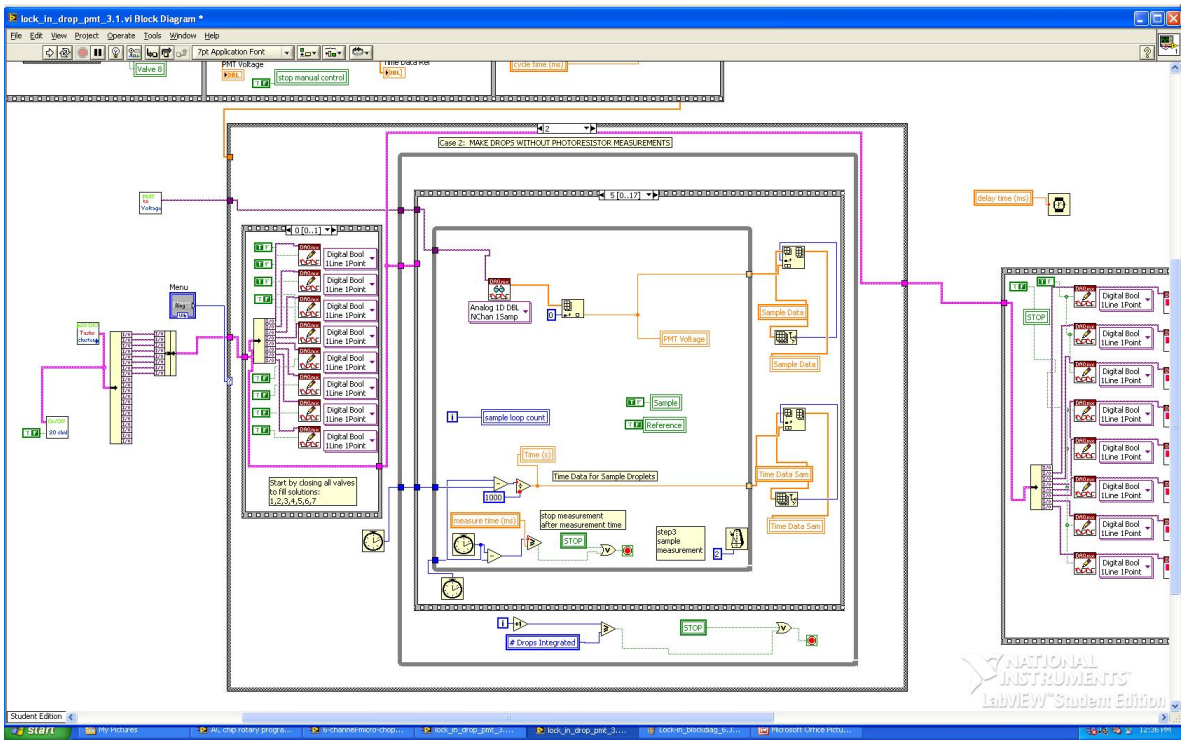

Figure 7.8: Automated Lock-in LabView Program block diagram step 6

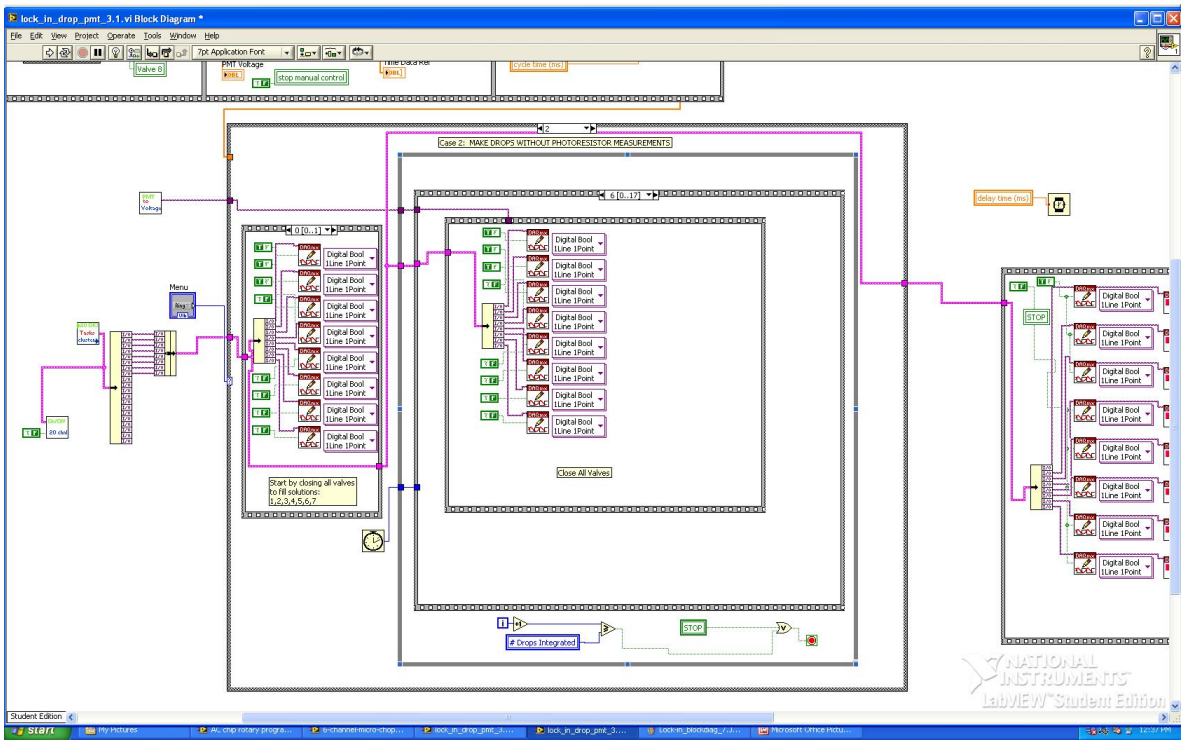

Figure 7.9: Automated Lock-in LabView Program block diagram step 7

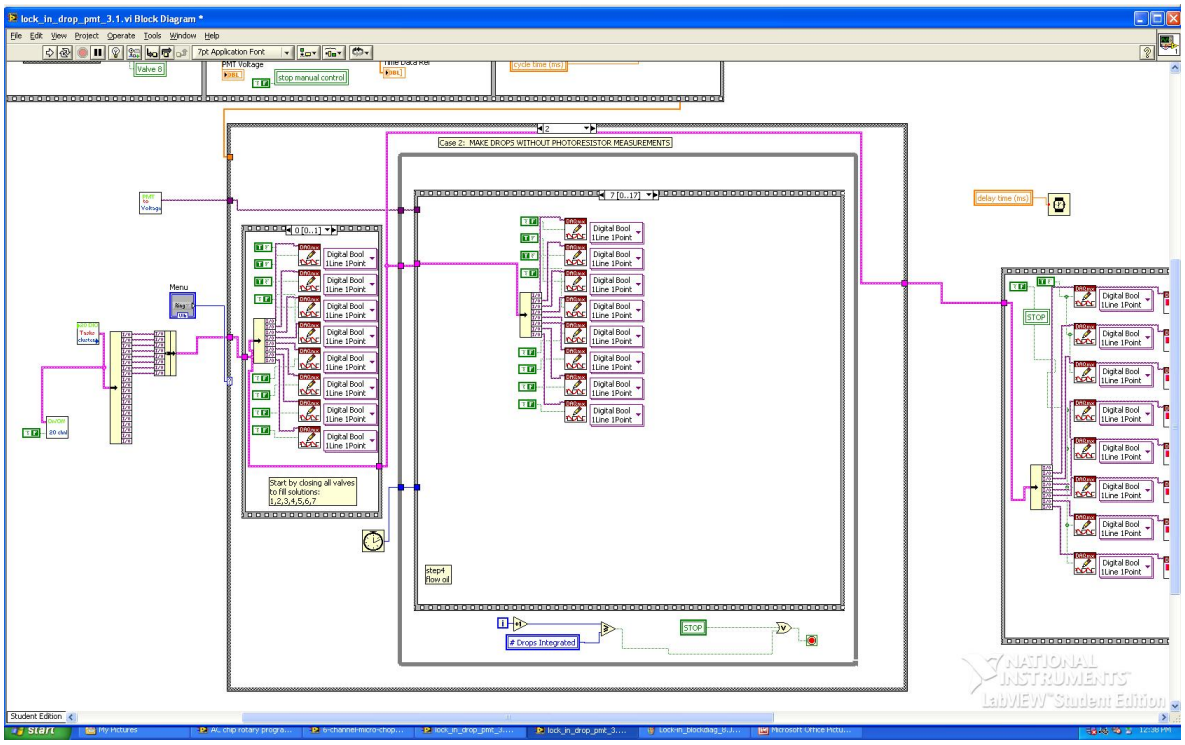

Figure 7.10: Automated Lock-in LabView Program block diagram step 8

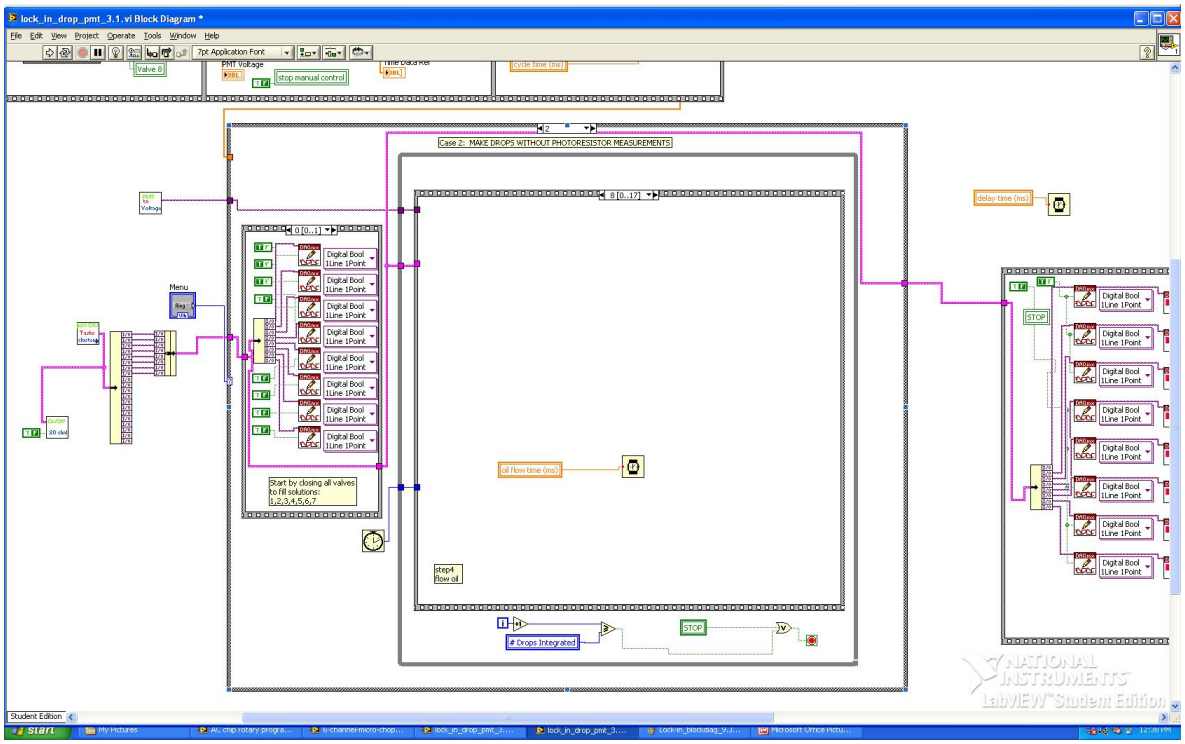

Figure 7.11: Automated Lock-in LabView Program block diagram step 9

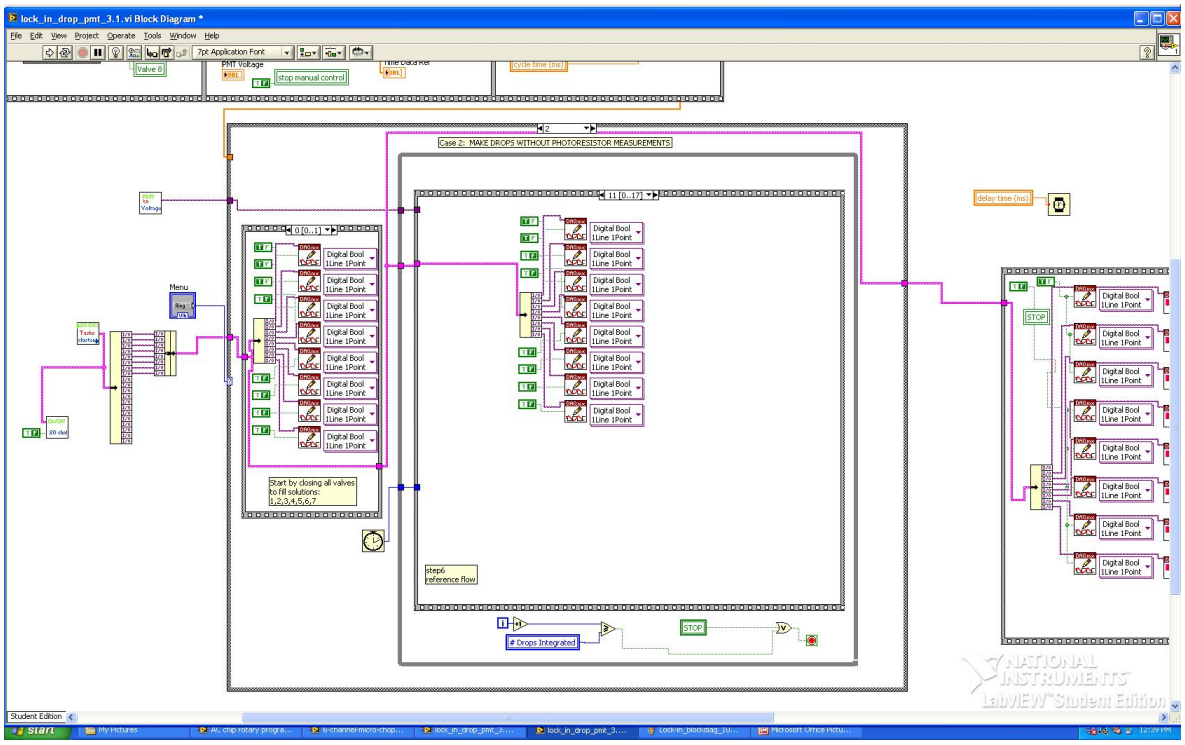

Figure 7.12: Automated Lock-in LabView Program block diagram step 10

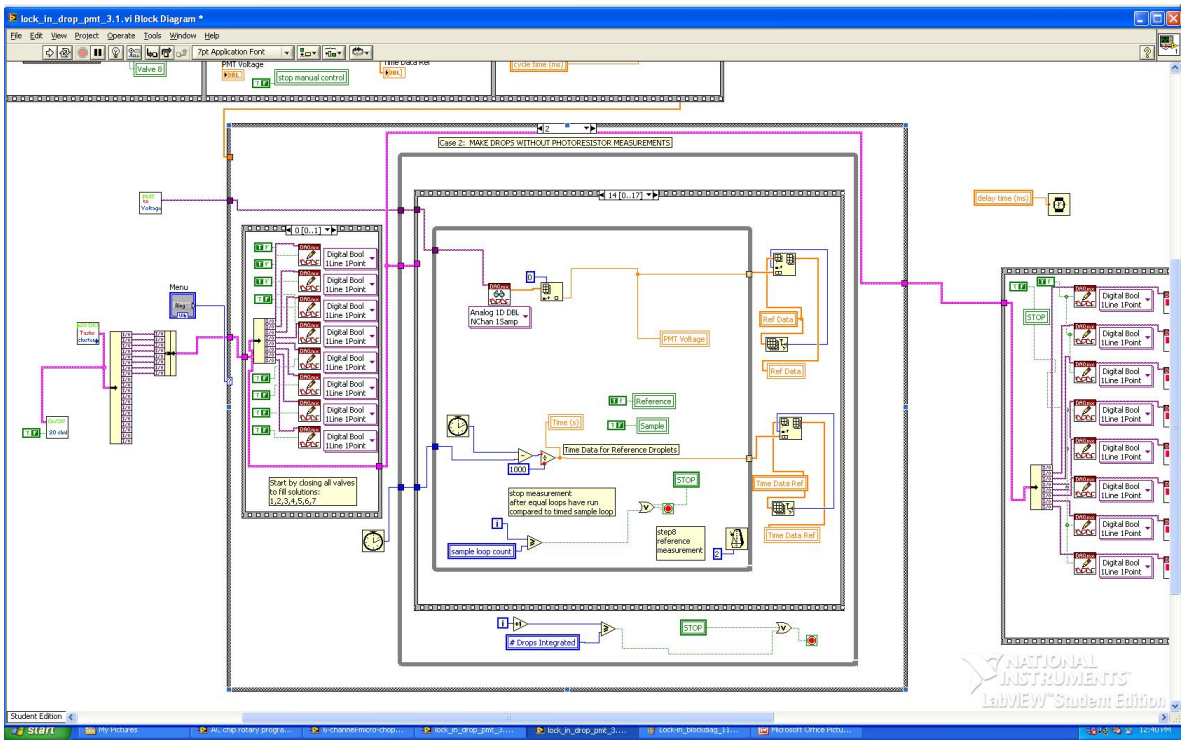

Figure 7.13: Automated Lock-in LabView Program block diagram step 11

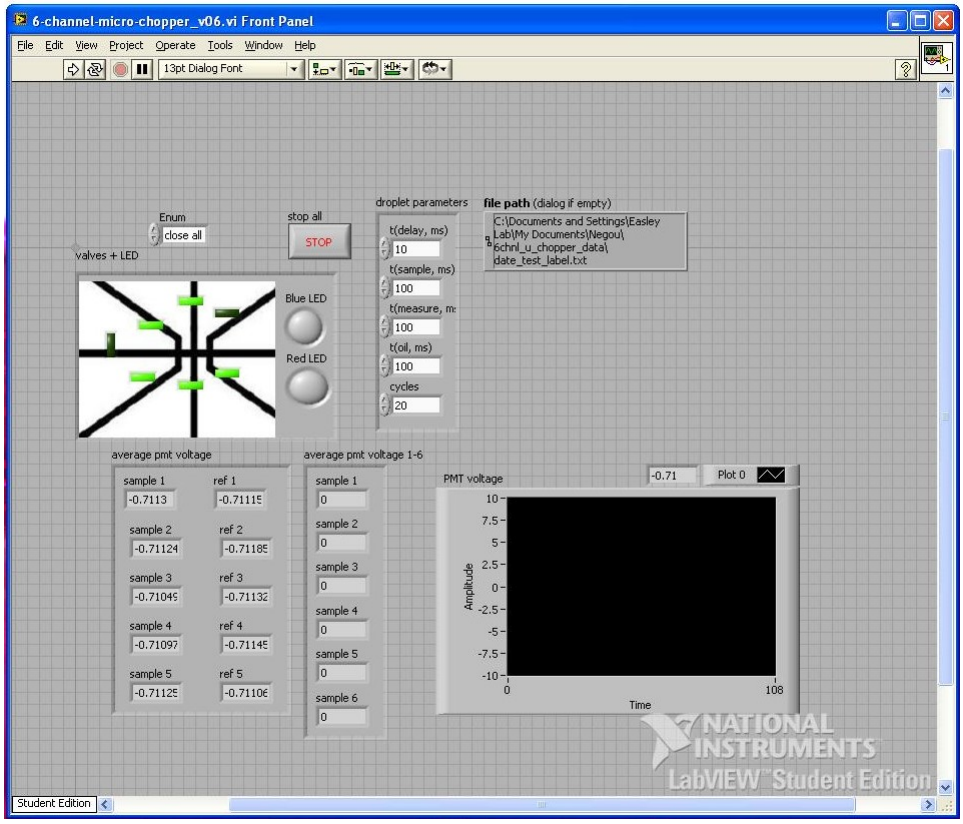

Figure 7.14: 6 channels automated Lock-in LabView Program front panel

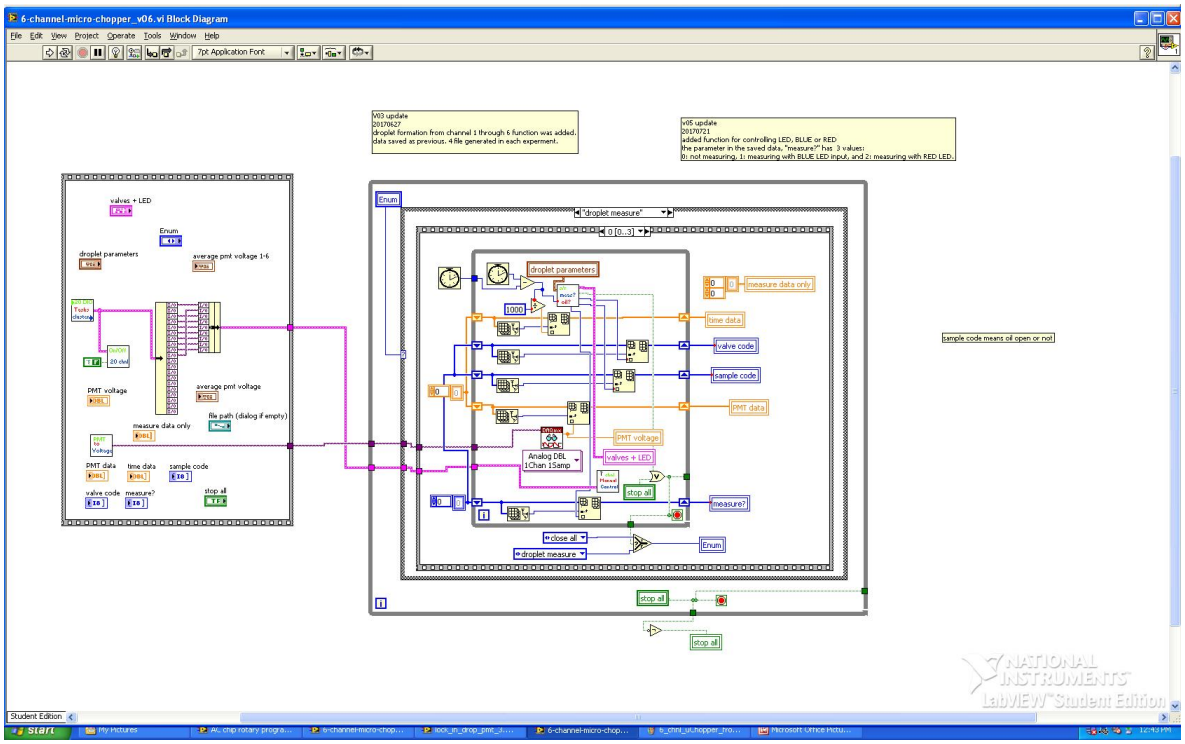

Figure 7.15: 6 channels automated Lock-in LabView Program block diagram step 1

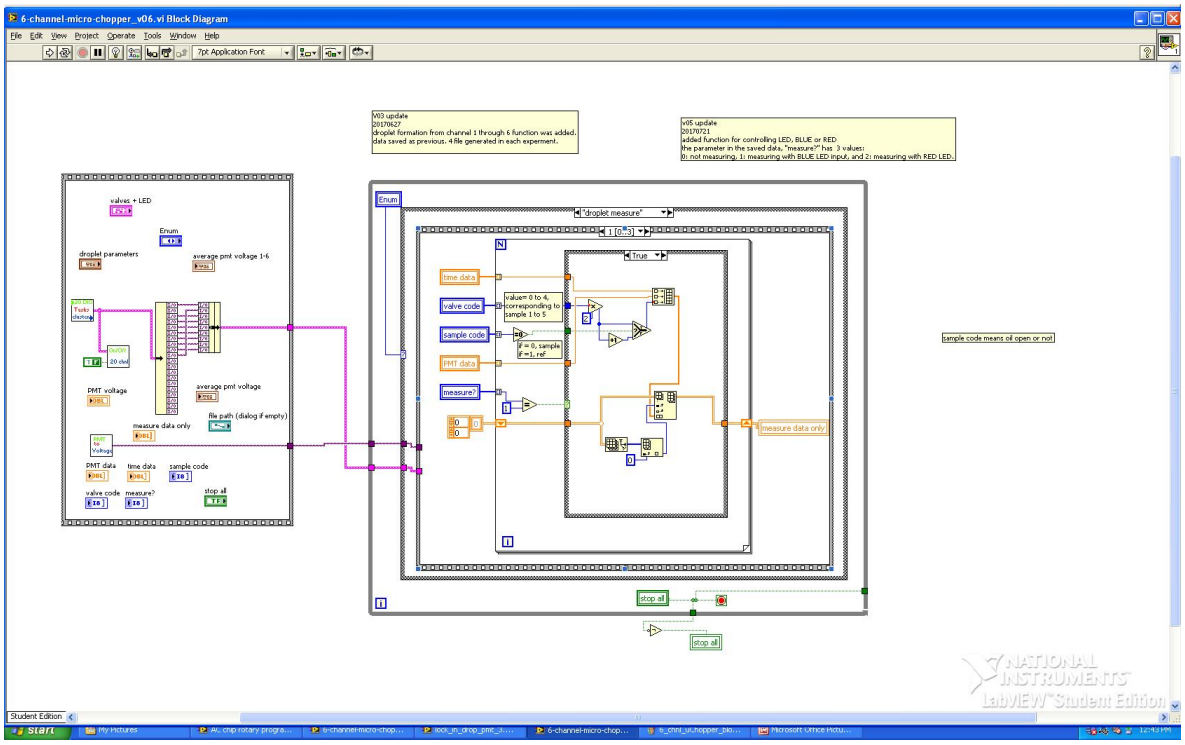

Figure 7.16: 6 channels automated Lock-in LabView Program block diagram step 2

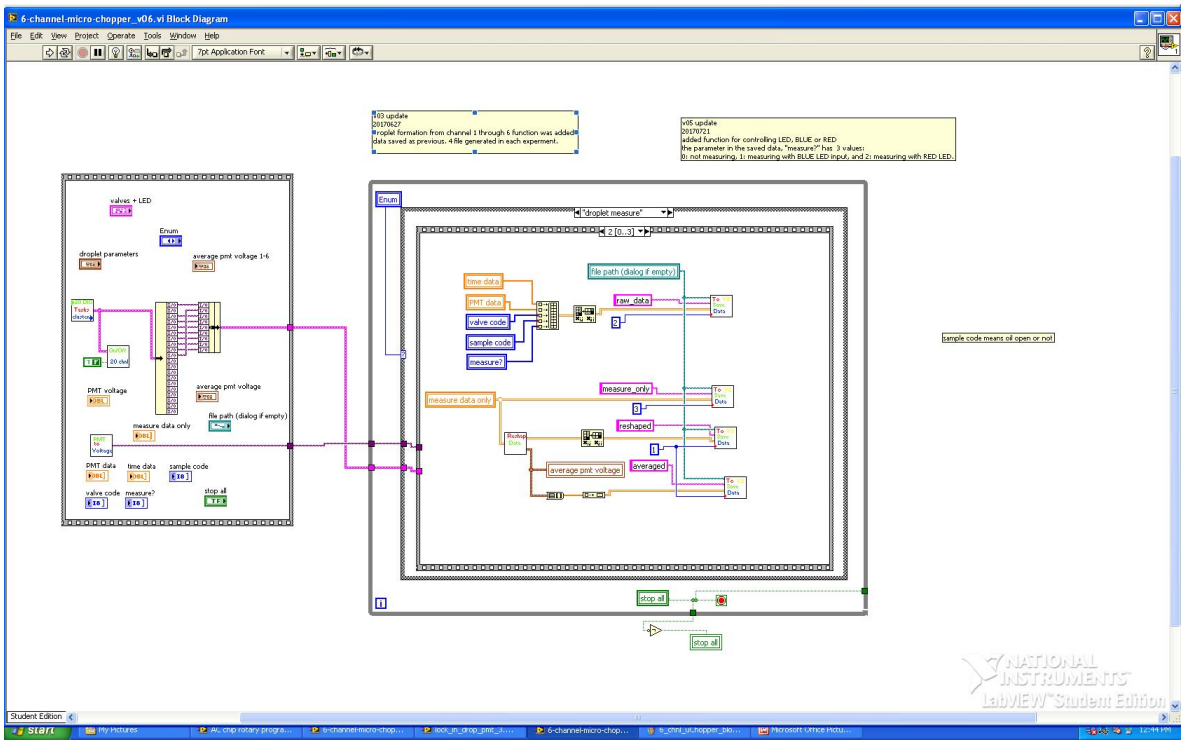

Figure 7.17: 6 channels automated Lock-in LabView Program block diagram step 3

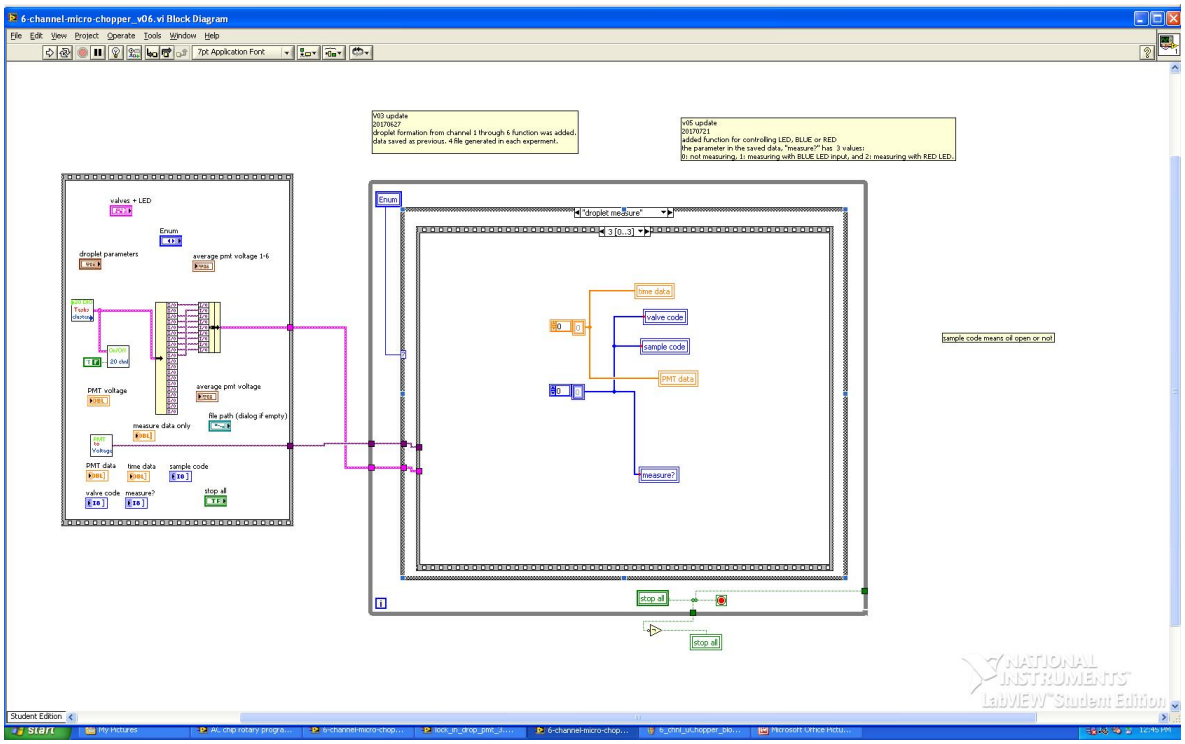

Figure 7.18: 6 channels automated Lock-in LabView Program block diagram step 4

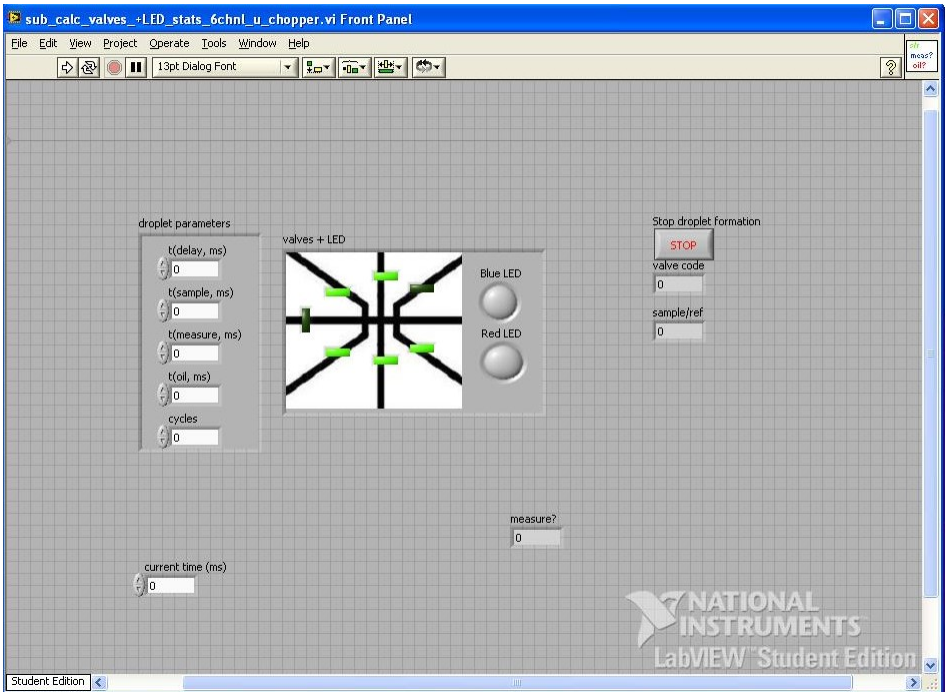

Figure 7.19: 6 channels automated Lock-in LabView SubVI front panel step 5

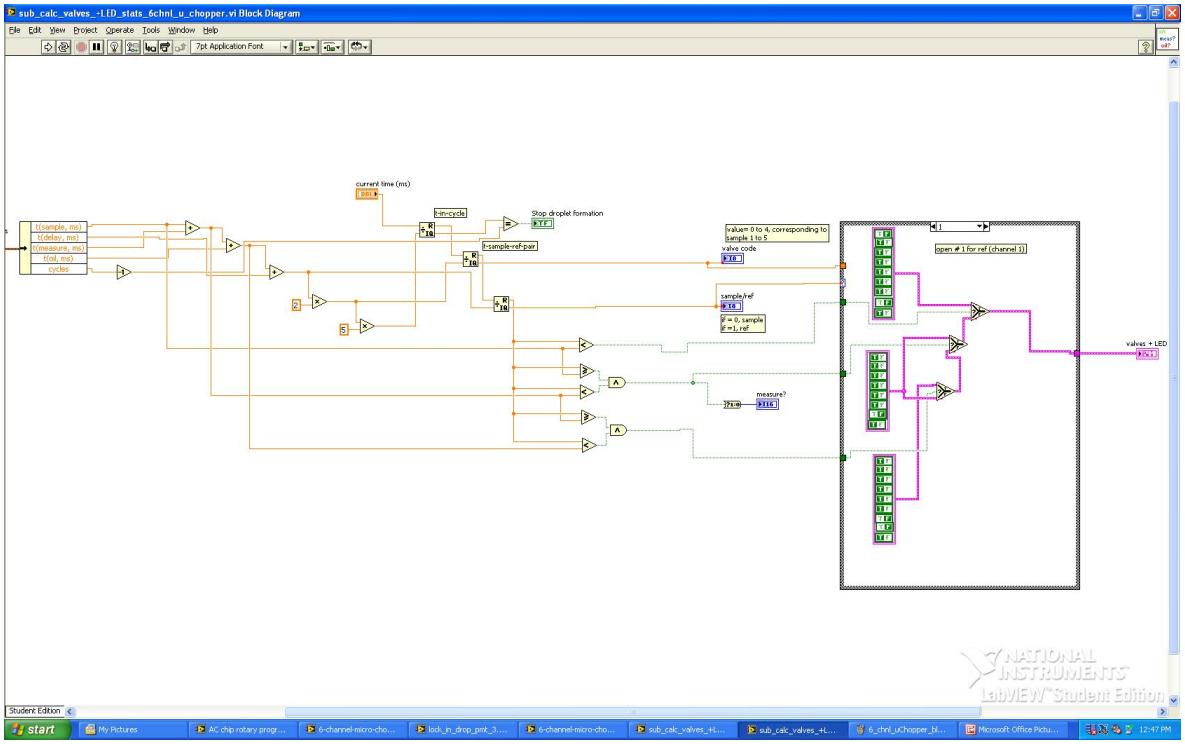

Figure 7.20: 6 channels automated Lock-in LabView SubVI block diagram

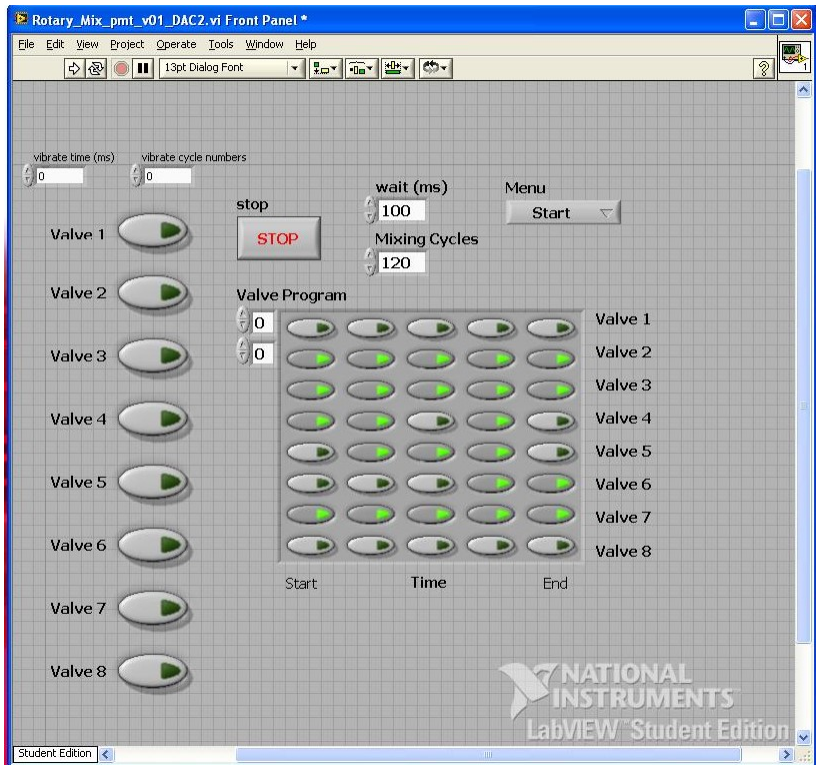

Figure 7.21: Rotary mixer LabView program front panel

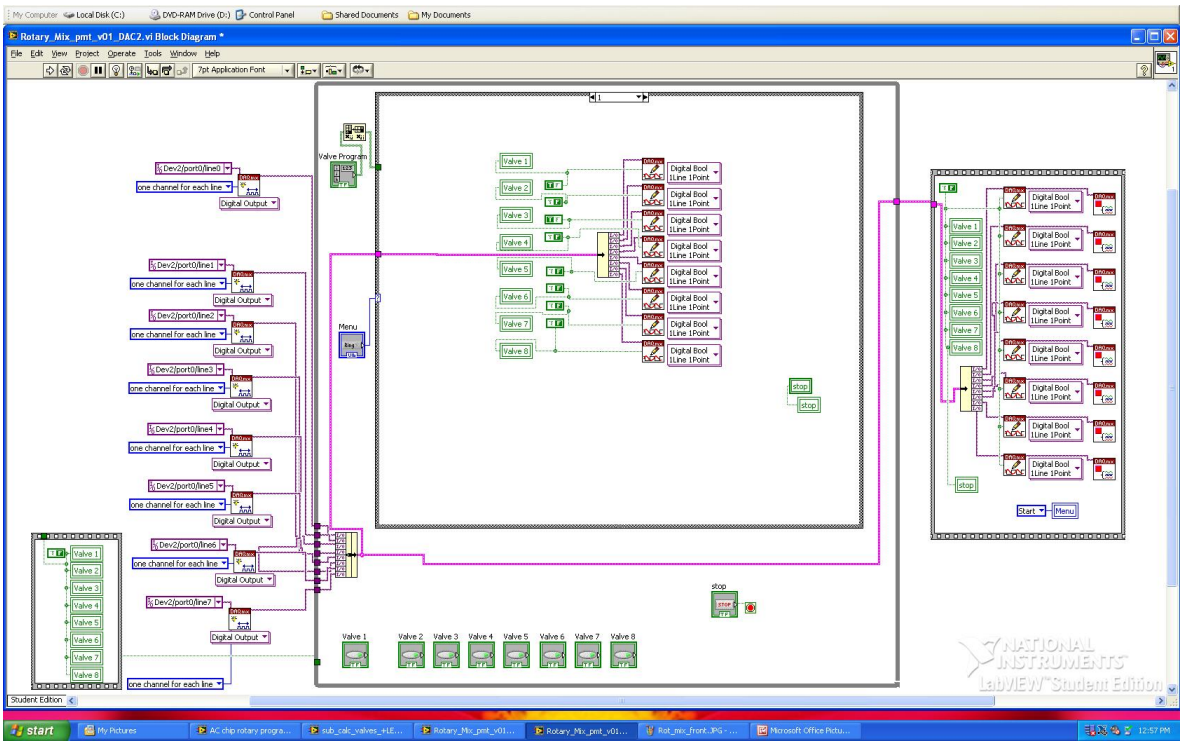

Figure 7.22: Rotary mixer LabView program blockdiagram step 1

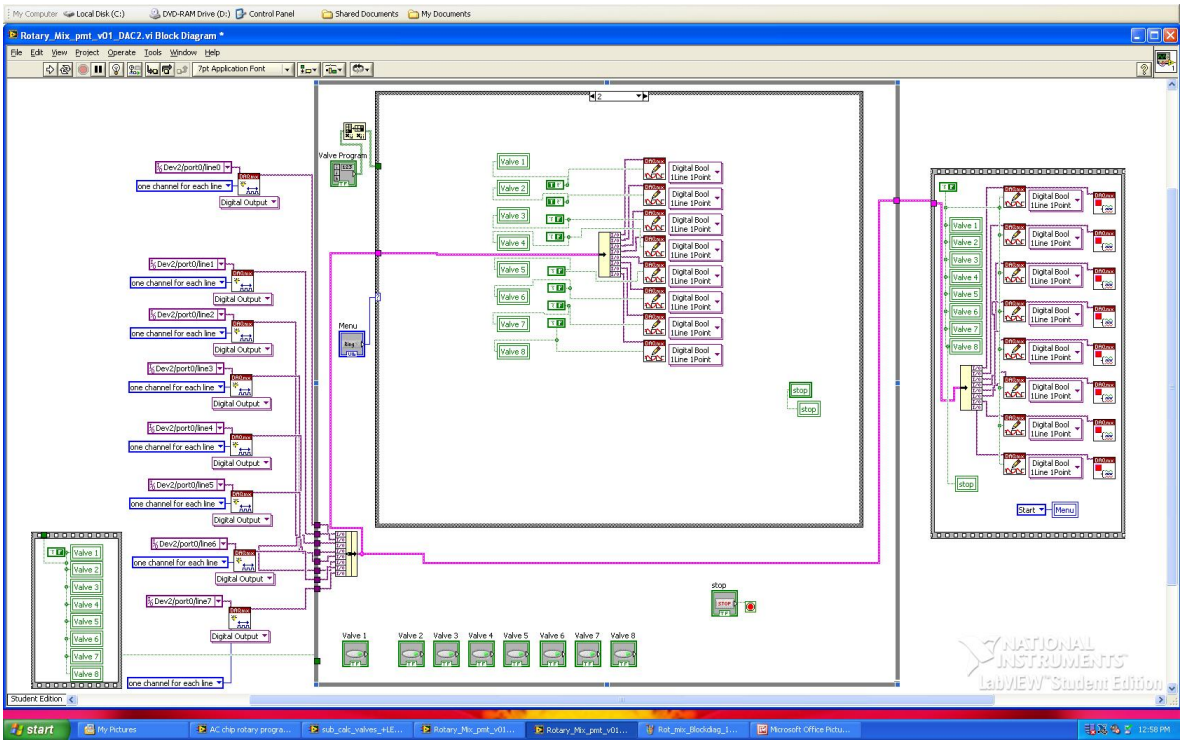

Figure 7.23: Rotary mixer LabView program blockdiagram step 2

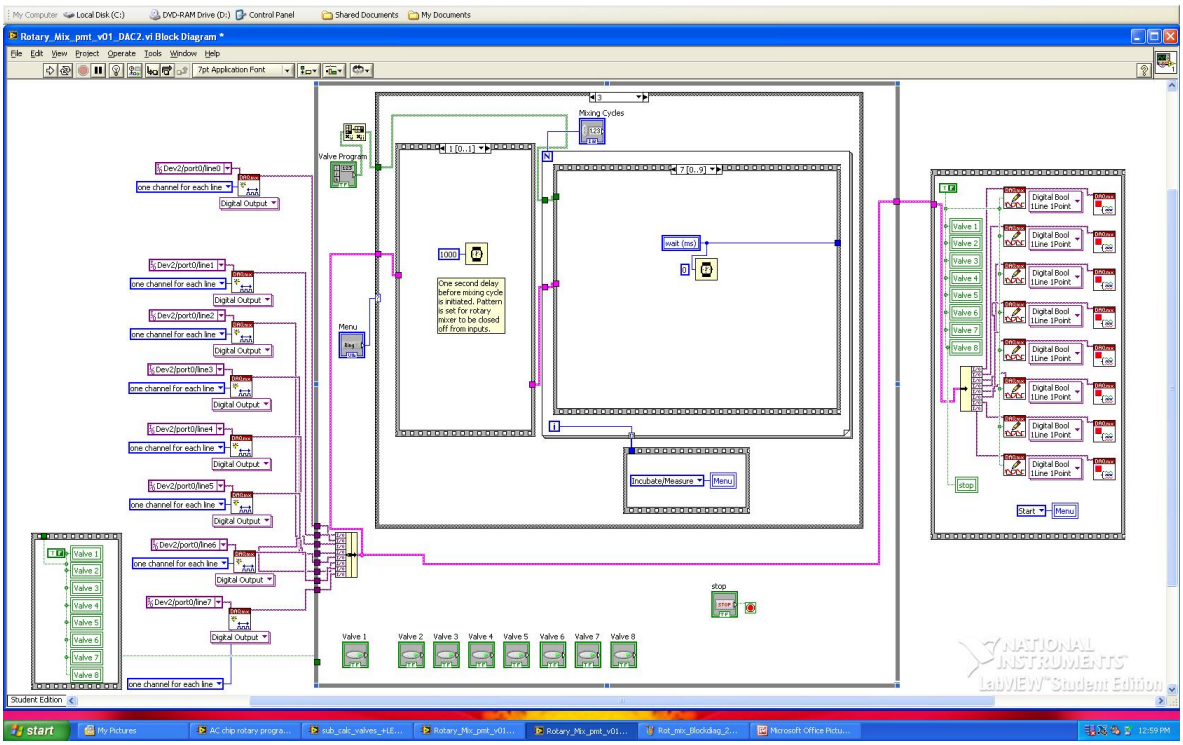

Figure 7.24: Rotary mixer LabView program blockdiagram step 3

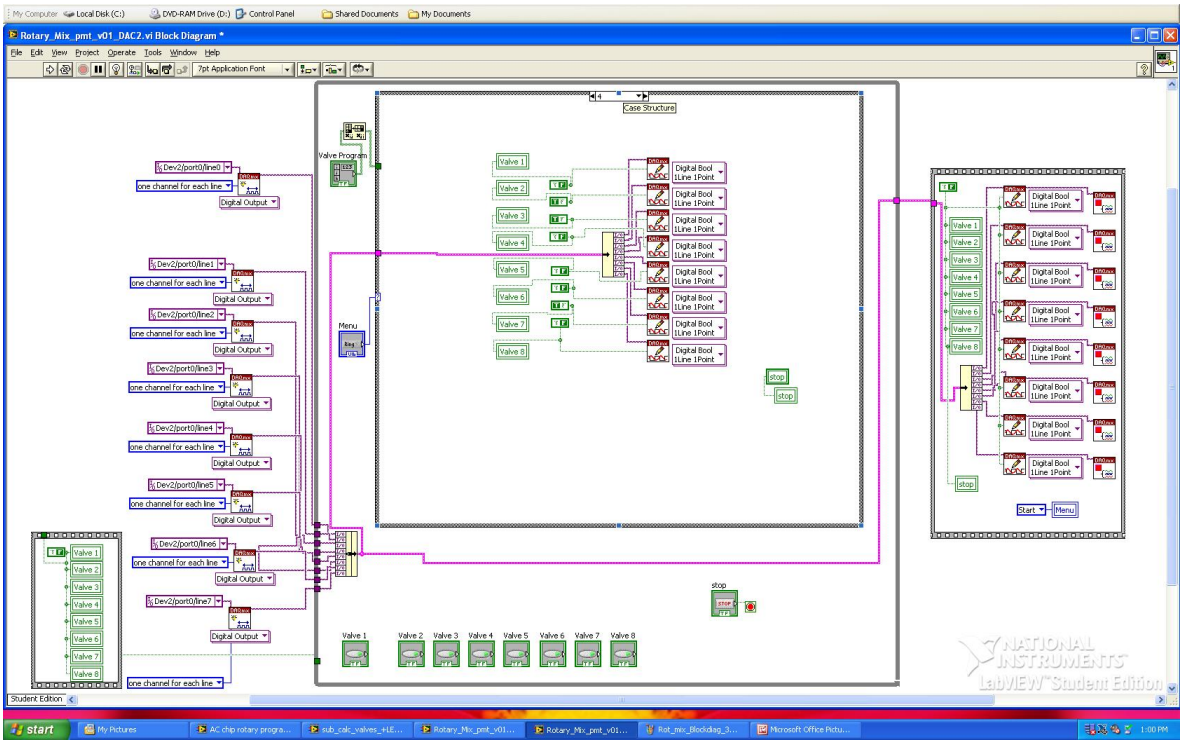

Figure 7.25: Rotary mixer LabView program blockdiagram step 4

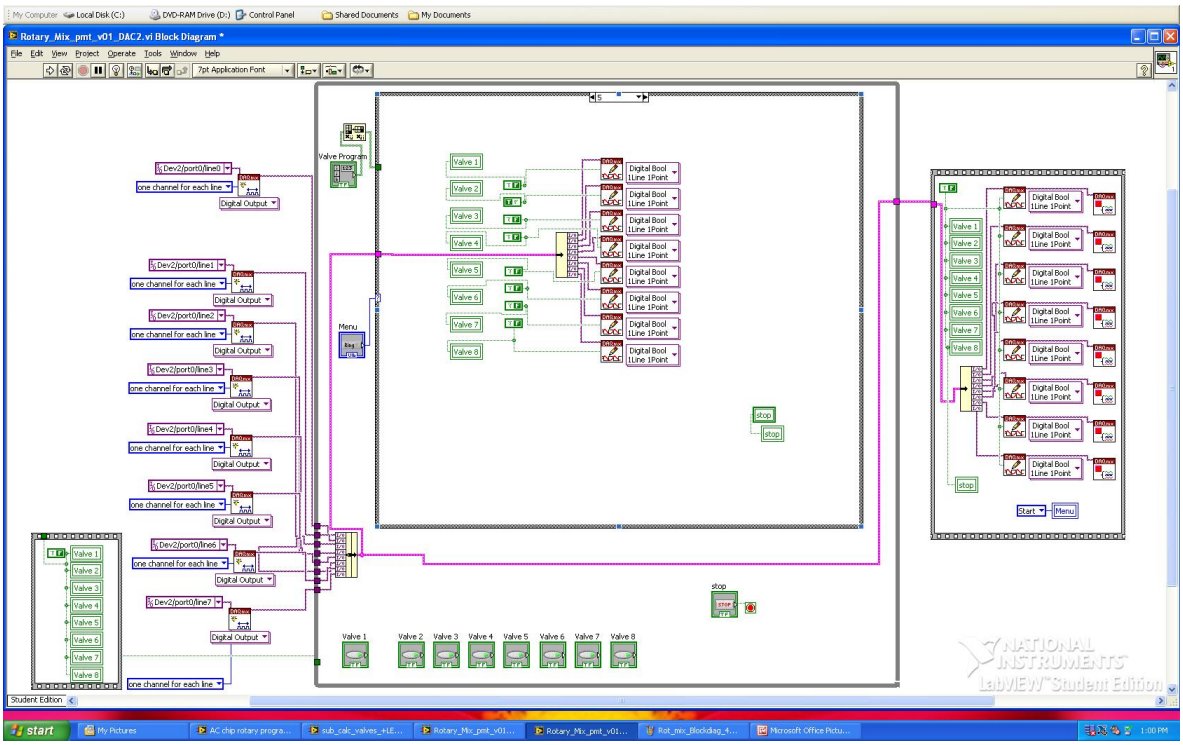

Figure 7.26: Rotary mixer LabView program blockdiagram step 5

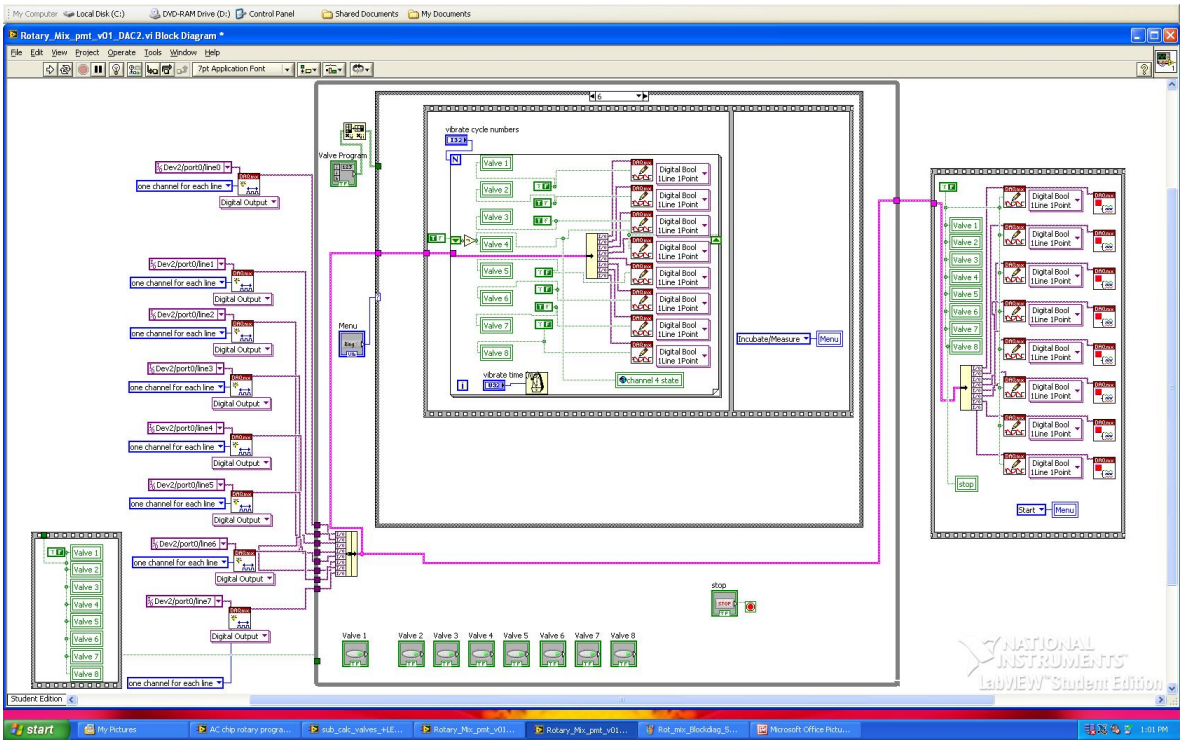

Figure 7.27: Rotary mixer LabView program blockdiagram step 6

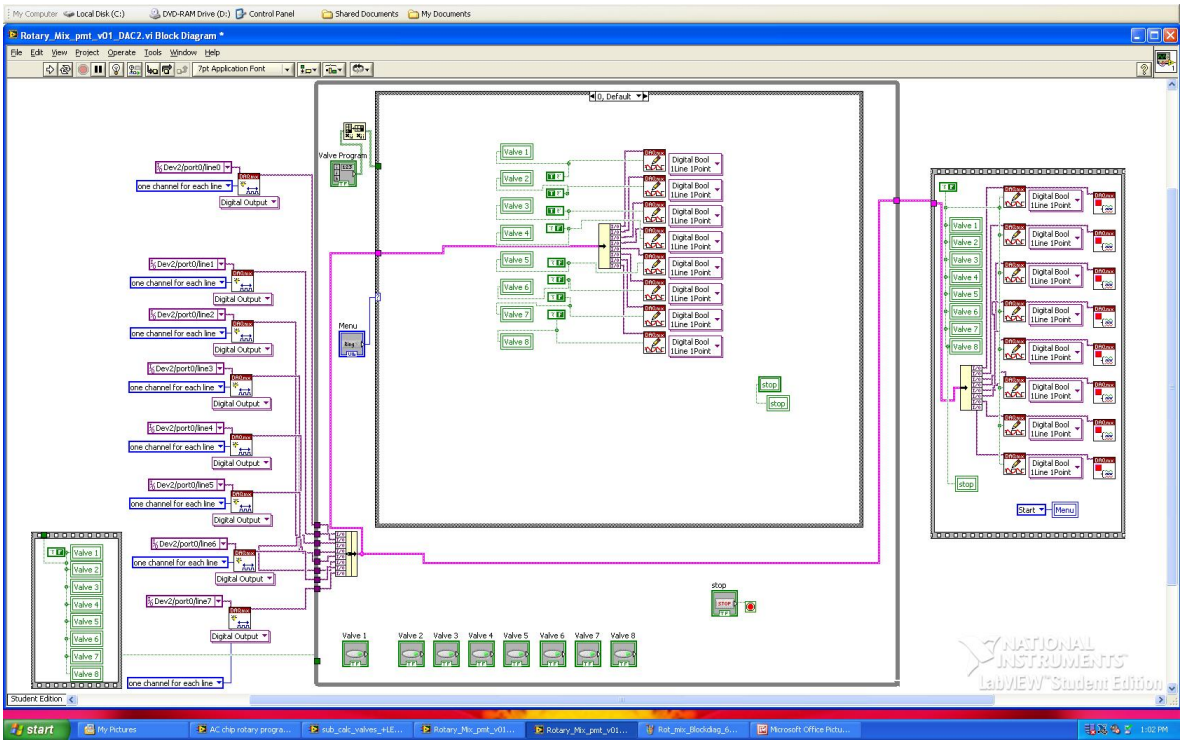

Figure 7.28: Rotary mixer LabView program blockdiagram step 7

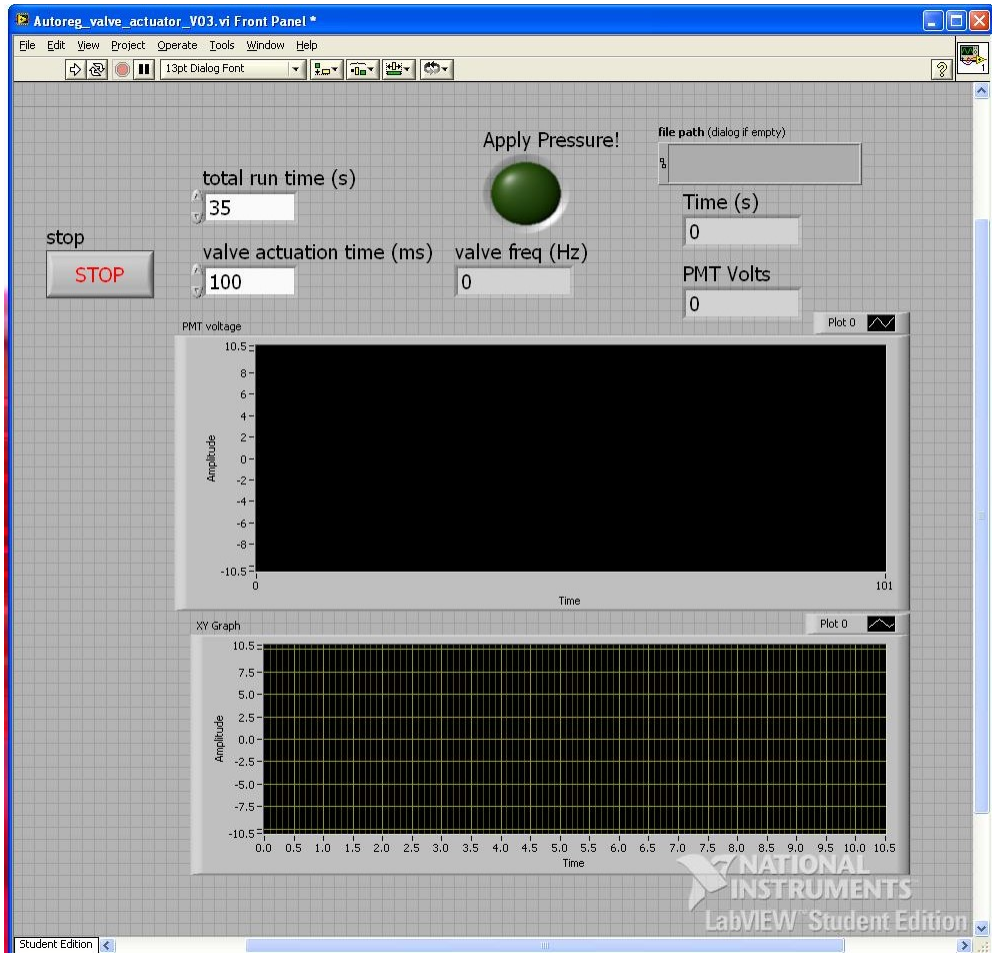

Figure 7.29: Autoregulators LabView program front panel

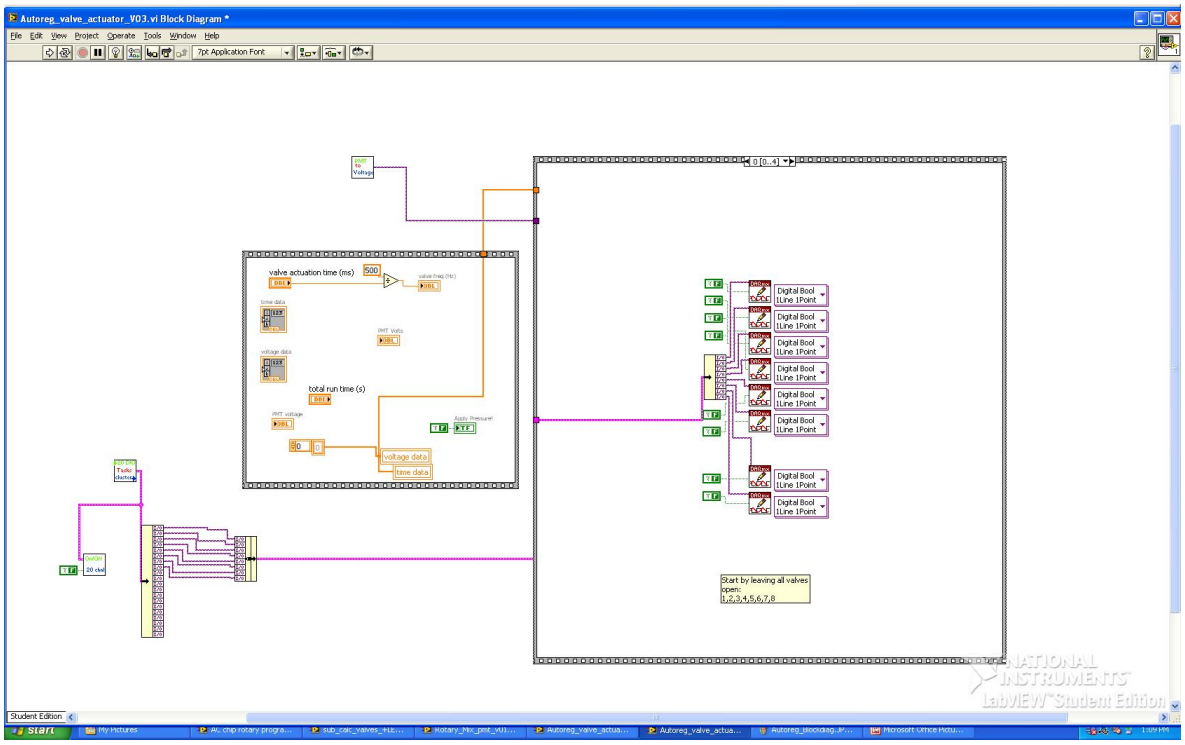

Figure 7.30: Autoregulators LabView program blockdiagram step 1

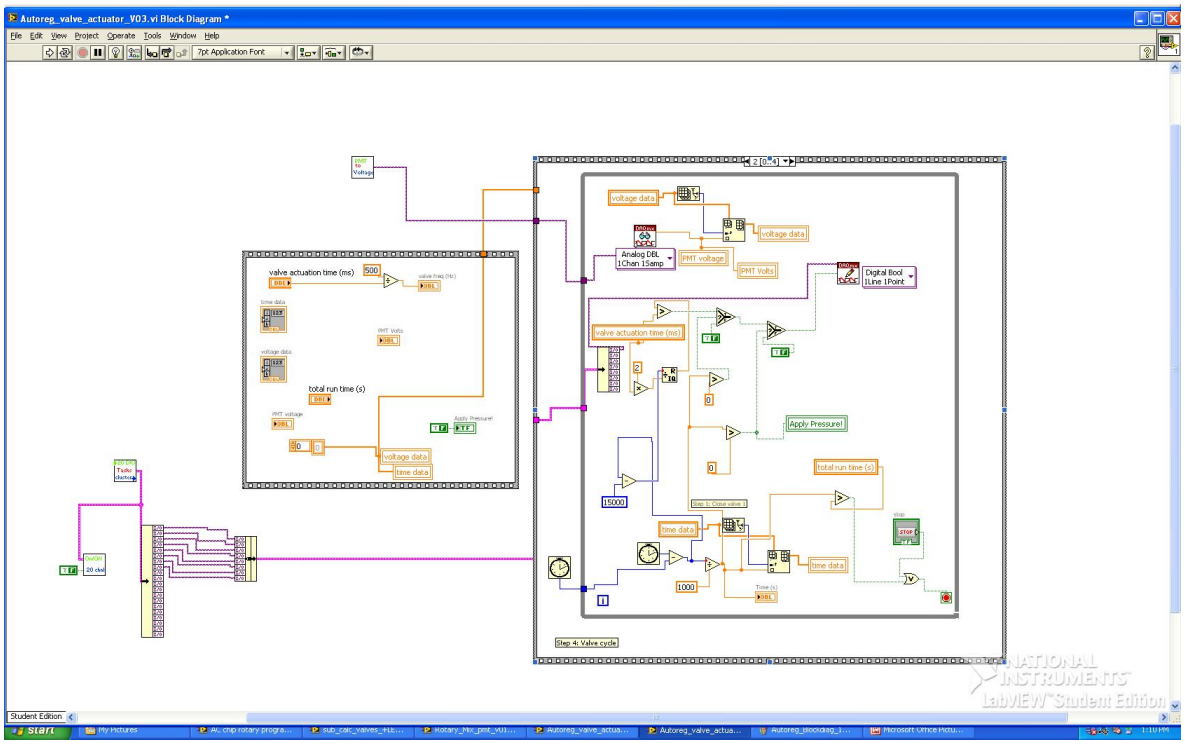

Figure 7.31: Autoregulators LabView program blockdiagram step 2

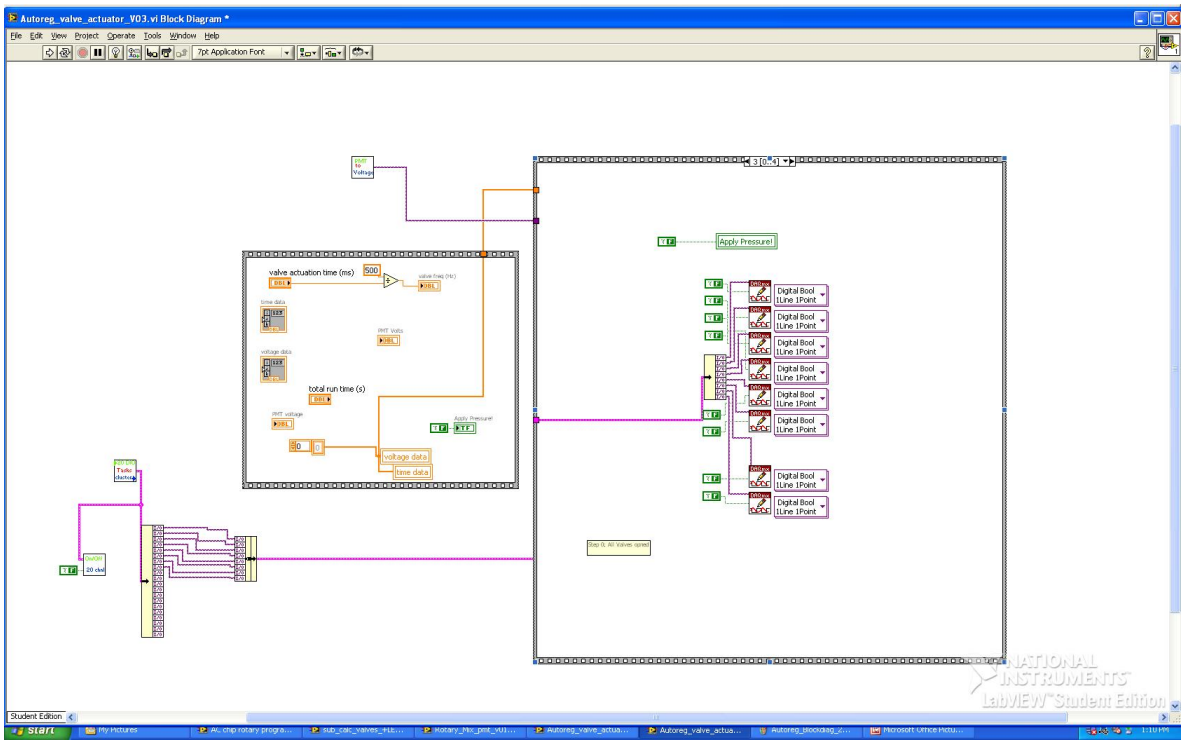

Figure 7.32: Autoregulators LabView program blockdiagram step 3

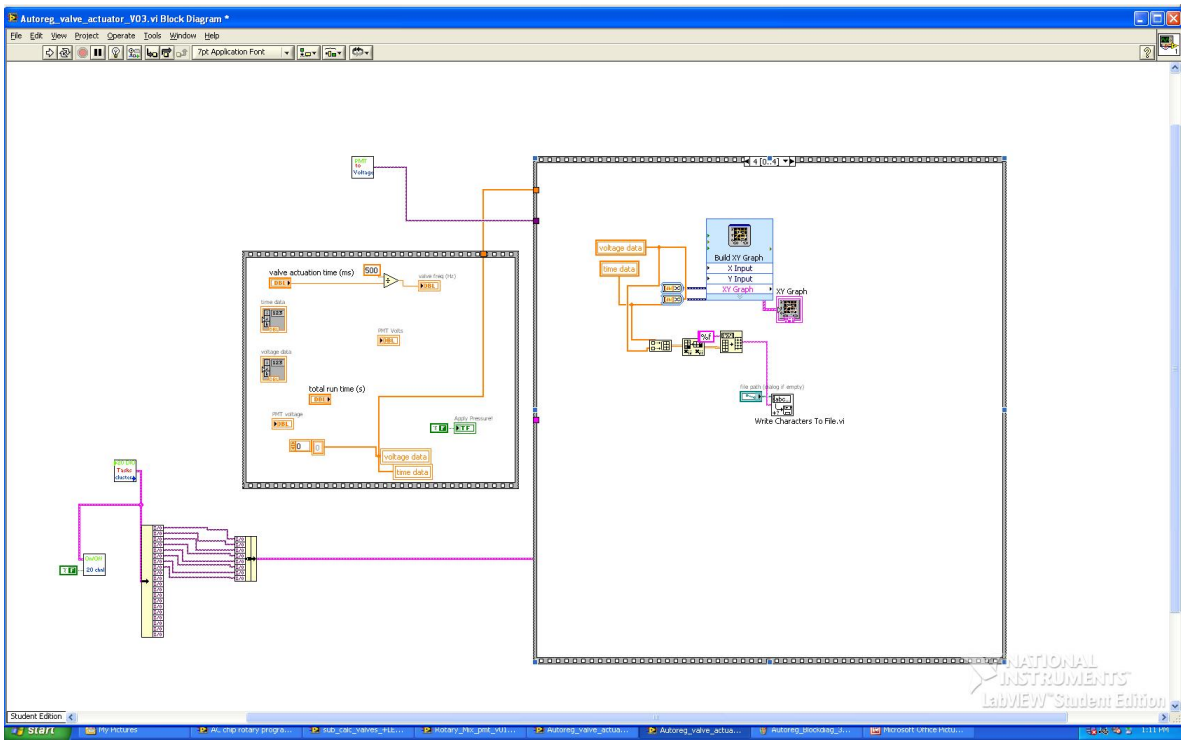

Figure 7.33: Autoregulators LabView program blockdiagram step 4

Chapter 8

Apendix B

8.1 Rights and permissions

Title: Quantitative and sensitive detection of rare mutations using droplet-based microfluidics

Author: Deniz Pekin,Yousr Skhiri,Jean-Christophe Baret,Delphine Le Corre,Linas Mazutis,Chaouki Ben Salem,Florian Millot,Abdeslam El Harrak,J. Brian Hutchison,Jonathan W. Larson,Darren R. Link,Pierre Laurent-Puig,Andrew D. Griffiths,Valérie Taly

Publication: Lab on a Chip

Publisher: Royal Society of Chemistry

Date: May 19, 2011

Order Completed

Thank you for your order.

This Agreement between Auburn University -- Jean Negou ("You") and Royal Society of Chemistry ("Royal Society of Chemistry") consists of your license details and the terms and conditions provided by Royal Society of Chemistry and Copyright Clearance Center.

Your confirmation email will contain your order number for future reference.

printable details

License Number	4211500617342
License date	Oct 17, 2017
Licensed Content Publisher	Royal Society of Chemistry
Licensed Content Publication	Lab on a Chip
Licensed Content Title	Quantitative and sensitive detection of rare mutations using droplet-based microfluidics
Licensed Content Author	Deniz Pekin,Yousr Skhiri,Jean-Christophe Baret,Delphine Le Corre,Linas Mazutis,Chaouki Ben Salem,Florian Millot,Abdeslam El Harrak,J. Brian Hutchison,Jonathan W. Larson,Darren R. Link,Pierre Laurent-Puig,Andrew D. Griffiths,Valérie Taly
Licensed Content Date	May 19, 2011
Licensed Content Volume	11
Licensed Content Issue	13
Type of Use	Thesis/Dissertation
Requestor type	academic/educational
Portion	figures/tables/images
Number of figures/tables/images	2
Distribution quantity	1
Format	print and electronic
Will you be translating?	no

Order reference number	
Title of the thesis/dissertation	Designing Microfluidics Components for Quantitative Bioanalysis and low limit of detection
Expected completion date	Dec 2017
Estimated size	200
Requestor Location	Auburn University 179 Chemistry Building AUBURN UNIVERSITY, AL 36849 United States Attn: Auburn University
Billing Type	Invoice
Billing address	Auburn University 179 Chemistry Building AUBURN UNIVERSITY, AL 36849 United States Attn: Auburn University
Total	0.00 USD

ORDER MORE CLOSE WINDOW

NATURE PUBLISHING GROUP LICENSE
TERMS AND CONDITIONS
Oct 15, 2017

This Agreement between Auburn University -- Jean Negou ("You") and Nature Publishing Group ("Nature Publishing Group") consists of your license details and the terms and conditions provided by Nature Publishing Group and Copyright Clearance Center.

License Number
4201071292250
License date
Oct 02, 2017
Licensed Content Publisher
Nature Publishing Group
Licensed Content Publication
Nature Physics
Licensed Content Title
Frequency-specific flow control in microfluidic circuits with passive elastomeric features
Licensed Content Author
Daniel C. Leslie, Christopher J. Easley, Erkin Seker, James M. Karlinsey, Marcel Utz et al.
Licensed Content Date
Feb 1, 2009
Licensed Content Volume
5
Licensed Content Issue
3
Type of Use
reuse in a dissertation / thesis
Requestor type
non-commercial (non-profit)
Format
print and electronic
Portion
figures/tables/illustrations
Number of figures/tables/illustrations
3
High-res required
no
Figures
Figure 1.2
Author of this NPG article
no
Your reference number
Title of your thesis / dissertation
Designing Microfluidics Components for Quantitative Bioanalysis and low limit of detection
Expected completion date
Dec 2017
Estimated size (number of pages)
200
Requestor Location
Auburn University
179 Chemistry Building

AUBURN UNIVERSITY, AL 36849

United States
Attn: Auburn University
Billing Type
Invoice
Billing Address
Auburn University
179 Chemistry Building

AUBURN UNIVERSITY, AL 36849
United States
Attn: Auburn University
Total
0.00 USD
Terms and Conditions

Terms and Conditions for Permissions

Nature Publishing Group hereby grants you a non-exclusive license to reproduce this material for this purpose, and for no other use,subject to the conditions below:

1. NPG warrants that it has, to the best of its knowledge, the rights to license reuse of this material. However, you should ensure that the material you are requesting is original to Nature Publishing Group and does not carry the copyright of another entity (as credited in the published version). If the credit line on any part of the material you have requested indicates that it was reprinted or adapted by NPG with permission from another source, then you should also seek permission from that source to reuse the material.

2. Permission granted free of charge for material in print is also usually granted for any electronic version of that work, provided that the material is incidental to the work as a whole and that the electronic version is essentially equivalent to, or substitutes for, the print version.Where print permission has been granted for a fee, separate permission must be obtained for any additional, electronic re-use (unless, as in the case of a full paper, this has already been accounted for during your initial request in the calculation of a print run).NB: In all cases, web-based use of full-text articles must be authorized separately through the 'Use on a Web Site' option when requesting permission.

3. Permission granted for a first edition does not apply to second and subsequent editions and for editions in other languages (except for signatories to the STM Permissions Guidelines, or where the first edition permission was granted for free).

4. Nature Publishing Group's permission must be acknowledged next to the figure, table or abstract in print. In electronic form, this acknowledgement must be visible at the same time as the figure/table/abstract, and must be hyperlinked to the journal's homepage.

5. The credit line should read:
   Reprinted by permission from Macmillan Publishers Ltd: [JOURNAL NAME] (reference citation), copyright (year of publication)
   For AOP papers, the credit line should read:
   Reprinted by permission from Macmillan Publishers Ltd: [JOURNAL NAME], advance online publication, day month year (doi: 10.1038/sj.[JOURNAL ACRONYM].XXXXX)

   Note: For republication from the *British Journal of Cancer,* the following credit lines apply.
   Reprinted by permission from Macmillan Publishers Ltd on behalf of Cancer Research UK: [JOURNAL NAME] (reference citation), copyright (year of publication)For AOP papers, the credit line should read:

Reprinted by permission from Macmillan Publishers Ltd on behalf of Cancer Research UK: [JOURNAL NAME], advance online publication, day month year (doi: 10.1038/sj.[JOURNAL ACRONYM].XXXXX)

6. Adaptations of single figures do not require NPG approval. However, the adaptation should be credited as follows:

   Adapted by permission from Macmillan Publishers Ltd: [JOURNAL NAME] (reference citation), copyright (year of publication)

   Note: For adaptation from the *British Journal of Cancer,* the following credit line applies.
   Adapted by permission from Macmillan Publishers Ltd on behalf of Cancer Research UK: [JOURNAL NAME] (reference citation), copyright (year of publication)

7. Translations of 401 words up to a whole article require NPG approval. Please visit http://www.macmillanmedicalcommunications.com for more information.Translations of up to a 400 words do not require NPG approval. The translation should be credited as follows:

   Translated by permission from Macmillan Publishers Ltd: [JOURNAL NAME] (reference citation), copyright (year of publication).

   Note: For translation from the *British Journal of Cancer,* the following credit line applies.
   Translated by permission from Macmillan Publishers Ltd on behalf of Cancer Research UK: [JOURNAL NAME] (reference citation), copyright (year of publication)

We are certain that all parties will benefit from this agreement and wish you the best in the use of this material. Thank you.
Special Terms:
v1.1
Questions? customercare@copyright.com or +1-855-239-3415 (toll free in the US) or +1-978-646-2777.

Title:	Microfluidic diagnostic technologies for global public health
Author:	Paul Yager,Thayne Edwards,Elain Fu,Kristen Helton,Kjell Nelson et al.
Publication:	Nature
Publisher:	Nature Publishing Group
Date:	Jul 27, 2006

Order Completed

Thank you for your order.

This Agreement between Auburn University -- Jean Negou ("You") and Nature Publishing Group ("Nature Publishing Group") consists of your license details and the terms and conditions provided by Nature Publishing Group and Copyright Clearance Center.

Your confirmation email will contain your order number for future reference.

printable details

License Number	4211530001878
License date	Oct 17, 2017
Licensed Content Publisher	Nature Publishing Group
Licensed Content Publication	Nature
Licensed Content Title	Microfluidic diagnostic technologies for global public health
Licensed Content Author	Paul Yager,Thayne Edwards,Elain Fu,Kristen Helton,Kjell Nelson et al.
Licensed Content Date	Jul 27, 2006
Licensed Content Volume	442
Licensed Content Issue	7101
Type of Use	reuse in a dissertation / thesis
Requestor type	academic/educational
Format	print and electronic
Portion	figures/tables/illustrations
Number of figures/tables/illustrations	1
High-res required	no
Figures	Figure 5
Author of this NPG article	no
Your reference number	
Title of your thesis / dissertation	Designing Microfluidics Components for Quantitative Bioanalysis and low limit of detection
Expected completion date	Dec 2017
Estimated size (number of pages)	200
Requestor Location	Auburn University 179 Chemistry Building

	AUBURN UNIVERSITY, AL 36849 United States Attn: Auburn University
Billing Type	Invoice
Billing address	Auburn University 179 Chemistry Building AUBURN UNIVERSITY, AL 36849 United States Attn: Auburn University
Total	0.00 USD

ORDER MORE CLOSE WINDOW

Order Completed

Thank you for your order.

This Agreement between Auburn University -- Jean Negou ("You") and Nature Publishing Group ("Nature Publishing Group") consists of your license details and the terms and conditions provided by Nature Publishing Group and Copyright Clearance Center.

Your confirmation email will contain your order number for future reference.

printable details

License Number	4211531503162
License date	Oct 17, 2017
Licensed Content Publisher	Nature Publishing Group
Licensed Content Publication	Nature Biotechnology
Licensed Content Title	Microfluidic organs-on-chips
Licensed Content Author	Sangeeta N Bhatia, Donald E Ingber
Licensed Content Date	Aug 5, 2014
Licensed Content Volume	32
Licensed Content Issue	8
Type of Use	reuse in a dissertation / thesis
Requestor type	academic/educational
Format	print and electronic
Portion	figures/tables/illustrations
Number of figures/tables/illustrations	1
High-res required	no
Figures	Figure 4C
Author of this NPG article	no
Your reference number	
Title of your thesis / dissertation	Designing Microfluidics Components for Quantitative Bioanalysis and low limit of detection
Expected completion date	Dec 2017
Estimated size (number of pages)	200
Requestor Location	Auburn University 179 Chemistry Building AUBURN UNIVERSITY, AL 36849

	United States Attn: Auburn University
Billing Type	Invoice
Billing address	Auburn University 179 Chemistry Building AUBURN UNIVERSITY, AL 36849 United States Attn: Auburn University
Total	0.00 USD

ORDER MORE CLOSE WINDOW

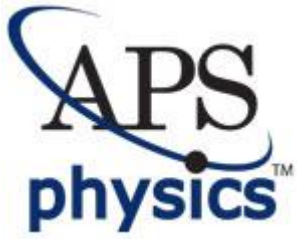

Title: Dynamic Pattern Formation in a Vesicle-Generating Microfluidic Device
Author: Todd Thorsen et al.
Publication: Physical Review Letters
Publisher: American Physical Society
Date: Apr 30, 2001

Review Order

Please review the order details and the associated terms and conditions.

No royalties will be charged for this reuse request although you are required to obtain a license and comply with the license terms and conditions. To obtain the license, click the Accept button below.

Licensed Content Publisher	American Physical Society
Licensed Content Publication	Physical Review Letters
Licensed Content Title	Dynamic Pattern Formation in a Vesicle-Generating Microfluidic Device
Licensed Content Author	Todd Thorsen et al.
Licensed Content Date	Apr 30, 2001
Licensed Content Volume	86
Type of use	Thesis/Dissertation
Requestor type	Student
Format	Print, Electronic
Portion	chart/graph/table/figure
Number of charts/graphs/tables/figures	1
Portion description	Figure 1
Rights for	Main product
Duration of use	Life of Current Edition
Creation of copies for the disabled	no
With minor editing privileges	no
For distribution to	United States
In the following language(s)	Original language of publication
With incidental promotional use	no
Lifetime unit quantity of new product	0 to 499
The requesting person/organization	Auburn University
Order reference number	
Title of your thesis / dissertation	Designing Microfluidics Components for Quantitative Bioanalysis and low limit of detection
Expected completion date	Dec 2017
Expected size (number of pages)	200

Requestor Location	Auburn University 179 Chemistry Building AUBURN UNIVERSITY, AL 36849 United States Attn: Auburn University
Total	0.00 USD

Edit Order Details

Edit Requestor Location This location may be used to determine your tax liability.

☐ I agree to these terms and conditions.

☐ I understand this license is for reuse only and that no content is provided.

Customer Code (if supplied) [ ] APPLY

BACK DECLINE ACCEPT

Please click accept only once.

Title: Biocompatible surfactants for water-in-fluorocarbon emulsions

Author: C. Holtze,A. C. Rowat,J. J. Agresti,J. B. Hutchison,F. E. Angilè,C. H. J. Schmitz,S. Köster,H. Duan,K. J. Humphry,R. A. Scanga,J. S. Johnson,D. Pisignano,D. A. Weitz

Publication: Lab on a Chip

Publisher: Royal Society of Chemistry

Date: Sep 2, 2008

Review Order

Please review the order details and the associated terms and conditions.

No royalties will be charged for this reuse request although you are required to obtain a license and comply with the license terms and conditions. To obtain the license, click the Accept button below.

Licensed Content Publisher	Royal Society of Chemistry
Licensed Content Publication	Lab on a Chip
Licensed Content Title	Biocompatible surfactants for water-in-fluorocarbon emulsions
Licensed Content Author	C. Holtze,A. C. Rowat,J. J. Agresti,J. B. Hutchison,F. E. Angilè,C. H. J. Schmitz,S. Köster,H. Duan,K. J. Humphry,R. A. Scanga,J. S. Johnson,D. Pisignano,D. A. Weitz
Licensed Content Date	Sep 2, 2008
Licensed Content Volume	8
Licensed Content Issue	10
Type of Use	Thesis/Dissertation
Requestor type	academic/educational
Portion	figures/tables/images
Number of figures/tables/images	1
Distribution quantity	1
Format	print and electronic
Will you be translating?	no
Order reference number	
Title of the thesis/dissertation	Designing Microfluidics Components for Quantitative Bioanalysis and low limit of detection
Expected completion date	Dec 2017
Estimated size	200
Requestor Location	Auburn University 179 Chemistry Building

	AUBURN UNIVERSITY, AL 36849 United States Attn: Auburn University
Total	0.00 USD

Edit Order Details

Edit Requestor Location This location may be used to determine your tax liability.

☐ I agree to these terms and conditions.

☐ I understand this license is for reuse only and that no content is provided.

Customer Code (if supplied) [ ] APPLY

BACK DECLINE ACCEPT

Please click accept only once.

Title: Droplet-based microfluidic system for individual Caenorhabditis elegans assay

Author: Weiwei Shi,Jianhua Qin,Nannan Ye,Bingcheng Lin

Publication: Lab on a Chip

Publisher: Royal Society of Chemistry

Date: Jul 7, 2008

Review Order

Please review the order details and the associated terms and conditions.

No royalties will be charged for this reuse request although you are required to obtain a license and comply with the license terms and conditions. To obtain the license, click the Accept button below.

Licensed Content Publisher	Royal Society of Chemistry
Licensed Content Publication	Lab on a Chip
Licensed Content Title	Droplet-based microfluidic system for individual Caenorhabditis elegans assay
Licensed Content Author	Weiwei Shi,Jianhua Qin,Nannan Ye,Bingcheng Lin
Licensed Content Date	Jul 7, 2008
Licensed Content Volume	8
Licensed Content Issue	9
Type of Use	Thesis/Dissertation
Requestor type	academic/educational
Portion	figures/tables/images
Number of figures/tables/images	1
Distribution quantity	1
Format	print and electronic
Will you be translating?	no
Order reference number	
Title of the thesis/dissertation	Designing Microfluidics Components for Quantitative Bioanalysis and low limit of detection
Expected completion date	Dec 2017
Estimated size	200
Requestor Location	Auburn University 179 Chemistry Building AUBURN UNIVERSITY, AL 36849

	United States Attn: Auburn University
Total	0.00 USD

Edit Order Details

Edit Requestor Location This location may be used to determine your tax liability.

☐ I agree to these terms and conditions.

☐ I understand this license is for reuse only and that no content is provided.

Customer Code (if supplied) [ ] APPLY

BACK DECLINE ACCEPT

Please click accept only once.

Title: Faster multiple emulsification with drop splitting
Author: Adam R. Abate,David A. Weitz
Publication: Lab on a Chip
Publisher: Royal Society of Chemistry
Date: Apr 19, 2011

Review Order

Please review the order details and the associated terms and conditions.

No royalties will be charged for this reuse request although you are required to obtain a license and comply with the license terms and conditions. To obtain the license, click the Accept button below.

Licensed Content Publisher	Royal Society of Chemistry
Licensed Content Publication	Lab on a Chip
Licensed Content Title	Faster multiple emulsification with drop splitting
Licensed Content Author	Adam R. Abate,David A. Weitz
Licensed Content Date	Apr 19, 2011
Licensed Content Volume	11
Licensed Content Issue	11
Type of Use	Thesis/Dissertation
Requestor type	academic/educational
Portion	figures/tables/images
Number of figures/tables/images	1
Distribution quantity	1
Format	print and electronic
Will you be translating?	no
Order reference number	
Title of the thesis/dissertation	Designing Microfluidics Components for Quantitative Bioanalysis and low limit of detection
Expected completion date	Dec 2017
Estimated size	200
Requestor Location	Auburn University 179 Chemistry Building AUBURN UNIVERSITY, AL 36849

	United States Attn: Auburn University
Total	0.00 USD

Edit Order Details

Edit Requestor Location This location may be used to determine your tax liability.

☐ I agree to these terms and conditions.

☐ I understand this license is for reuse only and that no content is provided.

Customer Code (if supplied) [ ] APPLY

BACK DECLINE ACCEPT

Please click accept only once.

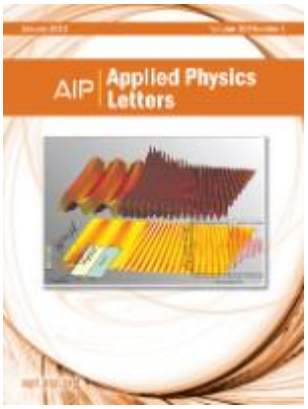

Title: Microfluidic sorting with high-speed single-layer membrane valves
Author: Adam R. Abate, Jeremy J. Agresti, David A. Weitz
Publication: Applied Physics Letters
Volume/Issue 96/20
Publisher: AIP Publishing LLC
Date: May 17, 2010
Page Count: 3

Review Order

Please review the order details and the associated terms and conditions.

No royalties will be charged for this reuse request although you are required to obtain a license and comply with the license terms and conditions. To obtain the license, click the Accept button below.

Licensed Content Publisher	AIP Publishing LLC
Licensed Content Publication	Applied Physics Letters
Licensed Content Title	Microfluidic sorting with high-speed single-layer membrane valves
Licensed Content Author	Adam R. Abate, Jeremy J. Agresti, David A. Weitz
Licensed Content Date	May 17, 2010
Licensed Content Volume	96
Licensed Content Issue	20
Requestor type	University or Educational Institution
Format	Print and electronic
Portion	Figure/Table
Number of figures/tables	1
Requestor Location	Auburn University 179 Chemistry Building AUBURN UNIVERSITY, AL 36849 United States Attn: Auburn University
Total	0.00 USD

Edit Order Details
Edit Requestor Location This location may be used to determine your tax liability.

☐ I agree to these terms and conditions.

I understand this license is for reuse only and that no content is provided.

Customer Code (if supplied) APPLY

BACK DECLINE ACCEPT

Please click accept only once.

Title:	Control and detection of chemical reactions in microfluidic systems
Author:	Andrew J. deMello
Publication:	Nature
Publisher:	Nature Publishing Group
Date:	Jul 26, 2006

Order Completed

Thank you for your order.

This Agreement between Auburn University -- Jean Negou ("You") and Nature Publishing Group ("Nature Publishing Group") consists of your license details and the terms and conditions provided by Nature Publishing Group and Copyright Clearance Center.

Your confirmation email will contain your order number for future reference.

printable details

License Number	4234350111858
License date	Nov 22, 2017
Licensed Content Publisher	Nature Publishing Group
Licensed Content Publication	Nature
Licensed Content Title	Control and detection of chemical reactions in microfluidic systems
Licensed Content Author	Andrew J. deMello
Licensed Content Date	Jul 26, 2006
Licensed Content Volume	442
Licensed Content Issue	7101
Type of Use	reuse in a dissertation / thesis
Requestor type	academic/educational
Format	print and electronic
Portion	figures/tables/illustrations
Number of figures/tables/illustrations	1
High-res required	no
Figures	Figure 2
Author of this NPG article	no
Your reference number	
Title of your thesis / dissertation	Microfluidic Circuit Designs for Nanoliter-Scale Flow Control and Highly Sensitive Quantitative Bioanalysis
Expected completion date	Dec 2017
Estimated size (number of pages)	200

Requestor Location	Auburn University 179 Chemistry Building AUBURN UNIVERSITY, AL 36849

	United States Attn: Auburn University
Billing Type	Invoice
Billing address	Auburn University 179 Chemistry Building AUBURN UNIVERSITY, AL 36849 United States Attn: Auburn University
Total	0.00 USD

ORDER MORE CLOSE WINDOW

Title: Measurement of microchannel fluidic resistance with a standard voltage meter

Author: Leah A. Godwin,Kennon S. Deal,Lauren D. Hoepfner,Louis A. Jackson,Christopher J. Easley

Publication: Analytica Chimica Acta

Publisher: Elsevier

Date: 3 January 2013

Order Completed

Thank you for your order.

This Agreement between Auburn University -- Jean Negou ("You") and Elsevier ("Elsevier") consists of your license details and the terms and conditions provided by Elsevier and Copyright Clearance Center.

Your confirmation email will contain your order number for future reference.

printable details

License Number	4234340845147
License date	Nov 22, 2017
Licensed Content Publisher	Elsevier
Licensed Content Publication	Analytica Chimica Acta
Licensed Content Title	Measurement of microchannel fluidic resistance with a standard voltage meter
Licensed Content Author	Leah A. Godwin,Kennon S. Deal,Lauren D. Hoepfner,Louis A. Jackson,Christopher J. Easley
Licensed Content Date	Jan 3, 2013
Licensed Content Volume	758
Licensed Content Issue	n/a
Licensed Content Pages	7
Type of Use	reuse in a thesis/dissertation
Portion	figures/tables/illustrations
Number of figures/tables/illustrations	1
Format	both print and electronic
Are you the author of this Elsevier article?	No
Will you be translating?	No
Original figure numbers	Figure 2
Title of your thesis/dissertation	Microfluidic Circuit Designs for Nanoliter-Scale Flow Control and Highly Sensitive Quantitative Bioanalysis
Expected completion date	Dec 2017
Estimated size (number of pages)	200
Requestor Location	Auburn University 179 Chemistry Building AUBURN UNIVERSITY, AL 36849

	United States Attn: Auburn University
Publisher Tax ID	98-0397604
Total	0.00 USD

ORDER MORE CLOSE WINDOW

Step 3: Order Confirmation

Thank you for your order! A confirmation for your order will be sent to your account email address. If you have questions about your order, you can call us 24 hrs/day, M-F at +1.855.239.3415 Toll Free, or write to us at info@copyright.com. This is not an invoice.

Confirmation Number: 11682949
Order Date: 11/22/2017
If you paid by credit card, your order will be finalized and your card will be charged within 24 hours. If you choose to be invoiced, you can change or cancel your order until the invoice is generated.

Payment Information

Jean Negou
Auburn University
jtn0002@auburn.edu
+1 (334) 844-4772
Payment Method: n/a

Order Details

Journal of micromechanics and microengineering : structures, devices, and systems

- **Order detail ID:**70801952

- **Order License Id:**4234361293621
- **ISSN:**0960-1317
- **Publication Type:**Journal
- **Volume:**
- **Issue:**
- **Start page:**
- **Publisher:**INSTITUTE OF PHYSICS PUBLISHING
- **Permission Status:** **Granted**
- **Permission type:**Republish or display content
- **Type of use:**Thesis/Dissertation
- View details

Title: Systematic characterization of feature dimensions and closing pressures for microfluidic valves produced via photoresist reflow

Author: P. M. Fordyce,C. A. Diaz-Botia,J. L. DeRisi,R. Gomez-Sjoberg

Publication: Lab on a Chip

Publisher: Royal Society of Chemistry

Date: Jul 11, 2012

Review Order

Please review the order details and the associated terms and conditions.

No royalties will be charged for this reuse request although you are required to obtain a license and comply with the license terms and conditions. To obtain the license, click the Accept button below.

Licensed Content Publisher	Royal Society of Chemistry
Licensed Content Publication	Lab on a Chip
Licensed Content Title	Systematic characterization of feature dimensions and closing pressures for microfluidic valves produced via photoresist reflow
Licensed Content Author	P. M. Fordyce,C. A. Diaz-Botia,J. L. DeRisi,R. Gomez-Sjoberg
Licensed Content Date	Jul 11, 2012
Licensed Content Volume	12
Licensed Content Issue	21
Type of Use	Thesis/Dissertation
Requestor type	academic/educational
Portion	figures/tables/images
Number of figures/tables/images	1
Distribution quantity	1
Format	print and electronic
Will you be translating?	no
Order reference number	
Title of the thesis/dissertation	Designing Microfluidics Components for Quantitative Bioanalysis and low limit of detection
Expected completion date	Dec 2017
Estimated size	200
Requestor Location	Auburn University 179 Chemistry Building AUBURN UNIVERSITY, AL 36849 United States Attn: Auburn University

Total	0.00 USD

Edit Order Details

Edit Requestor Location This location may be used to determine your tax liability.

☐ I agree to these terms and conditions.

☐ I understand this license is for reuse only and that no content is provided.

Customer Code (if supplied) [ ] APPLY

BACK DECLINE ACCEPT

Please click accept only once.

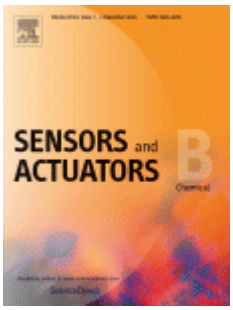

Title: Monolithic membrane valves and diaphragm pumps for practical large-scale integration into glass microfluidic devices

Author: William H Grover,Alison M Skelley,Chung N Liu,Eric T Lagally,Richard A Mathies

Publication: Sensors and Actuators B: Chemical

Publisher: Elsevier

Date: 1 April 2003

Review Order

Please review the order details and the associated terms and conditions.

No royalties will be charged for this reuse request although you are required to obtain a license and comply with the license terms and conditions. To obtain the license, click the Accept button below.

Licensed Content Publisher	Elsevier
Licensed Content Publication	Sensors and Actuators B: Chemical
Licensed Content Title	Monolithic membrane valves and diaphragm pumps for practical large-scale integration into glass microfluidic devices
Licensed Content Author	William H Grover,Alison M Skelley,Chung N Liu,Eric T Lagally,Richard A Mathies
Licensed Content Date	1 April 2003
Licensed Content Volume	89
Licensed Content Issue	3
Licensed Content Pages	9
Type of Use	reuse in a thesis/dissertation
Portion	figures/tables/illustrations
Number of figures/tables/illustrations	1
Format	both print and electronic
Are you the author of this Elsevier article?	No
Will you be translating?	No
Original figure numbers	Figure 1, and 2
Title of your thesis/dissertation	Designing Microfluidics Components for Quantitative Bioanalysis and low limit of detection
Expected completion date	Dec 2017
Estimated size (number of pages)	200
Requestor Location	Auburn University 179 Chemistry Building AUBURN UNIVERSITY, AL 36849 United States Attn: Auburn University
Publisher Tax ID	98-0397604
Total	0.00 USD

Edit Order Details

Edit Requestor Location This location may be used to determine your tax liability.

☐ I agree to these terms and conditions.

☐ I understand this license is for reuse only and that no content is provided.

Customer Code (if supplied) [ ] APPLY

BACK DECLINE ACCEPT

Please click accept only once.

Title:	Monolithic Microfabricated Valves and Pumps by Multilayer Soft Lithography
Author:	Marc A. Unger,Hou-Pu Chou,Todd Thorsen,Axel Scherer,Stephen R. Quake
Publication:	Science
Publisher:	The American Association for the Advancement of Science
Date:	Apr 7, 2000

Review Order

Please review the order details and the associated terms and conditions.

No royalties will be charged for this reuse request although you are required to obtain a license and comply with the license terms and conditions. To obtain the license, click the Accept button below.

Licensed Content Publisher	The American Association for the Advancement of Science
Licensed Content Publication	Science
Licensed Content Title	Monolithic Microfabricated Valves and Pumps by Multilayer Soft Lithography
Licensed Content Author	Marc A. Unger,Hou-Pu Chou,Todd Thorsen,Axel Scherer,Stephen R. Quake
Licensed Content Date	Apr 7, 2000
Licensed Content Volume	288
Licensed Content Issue	5463
Volume number	288
Issue number	5463
Type of Use	Thesis / Dissertation
Requestor type	Scientist/individual at a research institution
Format	Print and electronic
Portion	Figure
Number of figures/tables	1
Order reference number	
Title of your thesis / dissertation	Designing Microfluidics Components for Quantitative Bioanalysis and low limit of detection
Expected completion date	Dec 2017
Estimated size(pages)	200
Requestor Location	Auburn University 179 Chemistry Building

	AUBURN UNIVERSITY, AL 36849 United States Attn: Auburn University
Total	0.00 USD

Edit Order Details

Edit Requestor Location This location may be used to determine your tax liability.

☐ I agree to these terms and conditions.

☐ I understand this license is for reuse only and that no content is provided.

Customer Code (if supplied) [ ] APPLY

BACK DECLINE ACCEPT

Please click accept only once.